

**CATALYTIC DEHYDROCHLORINATION
OF 2-CHLOROBUTANE**

Thesis submitted for the degree of Doctor of Philosophy
by

Leng Leng Tan

Department of Chemistry

Cardiff University

January 2005

UMI Number: U583965

All rights reserved

INFORMATION TO ALL USERS

The quality of this reproduction is dependent upon the quality of the copy submitted.

In the unlikely event that the author did not send a complete manuscript and there are missing pages, these will be noted. Also, if material had to be removed, a note will indicate the deletion.



UMI U583965

Published by ProQuest LLC 2013. Copyright in the Dissertation held by the Author.
Microform Edition © ProQuest LLC.

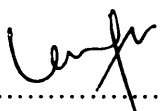
All rights reserved. This work is protected against
unauthorized copying under Title 17, United States Code.



ProQuest LLC
789 East Eisenhower Parkway
P.O. Box 1346
Ann Arbor, MI 48106-1346

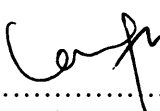
Declaration

This work has not previously been accepted in substance for any degree and is not being concurrently submitted in candidature for any degree

Signed  (candidate)
Date 15/6/2005

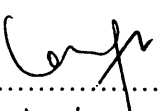
Statement 1

This thesis is the result of my own investigations, except where otherwise stated. Other sources are acknowledged by footnotes giving explicit references. A bibliography is appended.

Signed  (candidate)
Date 15/6/2005

Statement 2

I hereby give consent for my thesis, if accepted, to be available for photocopying and for inter-library loan, and for the title and summary to be made available to outside organizations.

Signed  (candidate)
Date 15/6/2005

Abstract

The catalytic dehydrochlorination of 2-chlorobutane has been studied using promoted alumina catalysts. The modified alumina ($\text{Al}_2\text{O}_3\text{-HCl}$, $\text{K-Al}_2\text{O}_3$), zirconia-alumina ($\text{ZrO}_2\text{-Al}_2\text{O}_3$) and silver-alumina ($\text{Ag/Al}_2\text{O}_3$) catalysts were synthesized and characterised before being tested for catalyst activity. In addition, silver-silica (Ag/SiO_2) and silver-zirconia-alumina ($\text{Ag/ZrO}_2\text{-Al}_2\text{O}_3$) were also prepared as different supported silver catalysts for dehydrochlorination of 2-chlorobutane. γ -alumina catalysts were active for the dehydrochlorination reaction due to the presence of Lewis acid sites. The catalyst performance and the acid-base properties suggest the reaction was acid-catalysed. Doping K or Na on γ -alumina inhibited the activity due to the loss of acidic sites from the alumina surface. Despite the inhibition effect of the alkaline doped catalyst, acid-base bifunctional catalysis was proposed over zirconia-alumina catalysts. The presence of Al-O-Zr surface structural defects on zirconia-alumina controlled the acid-base properties which relate to the catalytic activity. The role of basic sites is to stabilise the carbonium ion and activates the C-H bond, while the acid sites encourage the abstraction of Cl^- ions. A correlation between the ratio of base/acid sites and conversion is suggested, depending on the reaction conditions (i.e. space velocity). Finally, the silver-promoted catalysts were prepared, emphasis placed on the metal-support interaction. The results suggest that as well as the active species distribution which is important for the reaction, the acid-base properties of the support are vital.

Acknowledgement

I would like to thank all the following people who have contributed to the completion of this PhD thesis in one way or another.

Thanks to Prof. Graham Hutching, Dr. Colin Rhodes and Dr. Albert Carley who brought me to the world of “*Catalysis*” and giving me the opportunities to pursue this PhD study in Cardiff University.

Thanks to Dr. Colin Rhodes, Dr. Paul McMorn, Dr Phil Landon, Dr. Stuart Taylor and Dr. Albert Carley, my former and current supervisors, for their support, guidance and direction over the last three years.

Thanks to Dr Nicola Young, my industrial supervisor from Johnson Matthey Catalysts (formerly known as Syntex) for the industrial funding, and the memorable experiences in their research laboratory in Billingham as well as the annual industrial meeting.

Many thanks to my lab mates, Hong Mei, Nian Xue, Gerry, Fede, Javier, Pablo, Thomas, Marco, Tom, Chris, Nick, Becky, Owain, Darragh, Graham, Luisa, and so on, to fill my PhD life with joy, happiness, tears and courage.

Thanks to Kim, whose enthusiasm about research and I wish him to finish his PhD in Cambridge soon too!

Last but not least, I send my greatest acknowledgement to my parents, who support me all the way even before I started the PhD, their endless love are very much appreciated.

I also would like to give thanks to the internal examiner Dr Phil Davies and the external examiner Prof Jim Anderson for their participations and valuable opinions.

Contents

ABSTRACT

ACKNOWLEDGEMENT

1 INTRODUCTION

1.1 Background	1
1.2 Aims of Research	2
1.3 Research Approaches	2
1.3.1 The role of catalysis in dehydrochlorination of butyl chloride	2
1.3.2 Short survey of Mechanistic Concept	5
1.4 Catalytic Dechlorination Literatures Studies	6
1.4.1 Catalytic Dehydrochlorination	7
1.4.2 Catalytic Hydrodechlorination	12
1.4.3 Catalytic Oxidation	15
1.5 Miscellaneous	17
1.5.1 Economic Aspect	17
1.5.2 Environmental Aspect	20
References	23

2 EXPERIMENTAL

2.1 Introduction	27
2.2 Chemicals Preparation	27
2.2.1 Reagent	27
2.2.2 Catalyst Preparation	28
2.3 Catalyst Characterisation	32
2.3.1 Nitrogen adsorption (BET) isotherm	32
2.3.2 Powder x-ray diffraction (XRD)	33
2.3.3 Scanning electron microscopy (SEM)	35
2.3.4 Chemisorption/ Temperature programmed desorption (TPD)	35
2.3.5 Temperature programmed reduction (TPR)	37
2.3.6 Thermal gravimetric analysis (TGA)	37
2.3.7 X-ray photoelectron spectroscopy (XPS)	37
2.3.8 X-ray fluorescence analysis (XRF)	39
2.3.9 Atomic adsorption spectroscopy (AAS)	40
2.3.10 Infrared spectroscopy (IR)	41
2.3.11 Raman spectroscopy	41
2.3.12 Chloride analysis by columetric titration	42
2.4 Catalyst Testing	42
2.4.1 Process flow diagram	42
2.4.2 Reactor design	44
2.4.3 Gas analysis	46

2.5 Reaction Condition	48
2.5.1 Optimising reaction conditions	48
2.5.2 Alumina-based catalysts	49
2.5.3 Zirconia-promoted catalysts	51
2.5.4 Silver-promoted catalysts	52
References	53

3 OPTIMISING REACTION CONDITIONS

3.1 Introduction	54
3.2 The gas phase decomposition of butyl chloride/ Pyrolysis	54
3.2.1 Thermodynamic calculations	54
3.2.2 Experimental approach	56
3.3 Is there actually a REAL BLANK reaction?	57
3.4 Effect of silanisation of glass reactor on dehydrochlorination of t-BuCl	59
3.5 Optimised operating conditions for catalytic dehydrochlorination of t-BuCl	59
3.6 Discussions and conclusions	60
References	61

4 ALUMINA CATALYSTS

4.1 Introduction	62
4.2 Activated Aluminas	64
4.2.1 The characteristic of activated alumina	64
4.2.2 Catalytic activity	69
4.2.3 Post-reaction analysis	75
4.3 Effects of Acid-treatment	78
4.3.1 Catalyst characterisation	79
4.3.2 Catalytic activity	82
4.4 Effects of Thermal-treatment	84
4.4.1 The thermal stability of Al ₂ O ₃	84
4.4.2 Catalytic activity	88
4.5 Alkaline-doped Aluminas	89
4.5.1 K-doped aluminas	90
4.5.2 Na-doped alumina catalysts	101
4.6 Conclusions	107
References	109

5 ZIRCONIA PROMOTED CATALYSTS

5.1 Introduction	111
-------------------------	------------

5.2 Pure Zirconia	111
5.2.1 The characteristics of pure zirconia	113
5.2.2 ZrO ₂ as dehydrochlorination catalyst	118
5.2.3 Post-reaction analysis	120
5.3 Supported Zirconia on alumina	122
5.3.1 Characteristic of zirconia-alumina	123
5.3.2 Catalytic activity	131
5.3.3 Post-reaction analysis	137
5.4 Alkaline-doped zirconia-alumina	138
5.4.1 KOH/ZrO ₂ -Al ₂ O ₃ and ZrO ₂ /KOH-Al ₂ O ₃	139
5.5 Conclusions	145
References	147

6 SILVER DOPED CATALYSTS

6.1 Introduction	149
6.2 Silver-doped alumina	150
6.2.1 Catalyst characterisation	151
6.2.2 Catalytic activity	160
6.2.3 Post-reaction analysis	163
6.3 Al₂O₃-SS/ α-Al₂O₃/ SiO₂/ BN as alternative support	167
6.3.1 Catalytic performances	167
6.3.2 Evaluation of different supported Ag catalysts	168
6.4 Silver-doped silica	170
6.4.1 Catalyst characterisation	171
6.4.2 Catalytic activity	175
6.4.3 Post-reaction analysis	178
6.5 Silver-doped zirconia-alumina	180
6.5.1 Catalyst characterisations	180
6.5.2 Catalytic activity	183
6.5.3 Post-reaction analysis	185
6.6 Conclusions	186
References	188

7 CONCLUSIONS & FUTURE WORK **190**

APPENDIXES

Appendix A:	List of Priority Pollutants
Appendix B:	Physical Properties Data
Appendix C:	BET Isotherms
Appendix D:	Sample Calculations
Appendix E:	Case Studies – Chloride absorbent

1 INTRODUCTION

Background
Aims of Research
Research Approaches
Catalytic Dechlorination literature studies
Miscellaneous

1.1 Background

The disposal of the chlorinated waste is now recognised as a serious problem. The treatment technologies that are presently used are generally destructive in nature and typically involve landfill or incineration. These methods demand high energy and can result in the generation of toxic by-products¹ (e.g. dioxins, HCl, CO, CO₂). Therefore much effort has been put into searching for alternative disposal methods for chlorinated waste. These include chemical processes (catalytic or non-catalytic, air stripping, carbon absorption), biological or microbial¹, electrochemical², photochemical^{3,4}, ultrasonic, radiation⁵, radiolytic and thermal⁶ techniques. Among them, the catalytic dechlorination method seems to be more suitable, efficient and ecologically acceptable for handling chlorinated waste where the hazardous compound is transformed into recyclable products in a closed system with significant reduction of toxic emissions. Furthermore, the dechlorination process can also serve as a potential viable synthetic route to produce useful intermediates and the HCl is recovered.

1.2 Aims of Research

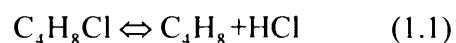
Our goal is to study the catalytic dehydrochlorination of chlorinated hydrocarbon over different catalysts under an inert condition. The monochlorobutanes or butyl chlorides (i.e. 1-chloro, 2-chlorobutane and tert-butyl chloride) were used as the model compounds of a weakly chlorinated volatile organic. We investigate the catalytic performance of acid, base, acid-base bifunctional and noble metal catalysts to develop new catalysts which allow the destruction of chlorinated compounds at low temperature, without need of an oxidant or reductant and allowing the recovery of chlorine as HCl.

1.3 Research Approaches

1.3.1 The role of catalysis in dehydrochlorination of butyl chloride

Keeping in mind the aims of research is to study the catalytic dehydrochlorination of butyl chlorides over different catalysts under an inert condition. Based on the fundamentals of catalysis, the choice of catalysts used, the operating conditions, and the possibly main side reactions were discussed.

The removal of chloride from monochlorobutane occurs by the overall reaction shown in equation (1.1):



The standard enthalpy energy of this reaction is positive, indicating an endothermic equilibrium reaction favoured by increasing temperature. No reaction takes place with the reactants at ambient temperature, and with an active catalyst a temperature between 50 to 400°C is needed for the reaction to proceed⁷. Gas phase decomposition (or pyrolysis)

takes place at temperature higher than 300°C to give butene and hydrochloric acid as the major products.

1.3.1.1 Catalysts

Pure γ -alumina, acid-treated alumina and alkaline-dope alumina (K-Al₂O₃, Na-Al₂O₃) were tested for the catalytic dehydrochlorination of butyl chloride to investigate the influence of the acid-base properties on the activity upon modification by thermal, acid- or base-treatment. γ -alumina was chosen owing to its large surface area, high porosity and its surface chemistry⁸. E. Iglesia *et al*⁹ proposed the amphoteric properties of γ -alumina that consists of basic oxygen, acidic hydroxyls and Al cation sites.

Pure zirconia and zirconia promoted (ZrO₂-Al₂O₃ and K-containing ZrO₂-Al₂O₃) catalysts were tested on this reaction for the first time as an acid-base bifunctional catalyst. ZrO₂ is known for its acid-base bifunctional¹⁰⁻¹² properties. The cooperation of weakly acid sites and weakly base sites makes zirconia an efficient catalyst for esterification, alkene hydrogenation¹¹ and dehydration-dehydrogenation of 2-propanol¹². Although zirconia shows interesting catalytic properties, its behaviour is still unclear. Extensive studies have been made of the effect of the synthetic procedure¹³⁻¹⁴ and the calcinations temperature^{12,15} on the change of textural properties and acid-base properties.

Ag catalysts are particularly interesting in catalytic dehalogenation due to the existence of silver ion in more than one valence state and are able to donate and accept halogen freely¹⁶. However, few studies has been published for the dehydrochlorination of butyl chloride using silver as an active catalyst due to catalyst poisoning by the formation

of stable chloride. A series of supported Ag catalysts were prepared by impregnating AgNO₃ salt onto the alumina, silica and zirconia-alumina support.

1.3.1.2 Main side reactions

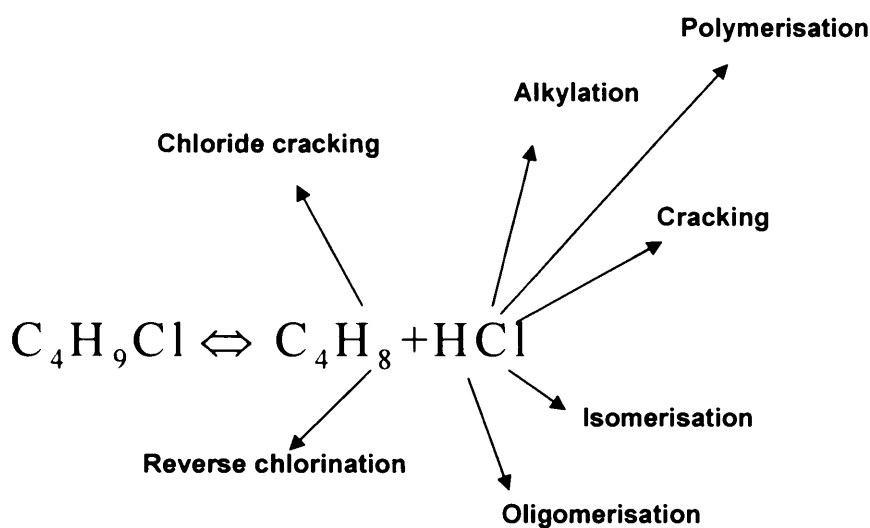
In the gas phase dehydrochlorination reactions, pure elimination products were obtained in most cases. Alkene and HCl were the major products from the contact elimination reaction. Unfortunately, the catalytic reaction is normally accompanied by side reactions, mostly due to carbon deposition which lead to catalyst deactivation increases with increasing temperature. For instance, with very strong acid catalyst like zeolites, fractionation products were obtained due to oligomerisation, cracking and aromatisation, in addition to the elimination products in dehydrochlorination of 2-chloropropane with the presence of oxygen¹⁷. Base catalysts like Al₂O₃ and MgO were ideal catalysts for the isomerisation of olefins⁹⁻¹⁰. Oxychlorination reaction occurred in the presence of CuCl₂-Al₂O₃ catalyst^{17,18}. Schematic below shows the possible side reactions might occur in the dehydrochlorination of butyl chloride, with a brief description of the types of reaction¹⁹.

Oligomerisation: Poly-olefins are formed by combining a low molecular weight compound into higher molecular weight olefin to form heavy unsaturated hydrocarbon (cyclic or aromatic compounds), which increase with increasing temperature.

Cracking: A reaction where large molecules break down to a smaller molecule. Typical products are ethene, hexene, propene, pentene, butene or isobutene.

Isomerisation: Double-bond shift or migration. Typical products are the different butene isomers (1-butene, cis/trans-2-butene, isobutene).

Polymerisation: Formation of large molecular weight compounds either by addition or condensation.



Scheme 1.1: Possible side reactions for the dehydrochlorination of butyl chlorides

1.3.2 Short Survey of Mechanistic Concept

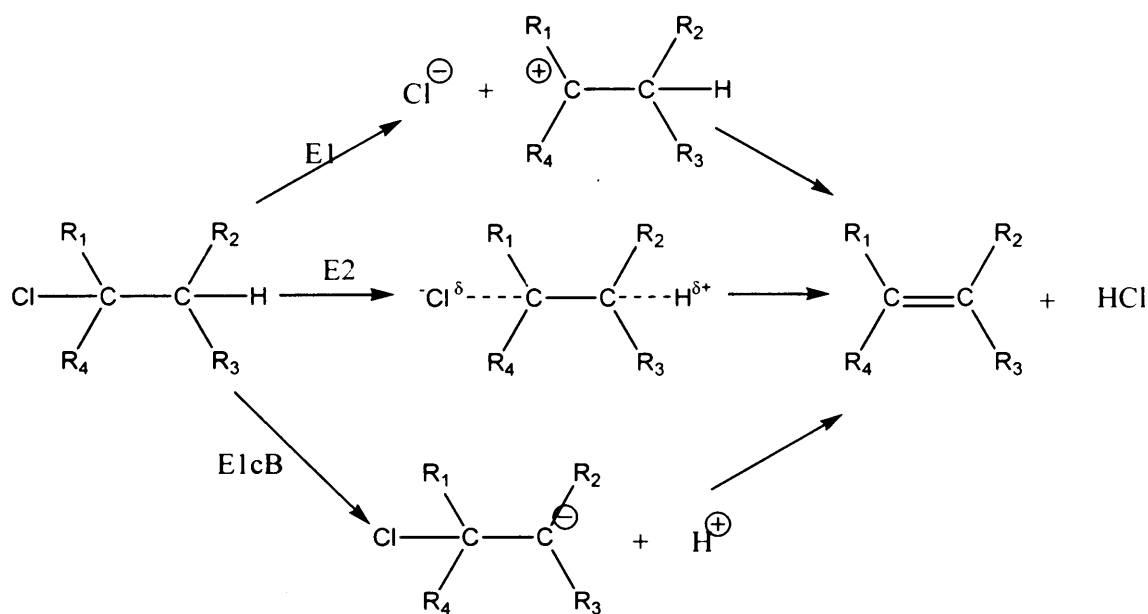
The “mechanism” refers mainly to the movement of the atoms in their rearrangement from the initial state to final state. In the gas phase, contact elimination is dominant, which are the E1, E2, and E1cB^{7,20} mechanism as shown in Scheme 1.2.

In the E1 mechanism, the reaction begins with the abstraction of Cl^- species generating a carbocation, which has a certain life time and can be subjected to rearrangement before loss of a proton in the second stage. The potential energy curve has two maxima separated by a minimum that corresponds to the carbonium ion.

In the case of the E1cB mechanism the reaction also consists of two distinct steps, beginning with the proton abstraction. The energy profile again has two maxima; the intervening minimum corresponds to the carbanion.

In the E2 (also called concerted) mechanism, H^+ and Cl^- removed simultaneously in a concerted process. The reaction begins with the lengthening of only one bond; before the rupture is complete, the other bond begins to loosen. The energy profile has only one maximum.

From the stereochemical point of view, two possibilities are distinguished: Abstraction of the leaving groups from the same side of the carbon chain called the cis- or syn-elimination, and the abstraction from the opposite sides called the trans- or anti-elimination.



Scheme 1.2: E1, E2 and E1cB, contact elimination mechanism

1.4 Catalytic Dechlorination literatures studies

Catalytic dechlorination can be performed under inert²¹ (dehydrochlorination), reducing^{22,23} (hydrogenolysis), or oxidizing^{17,24} (oxychlorination) conditions.

1.4.1 Catalytic Dehydrochlorination

Few studies are reported on the gas-phase dehydrochlorination for the disposal of chlorinated hydrocarbons. The catalysts commonly used are the supported or unsupported metal chlorides, metal oxides and zeolites.

Simkovich and Wagner²⁵ were the first to propose the presence of ionic effects such as ad-cations, ad-anions, cation vacancies, and anion vacancies can enhance the rate of dehydrochlorination of alkyl chlorides. The author found that the rate of the reaction of tert-butyl chloride to butene and HCl at 100°C on solid AgCl was enhanced accordingly upon doping AgCl with CdCl₂. Hauffe and Sitabkhan²⁶ found for the same reaction when the surface of AgCl was treated with Cl₂ vapour, that the surface becomes catalytically active. Maier *et al*^{27,28} demonstrated the influence of ionic defects on the dehydrochlorination of tert-butyl chloride using pure AgCl and doped AgCl with alumina. The presence of AgCl heterogeneously doped with alumina increases the rate of reaction significantly. The mechanism is interpreted in terms of Ag⁺-vacancy accumulation in the space charge region of AgCl. For the silica doped AgCl, no enhancement can be observed at low temperature and in the high temperature region, the conductance is lowered.

Ng and Leung subsequently investigated the ionic point defects for the same reaction over mixed copper chlorides²⁹ and first-row of transition metal chlorides³⁰. IR studies were carried out on MnCl₂, FeCl₂, FeCl₃, CoCl₂, NiCl₂, MgCl₂, CdCl₂, AlCl₃, CrCl₃ and FeCl₃ catalysts and the results show that tert-butyl chloride is associatively adsorbed onto the surfaces during the reaction. The resulting surface species, with a C-Cl bond and a highly perturbed methyl group, could possibly be an important reaction

intermediate. This was different from that reported for CuCl_2 where the tert-butyl chloride is dissociatively adsorbed resulting in a tert-butyl group bonded to a surface ion.

Various metal chloride oxides having layered structures, i.e. MClO ($\text{M} = \text{Bi}, \text{Sb}, \text{V}, \text{Fe}, \text{La}$), $\text{MBi}_3\text{Cl}_2\text{O}_4$ ($\text{M} = \text{Li}, \text{Na}$), $\text{Li}_3\text{Ca}_2\text{Bi}_9\text{Cl}_{10}\text{O}_{12}$ and $\text{LiCaBi}_3\text{Cl}_4\text{O}_4$, have been tested as catalysts for the dehydrochlorination of tert-butyl chloride to form olefins and were found active for the reaction, depending on the metal constituent and the structure³¹. Also, molten salt of ZnCl_2 and KCl supported on activated carbon, Al_2O_3 , or SiO_2 were used in the catalytic dehydrochlorination of butyl chloride and $\text{ClCH}_2\text{CHCl}_2$ at 300°C to give 1-butene, 2-butenes, 1,1- and 1,2-dichloroethylenes³²: the role of pore structure of carrier were determined.

Recently, Chihara *et al*³³ studied the catalytic dehydrochlorination of fluoro-, chloro-, bromo- and iodopentanes by Nb, Mo, Ta, and W halide clusters with an octahedral metal framework and by a Re chloride cluster with a triangular metal framework. All of the former clusters develop catalytic activity for dehydrohalogenation of 1-halogenated pentanes yielding 1-pentene and *cis*- and *trans*-2-pentenes in a helium or hydrogen stream when the clusters are preliminarily treated at 300°C . The Re cluster develops catalytic activity for the same reaction in a stream of helium above 175°C , while in a stream of hydrogen at 300°C , it is reduced to metallic Re to catalyze both dehydrohalogenation and hydrodehalogenation (hydrogenolysis) yielding pentenes and pentane. Even the C–F bond of 1-fluoropentane is hydrogenolyzed by the Re metal.

Metal oxides are important catalysts for catalytic dehydrochlorination (*via* elimination reaction)⁷, especially alkaline earth oxides attract significant attention as effective absorbent for toxic gases as NO_2 , SO_2 , SO_3 , and HCl , as well as chlorinated

compounds³⁴⁻³⁷. Misono and Yoneda³⁴ in 1974, investigated the stereoselectivity of the catalytic dehydrochlorination of 2,3-dichlorobutane, 2,3-dibromobutane and 2-bromobutane over MgO, CaO, SrO and Al₂O₃ at 100-250°C. The elimination of hydrogen halide proceeded selectively by anti- or trans- mode over fresh surface of these oxides below 200°C for dibromobutane and below 250°C for dichlorobutane, reflecting the surface basicity. Anti- mode was also favoured in the case of 2-bromobutane at about 100°C. However, due to the alteration of surface basicity by hydrogen halide formed, the stereoselectivity decreased with repeated pulses.

Klabunde and co-workers have performed extensive studies with the use of nanocrystalline MgO catalysts for dehydrochlorination of different chlorobutanes^{20,35,36}. The outcomes show both stoichiometric and catalytic dehydrochlorination of 1-chlorobutane took place, resulting in the topochemical conversion of MgO to MgCl₂. The obtained MgCl₂ appeared to be an active catalyst for the dehydrochlorination reaction, and the rate of conversion grows significantly with time. The reaction mechanism changes from predominantly E2 elimination on MgO to mostly E1 elimination over MgCl₂, which act as Lewis acid. Carbon coated MgO³⁷ was synthesised and the carbon coating acts as a hydrophobic barrier partially protecting the core metal oxide from water adsorption, however the destructive adsorption reaction can still proceed on the metal surface, as evidence by the dehydrochlorination of 1-chlorobutane. The overall stability of the material in the presence of water vapour is significant improved in comparison with non-coated nanocrystalline MgO.

Supported Cs⁺ or CsCl are effective catalysts for dehydrochlorination of chlorinated hydrocarbons and have been supported on activated carbon³⁸, and silica gel³⁹.

⁴¹. Trushechkina *et al*³⁸ tested the activated carbon (AC), 10%CsCl/AC, 11%CsCl/silica gel, and calcium aluminate catalysts on the 1,2-dichloroethane dehydrochlorination. Among them, Cs-containing catalysts and activated carbon showed good activity and selectivity attributed to the presence of basic sites on the surface. Mochida *et al* shows that the silica gel and the CsCl loadings most influenced the catalytic activity for dehydrochlorination of 1,1,2-trichloroethane (TCE). However significant decrease in activity was observed with repeated pulse or continuous gas flow, suggesting that desorption of HCl was limited³⁹. Bifunctional cooperation of OH groups on the silica surface was assumed to accelerate the elimination of HCl. The silica gel supported Cs⁺ salts was also examined for the dehydrochlorination of TCE and 1,1-dichloroethene (DCE). CsNO₃ showed the best activity due to its high dispersion obtained from supporting on silica gel, although it was converted into CsCl during the dehydrochlorination reaction^{40,41}.

Patent studies^{42,43} by Mochida *et al* showed that the activated carbon exhibited excellent activity and selectivity in particular for the dehydrochlorination of 1,2-dichloroethane without degradation in continuous use for long hours. The dehydrochlorination of 1,2-dichloroethane was performed at 350°C to give 69.5% of conversion. Szymanski and Zietek⁴⁴ investigated the catalytic dehydrochlorination of 2-chloropropane over activated carbon. The result shows that treating carbon with ammonia was an effective catalyst for dehydrochlorination, while oxidation with concentrated nitric acid diminishes the activity. The high activity of the ammonia treated carbon was due to the presence of pyridine-like species that act as additional basic sites.

Flid and co-workers published the use of series of Ni-Cr catalyst by co-precipitation, reduction and passivation, alumina supported Pd and Ni-Cr catalysts for catalytic dehydrochlorination of 1,2-dichloroethane⁴⁵ and 1,1,2-trichloroethane⁴⁶. Ni-Cr catalysts show good selectivity to ethylene depending on the temperature. The skeletal isomerisation of n-butene from dehydrochlorination of 1-chlorobutane over reduced WO₃ catalyst has also been reported⁴⁷. A unimolecular mechanism was concluded and the elimination reaction is always faster than the skeletal isomerisation.

There are only a few studies of dehydrochlorination on zeolites. Kladnig and Noller^{7,48} found the following activity series for dehydrochlorination of 1- and 2-chlorobutane over X-zeolites: Pr³⁺ > Mg²⁺ > Zn²⁺ > Co²⁺ > Ni²⁺ > Ca²⁺ > Cu²⁺ > Na⁺. Mochida reported that CsOH ion-exchanged ZSM-5 zeolites^{49,50} of high Si/Al ratios were found to exhibit distinct catalytic activity for selective dehydrochlorination of 1,1,2-trichloroethane into 1,1-dichloroethene. The result shows initial high activity due to the presence of silanol, but catalyst deactivation was observed after the CsOH was converted into CsCl on the zeolite. The catalytic conversion of methyl chloride over zeolite catalysts has been investigated in detailed by Lunsford and co-workers⁵¹. The motivation behind this work emphasized on maximising the yield of ethylene and propylene from the reaction of methyl chloride by modifying ZSM-5 zeolites. The phosphorus modified MgZSM-5 was found to obtain high activity and selectivity to the formation of propylene. Test reactions and spectroscopic studies confirm that the phosphorus modified MgZSM-5 decreases the strong Bronsted acidity of the zeolite, inhibiting the undesired further oligomerisation of ethylene to paraffins and aromatics.

1.4.2 Catalytic hydrodechlorination

Among the techniques of catalytic dechlorination, reductive dechlorination or hydrodechlorination is of the most commonly used for the hydrogenolysed of chlorinated hydrocarbon^{22,23}. In general, the cleavage of carbon-chlorine bonds is the rate-determining step in the hydrodehalogenation reaction. The order of the ease of hydrodehalogenation for organic halides is related to the dissociation energy of these bonds (C-F, 108 kcal mol⁻¹; C-Cl, 81 kcal mol⁻¹; C-Br, 67 kcal mol⁻¹; C-I, 53 kcal mol⁻¹), which is: I > Br > Cl >> F and tertiary halide > secondary > primary.

Catalysts mostly used for reductive dechlorination of chlorinated hydrocarbon are noble metal types (Pt, Pd, Rh) with or without support. Pt and Pd catalysts seem to play the most important role in chlorine removal from organic chloride. Morikawa *et al*⁵² investigated the reduction of chloroacetone over silica-supported noble metal catalysts. The results show different selectivities depending on the catalyst used: Pd/SiO₂ catalysed the hydrodechlorination to give acetone; Pt/SiO₂ promoted the hydrogenation to give 1-chloro-2-propanol and 2-propanol; and Rh/SiO₂ transformed acetone to 1-chloro-2-propanol through the addition of hydrogen chloride. The hydrodechlorination activity of noble metals followed the order of Pd > Pt >> Rh > Ru.

Diez *et al*⁵³ compare the hydrodechlorination activity of eight commercial catalysts (Nickel-Raney, Ni on SiO₂, Pd on alumina, Pt on both alumina and activated carbon, Rh on alumina and sulfided Ni-Mo on alumina) for the hydrodechlorination of the six organochlorinated compounds that are released into the environment in the greatest amounts: dichloromethane (DCM), chloroform (CLF), carbon tetrachloride

(CTC), 1,1,1-trichloroethane (TCA), trichloroethylene (TCE) and tetrachloroethylene (TTCE). Pt catalysts were found to yield the highest conversions.

Supported Pt⁵⁴, Pd and Rh⁵⁵ on Al₂O₃ catalysts showed high activity in the hydrodechlorination of chlorobenzene. The kinetics of the hydrodechlorination of chlorobenzene has been investigated over Pd/Al₂O₃ and Rh/Al₂O₃ catalysts of varying dispersion⁵⁵. A reaction scheme was proposed, in which a surface chloride was formed due to strong interaction between chlorobenzene and catalyst; hydrogen was served to displace the chloride from the catalyst surface. The particle size and the metal dispersions are strongly influenced the catalyst performance, and Pd catalysts appeared to be a better catalyst than Rh catalysts.

Keane and co-worker^{56,57} have performed extensive studies on the use of Ni/SiO₂ catalysts to hydrotreat a range of chlorinated feedstock: cyclochloride⁵⁸, chlorobenzene, chlorotoluene, chlorophenol, dichlorobenzene, dichlorophenol, trichlorophenol, and pentachlorophenol. In the case of polychlorinated compounds, dechlorination proceeded in a stepwise manner to generate a partial dechlorinated product. Hydrodechlorination occurred *via* an electrophilic mechanism where the presence of electron-donating substituents (inductive effect) on the benzene ring enhances the rate of reaction. The gas phase dechlorination of aliphatic chloride such like cyclohexyl chloride, took place *via* the internal elimination of the corresponding hydrogen chloride. The catalyst exhibited both short term and irreversible long term deactivation due to surface poisoning (chloride or carbon cracking), and the presence of hydrogen served to displace the inorganic chloride from the surface poisoning and extend the productive lifetime of the catalysts^{21,58}. The reaction is shown to be structure sensitive over Ni/SiO₂ where the

hydrodechlorination rate and the yield of parent aromatic is favoured by larger Ni particle sizes⁵⁶. A direct contact of the freshly activated catalyst with HCl induced an appreciable growth of the supported metal crystallites. In addition, Cesteros and Cho prepared several Ni catalysts including bulk nickel⁵⁹, Ni/Al₂O₃⁶⁰, Ni/NiAl₂O₄⁶¹, and Ni/Al-MCM-41⁶², Ni/SBA-15⁶³ for the hydrodechlorination of di- or trichlorobenzene and trichloroethane.

Zeolites as catalysts or catalysts supports offer a number of advantages over metal oxide or supported metal catalysts due to its high internal surface area and the cation exchange capacity. This feature makes zeolite a potential active catalyst for catalytic dehalogenation processes⁶⁴. Schuth *et al* have developed zeolite supported palladium catalysts which are resistant to sulfite poisoning and they can be effectively for treating groundwater contaminants like 1,2-dichlorobenzene⁶⁵. Palladium was supported on zeolites ZSM-5, zeolite Y and mesoporous MCM-41, in which the hydrodechlorination of 1,2-dichlorobenzene in water investigated at room temperature.

Creyghton *et al*⁵⁴ compare the catalytic activity of Pt/H-BEA zeolite and Pt/Al₂O₃ catalysts for the gas phase hydrodechlorination of chlorobenzene. Both catalysts show high activity in the hydrogenolysis of the carbon-halogen bond; however, deactivation of Pt/H-BEA is ascribed to acid-catalysed oligomerisation reaction and coke formation limit the access of reactant molecules to the platinum clusters in the zeolite matrix. A similar conclusion was drawn from the work of Keane *et al*⁵⁸, who compared the performance of Ni/SiO₂ and Ni/Na-Y zeolite catalysts for the decomposition of cyclohexyl chloride and cyclohexyl bromide.

The gas-phase hydrochlorination of pentachlorophenol over the same Ni/SiO₂ and Ni/Na-Y zeolite catalysts⁶⁶ shows 100% selective in cleaving the C-Cl bond, leaving the

hydroxyl substituent and benzene ring intact. Increasing the Ni loading on SiO₂ was found to raise the overall level of dechlorination while the use of a zeolite support introduced spatial constraints that severely limited the extent of dechlorination.

1.4.3 Catalytic oxidation

The catalytic oxidation at less severe conditions (low temperature) is also a promising alternative for removal of chlorinated hydrocarbons^{17,24,67-77}. The desired reaction is a complete oxidation to produce CO₂ and HCl. The oxidative dechlorinating catalysts include the noble metal-based, transition metal oxides and zeolites.

Noble metal-based catalysts have been extensively used for the combustion of chlorinated volatile organic compounds (VOCs), especially Pt and Pd-based catalysts due to their high intrinsic activity and selectivity. Gonzalez-Velasco^{67,68} evaluated the catalytic oxidation of 1,2-dichloroethane (DCE) and trichloroethylene (TCE) over alumina supported noble metal catalysts (Pt and Pd) in a range of metal contents from 0.1 to 1wt%. Pd/ γ -Al₂O₃ resulted to be more active than Pt/ γ -Al₂O₃ catalysts in the oxidation of both chlorinated compounds. As a continuation of his research, the author investigated the complete oxidation of TCE using the same catalysts (Pt and Pd on γ -Al₂O₃) in the presence of hydrogen-rich compounds, namely water, hexane and toluene⁶⁸. It was found that the presence of water promote the complete oxidation of CO to CO₂ by the water-gas-shift reaction.

Busca and co-worker^{17,69} investigated the conversion of 2-chloropropane as a weakly chlorinated VOCs in the presence of oxygen over a series of catalysts including Al₂O₃, SiO₂-Al₂O₃, CuCl₂-Al₂O₃⁷⁰, WO₃-Al₂O₃, MnO_x-Al₂O₃, W-Mn-Al₂O₃, V₂O₅-WO₃-

TiO₂ and H-ZSM-5 zeolite. SiO₂-Al₂O₃ appeared to be the best catalyst among all the catalysts tested. The selectivities to propene differ significantly from catalyst to catalyst.

FT-IR and reactor study of the dehydrochlorination activity of CuCl₂-Al₂O₃ confirmed that the exposed alumina support surface are responsible for the dehydrochlorination of 1,2-dichloroethane (DCE) to vinyl chloride monomer^{71,72}. The FTIR spectra of ethylchloride adsorbed on γ -Al₂O₃ show weakly molecularly adsorbed species and ethoxy groups formed by nucleophilic substitution. Additionally, adsorbed diethylether is also observed. Experiments performed on alumina doped with MgCl₂ and KCl⁷¹ indicated that the site reactivity scale for ethylchloride conversion to ethylene is followed: γ -Al₂O₃ > CuCl₂/Al₂O₃ > MgCl₂/Al₂O₃ > KCl/Al₂O₃. Doping alumina with MgCl₂ and in particular with KCl limits the activity of the bare support in the dehydrochlorination.

Nevertheless, MnO_x-Al₂O₃, W-Mn-Al₂O₃, and V₂O₅-WO₃-TiO₂ are active in the dehydrochlorination of 2-chloropropane¹⁷, but Mn-containing catalysts are deactivated as combustion catalysts by chlorine. V₂O₅-WO₃-TiO₂ catalysts appear to be more selective to propene, whose oxidation activity retained is not affected by chlorine or HCl. The catalyst promotes oxidation to CO and CO₂ with higher V contents^{73,74}. The V-W-Ti catalysts are also very active in the dehydrochlorination of 1-chloropropane⁷⁴, *ortho*-dichlorobenzene (*o*-DCB) and dibenzofuran (DBF)⁷⁵.

The use of zeolite catalysts for deep oxidation of 1,2-dichloroethane (DCE) to CO₂, HCl and H₂O was recently reported by Gonzalez-Velasco²⁴. The conversion followed the order of H-ZSM-5 > H-MOR > H-Y. The higher activity of H-ZSM-5 catalyst was ascribed to the high density of strong Bronsted sites. However, vinyl

chloride was formed as an intermediate which required higher temperature for complete destruction to CO, CO₂ and HCl. H-Y and H-MOR appeared to be more selective to CO₂ than H-ZSM-5. The presence of water in the feed stream has significantly reduced the formation of vinyl chloride and the CO₂ selectivity was largely enhanced²⁴. A similar conclusion was drawn for the catalytic combustion of dichloromethane (DCM) and trichloroethylene (TCE) over H-BEA and PdO/H-BEA catalysts⁷⁶.

Finocchio and Busca have compared the conversion of 1-, 2-chloropropane, 1,2-dichloropropane and trichloroethylene (TCE) over H-ZSM-5 with H-Y and SiO₂-Al₂O₃ catalysts in the presence of oxygen^{17,69,77}. The conversion of mono- and dichloropropane: SiO₂-Al₂O₃ performs the best catalytic activity in terms of conversion and selectivity to alkenes and HCl, while significant formation of chlorinated by-products is observed over H-ZSM-5 zeolite. Water vapour is needed to perform the “steam reforming” of TCE and the zeolite catalysts appear to be more effective than the SiO₂-Al₂O₃ catalyst.

Please refer to the end of this chapter to obtain a summary table of the selections of literatures reviewed.

1.5 Miscellaneous

1.5.1 Economic Aspect

Dechlorination of chlorinated hydrocarbon (also known as organic chloride) is an important, well-established reaction which is frequently used in organic synthesis. Since 1920s, catalytic dechlorination was already used for the production of additive resin⁷⁸,

lubricant oil^{79,80,81}, chemical solvents^{82,83}, fatty acid^{84,85}, motor fuel⁸⁶, sugar⁸⁷, and vinyl chloride^{88,89,90}, which were the major contributions to the paint, pharmaceutical, chemical processing, petrochemical and fine chemical industries.

Among them, the manufacture of lubricant oil considering the most entrenched process with numerous patents registered at United States^{80,91} and Japan^{81,92,93}. The lubricant oils were produced by catalytic dechlorination of chlorinated hydrocarbon to yield oil with high viscosity that was the major applications (e.g. crude oil) of petroleum refining. Unfortunately, petroleum refiners worldwide also face a common problem that the chlorinated hydrocarbons have caused poisoning of downstream catalysts, corrosion cracking and plugging, where the crude oil or the lubrication oil were identified as one of the sources of these chlorides^{94,95}. The chloride contaminants from compressor lubrication oil leads to throughput-reducing fouling by thermal or catalytic cracking of higher hydrocarbon. This effect can be partly reversible, provided that the problem is recognised quickly and rectified. However, minor leakage of oil is not easily identified and permanent damage to the overall operation can occur.

In fine chemical industry, chlorinated hydrocarbon have been widely used as solvent^{82,83}, such as methylene chlorides (applied in pharmaceuticals, chemical processing, aerosol, and surface treatment including paint stripping and urethane foam blowing), tetrachloroethane (pesticides, metal cleaning) and trichloroethylene (speciality adhesive). Methylene chloride²³ is completely biodegradable under both aerobic and anaerobic conditions, therefore, is not being regulated by the Montreal Protocol⁹⁶. Tetrachloroethane^{82,83} (e.g. 1,1,2,2-tetrachloroethane) was used in large amounts to produce trichloroethylene, tetrachloroethylene, and 1,2-dichloroethylene. These aliphatic

chlorinated hydrocarbons have recently been recommended by the Environmental Protection Agency⁹⁷ (EPA) to be phase out of production, as it displayed serious environmental issue. There are considered very dangerous environmental pollutants, can be detected in air, surface water and ground water. EPA has classified these compounds as possible human carcinogen.

In the 1940s the industry of chlorinated pesticides reached maximum production and development, lindane, DDT, chlordane and dieldrin representing the most important members of this family¹. Perhaps the most infamous of all chlorinated pesticides is DDT. It is a useful insecticide particularly good against the mosquito that is the carrier of malaria disease. DDT is very resistant to biodegradation. Its accumulation in the food chain causes low fertility of birds and fish, and is carcinogenic to human. Therefore, it has been banned²³ by the EPA since 1972. In addition, extensive studies have been carried out for the detection and determination of residual DDT content⁹⁸.

The polymeric form of organic chlorides, such as polyvinylchloride (PVC)⁸⁸, vinylidene chloride⁹⁹, dichlorostyrene¹⁰⁰ and chloroprene¹⁰¹ are commercially valuable. These materials are important in manufacturing of plastic products, such like toys, shoes, raincoats, umbrella, computer and keyboards, magnetic recording tape, food packaging, and more. They are useful due to the ability of plastic to resist water, fire-proof, and as a barrier to prevent entry of oxygen into food container and to prolong the storage period. Although these polymers display outstanding characteristic, they cause serious environmental issues as they are not biodegradable and release toxic emission upon thermal treatment, which are harmful to humans²³.

1.5.2 Environmental Aspect (Health & Safety)

The two main Federal agencies involved in the protection of human health and environment are the Environmental Protection Agency (EPA) and the Occupational Safety and Health Administration (OSHA)¹⁰². Chlorinated hydrocarbons are recognized as the most widespread and persistent contaminants of ground and surface water; at least 15 of these contaminants are listed as the priority pollutants by the EPA under the Clean Water Act (CWA) of 1977¹⁰³, referring to Appendix A. Some chlorinated organic compounds with low molecular weight are categorised as the volatile organic compound (VOC), which are the major air pollutants under the Clean Air Act¹⁰⁴. The three of the most recalcitrant toward degradation: chlorofluorocarbons (CFCs), polychlorinated biphenyl (PCBs), dibenzo-*p*-dioxins (e.g. 2,3,7,8-TCDD or dioxins) and dibenzofurans (furans) has been widely studied and reviewed^{23,105}. Special attentions were drawn to the volatile organic compounds (VOCs), whose is more relevant to our studies.

The chlorinated volatile organic compounds (VOCs)^{17,24} emission such like 1,2-dichloroethane (DCE) are associated to a wide range of industrial processes from the vinyl chloride production plants, and is also found in ground water air-stripping emissions admixed with other chlorinated solvents such as trichloroethylene, dichloromethane and 1,2-dichloroethylene. Such compounds are known to be hazardous to the environment and public health, typically carcinogens, mutagens and tetratogens. Hence, public awareness of the harmful effects of VOCs emissions has led to increasingly stringent environmental regulations. The Clean Air Act Amendments of 1990 establish health based air quality standards to significantly improve the reduction of emissions.

Tables below are a selection of publications that was referred for the current studies.

Catalytic dehydrochlorination

Reactant	Catalyst	Ref.
t-butyl chloride	AgCl, AgCl:CdCl ₂	25
	AgCl treated with Cl ₂ vapour	26
	AgCl, AgCl:Al ₂ O ₃	27,28
	CuCl ₂	29
	First-row transition metal chloride	30
	MCIO (M = Bi, Sb, V,	31
butyl chloride and trichloroethane (TCE)	molten salt of ZnCl ₂ and KCl supported on activated carbon, Al ₂ O ₃ , or SiO ₂	32
	Nb, Mo, Ta, and W halide clusters with Re chloride cluster	33
2,3-dichlorobutane, 2,3-dibromobutane and 2-bromobutane chlorobutanes	MgO, CaO, SrO and Al ₂ O ₃	34
	MgO, Carbon coated MgO	35,36,37
1,2-dichloroethane (DCE)	activated carbon (AC), 10%CsCl/AC, 11%CsCl/silica gel, and calcium aluminate	38
1,1,2-trichloroethane (TCE)	silica gel supported Cs ⁺ salts (nitrate, chloride), activated carbon	39-43
2-chloropropane	Activated carbon (AC), AC treated with ammonia	44
1,2-dichloroethane and 1,1,2-trichloroethane	Pd and Ni-Cr on alumina	45,46
1-chlorobutane	WO ₃	47
1- and 2-chlorobutane	X-zeolites (X = Pr ³⁺ , Mg ²⁺ , Zn ²⁺ , Co ²⁺ , Ni ²⁺ , Ca ²⁺ , Cu ²⁺ , Na ⁺)	48
1,1,2-trichloroethane into 1,1-dichloroethene	CsOH ion-exchanged ZSM-5 zeolites	49,50
Methyl chloride	phosphorus modified MgZSM-5	51

Catalytic hydrodechlorination (Reductive dechlorination)

Reactant	Catalyst	Ref.
chloroacetone	silica-supported noble metal (Pd, Pt, Rh, Ru)	52
dichloromethane (DCM), chloroform (CLF), carbon tetrachloride (CTC), 1,1,1-trichloroethane (TCA), trichloroethylene (TCE) and tetrachloroethylene (TTCE)	Raney Ni, Ni/SiO ₂ , Pd /Al ₂ O ₃ , Pt/Al ₂ O ₃ , Pt/C, Rh/Al ₂ O ₃ and sulfided Ni-Mo/Al ₂ O ₃	53
chlorobenzene	Pt, Pd and Rh on Al ₂ O ₃ , Pt/H-BEA zeolite	54,55
cyclochloride, chlorobenzene, chlorotoluene, chlorophenol, dichlorobenzene, dichlorophenol, trichlorophenol, and pentachlorophenol	Ni/SiO ₂ , Ni/Na-Y zeolite	56-58,66
di- or trichlorobenzene and trichloroethane	bulk nickel, Ni/Al ₂ O ₃ , Ni/NiAl ₂ O ₄ , and Ni/Al-MCM-41, Ni/SBA-15	59-63
1,2-dichlorobenzene	Palladium was supported on zeolites ZSM-5, zeolite Y and mesoporous MCM-41	65

Catalytic oxidation (oxidative dechlorination)

Reactant	Catalyst	Ref.
1,2-dichloroethane (DCE) and trichloroethylene (TCE)	Pt and Pd on Al ₂ O ₃	67,68
2-chloropropane	Al ₂ O ₃ , SiO ₂ -Al ₂ O ₃ , CuCl ₂ -Al ₂ O ₃ , WO ₃ -Al ₂ O ₃ , MnO _x -Al ₂ O ₃ , W-Mn-Al ₂ O ₃ , V ₂ O ₅ -WO ₃ -TiO ₂ and H-ZSM-5 zeolite.	69
1,2-dichloroethane (DCE)	Al ₂ O ₃ , CuCl ₂ /Al ₂ O ₃ , MgCl ₂ /Al ₂ O ₃ , KCl/Al ₂ O ₃	70-72
1-chloropropane, <i>ortho</i> -dichlorobenzene (<i>o</i> -DCB) and dibenzofuran (DBF)	V ₂ O ₅ -WO ₃ -TiO ₂	73-75
1,2-dichloroethane (DCE)	H-ZSM-5, H-MOR, H-Y	24
dichloromethane (DCM) and trichloroethylene (TCE)	H-BEA and PdO/H-BEA	76
1-, 2-chloropropane, 1,2-dichloropropane and trichloroethylene (TCE)	H-ZSM-5, H-Y and SiO ₂ -Al ₂ O ₃	17,69,77

References

1. M.D. LaGrega, P.L. Buckingham, J.C. Evans, "Hazardous Waste Management". (1994), McGraw-Hill Inc.
2. R. Chetty, P.A. Christensen, B.T. Golding, K. Scott, *Applied Catalysis A-General*, **271** (2004) 185-194
3. R.L. Gross, X. Liu, A.G. Suits, *Chemical Physics Letters*, **362** (2002) 229-234
4. M. Hegedus, A. Dombi, *Applied Catalysis A-General*, **271** (2004) 177-184
5. V. Mucka, V. Cuba, M. Pospisil, R. Silber, *Applied Catalysis A-General*, **271** (2004) 195-201
6. Y. Yamamoto, S. Tagawa, *Environmental Science & Technology*, **35** (2001) 2122-2127
7. H. Noller, W. Kladnig, *Catalysis Review- Science and Engineering* **13** (1976) 149-207.
8. M. Howe-Grant, Kirk-Othmer Encyclopedia of Chemical Technology (1985). John Wiley & Sons. **Vol.2:** p140.
9. E. Iglesia, D. G. Barton, J.A. Biscardi, M.J.L. Gines, S.L. Soled, *Catalysis Today*, **38** (1997) 339-360
10. H. Hattori, *Chemical Review* **95** (1995) 537-558.
11. K. Tanabe, T. Yamaguchi, *Catalysis Today* **20** (1994) 185-198.
12. M.A. Aramendia, V. Borau, C. Jimenez, J.M. Marinas, A. Porras, F.J. Urbano, *Journal of Chemical Society: Faraday Transaction* **93:7** (1997), 1431-1438.
13. G.K. Chuah, S.H. Liu, S. Jaenicke, J. Li, *Microporous and Mesoporous Materials* **39** (2000) 381-392.
14. A. Kaddouri, C. Mazzocchia, E. Tempesti, R. Anouchinsky, *Journal of Thermal Analysis*, **53** (1998) 97-109.
15. P.D.L. Mercera, J.G. Van Ommen, E.B.M. Doesburg, A.J. Burggraaf, J.R.H. Ross, *Applied Catalysis*, **57** (1990) 127-148.
16. Robert H. Perry and Don W. Green, "Perry's Chemical Engineering Handbook" 7th edition, published by McGraw-Hill, 23-28.
17. C. Pistarino, E. Finocchio, G. Romezzano, F. Briccese, R. Di Felice, G. Busca; M. Baldi, *Industrial & Engineering Chemistry Research*, **39** (2000) 2752-2760
18. C.F. Ng, K. S. Leung, *Journal of Catalysis* **67** (1981) 410-423
19. M. Howe-Grant, Kirk-Othmer Encyclopedia of Chemical Technology (1985). John Wiley. **Vol.4:** p.346, **18:** p.720.
20. I. Mishakov, A.F. Bedilo, R. Richard, V. Chesnokov, A. Volodin, V. Zaikovski, R.A. Buyanov, K.J. Klabunde, *Journal of Catalysis* **206** (2002) 40-48
21. G. Tavoularis, M. A. Keane, *Journal of Molecular Catalysis A: Chemical*, **142** (1999) 187-199
22. A. R. Pinder, *Synthesis*, (1980) 425-452
23. F. Alonso, I. P. Beletskaya, M. Yus, *Chemical Review*, **102** (2002) 4009-4091
24. R. Lopez-Fonseca, A. Aranzabal, P. Steltenpohl, J.I. Gutierrez-Ortiz, J.R. Gonzalez-Velasco, *Catalysis Today*, **62** (2000) 367-377

25. G. Simkovich, C. Wagner, *Journal of Catalysis* **1** (1962) 521-525.
26. K. Hauffe, F. Sitabkhan, *Journal of Catalysis* **8** (1967) 340-347.
27. J. Maier, *Journal of Physical Chemistry Solids* **46:3** (1985) 309-320.
28. J. Maier, P. Murugaraj, *Solid State Ionics* **40/41** (1990) 1017-1020.
29. C.F.Ng, K. S. Leung, *Journal of Catalysis* **67** (1981) 410-423.
30. C.F. Ng, C.K. Chan, *Journal of Catalysis* **89** (1984) 553-559.
31. W. Ueda, M. Yamazaki, Y. Morikawa, *Bulletin of Chemical Society of Japan* **66:1** (1993), 347-349.
32. J. Kobayashi, H. Sofugawa, M. Asaba, H. Masaaki, H. Kosugi, Y. Yoshio, *Kenkyu Hokoku - Asahi Garasu Kogyo Gijutsu Shoreikai (written in Japanese)*, **37** (1980) 251-265
33. S. Kamiguchi, M. Watanabe, K. Kondo, M. Kodomari, T. Chihara, *Journal of Molecular Catalysis A: Chemical*, **203** (2003) 153-163
34. M. Misono, Y. Yoneda, *Journal of Catalysis*, **33** (1974) 474-479
35. R. Richard, R.S. Mulukutla, I. Mishakov, V. Chesnokov, A. Volodin, V. Zaikovski, N. Sun, K.J. Klabunde, *Scripta mater.* **44** (2001) 1663-1666.
36. V.B. Fenelonov, M.S. Melgunov, I. Mishakov, R. Richard, V. Chesnokov, A. Volodin, K.J. Klabunde, *Journal Physical Chemistry B* **105** (2001) 3937-3941.
37. A.F. Bedilo, M.J. Sigel, O.B. Koper, M.S. Melgunov, K.J. Klabunde, *Journal of Material Chemistry* **12** (2002) 3599-3604.
38. M.A. Trushechkina, B. I. Azbel, I.I. Kurlyandskaya, I.G. Solomonik, M.R. Flid, *NATO series. II: Mathematics, Physics and Chemistry*, **69** (2002) 399-405
39. I. Mochida, T. Takagi, H. Fujitsu, *Applied Catalysis*, **18: 1** (1985) 105-15
40. I. Mochida, Y. Kojima, H. Tejima (1993), Patent: JP 051324376 19930528
41. I. Mochida, Y. Yasumoto, H. Fujitsu, Y. Kojima, *Chemistry Letters*, **3** (1992) 461-4
42. I. Mochida (1997), Patent: JP 09249590 19970922
43. I. Mochida, Y. Kojima, H. Tejima, M. Morita (1993), Patent: JP 05271123 19931019
44. G.S. Szymanski, S. Zietek, *Carbon'01* (2001). Lexington, KY, United State, University of Kentucky Centre for Applied Energy Research Library, Lexington, KY.
45. G.S. Dasaeva, M.R. Flid, Y.K. Dmitriev, L.M. Kartashov, Y.A. Treger, *Khimicheskaya Promyshlennost (Moscow. written in Russian)*, **3** (2000) 173-178
46. G.S. Dasaeva, M.R. Flid, Y.K. Dmitriev, L.M. Kartashov, Y.A. Treger, *Khimicheskaya Promyshlennost (Moscow. written in Russian)*, **4** (2000) 225-228
47. Z.X. Cheng, V. Ponec, *Catalysis Letters* **27** (1994) 113-117.
48. W. Kladnig, H. Noller, *Journal of Catalysis*, **29** (1973) 385
49. I. Mochida, Y. Kojima, H. Tejima (1993), Patent: JP 05132435 19930528
50. I. Mochida, Y. Yasumoto, H. Fujitsu, Y. Kojima, *Sekiyu Gakkaishi*, **36: 6** (1993) 498-501
51. Y. Sun, S. M. Campbell, J.H. Lunsford, G.E. Lewis, D. Palke, L.-M. Tau, *Journal of Catalysis*, **143** (1993) 32-44
52. T. Mori, D. Tomikawa, Y. Katano, J. Kubo, Y. Morikawa, *Applied Catalysis A: General* **271** (2004) 77-84.
53. S. Ordonez, H. Sastre, F.V. Diez, *Applied Catalysis B- Environmental*, **25** (2000) 49-58

-
54. E.J. Creighton, *Applied Catalysis A: General* **128** (1995) 275-288.
 55. B. Coq, G. Ferrat, F. Figueras, *Journal of Catalysis* **101** (1986) 434-445
 56. C. Menini, C. Park, E.-J. Shin, G. Tavoularis, M.A. Keane, *Catalysis Today*, **62**: 4 (2000) 355-366
 57. E. -J. Shin, M.A. Keane, *Applied Catalysis B: Environmental* **18** (1998) 241-250.
 58. G. Tavoularis, M.A. Keane, *Applied Catalysis A: General* **182** (1999) 309-316.
 59. J. Estelle, J. Ruz, Y. Cesteros, R. Fernandez, P. Salagre, F. Medina, J.E. Sueiras, *Journal of Chemical Society Faraday Transaction* **92**:15 (1996) 2811-2816.
 60. Y. Cesteros, P. Salagre, F. Medina, J.E. Sueiras, *Applied Catalysis B: Environmental* **22** (1999)135.
 61. Y. Cesteros, P. Salagre, F. Medina, J.E. Sueiras, *Applied Catalysis B: Environmental* **25** (2000)213.
 62. Y. Cesteros, P. Salagre, F. Medina, J.E. Sueiras, *Catalysis Letters* **79**:1-4 (2002) 83-88.
 63. Y.S. Cho, J. C. Park, B. Lee, Y. Kim, J. Yi, *Catalysis Letters*, **81**: 1-2 (2002) 89-96
 64. R. F. Howe, *Applied Catalysis A-General*, **271** (2004) 3-11
 65. C. Schuth, S. Disser, F. Schuth, M. Reinhard,, *Applied Catalysis B: Environmental*, **28** (2000) 147-152
 66. E.-J. Shin, M. A. Keane, *CATALYSIS Letters*, **58** (1999) 141-145
 67. J.R. Gonzalez-Velasco, A. Aranzabal, J.I. Gutierrez-Ortiz, R. Lopez-Fonseca, M.A. Gutierrez-Ortiz, *Applied Catalysis B-Environmental*, **19** (1998) 189-197
 68. J.R. Gonzalez-Velasco, A. Aranzabal, R. Lopez-Fonseca, R. Lopez-Fonseca, R. Ferret, J.A. Gonzalez-Marcos, *Applied Catalysis B-Environmental*, **24** (2000) 33-43
 69. C. Pistarino, F. Bricchese, E. Finocchio, G. Romezzano, R. Di Felice, and G. Busca, *Studies in Surface Science and Catalysis*, **130**: B (2000) 1613-1618
 70. E. Finocchio, N. Rossi, G. Busca, M. Padovan, G. Leofanti, B. Cremaschi, A. Marsella, D. Carmello, *Journal of Catalysis*, **179**: 2 (1998) 606-618
 71. D. Carmello, E. Finocchio, A. Marsella, B. Cremaschi, G. Leofanti, M. Padovan, G. Busca, *Journal of Catalysis*, **191**: 2 (2000) 354-363
 72. A. Marsella, D. Caemello, E. Finocchio, B. Cremaschi, G. Leofanti, M. Padovan, G. Busca,, *Studies in Surface Science and Catalysis*, **130**: B (2000) 1823-1828
 73. G. Busca, M. Baldi, C. Pistarino, J.M. Gallardo Amores, V. Sanchez Escribano, E. Finocchio, G. Romezzano, F. Bregani, G.P. Toledo, *Catalysis Today*, **53** (1999) 525-533
 74. E. Finocchio, M. Baldi, G. Busca, C. Pistarino, G. Romezzano, F. Bregani, G.P. Toledo, *Catalysis Today*, **59** (2000) 261-268
 75. M.A. Larrubia, G. Busca, *Applied Catalysis B: Environmental*, **39** (2002) 343-352
 76. R. Lopez-Fonseca, J. I. Gutierrez-Ortiz, J.R. Gonzalez-Velasco, *Applied Catalysis A-General*, **271** (2004) 39-46
 77. E. Finocchio, C. Pistarino, S. Dellepiane, B. Serra, S. Braggio, M. Baldi, G. Busca, *Catalysis Today*, **75** (2002) 263-267
 78. E. Bielouss, (1921), Patent: US 1384423 19210712.
 79. F.C. Hall, W.R. Wiggins, A.W. Nash, *Journal of the Institute of Fuel*, **9** (1935) 106-117.

80. E.W. Gardiner, J. W. G., A.L. Lyman (1937), Patent: US 2082203 19370601
81. S. Nisimura, (1939), Patent: JP 129436 19390328
82. S. Yamaguchi, *Nippon Kagaru Kaishi (1921-47)*, **55** (1934) 1227-31
83. S. Yamaguchi, *Nippon Kagaru Kaishi (1921-47)*, **55** (1934) 1232-5
84. J.S. Vibar, D. M. B. *Natural and Applied Science Bulletin*, **5** (1936) 123-8.
85. W.J. Kirkpatrick, (1945). Patent: US 2367287 19450116.
86. E.M. Marks, (1939), Patent: US 2164334 19390704.
87. R.N.D. Puis, (1942), Patent: US 2282603 19420512.
88. T. Miwa, (1944), Patent: JP 162228 19440301
89. S.S. Bobkov, P.P. Shepeneva (1946). Patent: SU 66688 199460731
90. W. L. J. de Nie (1949), Patent: US 2474206 19490628
91. V.N. Jenkins, (1946), Patent: US 2410381 19461029
92. N. Nakahara, Y. Koga (1939), Patent: JP 132553 19391009
93. D. Nakamori, Y. Ohata, T. Arakawa (1948), Patent: JP 175752 19480228
94. M.V. Twigg, "Catalyst Handbook". 2nd edition. (1989) London, England, Wolfe Publishing Ltd. p408.
95. M.V. Veazey, *Material Performance*, (May 2002) 17-19.
96. K.M. Sarma, G. M. Bankobeza, M.A. Mulumba,, The Montreal Protocol on Substances that Deplete the Ozone Layer (2000). London 1990, Copenhagen 1992, Vienna 1995, Montreal 1997, Beijing 1999, United Nations Environment Programme
97. U.S. Environmental Protection Agency. Interhrated Risk Information System (IRIS) on 1,1,2,2-Tetrachloroethane. National Centre for Environmental Assessment, Office of Research and Development, Washington, DC. 1999. (<http://www.epa.gov/ttn/atw/hlthef/tetrachl.html>)
98. M. E. Alessandrini, *Bulletin of World Health Organization*, **2** (1950) 629-36
99. B.A. Howell, F. M. Uhl, *Thermochimica Acta*, **357-358** (2000) 113-117
100. E. R. Erickson, Michalek, John C. (1947), US 2432737 19271216
101. G. W. Hearne, Adams, Merrill L. (1945), Patent: US 2391827 19451225
102. Howe-Grant, M., Kirk-Othmer Encyclopedia of Chemical Technology (1985). John Wiley & Sons. **Vol.20**: p. 108.
103. Clean Water Act of 1977. 33 USC §1251, section 101, PL95-217; most recent amendment, PL96-510.
104. Clean Air Act 42 USC §1857 *et seq.*; Air Quality Act of 1967, PL90-148; CAA of 1970 42 USC §7401 *et seq.*, PL91-604; CAA of 1977 PL95-95; most recent amendment, PL97-23.
105. V.I. Kovalchuk, J. L. d'Itri. *Applied Catalysis A-General*, **271** (2004) 13-25

2 EXPERIMENTAL

Chemicals Preparation
Catalyst Characterisation
Catalyst Testing
Reaction Conditions

2.1 Introduction

In this chapter, we discuss the techniques that were used for the preparation of reagents and catalysts, catalyst characterisation, and catalyst testing for the dehydrochlorination reaction. The primary, secondary and tertiary butyl chlorides were chosen as the model compounds for these studies. The catalysts that were employed are distinguished into three categories, which are alumina-based catalysts, zirconia-promoted catalysts and silver-promoted catalysts. Each of these catalysts was prepared by a variety of methods, including dry and wet impregnation, precipitation and co-precipitation techniques, each of these are discussed in section 2.2. Section 2.3 describes all the characterisation techniques that were employed and section 2.4 summarises the reaction conditions for catalyst testing.

2.2 Chemicals Preparation

2.2.1 Reagent

1-chloro, 2-chlorobutane and *2-chloro-2-methylpropane* (primary, secondary and tertiary butyl chloride, C_4H_9Cl ; see Appendix B for individual physical properties) were chosen for the study of dehydrochlorination reaction. These reagents were supplied by Aldrich and were purified before use. The purification method followed the procedure that was published by Armarego & Perri¹. Pure reagent was

prepared by shaking repeatedly with concentrated sulfuric acid until no further colour developed in the acid to remove any impurities such like metal ions. The reagent was then washed with sodium carbonate or sodium hydrogen carbonate, and more water. The reagent was separated from the solution in a separating funnel. Finally, it was dried with calcium chloride and distilled. The distillation was performed to separate the corresponding butanol. The reagent was heated in the round bottom flask with an isomantle. When the temperature reached the boiling point of each butyl chloride, total reflux was achieved. The vapour was condensed using a condenser circulated with cold water and collected in another flask that is connected to the vacuum line. Dry nitrogen was introduced to keep the reagent under inert condition. The contents of the reagent were confirmed by NMR technique.

2.2.2 Catalyst Preparation

2.2.2.1 Alumina-based catalysts

γ -alumina was used as a catalyst and catalyst support, owing to its high surface area and its amphoteric properties. Practically all alumina is obtained by processing bauxite, mostly performed *via* Bayer process² that is the most economic method for alumina production. It has been widely used in the chemical industry as a catalyst, catalyst support and adsorbent, was generally prepared by firing at below 500°C to give a γ -phase alumina. It contains a certain degree of impurities; typically 0.35-0.45% of Na₂O can be obtained. Syntex plc supplied the γ -alumina that was used in most cases in this study as a catalyst support (Katalco-55-1, BET = $\sim 300 \text{ m}^2\text{g}^{-1}$ & bulk density = $0.75 \text{ g}\cdot\text{cm}^{-3}$). A short study of ultra-pure γ -alumina supplied by Sasol (Puralox SBA-200, BET = $\sim 202 \text{ m}^2\text{g}^{-1}$ & bulk density = $0.71 \text{ g}\cdot\text{cm}^{-3}$) was also carried out for comparison. γ -alumina was pre-calcined at 500°C for 3h before use.

γ -alumina was modified by acid-treating the γ -alumina supplied by Syntex plc with hydrogen chloride ($\text{Al}_2\text{O}_3\text{-HCl}$) to remove impurities present in the industrial alumina. γ -alumina was immersed in a 3M of hydrogen chloride solution overnight under a constant stirring at room temperature. The sample was then filtered and washed several times with distilled water. The sample was again immersed in distilled water overnight, followed by filtering. Finally, the sample was dried in an oven at 100°C overnight and was subjected to a calcination step at 600°C for 3h.

γ -alumina was calcined at 800 and 1200°C to observe the *effect of thermal treatment*. It is well known that the chemical and physical properties of γ -alumina change significantly depending on the degree of dehydration.

Alkaline-doped alumina was prepared by impregnating the γ -alumina support with potassium loading ranges from 0.1 to 20wt%, where the potassium salts (K_2CO_3 , KOH, KCl, and KF) were used as the precursors. To 1g of the support, the desired amount of the potassium solution was impregnated dropwise onto the support. The sample was then dried in the oven overnight and subjected to calcination at 400°C for 3 to 5h. Table 2.1 shows a list of the alumina-based catalysts that were prepared, together with the preparation method, calcination conditions and precursor used.

Table 2.1: List of alumina-based catalysts

	Prepared by	Calcination temperature, $^\circ\text{C}$ (duration, h)	Precursors
$\gamma\text{-Al}_2\text{O}_3$	Syntex	500 (3)	Al_2O_3
$\gamma\text{-Al}_2\text{O}_3$ SS	Sasol	500 (3)	Al_2O_3
$\text{Al}_2\text{O}_3\text{-HCl}$	Acid-treatment	600 (3)	Al_2O_3
$\text{Al}_2\text{O}_3\text{-800}$	Thermal-treatment	800 (3)	Al_2O_3
$\text{Al}_2\text{O}_3\text{-1200}$	Thermal-treatment	1200 (8)	Al_2O_3
KOH- Al_2O_3	Incipient wetness	400 (5)	KOH, Al_2O_3
$\text{K}_2\text{CO}_3\text{-Al}_2\text{O}_3$	Incipient wetness	400 (3)	K_2CO_3 , Al_2O_3
KF- Al_2O_3	Incipient wetness	400 (3)	KF, Al_2O_3
KCl- Al_2O_3	Incipient wetness	400 (3)	KCl, Al_2O_3

2.2.2.2 Zirconia-promoted catalysts

Zirconia was used as a catalyst and catalyst promoter due to its acid-base bifunctional properties^{3,4}. Pure zirconia was prepared by precipitation, following the procedure reported elsewhere⁵. 10ml of zirconyl oxynitrate ($\text{ZrO}(\text{NO}_3)_2$ in dilute HNO_3) was used as the precursor and was hydrolysed by 20ml of concentrated ammonia solution (volume ratio of zirconia:ammonia is 1:2). The mixture was heated at 70°C under vigorous stirring, and some water was added to maintain a pH of 7-8. After the gel was formed, it was filtered and dried in oven overnight at 100°C. Finally, the sample was calcined at 600°C for 24h to give the pure zirconia. Zirconia supplied by Aldrich was used as a reference material.

Zirconia-alumina catalysts were prepared by co-precipitation and impregnation techniques. Co-precipitated prepared zirconia-alumina (ZAC) was made using zirconyl oxynitrate ($\text{ZrO}(\text{NO}_3)_2$ in dilute HNO_3) and aluminium nitrate as the precursors. Zirconia-alumina prepared by the wet impregnation (ZAI) method was made using zirconia oxynitrate ($\text{ZrO}(\text{NO}_3)_2$ in dilute HNO_3) as the precursor. It was also prepared by dry impregnation (ZAH) using dry zirconyl oxynitrate powder as precursor. 25, 50 and 75wt% of $\text{ZrO}(\text{NO}_3)_2$ loading were prepared. The sample was dried overnight in the oven at 100°C and calcined at 500°C for 3h.

$\text{KOH}/\text{ZrO}_2\text{-Al}_2\text{O}_3$ and $\text{ZrO}_2/\text{KOH-Al}_2\text{O}_3$ catalysts were prepared by introducing the second and third metal salt followed the sequence as indicated. $\text{KOH}/\text{ZrO}_2\text{-Al}_2\text{O}_3$ termed KZA catalyst was prepared by impregnating 1wt% of KOH solution on the $\text{ZrO}_2\text{-Al}_2\text{O}_3$ support prepared by co-precipitation (ZAC) with 50wt% of zirconium salt contents. $\text{ZrO}_2/\text{KOH-Al}_2\text{O}_3$ termed ZKA catalyst was prepared by impregnating 50wt% of $\text{ZrO}(\text{NO}_3)_2$ on 1wt% $\text{KOH-Al}_2\text{O}_3$ catalyst. The samples were subjected to calcination at temperature as stated in Table 2.2.

Table 2.2: List of zirconia-based catalysts

Catalysts	Prepared by	Calcination temperature °C (h)	Precursor(s)
ZrO ₂	Precipitation	600 (24)	ZrO(NO ₃) ₂ in dilute HNO ₃
ZrO ₂ -ADH	Aldrich	600 (24)	
ZrO ₂ -Al ₂ O ₃ (ZAC)	Co-precipitation	500 (3)	ZrO(NO ₃) ₂ in dilute HNO ₃ , Al(NO ₃) ₃
ZrO ₂ -Al ₂ O ₃ (ZA I)	Incipient wetness	500 (3)	ZrO(NO ₃) ₂ in dilute HNO ₃ , Al ₂ O ₃
ZrO ₂ -Al ₂ O ₃ (ZAH)	Incipient wetness	500 (3)	ZrO(NO ₃) ₂ , Al ₂ O ₃
ZrO ₂ -KOH- Al ₂ O ₃	Sequential impregnation	500 (3)	ZrO(NO ₃) ₂ , KOH- Al ₂ O ₃
KOH-ZrO ₂ - Al ₂ O ₃	Sequential impregnation	500 (3)	KOH, ZrO ₂ -Al ₂ O ₃ (ZAC)

2.2.2.3 Silver promoted catalysts

Silver-alumina, silver-silica and silver-zirconia-alumina were prepared by the incipient wetness technique with silver loading ranges from 1 to 20wt%, where silver nitrate solution was used as the precursor. To 1g of the support, the desired amount of the silver nitrate was impregnated. The sample was heated in oven overnight at about 100°C and was subjected to a calcination at 450°C for 3h.

Table 2.3: List of silver promoted catalysts

	Prepared by	Calcination temperature °C (h)	Precursor(s)
Ag-Al ₂ O ₃	Incipient wetness	450 (3)	AgNO ₃ , Al ₂ O ₃
Ag-SiO ₂	Incipient wetness	450 (3)	AgNO ₃ , SiO ₂
Ag-ZrO ₂ -Al ₂ O ₃ (Ag-ZAC)	Incipient wetness	450 (3)	AgNO ₃ , ZrO ₂ -Al ₂ O ₃
Ag-ZrO ₂ -Al ₂ O ₃ (Ag-ZAH)	Incipient wetness	450 (3)	AgNO ₃ , ZrO ₂ -Al ₂ O ₃
Boron nitride (BN)	Aldrich	-	-
Fused SiO ₂	Aldrich	-	-
SiO ₂ (non-porous)	Aldrich	-	-

In the search for an alternative support for Ag catalyst, the Sasol alumina (Al₂O₃-SS), alpha-alumina (α -Al₂O₃ or Al₂O₃-1200), fused (<5m²g⁻¹) and non-porous

silica (SiO₂, grade 7754, high purity) and Boron nitride (BN, c.a. 1 μm & S.G. = 2.29) were tested for the dehydrochlorination of 2-chlorobutane. Table 2.3 lists the silver promoted catalysts and the supports that were used in this study. All catalysts were pelletised, crushed, and sieved to an average particle size between 150 ~ 250 μm mesh.

2.3 Catalyst Characterisations

2.3.1 Nitrogen adsorption (BET) isotherm

The nitrogen adsorption was performed based on the BET (Brunauer-Emmett-Teller) isotherm to determine the specific surface area, specific pore volume and pore size distribution of the catalyst. The BET isotherm at -196°C (77K) was obtained using a Micrometrics Gemini 2360 surface analyser. Prior to analysis, the sample was degassed at 150°C under flow of nitrogen for 1h.

Based-on the BET isotherm (see Appendix C), the BET equation^{6,7} was derived.

$$\frac{P}{N_s(P_o - P)} = \frac{1}{NC} + \frac{(C-1)}{NC} \times \frac{P}{P_o} \quad (2.1)$$

Where the N_s can be written in terms of the volumes and masses.

$$\frac{P}{V_s(P_o - P)} = \frac{1}{V_m C} + \frac{(C-1)}{V_m C} \times \frac{P}{P_o} \quad (2.2)$$

Where

- V_s = Volume of gas adsorbed at pressure P, cm³g⁻¹
- V_m = Volume of gas adsorbed at monolayer, cm³g⁻¹
- P_o = Saturation pressure of adsorbate gas at the experimental temperature, mmHg
- C = A constant related exponentially to the heats of adsorption and liquefaction of gas. $C = e^{(q_1 - q_L)RT}$ where q_1 = heat of adsorption on the first layer; q_L = heat of liquefaction of adsorbed gas on all other layers

A plot of $P/V_S(P_o - P)$ versus P/P_o give a straight line with Y-intercept represents $1/V_m C$ and gradient represents $(C - 1)/V_m C$. By solving the both equations, the value of C and V_m can be evaluated. Assuming that one specific site was occupied by one molecule of nitrogen.

$$S_A = N \times A_m \quad (2.3)$$

The total surface area (S_A , m^2g^{-1}) is the number of sites in a monolayer (N) multiply by the area of one molecule of nitrogen (A_m , $0.162\text{nm}^2\text{molecule}^{-1}$).

2.3.2 Powder x-ray diffraction (XRD)

X-ray diffraction patterns were recorded using a Enraf Nonius FR590 sealed tube diffractometer with Cu K_α radiation (1.5418\AA). Samples were ground and mounted on an aluminium holder. The sample was spun while the patterns were collected over the range $10^\circ \leq 2\theta \leq 120^\circ$, and crystalline phases were identified using the JCPDS files version 2.16. The tube voltage employed was 40kV and the current was 30mA. Each sample was scanned for 30min.

In situ XRD was employed to perform the analysis under a controlled environment. An Enraf Nonius FR591 rotating anode diffractometer with a Cu anode was used for this type of analysis. The sample was mounted in a stainless steel cell (*in situ* cell) with windows which are transparent to x-rays and a heating stage covered by a platinum foil, which served as a thermally conducting sample holder. The *in situ* cell can be heated up to temperatures of 900°C . The voltage used was 40kV and the current was 100mA.

The basis of the technique is based on the diffraction of an x-ray beam from the sample. When a monochromatic x-ray beam is incident on a finely powdered sample, the x-rays are scattered by atoms in an ordered lattice plane, according to

Bragg's law^{8,9}. For constructive interference to occur between two lattice planes, the path difference (x) must be an integral number of wavelengths (λ):

$$n\lambda = 2x \quad (2.4)$$

By definition of $\sin\theta = x/d$ (Fig 2.1), substitute into the equation:

$$n\lambda = 2d \sin \theta \quad (2.5, \text{Bragg equation})$$

Where λ is the wavelength of the x-rays (ca. 1 Å), d is the distance between two lattice planes θ is the incident angle and n is an integer. Note that the range for XRD technique limited to not less than 25 Å of crystallite size.

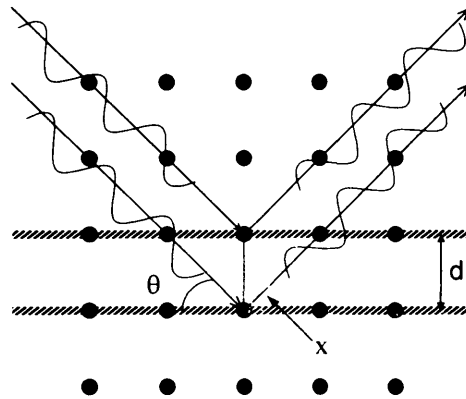


Fig 2.1: Diffraction of x-rays from two planes of atoms in a solid

The x-ray line broadening is defined by the Scherrer equation, as a function of crystallite size:

$$\text{Av. Crystallite size}/\text{\AA} = 0.9\lambda/B \cos \theta$$

Where λ = radiation wavelength/Å
 B = line broadening constant
 θ = diffraction angle

B is derived from the full width at half maximum (FWHM) by:

$$B^2 = B_u^2 - B_s^2$$

B_u = FWHM for unknown in radians
 B_s = FWHM for standard in radians

The standard is a sample with high crystallinity ($>1000\text{\AA}$) and B_s is determined at a similar Bragg angle to that of the unknown sample. Method best applied to crystallite sized 50 – 500 \AA .

2.3.3 Scanning electron microscopy (SEM)

Scanning electron micrographs were obtained with a Veeco FEI (Philips) XL30 ESEM (Environmental Scanning Electron Microscope) FEG (Field Emission Gun) with a secondary electron detector for surface imaging. The analytical instrumentation is comprised of an Oxford Instrument INCA ENERGY (EDX) x-ray analysis system. Magnifications up to $\times 500k$ can be obtained. Samples were mounted on a stub and were coated with a very thin layer of gold film using a sputter coater to make them conductive. Prior to EDX analysis, samples were carbon coated to prevent overlapping of signal due to high response of gold element. The instrument was operated under high vacuum conditions.

2.3.4 Chemisorption/ Temperature programmed desorption (TPD)

The selective chemisorption and temperature programmed desorption were performed using a Micrometric AutoChem 2910 in a flow type reactor fitted with a TCD detector. Carbon dioxide (an acid) and ammonia (a base) were used as the probe molecules to determine the total basic sites and the total acidic sites.

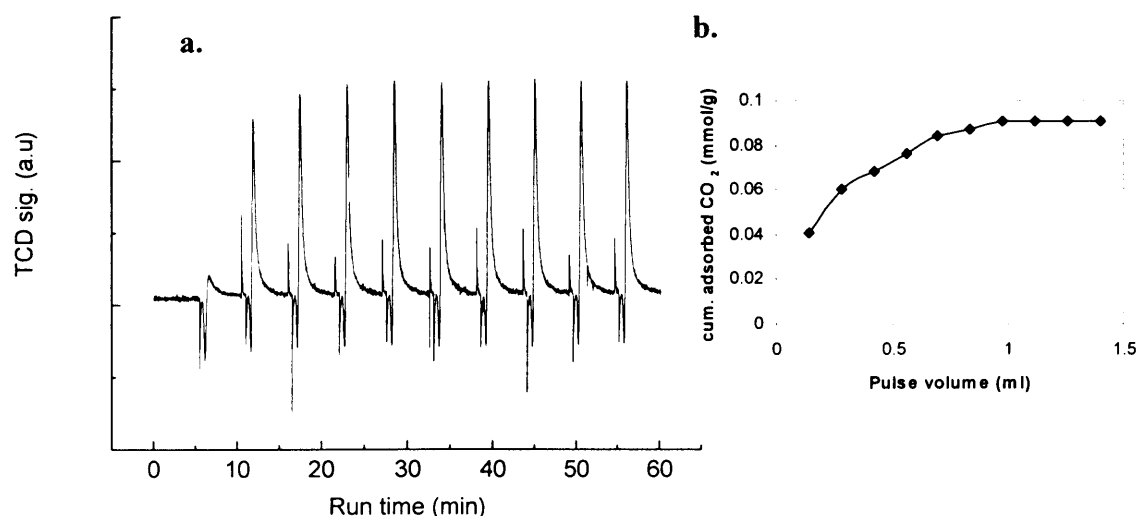
100mg of sample was placed in the quartz reactor and was degassed at the calcination temperature under a flow of $50\text{ml}\cdot\text{min}^{-1}$ of argon for 30min prior to analysis. After the sample was returned to ambient temperature, the CO_2 chemisorption was performed by injecting a fixed volume of CO_2 probe to the sample. A consistent flow of $20\text{ml}\cdot\text{min}^{-1}$ of argon to the sample was maintained, and the CO_2

flow was $20\text{ml}\cdot\text{min}^{-1}$. After the sample was saturated with CO_2 , it was purged for 30min under flow of argon to remove any physisorption. CO_2 -TPD was obtained by heating the sample from ambient to 850°C at a temperature ramp rate of $20^\circ\text{C}\cdot\text{min}^{-1}$ under flow of $50\text{ml}\cdot\text{min}^{-1}$ of argon.

NH_3 chemisorption was performed by injecting a fixed volume of NH_3 to the sample at 100°C to avoid any condensation. NH_3 -TPD was carried out from 100 to 850°C at a temperature rate of $20^\circ\text{C}\cdot\text{min}^{-1}$ and $10\text{ml}\cdot\text{min}^{-1}$ of argon flow.

Chemisorption analysis gives a quantitative measurement of active sites by measuring the amount of adsorbed gas, assuming one molecule of the reactive gas reacts with one corresponding active site. Fig 2.2a shows a typical chemisorption plot, where a fixed amount of the reactive gas was injected to the sample using a pulse technique *via* a sample loop. By integrating the area under the graph, the total number of active sites can be estimated (Fig 2.2b). The TPD desorption peak temperatures is used to estimate the strength of the active sites. The higher the desorption temperature indicates stronger strengths for the active site.

Fig 2.2: A chemisorption of CO_2 on activated alumina from Syntex plc



2.3.5 Temperature programmed reduction (TPR)

Temperature programmed reduction in hydrogen was also performed using a Micrometric AutoChem 2910 in a flow type reactor with a TCD detector. 100mg of the catalyst was degassed at 120°C under flow of 50ml·min⁻¹ of argon for 30min. After the temperature returned to ambient, TPR was carried out by heating the sample at a rate of 10°C·min⁻¹ from 0 to 450°C in 10%v/v H₂-Ar flow (50ml·min⁻¹). The amount of hydrogen consumption and the reduction process was determined.

2.3.6 Thermal gravimetric analysis (TGA)

Thermal gravimetric analysis was performed in a Perkin Elmer TGA 7 connected to a TAC/DX Thermal Analysis Controller to record the change in weight of the sample as a function of temperature. The instrument comprised of a microbalance with a furnace programmed for temperature control. 10mg of sample was placed in a platinum crucible that is connected to a microbalance and heated at a rate of 20°C·min⁻¹ up to 900°C under a stream of N₂ (60ml·min⁻¹). Oxygen or air can also be used as the reactive gas. The decomposition temperature and the weight losses were determined. The result can be presented as a thermogravimetric (TG) curve, in which the weight change was recorded as a function of temperature; or as a derivative thermogravimetric (DTG) curve, where the derivative weight is plotted against the temperature.

2.3.7 X-ray photoelectron spectroscopy (XPS)

X-ray photoelectron spectroscopy was performed using a VG Escalab 220 equipped with Mg K_α (1253.6eV) and Al K_α (1486.6eV) twin anodes to monitor the surface composition of catalysts. The instrument comprised an x-ray gun, an ultra-

high vacuum chamber, a multichanneltron detector and a Concentric Hemispherical Analyzer. The sample was mounted on a stub using a double-sided sticky tape. The spectra were collected with an analyser at pass energy of 20eV. The anode voltage used was 15kV and the current was 20mA. The XPS spectrum is usually a plot of the intensity of photoelectron versus the binding energy.

When a primary x-ray excitation source from an x-ray tube or a radioactive source strikes a sample, the x-ray can either be absorbed or scattered by the sample. The process in which an x-ray is absorbed by the atom and induces electron emission from its inner shell is called the “photoelectric effect”. Einstein’s theory⁶ explained that the photons can induce electron emission from a solid provided the photon energy ($h\nu$) is greater than the work function (ϕ). The work function of a solid is defined as the minimum energy required to remove an electron from the highest occupied energy level in the solid to the vacuum level. The vacuum level may be used as “energy zero”.

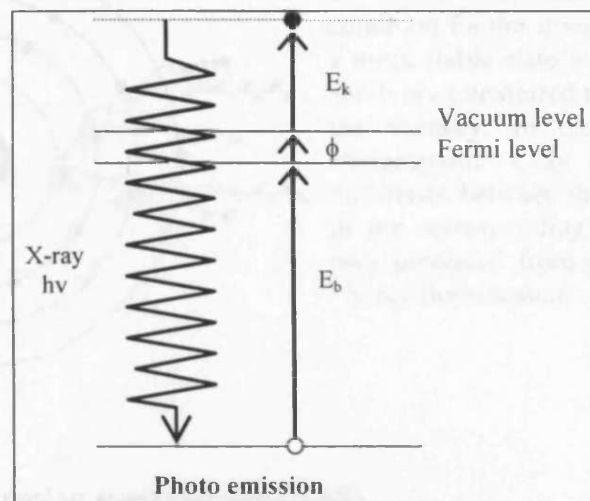
By applying the principle of energy conservation (Einstein’s photoelectric equation), the kinetic energy of emitted photoelectrons (E_k) defined as:

$$E_k = h\nu - (E_b + \phi) \quad (2.6)$$

where	E_k	is the kinetic energy of the photoelectron
	h	is Planck’s constant
	ν	is the frequency of the exciting radiation
	E_b	is the binding energy of the photoelectron with respect to the Fermi level of the sample
	ϕ	is the work function of the spectrometer.

In practice we use the Fermi level of the spectrometer as a reference level, in which case the work function (ϕ) disappear from equation (2.6) to give $E_k = h\nu - E_b$.

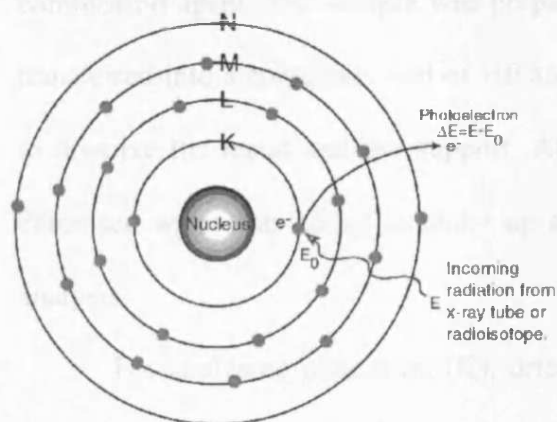
Fig 2.3: X-ray photoemission process.



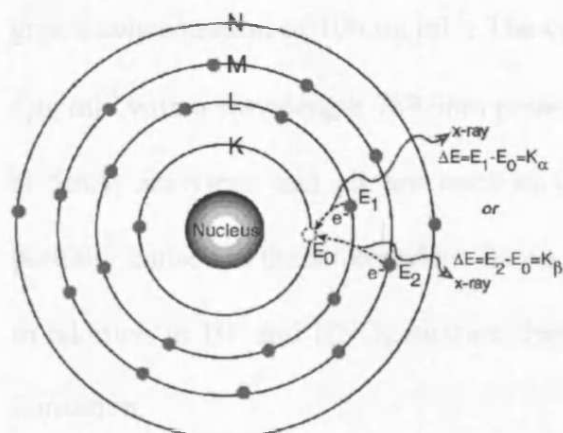
2.3.8 X-ray Fluorescence analysis (XRF)

X-ray fluorescence analysis (XRF) was performed with a Philips MagiX PRO XRF spectrometer at the industrial laboratory of Syntex. The instrument comprised a wavelength dispersive x-ray analysis system with rhodium anode operating at 4kW power. The software used for quantitative and qualitative analysis is produced by Philips, and is called SuperQ. XRF interprets the characteristic radiation emitted by the elements of the sample upon excitation, enabling a good and accurate determination of the elemental composition.

Fig 2.4: The X-ray fluorescence process



1) The process in which an x-ray is absorbed by the atom by transfer all the energy to an innermost electron is called the "photoelectric effect". If the primary x-ray had sufficient energy, electrons are ejected from the inner shell creating vacancies.



2) These vacancies present an unstable condition for the atom. To restore the atom to a more stable state, electrons from the outer shells are transferred to the inner shells to fill the vacancy. In the process, it emits a characteristic x-ray whose energy is the difference between the two binding energies of the corresponding shells. The emitted x-rays produced from this process are called "X-ray fluorescence".

2.3.9 Atomic absorption spectroscopy (AAS)

Atomic absorption spectroscopy was performed using a double beam Varian SpectrAA 55B instrument, which is the flame atomisation system, used to determine the amount of metal loading of the samples. These include silver and potassium loadings for different catalysts that were prepared.

To prepare the standard solutions for analysing silver (Ag), pure silver nitrate (AgNO_3 , 99.99%) was used. 0.1574g of dried AgNO_3 was dissolved in water and was diluted to 1 litre to give $100 \mu\text{g}\cdot\text{ml}^{-1}$ (100ppm) Ag. Further dilution to 1, 5, & $10 \mu\text{g}\cdot\text{ml}^{-1}$ before it was used for calibration. The resonance line source was produced by a silver lamp with wavelength 328.1nm. The working conditions for atomic absorption were a lamp current of 4mA, and use of acetylene and air as the combustion agent. The sample was prepared first weighing the sample before it was transferred into a container. 4ml of HF and 2ml of HNO_3 were added to the container to dissolve the metal and the support. After all samples were completely dissolved, deionised water was added to make up a total volume of 35ml of solution, prior to analysis.

For analysing potassium (K), dried potassium chloride was used as standard. 0.1907g of dried potassium chloride was dissolved in water and diluted to 1 litre to

give a concentration of $100 \mu\text{g}\cdot\text{ml}^{-1}$. The optimum working range for K is between $1-6 \mu\text{g}\cdot\text{ml}^{-1}$ with a wavelength 769.9nm potassium lamp. The lamp current was operated at 5mA ; acetylene and air are used as the combustion fuel. As the potassium is partially ionised in the air-acetylene flame, cesium nitrate ($1000 \mu\text{g}\cdot\text{ml}^{-1}$ Cs) was added in addition to HF and HNO_3 mixture during the sample preparation to suppress the ionisation.

2.3.10 Infrared spectroscopy (IR)

The infrared spectra were recorded with a Perkin Elmer 2000 FT-IR spectrometer range from 4000 to 400cm^{-1} of wavenumber. The samples were prepared by pressing a mixture of 300mg of KBr and 10mg of catalysts into a self supporting wafer. Typical procedure was with 10 scans and 2cm^{-1} of resolution.

In infrared spectroscopy a molecule absorbs photon with the same frequency as its vibrations. A wavenumber is the inverse of the wavelength in cm. An increase in wavenumber corresponds to an increase in energy. A typical IR spectrum is a plot of the percent transmittance (%T) against the wavenumber (cm^{-1}). A zero transmittance corresponds to 100% absorption of light at that wavelength.

2.3.11 Raman spectroscopy

Raman spectra were obtained at room temperature with a Renishaw Ramascope spectrometer using a 514.5 nm Ar^+ laser. Powdered samples were pressed in a holder and analyzed without further treatment (10 scans). The scanning ranges from 100 to 2000cm^{-1} . Raman spectroscopy is based on the inelastic scattering of photons, which lose energy by exciting vibrations in the sample.

2.3.12 Chloride analysis by coulometric titration

The coulometric titration of chloride was performed using a Corning 926 analyser fitted with a silver electrode, the end points being determined potentiometrically. 0.1g to 0.3g of sample was ground and dissolved in 25ml of 50:50v/v HNO₃. The mixture was made up to 75ml in volume using deionised water. This was covered and boiled gently for 30 minutes with cover, then left to cool before analysis. The mixture was again made up to 250ml in a volumetric flask with deionised water and the sample was ready for analysis. Prior to analysis, the electrode was immersed in 25ml of acetic acid buffer solution, and the instrument calibrated with standard NaCl solution. For each analysis, 0.5ml of the sample was injected to the buffer solution. The coulometric reading was recorded. The percentage of chloride from the sample was calculated using the following formula:

$$\% \text{ Cl by weight} = \frac{\text{Coulometric reading (mg/L Cl)}}{\text{Sample weight} \times 40} \quad (2.7)$$

2.4 Catalyst Testing

2.4.1 Process flow diagram

A process flow diagram is shown in Fig 2.5. Helium was used as the carrier gas and it was controlled by a Brooke Instrument mass flow controller. Helium was bubbled through the saturator that contains the reaction reagent to generate saturated vapour. The saturator was filled with glass beads to increase the contact time improving in the mass transfer and was submerged in an ice-bath. The saturated vapour (feed gas) was made-up with helium gas to the desired flow, before it was introduced to the reactor. A continuous flow fixed bed reactor was used at atmospheric pressure. The reactor consists of a glass (Pyrex/Quartz) tube with inner

diameter of 9mm and is placed inside a conventional electric furnace. A septum was fitted at the reactor exit for sample collection. The exit gas was filtered to prevent transportation of particulate and was maintained at the reaction temperature to avoid condensation. The hydrocarbon reactants and the products were analysed by an online gas chromatograph fitted with a flame ionisation detector (FID) and a DB1 capillary column (30m, J&W). The acid gas was trapped in a sodium hydroxide scrubber for further analysis.

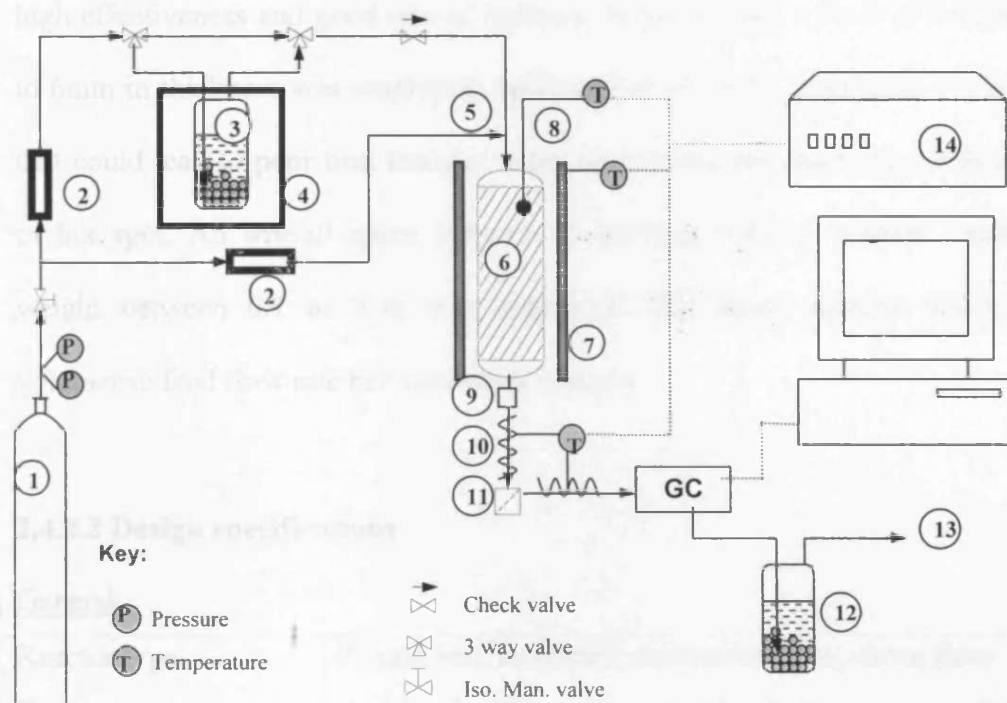


Fig 2.5: A process flow diagram for catalytic dehydrochlorination reaction. 1 = He carrier gas, 2 = mass flow control valve, 3 = reagent saturator filled with glass beads, 4 = iced bath, 5 = helium make-up, 6 = continuous flow fixed-bed reactor, 7 = furnace, 8 = thermocouple, 9 = septum, 10 = heating tape, 11 = filter, 12 = NaOH scrubber, 13 = outlet, 14 = temperature controller

2.4.2 Reactor design

2.4.2.1 Catalyst

Catalyst particle sizes used are a compromise between pressure drop, heat and mass transfer between the pore structures (porosity, pore size) of the catalyst. Alumina-based, zirconia-promoted or silver-promoted catalysts were employed for the dehydrochlorination reaction. Most catalysts have BET surface area above $100\text{m}^2\text{g}^{-1}$. All catalysts were pelletised and were sieved to an average size between $150 \sim 250 \mu\text{m}$ in diameter before used. One of the advantages of these catalysts is the high effectiveness and good rate of reaction. In most cases, a layer of fine granules 2 to 6mm in thickness was employed, sufficient to avoid the possibility of channelling that could lead to poor heat transfer, poor conversion, and harm the catalyst because of hot spot. An overall space velocity of between 9500 to 50000h^{-1} and catalyst weight between 0.1 to 0.3g was employed. The space velocity defines as the volumetric feed flow rate per volume of catalyst.

2.4.2.2 Design specifications

General

Reactor type	Single bed, fixed-bed, continuous flow, down flow
Reactants	1-chlorobutane or 2-chlorobutane or 2-chloro-2-methylpropane (with helium balance)
Catalysts	Alumina supported, zirconia promoted, silver promoted
Support	Silica wool

Operating condition

Operating temperature	$25 - 350^\circ\text{C}$
Operating pressure	1 atm
Total flowrate	$50 - 120 \text{ ml}\cdot\text{min}^{-1}$

Total reactor volume	
Catalyst charge	0.1 – 0.3g

Catalyst bed

Catalyst fill height	2 – 5.2mm
Catalyst volume	0.11 – 0.33 ml
Particle size	150 – 250 μ m

Material properties

Reactor material	Pyrex (600°C) or quartz (1200°C)
Tube material	1/2", 1/4", 1/8", 1/16" (316-SS)

2.4.2.3 Conversion and selectivity

The conversion can be calculated either based on the total consumption of the reactants or the total products yielded. In our studies, due to the reactant feed concentration changes as a consequent of gas phase reaction¹⁰, the catalyst activity was present in term of the conversion, based on the total product yielded. Considering the stoichiometric ratio might change depending on the products yielded, the concentration of the product need to be corrected before use. The formula for conversion as followed:

$$\text{conv (\%)} = \frac{\text{total products with correction}}{\text{total reactant in feed}} \times 100 \quad (2.8)$$

Assuming that all products have been identified and there is not significant coking occurred.

Product selectivity is defined as the number of moles of the desire product dividing the total number of moles of products.

$$\text{selectivity} = \frac{\text{desire product}}{\text{total product}} \times 100 \quad (2.9)$$

Carbon balance was calculated based on the total number of moles of carbon obtained for feed and products.

$$\text{C bal} = \frac{C_{\text{in}}}{C_{\text{out}}} \times 100 \quad (2.10)$$

An experimental error of about 5% was estimated. Refer to Appendix D for a sample calculation of mass balance.

2.4.3 Gas analysis

2.4.3.1 Hydrocarbons analysis by Gas chromatography

Gas chromatography separates a mixture into its constituents by passing a moving gas over a stationary adsorbent. Generally, gas chromatography comprises an injector, a column and a detector. For the injector, an automatic six port gas sampling valve (GSV) was used for the injection port, controlled by a pneumatic actuator connected to a time event facility. A DB-1 column supplied by J&W (30m × 0.531mm × 5µm) was installed for separation of the compounds. The fused silica capillary column consists of an amber-brown polyamide exterior coating that protects the tubing from breakage. DB-1 is coated with 100% dimethylpolysiloxane, and the separation was based on the boiling point. Helium was used as the carrier gas for the capillary column. A flame ionisation detector (FID) was used for the quantitative analysis of the separated compounds.

The basis of operation of the FID detector is that the effluent from the column is combusted in the mixture of air and hydrogen to cause ionisation of molecule. The ionisation produces a large increase in the electrical conductivity of the flame and a quantitative signal was collected. The FID is mass sensitive, so the response is

unaffected by changes of flow to the detector. The optimum operating conditions were: sample loop size 5 μ L; initial oven temperature at 40 or 70°C for 3min; temperature ramp 20°C·min⁻¹, final temperature 165°C for 2min; injector temperature 170°C; detector temperature 260°C. GC-MS was also used to confirm the identity of products.

To calibrate the concentration with response to the raw count, a known amount of a reference compound was injected. The FID relative response factor and relative carbon response factor of a compound are calculated as follows:

$$\text{FID relative response factor} = \frac{\text{FID response factor of compound}}{\text{FID response factor of reference}}$$

Where $\text{FID response factor} = \frac{\text{peak area of compound}}{\text{quantity of compound injected}}$

& $\text{FID relative carbon response factor} = \frac{\text{FID carbon response factor of compound}}{\text{FID carbon response factor of reference}}$

Where

$$\text{FID carbon response factor of compound} = \text{FID response factor} \times \frac{\text{molecular weight}}{\text{total C at wt in compound}}$$

2.4.3.2 Chloride analysis by sodium hydroxide scrubber (NaOH)

A bubbler filled with 40ml of NaOH (0.43-4.3M) was used as a chloride trap. It was assumed that HCl was the only acid product from the reaction. The bubbler was filled with glass beads to increase the contact time of the reaction. The pH change was monitored by using phenolphthalein as indicator, the colour changing from colourless to red when the pH changes from acid to base. A chlorine mass balance calculation was obtained by quantifying the amount of hydrochloric acid produced. At the end of each reaction, 10ml of the mixture was used for the analysis.

2.5 Reaction conditions

2.5.1 Optimising reaction conditions

2.5.1.1 Blank reactions

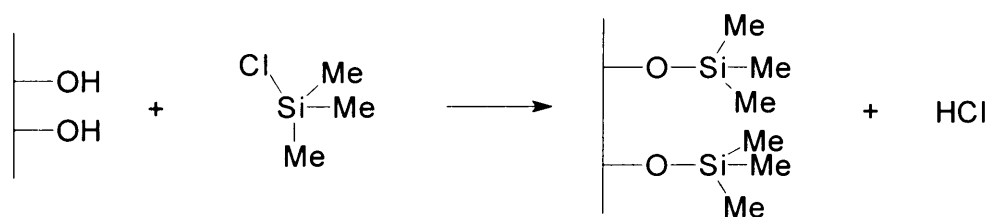
Blank reactions were carried out for 1-chlorobutane, 2-chlorobutane and 2-chloro-2-methylpropane dehydrochlorination over the empty glass reactor. The reactions were performed at temperature ranges between 35 to 335°C to observe the gas-phase decomposition of butyl chlorides. A total flow of 60ml·min⁻¹ of carrier gas was bubbled through the reagent saturator at 0°C (273K). Note that the vapour pressure for different butyl chlorides at 273K is 29mm·Hg (for 1-chlorobutane), 47mm·Hg (for 2-chlorobutane) and 99mm·Hg (for tert-butyl chloride).

2.5.1.2 Effect of silanised glass reactor for gas phase dehydrochlorination of tert-butyl chloride

2-methyl-2-chloropropane dehydrochlorination was performed at 35°C over the silanised glass reactor tube with total feed flowrate of 60ml·min⁻¹.

In theory, the reactive groups of the physisorbed silanisation compound undergo nucleophilic attack by the surface silanol groups on a hydrated glass surface, which leaves the silane covalently bound to the oxide surface (Scheme 2.1). This application will make the surface relatively more inert toward the reaction studied.

Scheme 2.1: Silanisation of glass with trimethylchlorosilane



Liquid-phase silanisation: 450ml of trimethylchlorosilane in toluene solution (5% v/v) was added to a 500ml clean and dry glass flask with cover. The Pyrex glass reactor tube was immersed in the flask at 35°C, with gently agitation for 4hrs. The Pyrex glass reactor tube was then removed and rinsed repeatedly with toluene. The glass reactor tube was thermally cured in an oven at 100°C for 16hr.

2.5.1.3 Optimised operating conditions for catalytic dehydrochlorination of butyl chloride

γ -alumina catalyst was chosen as the reference material to optimise the operating conditions for the catalytic dehydrochlorination of 2-chlorobutane. The reaction was performed at temperature ranges from 35 to 335°C, with 100mg of catalyst and 60ml·min⁻¹ of total feed flow rate (GHSV = 33000h⁻¹).

2.5.2 Alumina-based catalysts

2.5.2.1 γ -alumina catalyst for dehydrochlorination of 2-chlorobutane

A preliminary study of the dehydrochlorination of 2-chlorobutane was performed over the activated alumina at 135°C for 3h. Two types of activated alumina were compared, which are the activated alumina supplied by Syntex and Sasol. 100mg of catalyst was supported by a plug of glasswool and was placed in a fixed-bed reactor. A total feed flow rate of 60ml·min⁻¹ (GHSV=33000h⁻¹) and 55000ppm concentration of 2-chlorobutane was fed into the reactor.

An extension of the study was carried out to investigate the catalyst life for activated alumina. Prior to the reaction, a total feed flow rate of 100ml·min⁻¹ (GHSV=55000h⁻¹) and 30000ppm of 2-chlorobutane were employed. The reaction

was performed over activated alumina from Syntex plc at 135°C for 18h, as a representative result.

2.5.2.2 Effect of acid treatment on activated alumina

Activated alumina was modified with acid treatment ($\text{Al}_2\text{O}_3\text{-HCl}$) to observe the influence on the activity. The reaction was performed over the acid-treated alumina at 135°C for 3h, pure alumina as reference. 100mg of catalyst, $60 \text{ ml}\cdot\text{min}^{-1}$ of total feed flow rate ($\text{GHSV}=33000\text{h}^{-1}$) and 55000ppm of 2-chlorobutane were used.

2.5.2.3 Effect of thermal treatment on activated alumina

Activated alumina was thermal treated at 500 (Al_2O_3), 800 ($\text{Al}_2\text{O}_3\text{-800}$) and 1200°C ($\alpha\text{-Al}_2\text{O}_3$) to represent hydrated, partial dehydrated and complete dehydrated alumina. They were used as catalyst for the dehydrochlorination of 2-chlorobutane to observe the influence of the thermal treatment on the catalytic activity. The reaction was performed at 135°C for 6h, 100mg of catalyst and $60\text{ml}\cdot\text{min}^{-1}$ of total flow rate ($\text{GHSV}=33000\text{h}^{-1}$) were employed. The feed concentration was 55000ppm.

2.5.2.4 K-doped alumina catalysts for dehydrochlorination of 2-chlorobutane

Different loadings of $\text{KOH-Al}_2\text{O}_3$ catalysts ranges from 0.2 to 5wt% potassium loadings were tested for the dehydrochlorination of 2-chlorobutane to investigate the influence of the potassium loadings (K^+) on the activity. Whereby, a series of $\text{K-Al}_2\text{O}_3$ catalysts (KF , KCl , KOH and K_2CO_3 on alumina) with 1wt% of potassium loading was prepared using different type of precursors to investigate the effect of the anion. The reactions were performed at 135°C, 100mg of catalyst and

100ml·min⁻¹ of total flow rate (GHSV= 55000h⁻¹) were employed. The feed concentration was 30000ppm.

Prior to the reaction, the space velocity was modified by increasing the catalyst volume and decreasing the total flow rate. The 2-chlorobutane conversion was performed over KF, KCl, KOH and K₂CO₃ on alumina with 1wt% K loadings. 300mg of catalyst and 60ml·min⁻¹ of total feed flow (GHSV=9509h⁻¹) were employed. The 2-chlorobutane concentration was 22000ppm.

2.5.2.5 Sodium-alumina catalyst for dehydrochlorination of 2-chlorobutane

Dehydrochlorination of 2-chlorobutane was performed over Na₂CO₃-Al₂O₃ at 135°C for 20h. Prior to the reaction, 300mg of catalyst and 60ml·min⁻¹ of total feed flow rate (GHSV=9509h⁻¹) were used. 1wt%K₂CO₃-Al₂O₃ used as reference.

2.5.3 Zirconia-promoted catalysts

2.5.3.1 Pure zirconia for dehydrochlorination of 2-chlorobutane

Precipitation prepared zirconia (ZrO₂-P) and commercial zirconia (ZrO₂-ADH) were tested on the catalytic dehydrochlorination of 2-chlorobutane at 135°C for 20h. The reaction was performed using 100mg of catalyst and 100ml·min⁻¹ of feed flowrate (GHSV=55000h⁻¹) with 30000ppm of gas concentration.

2.5.3.2 Zirconia-alumina for dehydrochlorination of 2-chlorobutane

25, 50 and 75wt% of ZrO₂-Al₂O₃ catalysts prepared by co-precipitation (ZA-C) and impregnation (ZA-I & ZA-H) methods were tested for the catalytic dehydrochlorination of 2-chlorobutane. The reactions were carried out at 135°C for

5h, 100mg of catalyst and total gas flow of $100\text{ml}\cdot\text{min}^{-1}$ (GHSV = 55000h^{-1}). Feed concentration was 30000ppm.

2.5.3.3 Addition of KOH as base modified zirconia alumina catalysts

KOH/ZrO₂-Al₂O₃ (KZA) and ZrO₂/KOH-Al₂O₃ (ZKA) catalysts were tested on the dehydrochlorination of 2-chlorobutane. Pure alumina, zirconia and 1wt%KOH/Al₂O₃ were used as references. The reactions were performed at 135°C for 20h, 300mg of catalyst and total gas flow of $60\text{ml}\cdot\text{min}^{-1}$ (GHSV = 9509h^{-1}). Feed concentration is 22000ppm.

2.5.4 Silver-promoted catalysts

2.5.4.1 Ag/Al₂O₃ as dehydrochlorination catalysts

1, 5, 10 and 20 wt% Ag/Al₂O₃ catalysts were prepared by the incipient wetness techniques and were tested for the dehydrochlorination of 2-chlorobutane at 135°C for 5h. Reaction conditions: 100mg of catalyst with total feed flow rate of $100\text{ml}\cdot\text{min}^{-1}$ (GHSV = 55000h^{-1}). Gas concentration is 30000ppm.

2.5.4.2 Al₂O₃-SS, α -Al₂O₃, SiO₂ and BN as alternative supports

Al₂O₃-SS, α -Al₂O₃, SiO₂ and BN were tested for the dehydrochlorination of 2-chlorobutane at reaction temperatures between 35°C and 335°C with an interval of 100°C. Reaction conditions: 100mg of sample with feed flow rate of $100\text{ml}\cdot\text{min}^{-1}$ (GHSV = 55000h^{-1}) and 33000ppm of gas concentration.

Supported Ag catalysts were subsequently prepared by impregnating silver nitrate on γ -Al₂O₃, α -Al₂O₃ and SiO₂ were tested on the same reaction to investigate their catalytic performances.

2.5.4.3 Ag/SiO₂ as dehydrochlorination catalyst

1, 5, 10 and 20wt% Ag/SiO₂ catalysts were tested for the dehydrochlorination of 2-chlorobutane at 135°C. Reaction conditions: 100mg of catalyst, 100mlmin⁻¹ (GHSV = 55000h⁻¹) and 30000ppm feed concentration.

2.5.4.4 Ag/ZrO₂-Al₂O₃ as dehydrochlorination catalysts

10wt% of Ag/ZAH and Ag/ZAC catalysts were tested for the dehydrochlorination of 2-chlorobutane at 135°C to investigate their catalytic performances. Reaction conditions: 135°C of reaction temperature, 100mg of sample, 90mlmin⁻¹ of total flow rate (GHSV = 48000h⁻¹) and 27000ppm of feed concentration.

References

1. Armarego, & Perrin, "Purification of Laboratory Chemicals" 4th edition, published by Butterworth Heinemann.
2. Kirk-Othmer, Encyclopedia of Chemical Technology (3rd Edn), Vol. 2, John Wiley & Son.
3. H. Hattori, *Chemical Review* **95** (1995) 537-558.
4. K. Tanabe, W.F. Holderich, *Applied Catalysis A: General* **181** (1999) 399-434.
5. B. Q. Xu, T. Yamaguchi and K. Tanabe, *Applied Catalysis*, **64** (1990) 41-54.
6. Attard and Barnes, "Surface", 1998, Oxford University Press.
7. P.W. Atkins, "Physical Chemistry", 1982, Oxford University Press.
8. J. W. Niemantsverdriet, "Spectroscopy in Catalysis", 2nd edition (2000), Wiley.
9. S. H. Taylor, Lecture note, Cardiff University.
10. D.H.R. Barton, P.F. Onyon, *Transaction Faraday Society* **45**, (1949), 725-735

3 OPTIMISING REACTION CONDITIONS

The gas phase decomposition of butyl chloride/ Pyrolysis

Is there actually a REAL BLANK reaction?

Effect of silanisation of glass reactor on dehydrochlorination of t-BuCl

Optimised operating conditions for catalytic dehydrochlorination of BuCl

3.1 Introduction

This chapter consists of some general consideration for optimising the operating conditions of the reactor. These include the thermodynamic calculation and experimental approaches to the reactivity of the compounds. Operating conditions including the pressure, temperature, conversion and selectivity were considered.

3.2 The gas phase decomposition of butyl chlorides/ Pyrolysis

3.2.1 Thermodynamic calculations

According to the thermodynamic literature data¹ (see Appendix B), the associated standard enthalpy heat of reaction and the standard Gibb's free energy for the decomposition of butyl chlorides at 298K are as follows:

Table 3.1: The standard Gibb's free energy and standard enthalpy heat of reaction for the decomposition of butyl chlorides

$\Delta H_r^{\circ} = \sum \Delta H_f^{\circ}(\text{product}) - \sum \Delta H_f^{\circ}(\text{reactant})$	$\text{kJ}\cdot\text{mol}^{-1}$	$\text{kJ}\cdot\text{mol}^{-1}$
1-chlorobutane --> cis-2-butene + HCl	$\Delta H_r^{\circ} = 48.03$	$\Delta G_r^{\circ} = 9.38$
2-chlorobutane --> cis-2-butene + HCl	$\Delta H_r^{\circ} = 62.26$	$\Delta G_r^{\circ} = 24.08$
2-chloro-2-methylpropane --> isobutene + HCl	$\Delta H_r^{\circ} = 74.11$	$\Delta G_r^{\circ} = 26.92$

The standard enthalpy heat of reaction (ΔH_r°) that is positive indicates these reactions are endothermic and are favoured by increasing temperature and by decreasing pressure.

In order to calculate the equilibrium constant (K_a) for each butyl chloride, the Gibb's free energy equation applied:

$$\Delta G^\circ = -RT \ln K_a \quad (3.1)$$

And
$$\Delta G^\circ = \Delta H^\circ - TS \quad (3.2)$$

Dividing equation (3.2) by T, the temperature leads to:

$$\frac{\Delta G^\circ}{T} = \frac{\Delta H^\circ}{T} - S^\circ \quad (3.2a)$$

Applying the standard Gibb's energy (ΔG_{298}) and enthalpy heat energy (ΔH_{298}) into equation (3.2a) and the entropy (S) was taken as a constant:

$$\frac{\Delta G_{298}}{298} = \frac{\Delta H_{298}}{298} - \text{const.}$$

	constant
1-chlorobutane	0.1297
2-chlorobutane	0.1281
2-chloro-2-methylpropane	0.1584

$$\frac{\Delta G_T}{T} = \frac{\Delta H_T}{T} - \text{const} \quad (3.3)$$

Alternatively, the enthalpy heat of reaction (ΔH) can be calculated from the specific heat capacity (C_p):

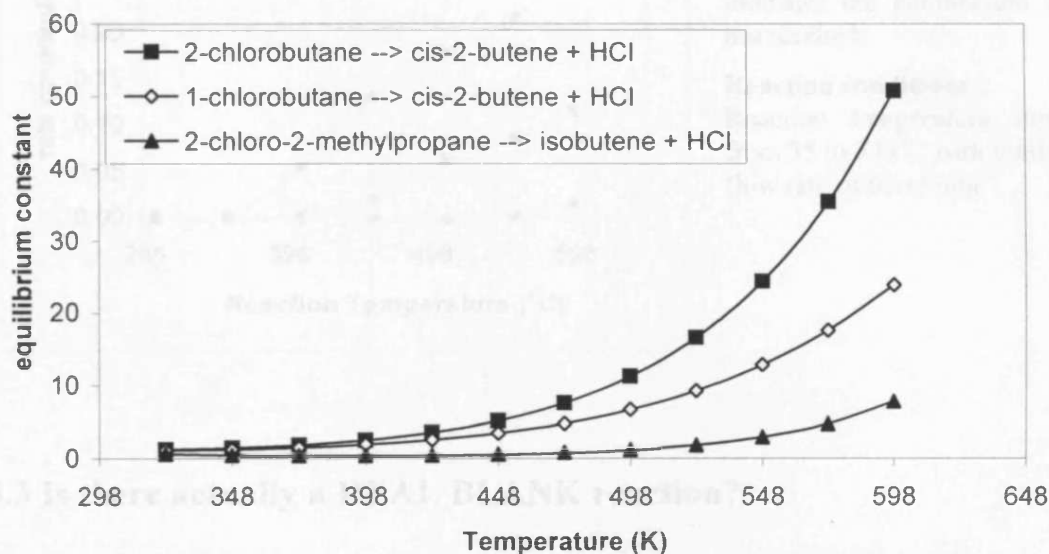
$$\Delta H = \int_{T_1}^{T_2} C_p dT \quad (3.4)$$

The temperature (T) value ranges from 50 – 300°C (323 - 573K). Therefore, solve equation (3.4) to give ΔH , equation (3.3) to give ΔG and equation (3.1) to give K_a .

Fig 3.1 shows the theoretical thermodynamic equilibrium constant for different butyl chloride at temperature ranges from 50 to 350°C (303 - 603K). It is

shown that at room temperature the reaction is thermodynamically not favoured. The order for the ease of chloride based on the thermodynamic calculation is 2-chlorobutane > 1-chlorobutane > 2-chloro-2-methylpropane.

Fig 3.1 Temperature dependence of the equilibrium constant for dehydrochlorination of butyl chloride



3.2.2 Experimental approach

Blank reactions were performed by introducing 1-chlorobutane (1-CB), 2-chlorobutane (2-CB) and 2-chloro-2-methylpropane (t-BuCl) over an empty glass reactor tube at temperature ranges from 35 to 335°C (308 – 603K) under atmospheric pressure. Fig 3.2 illustrates the gas-phase decomposition of different butyl chlorides. The conversion of 2-chloro-2-methylpropane started to be detectable at 35°C and showed above 20% conversion at 135°C. 2-Chlorobutane and 1-chlorobutane decomposition started to be detectable at 135°C, the conversion raised with increasing temperature. The reactivity order of the gas-phase decomposition is 2-chloro-2-methylpropane > 2-chlorobutane > 1-chlorobutane. This order matches the well-known order for the ease of chloride removal^{2,3}. This indicates that the chloride removal is strongly influenced by the structure environment of the halogen atom in

the molecule. Notably, thermodynamic calculations reported above give us a different order, implying that the reaction was not reached equilibrium.

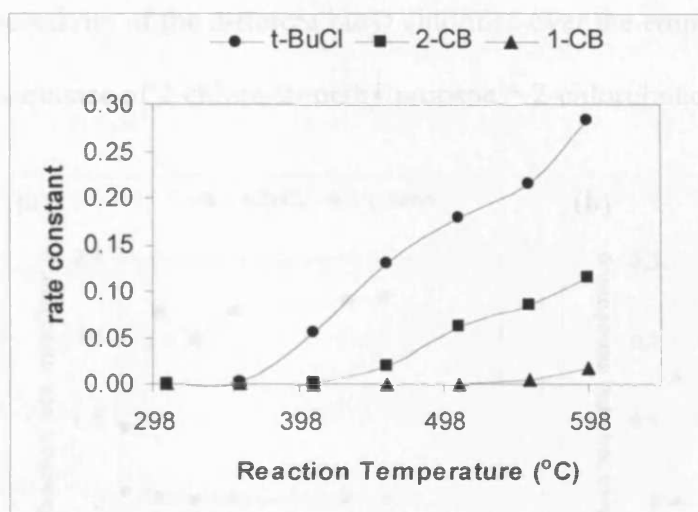


Fig 3.2: Experimental obtained rate constant for the butyl chlorides dehydrochlorination indicates the equilibrium was not reached.

Reaction conditions:

Reaction temperature ranges from 35 to 335°C with total gas flow rate of 60ml·min⁻¹.

3.3 Is there actually a REAL BLANK reaction?

As mentioned above, the decomposition of 2-chloro-2-methylpropane started to be detectable at 35°C. The reaction profiles for (a) tert-butyl chloride, (b) 2-chlorobutane, and (c) 1-chlorobutane dehydrochlorination over empty reactor tube at 35°C were examined and were showed in Fig 3.3. The result showed that at close to ambient temperature (35°C), the tert-butyl chloride decomposed over the empty reactor tube to give isobutene as the major hydrocarbon product. However, the mass balance revealed carbon losses that indicate some adsorption of the reactant on the glass reactor wall may occur. This phenomenon has also been observed by Barton⁴ and Brearley⁵, in which the glass reactor was active to the decomposition of tert-butyl chloride. Initially, the glass reactor wall was promoting the heterogeneous decomposition of tert-butyl chloride. Only after the reactor was coated with a carbonaceous film, the pyrolysis of tert-butyl chloride took place. Thus, reproducible results can be obtained. Schematic 3.1 demonstrate the heterogeneous decomposition

of tert-butyl chloride over the glass reactor tube. 2-chlorobutane and 1-chlorobutane were also tested for the dehydrochlorination reaction over empty reactor tube. The reactivity of the different butyl chlorides over the empty reactor tube was followed the sequence of 2-chloro-2-methylpropane > 2-chlorobutane > 1-chlorobutane.

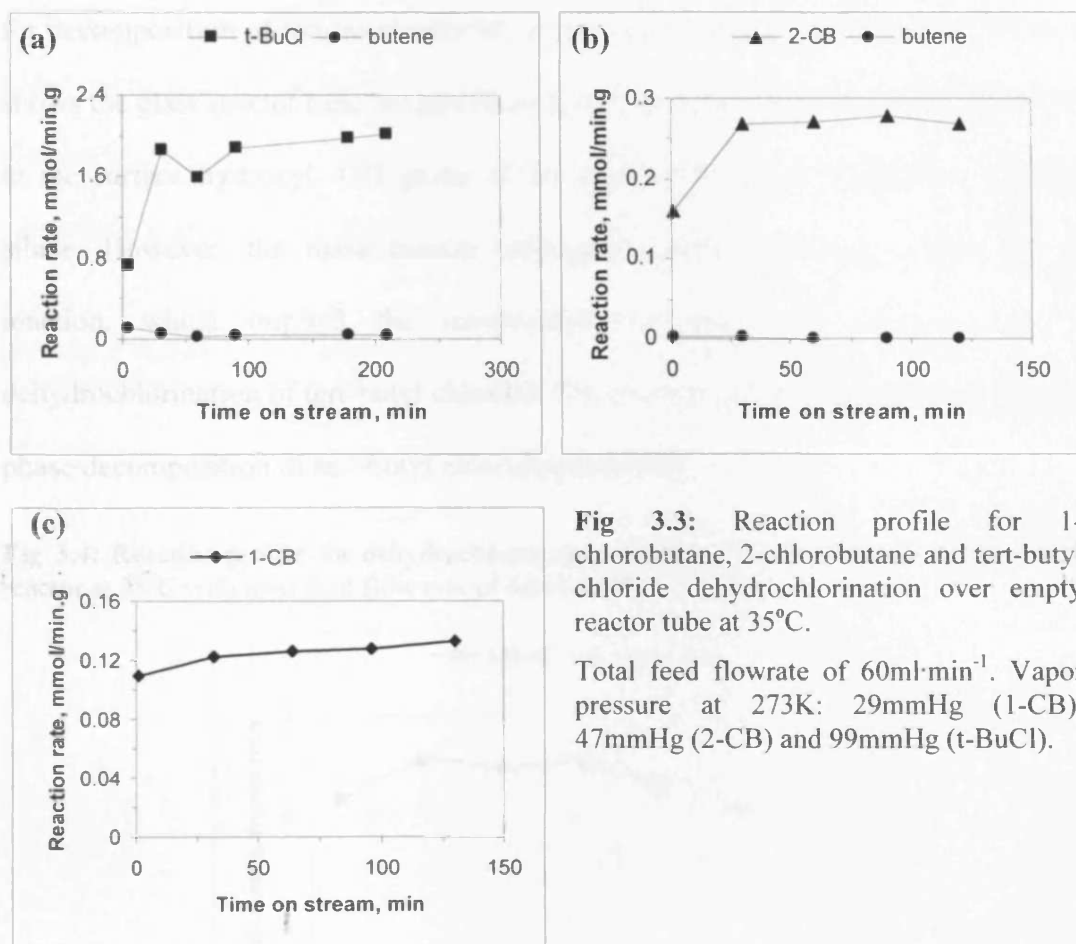
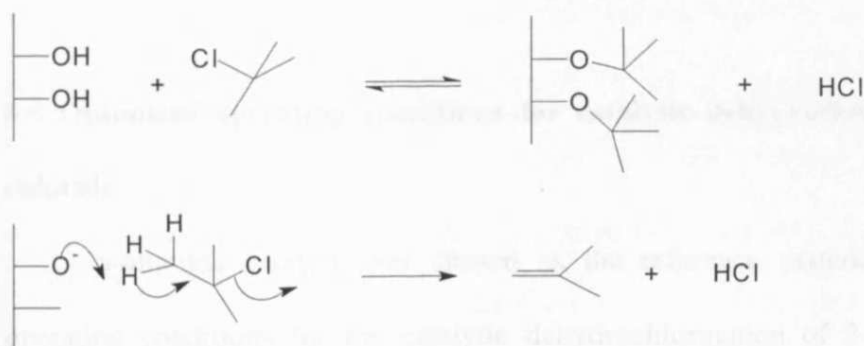


Fig 3.3: Reaction profile for 1-chlorobutane, 2-chlorobutane and tert-butyl chloride dehydrochlorination over empty reactor tube at 35°C.

Total feed flowrate of $60\text{ml}\cdot\text{min}^{-1}$. Vapor pressure at 273K: 29mmHg (1-CB), 47mmHg (2-CB) and 99mmHg (t-BuCl).

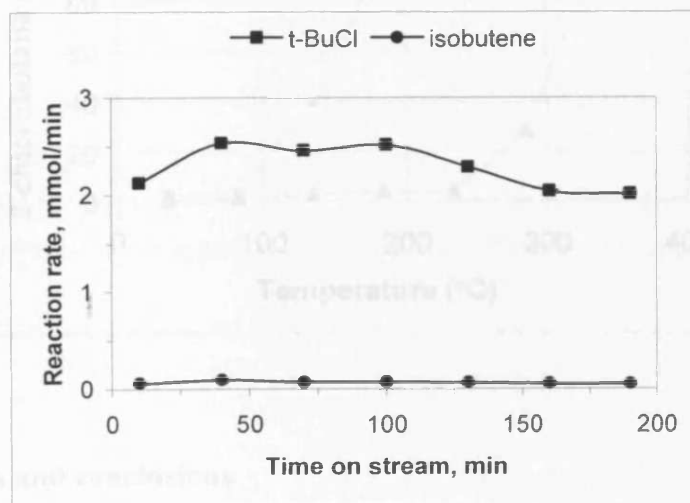
Scheme 3.1: Heterogeneous decomposition of tert-butyl chloride over empty glass reactor tube



3.4 Effect of silanisation of glass reactor on the dehydrochlorination of t-BuCl

In order to achieve “zero conversion” and to obtain reproducible results, the glass reactor was undergone a silane treatment⁶. Fig 3.4 illustrates the reaction profile for decomposition of tert-butyl chloride over a silanised glass reactor tube. The result shows the glass reactor tube became more active after the silane treatment. This is due to the surface hydroxyl -OH group of the glass reactor was masked by the bulky silane. However, the mass balance indicates slightly increasing carbon for this reaction, which implied the involvement of the silane polymer into the dehydrochlorination of tert-butyl chloride. The presence of isobutene showed that gas-phase decomposition of tert-butyl chloride proceeded.

Fig 3.4: Reaction profile for dehydrochlorination of tert-butyl chloride over silanised glass reactor at 35°C with total feed flow rate of 60ml·min⁻¹.

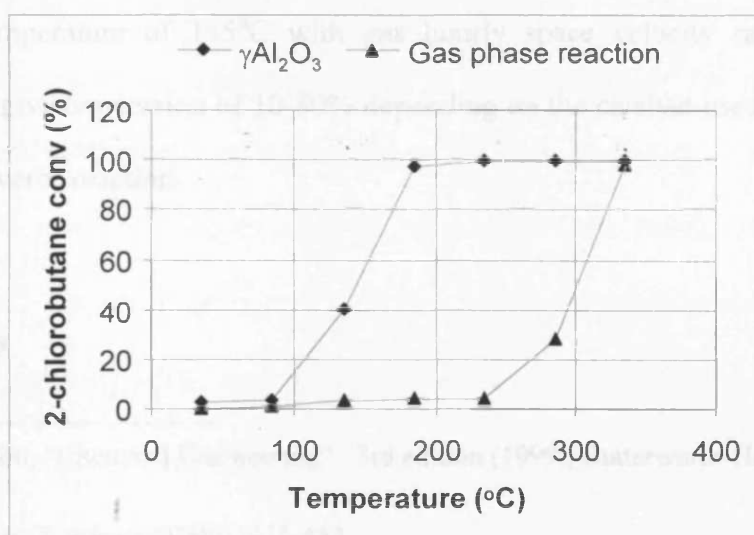


3.5 Optimised operating conditions for catalytic dehydrochlorination of butyl chloride

γ -alumina catalyst was chosen as the reference material to optimise the operating conditions for the catalytic dehydrochlorination of 2-chlorobutane. The

reaction was performed at temperature ranges from 35 to 335°C, with 100mg of catalyst and 60ml·min⁻¹ of total feed flow rate. Fig 3.5 shows the gas-phase decomposition of 2-chlorobutane with and without the presence of a catalyst. The result showed that with the presence of γ -alumina, the conversion raised from 4% to 40% at 135°C and reached above 95% at temperature above 185°C. Therefore, in order to compare the activity between different catalysts, the optimised conditions for the catalytic studies are reaction temperature at 135°C under atmospheric pressure and gas hourly space velocity (GHSV) of 9500-55000h⁻¹.

Fig 3.5: Decomposition of 2-chlorobutane with or without a catalyst. The reaction was performed at temperature ranges from 35 to 335°C, with 100mg of catalyst and 60ml·min⁻¹ of total feed flow rate (GHSV = 33000h⁻¹).



3.6 Discussions and conclusions

Based on the thermodynamic calculations and the experimental results obtained, performing dehydrochlorination of butyl chloride under atmospheric pressure is feasible to maintain activity. Blank reaction with 2-chloro-2-methylpropane, 2-chlorobutane and 1-chlorobutane over empty reactor tube showed a reactivity order of 2-chloro-2-methylpropane > 2-chlorobutane > 1-chlorobutane. This

is consistent with the well-known order of ease of chloride removal. The high reactivity of 2-chloro-2-methylpropane to the empty reactor was due to a heterogeneous decomposition over the glass reactor wall. Reproducible results can only be obtained after the glass reactor wall was coated with a carbonaceous film.

Silanisation of glass reactor was performed to mask the activity due to the silanol group of the glass. However, the silane treatment also induced some side reaction due to the exchange reaction between the reactant and bulky silane. Consequently, 2-chlorobutane was chosen as a representative compound to study the dehydrochlorination reaction to minimise the "glass effect". Nevertheless, the result from the decomposition of 2-chlorobutane over alumina catalyst suggested an operating temperature of 135°C with gas hourly space velocity ranges 9500 to 55000h⁻¹, to give conversion of 10-80% depending on the catalyst used and to assure negligible reverse reaction.

References

-
1. R.K. Sinnott, "Chemical Engineering". 3rd edition (1999), Butterworth-Heinemann. Vol. 6
 2. A.R. Pinder, *Synthesis* (1980), 425-452.
 3. H. Noller, W. Klading, *Catalyst Review- Science and Engineering* **13**, (1976), 149-207.
 4. D.H.R. Barton, P.F. Onyon, *Transaction Faraday Society* **45**, (1949), 725-735.
 5. Brearley, Kistiakowsky and Stauffer, *Journal of American Society* **58**, (1936), 43.
 6. C.M. Halliwell, A.E.G. Cass, *Analytical Chemistry* **73**, (2001) 2476-2483.

4 ALUMINA CATALYSTS

Activated Aluminas
Effects of Acid-treatment
Effects of Thermal-treatment
Alkaline-doped Aluminas

4.1 Introduction

Activated aluminas are widely used in adsorption and catalysis where their large surface area, pore structure and surface chemistry play an essential role¹. They are obtained from various hydrated aluminas by controlling the thermal treatment and degree of dehydration to produce aluminas of different types^{1,2}. A wide variety of chemical sites can be found on the surface of alumina attributed to its defect spinel structure, where Al^{3+} can be in either in the octahedral or tetrahedral holes of the oxygen lattice⁴. Their various transitional aluminas have crystal structure of γ , η , χ , ρ or α -phase³, as classified by the ratio of octahedral and tetrahedral Al^{3+} coordinated ions and the oxygen lattice density.

γ -alumina is obtained by dehydration of the hydrous oxide at low temperature ($\sim 450^\circ\text{C}$), and is the amorphous form of alumina that is hygroscopic and can be dissolved in acid⁴. α -alumina is the most stable form of alumina that occurs in *nature* as corundum and can be prepared by heating γ -alumina or any hydrous oxides above 1000°C . α -alumina is very hard, resistant to hydration and attack by acids, and is chemically inert. For industrial applications¹, γ -alumina is generally used as an adsorbent (drying agent and in chromatography), catalyst (Claus process, dehydration of alcohols, isomerisation of olefins and dehydrochlorination, and catalyst support).

γ -alumina is one of the most frequently used catalysts or catalyst supports for catalytic dehydrochlorination, in addition to the active carbon⁵, clays⁶, silica-alumina and silica gel⁷. Suzuki *et al*⁸ investigated the catalytic dehydrochlorination of trichloroethane (TCE) over an activated alumina catalyst at 250-330°C. The results suggested that the reaction proceeded *via* acid catalysis, and the *cis*-isomer was predominant while the activity was high. However as the catalyst activity declined, the *trans*-isomer and dichloroethene (CH₂=CCl₂) predominated.

A similar conclusion was drawn by Mochida *et al*^{9,10} that the *cis*-isomers were predominant on alumina in the dehydrochlorination of five chloroethanes, where the reaction proceeded *via* an E2 concerted mechanism. The author explained that the reactivity order of the chloroethane on various acidic and basic oxides changed continuously according to the acidity of the catalyst and the E2 concerted mechanism may occur on alumina which consists of binary sites of acidity and basicity¹¹. Catalysts with strong acidity or basicity proceed *via* E1 or E1cb mechanism. A later study investigated the use of steam to regenerate sites for dehydrochlorination of 1,1,2-trichloroethane¹². By introducing water into the reactor system at 500°C, HCl was liberated from the alumina surface to maintain the dehydrochlorination activity.

On the other hand, Noller *et al*¹³ reported the mechanistic displacements in the elimination of HCl from chlorobutane at 150-400°C over γ -Al₂O₃, MO-Al₂O₃ (M=Zn, Mg, Ni) and MAl₂O₄ (M=Zn, Mg, Ni) catalysts. In relation to the electron pair acceptor (EPA) centres of the catalysts, the tendency towards an E2 mechanism increased in the order Mg < Zn < Ni. The E1 mechanism was favoured by higher temperature. In particular, γ -Al₂O₃ was tested on the same reactions with addition of water to observe catalytic activity¹⁴. The addition of water and the use of previously dried catalysts sharply decreased the activity. The result indicated that Al ions in

tetrahedric surrounding are the active sites. This reaction is entirely different from the decomposition of multi-chlorinated ethane reported by Mochida *et al.*

In our studies, the pure γ -alumina, acid- or thermal treated aluminas, and alkaline-doped aluminas were tested for the dehydrochlorination of 2-chlorobutane, as a catalyst and catalyst support, to investigate the influences of the structures and acid-base properties on the activity. Each of these catalysts were characterised by various techniques, include nitrogen adsorption (BET), x-ray diffraction (XRD), scanning electron microscopy (SEM), x-ray photoelectron spectroscopy (XPS), selective chemisorption/ temperature programmed desorption (TPD) of carbon dioxide and ammonia, thermogravimetric analysis (TGA) and others. The catalytic activities were compared.

4.2 Activated aluminas

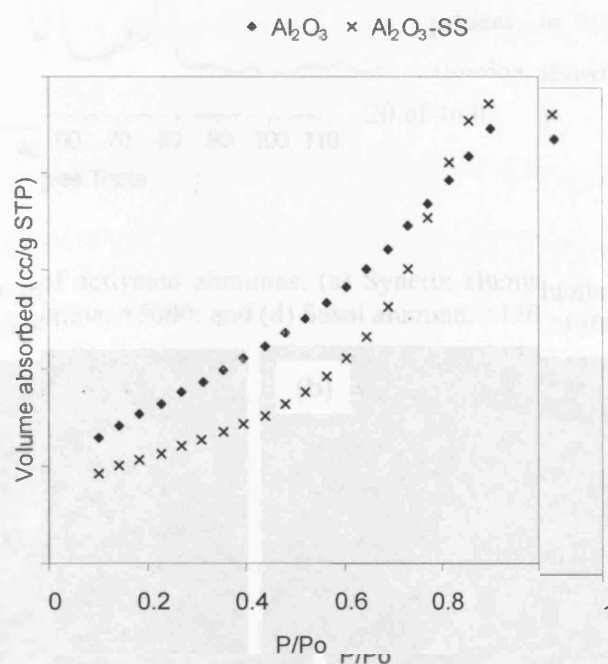
Two sources of commercial activated aluminas were compared here, namely Syntex alumina (Al_2O_3) and Sasol alumina ($\text{Al}_2\text{O}_3\text{-SS}$). Syntex alumina is an amorphous form of alumina commonly used as a catalyst support. It has a surface area of about $300 \text{ m}^2\text{g}^{-1}$ and bulk density of $0.75 \text{ g}\cdot\text{cm}^{-3}$. The Sasol alumina, so called the “ultra-pure” grade alumina has a typical surface area of about $202 \text{ m}^2\text{g}^{-1}$ and bulk density of $0.71 \text{ g}\cdot\text{cm}^{-3}$. All samples were pretreated by heating at 500°C for 3h before use.

4.2.1 The characteristics of activated alumina

N_2 -adsorption (BET) was used to measure the surface area and the pore size distributions for activated aluminas. The BET isotherm¹⁵ shows the typical plot for activated alumina, which suggests a non porous alumina was obtained (Fig 4.1, also

see Appendix C). After the samples were dehydrated at 500°C, the Syntex alumina (Al_2O_3) has a surface area of $290 \text{ m}^2\text{g}^{-1}$, total pore volume of $0.34\text{cm}^3\text{g}^{-1}$ with pore size diameter of 3.5 nm, whereas Sasol alumina ($\text{Al}_2\text{O}_3\text{-SS}$) has a surface area of $195 \text{ m}^2\text{g}^{-1}$, total pore volume of $0.37\text{cm}^3\text{g}^{-1}$ with pore size diameter of 8.5 nm. The samples do not exhibit loss of surface area due to dehydration, which was generally observed with increasing temperature¹.

Fig 4.1: The BET isotherm for Syntex alumina (diamond) and Sasol alumina (cross)



X-ray diffraction analysis (XRD) of the activated aluminas shows a pattern of γ -phase alumina, as shown in Fig 4.2. The results reveal that the amorphous form of alumina was obtained for both Syntex (Al_2O_3) and Sasol ($\text{Al}_2\text{O}_3\text{-SS}$) alumina, the Sasol alumina exhibited higher line broadening than the Syntex alumina. Broad peaks at 2θ of 32.8° , 37.4° , 46.0° and 66.8° are ascribed to the distinct γ -phase of alumina.

In addition, scanning electron micrographs (SEM) were used to illustrate the particle shape and size of activated alumina, as shown in Fig 4.3. The pictures show aggregates of activated alumina in sphere and other shapes of varying size. Small

particles of about 1 μm in diameter can be observed on the surface of activated alumina.

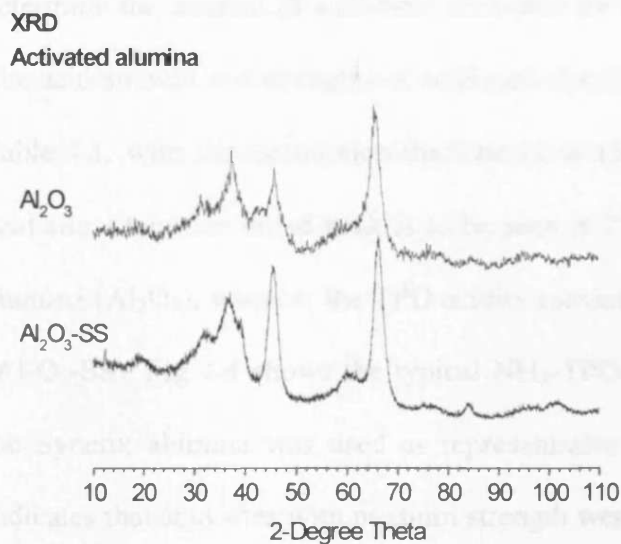
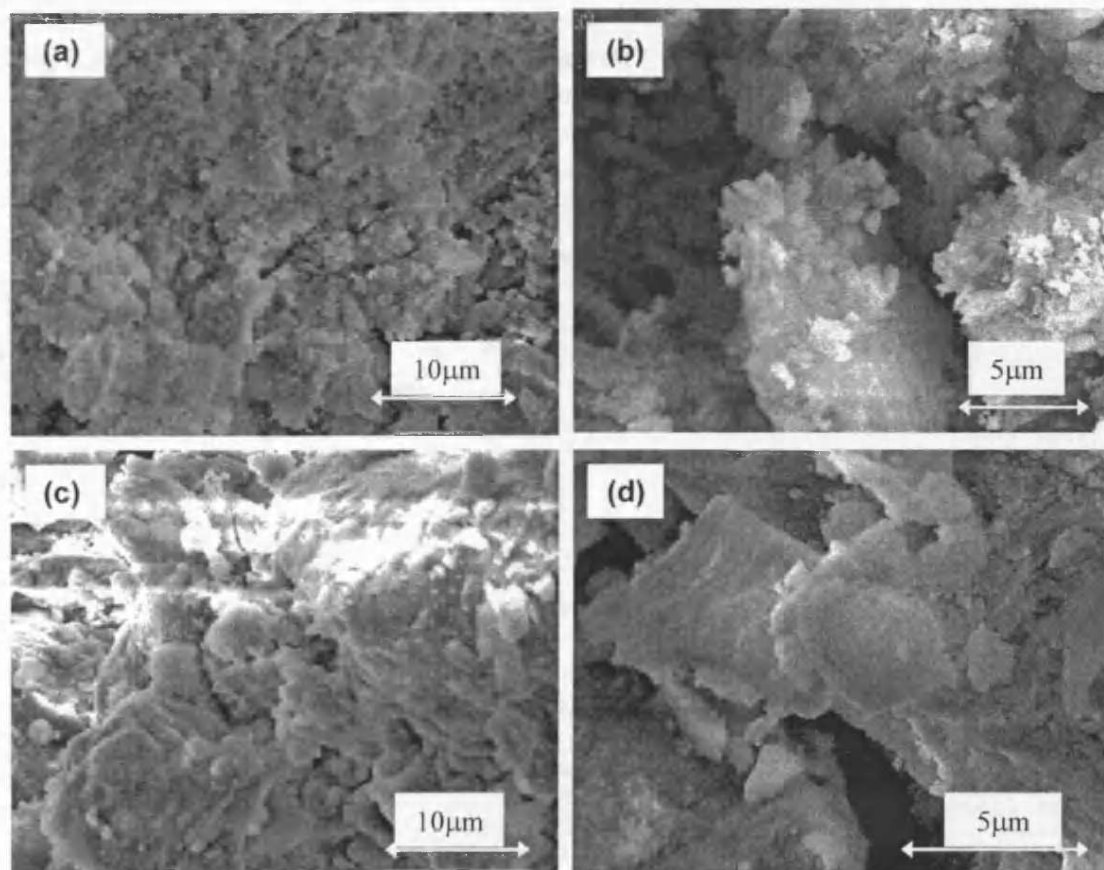


Fig 4.2: X-ray diffraction patterns of activated alumina. Alumina supplied by Syntex is shown at the top, and alumina supplied by Sasol at the bottom. The XRD patterns show that both aluminas were present in γ -phase, with Sasol alumina showing sharper peak at 2θ of 46.0° .

Fig 4.3: SEM micrographs of activated aluminas. (a) Syntex alumina, $\times 5000$; (b) Syntex alumina, $\times 9000$; (c) Sasol alumina, $\times 5000$; and (d) Sasol alumina, $\times 13000$ of magnification.



4.2.1.1 Acid-base properties by chemisorption of carbon dioxide or ammonia

The chemisorption of carbon dioxide and ammonia was employed to determine the amount of acid-base sites and the strength of the acidity and basicity. The acid amount and strengths of activated alumina heat-treated at 500°C are given in Table 4.1, with the assumption that one molecule of ammonia could react with one acid site. Only one broad peak is to be seen at 200°C from the NH₃-TPD of Syntex alumina (Al₂O₃), whereas the TPD acidity maximum falls at 260°C for Sasol alumina (Al₂O₃-SS). Fig 4.4 shows the typical NH₃-TPD curve for activated alumina, where the Syntex alumina was used as representative result. The TPD peak temperature indicates that acid sites with medium strength were obtained for the activated alumina. The higher TPD peak temperature for Sasol alumina than Syntex alumina, suggests that stronger acidity was observed for Sasol alumina.

Fig 4.4: TPD curve of ammonia adsorbed at 100°C over Syntex alumina, followed by a temperature programmed from room temperature to 500°C with 20°C·min⁻¹ of ramp rate.

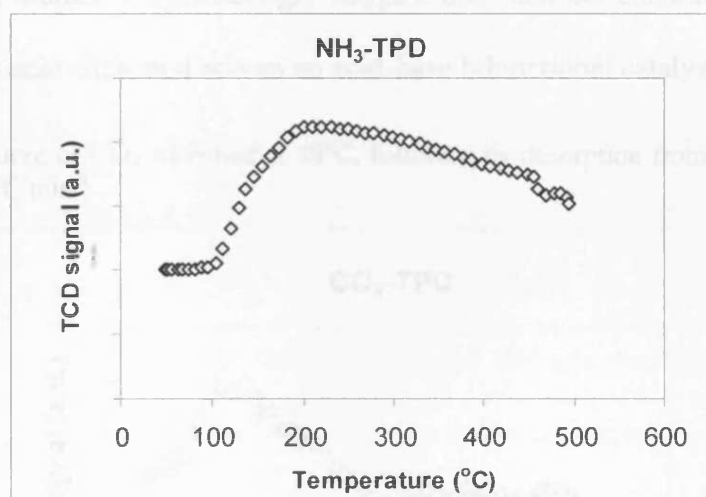


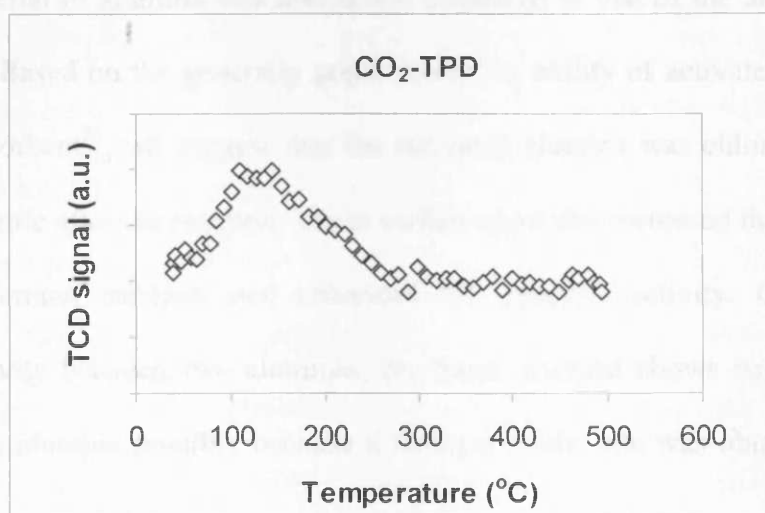
Table 4.1: The acid-base properties of activated aluminas

samples	Acidity (NH ₃)		Basicity (CO ₂)	
	Al ₂ O ₃	Al ₂ O ₃ -SS	Al ₂ O ₃	Al ₂ O ₃ -SS
TPD, T _{max} (°C)	200	260	115	120
Active sites (μmol.g ⁻¹)	96	88	95	46
Active sites (molecule.m ⁻² × 10 ¹⁶)	20	27	20	14

The acidity of activated alumina has been studied using a wide variety of techniques¹⁶ include titration with KOH, calorimetric titration with dioxane, and the chemisorption of gaseous ammonia, trimethylamine and pyridine. In particular, the determination of surface acidity of alumina by ammonia adsorption has been reported¹⁷. In order to distinguish the acid sites of alumina between Bronsted and Lewis type, various methods have been applied. Pines and Haag¹⁸, using a range of indicators concluded that alumina displayed Lewis acidity. Infrared adsorption band of pyridine adsorbed on alumina provide additional evidence that the acid sites of alumina are of the Lewis type¹⁹.

The CO₂-TPD of activated aluminas (Fig 4.5) shows only one broad peak at 120°C. The number of surface basic sites for Syntex alumina is greater than the Sasol alumina. Comparatively little work has been done on investigating the basic properties of alumina¹⁶. Pines and Manassen²⁰ have carried out a series of interesting stereochemical studies which strongly suggest that alumina contains intrinsic basic sites as well as acid sites, and acts as an acid-base bifunctional catalyst.

Fig 4.5: TPD curve of CO₂ adsorbed at 40°C, followed by desorption from 40 to 500°C with ramp rate of 20°C·min⁻¹

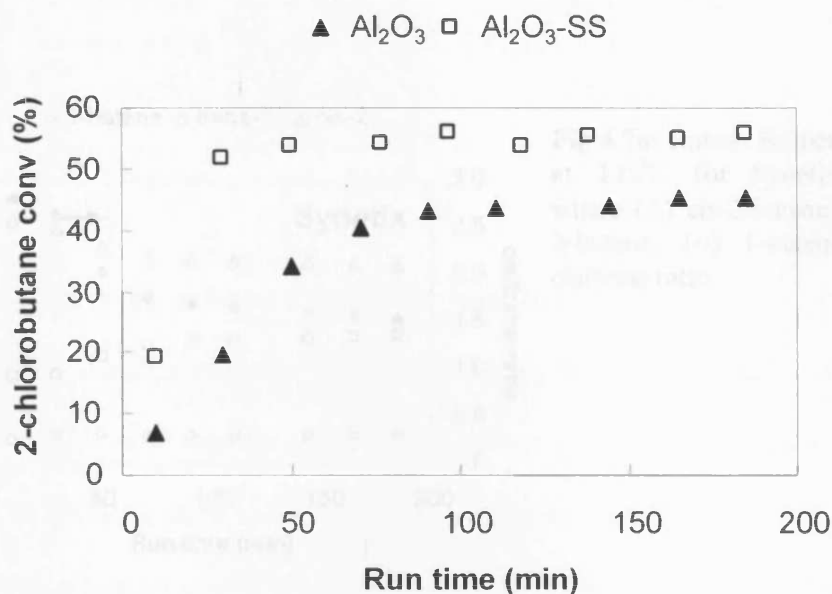


agreement with the published work by Hindin²¹ and Knozinger²², regarding the use of alumina as catalysts for ethylene hydrogenation and dehydration of alcohols, respectively.

4.2.2 Catalytic activity

A preliminary study of dehydrochlorination of 2-chlorobutane was performed over activated aluminas. Fig 4.6 shows the catalyst performance over Syntex and Sasol alumina within a time scale of 3h at 135°C. The activity is presented in terms of conversion, by measuring the exit gas concentration. The reaction profile shows that the catalyst activity was initially low, and reached a steady state after 2h of reaction online. The maximum conversion reached at steady state, was 45% for Syntex alumina (Al_2O_3) and 55% for Sasol alumina (Al_2O_3 -SS). The result indicates that the starting material of alumina was less active compared to that of the alumina after 2h of reaction. Based on the generally good absorptive ability of activated alumina as a chloride absorbent²³, we suggest that the activated alumina was chlorinated to form surface chloride after the reaction. These surface chlorides increased the acidity of the activated alumina catalysts and enhanced the catalysts activity. Comparing the catalyst activity between two aluminas, the Sasol alumina shows better conversion than Syntex alumina possibly because a stronger acidic site was obtained for Sasol alumina.

Fig 4.6: Catalytic activity for activated aluminas: (▲) Syntex alumina and (□) Sasol alumina. Reaction conditions: 135°C for 3h, 100mg of catalyst and 60ml·min⁻¹ total flow rate (GHSV= 33000h⁻¹).



The product distributions changed continuously according to the reaction time. The activated alumina was found to be highly selective to the isomers of butene as the major hydrocarbon product with above 99.9% of selectivity, and less than 0.1% of octene isomers were detected as secondary product. HCl was the only chlorinated product obtained from the reaction and was collected in a sodium hydroxide solution for further analysis. Fig 4.7 shows the product distributions and the ratio of cis to trans isomers changed with time over activated aluminas at 135°C. It was observed that the cis isomer was predominant, followed by the trans isomer and 1-butene. The cis/trans ratio was high when the activity was low at the start of the reaction. When the steady state was reached, Syntex alumina has a cis/trans ratio of 1.5 while Sasol alumina has a cis/trans ratio close to unity. The result indicates that the catalytic dehydrochlorination of 2-chlorobutane over activated alumina took place *via* acid catalysis to form the preferential cis-2-butene, according to Mochida *et al.* The alteration of the cis/trans ratio implied that the surface acidity was increased by the

hydrogen chloride formed. It was found that Sasol alumina exhibited greater acidity than Syntex alumina.

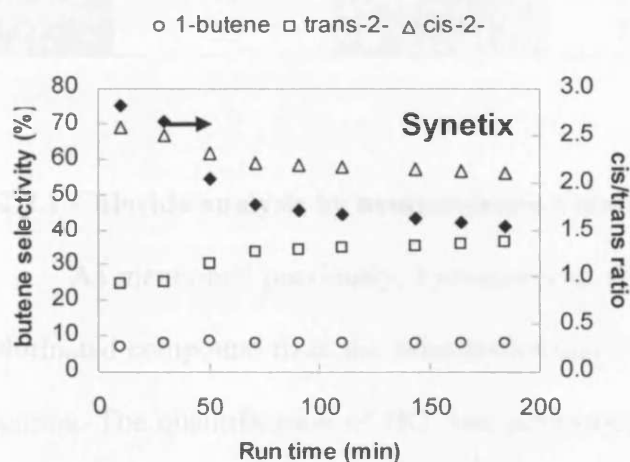


Fig 4.7a: Butene isomer selectivity at 135°C for Syntex alumina, where (Δ) cis-2-butene, (□) trans-2-butene, (o) 1-butene and (◆) cis/trans ratio.

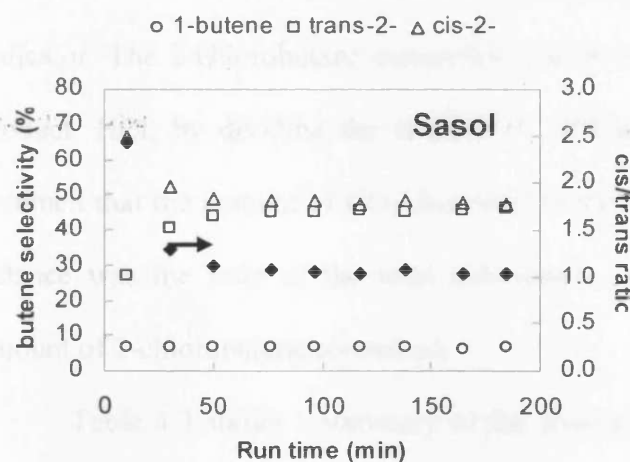


Fig 4.7b: Butene isomer selectivity at 135°C for Sasol alumina, where (Δ) cis-2-butene, (□) trans-2-butene, (o) 1-butene and (◆) cis/trans ratio.

Mochida *et al*^{9,11} reported that the cis isomers were preferred on an acid catalyst and the trans isomers were preferred on a base catalyst in a dehydrochlorination process. The cis to trans ratio in 2-butenes produced could be used to judge whether the reaction is a base-catalysed or acid-catalysed one. A high cis/trans ratio observed for the base-catalysed isomerisation is in contrast to the value close to unity for acid-catalysed isomerisation²⁴. A summary of the results from the catalyst performance is showed in Table 4.2.

Table 4.2: Summary of catalyst performance, result recorded at 180min on stream at steady state. Reaction condition: 135°C for 3h, 100mg of catalyst and 60ml·min⁻¹ total flow rate (GHSV= 33000h⁻¹).

	2-chlorobutane	Butene	Distribution of products (%)			cis/trans ratio
	Conversion (%)	Selectivity (%)	1-butene	trans-2-	cis-2-	
Al ₂ O ₃	45	99.9	8	37	56	1.5
Al ₂ O ₃ -SS	55	99.9	7	46	47	1.0

4.2.2.1 Chloride analysis by neutralisation titration

As mentioned previously, hydrogen chloride (HCl) was found to be the only chlorinated compound from the dehydrochlorination of 2-chlorobutane over activated alumina. The quantification of HCl was performed by dissolving the HCl in a fixed amount of NaOH solution in a scrubber for further titration using phenolphthalein as the indicator. The 2-chlorobutane conversion can be evaluated based on the chlorinated product, HCl, by dividing the amount of HCl produced to the total feed. It was assumed that the amount of CO₂ dissolved in the solution is negligible. The chlorine balance was the ratio of the total chlorinated compounds produced and the total amount of 2-chlorobutane consumed.

Table 4.3 shows a summary of the conversions, chlorine balance and carbon balance for dehydrochlorination of 2-chlorobutane over activated alumina (Synetix). The results showed inconsistency for the conversion and mass balance calculated from the HCl. The chlorine balance deviates from 68 to 115%, despite the same catalyst under same reaction conditions was used. In contrast, a more reliable hydrocarbon conversion was observed with close to 100% carbon balance obtained. The results suggest that quantitative analysis was not possible as the neutralisation process is strongly dependent on the concentration of the titrant or titrand. This may be due to a rapid rate of pH change near the equivalent point when a strong acid was neutralised by a strong base²⁵.

Table 4.3: The conversion and mass balance calculated based on the HCl product from the dehydrochlorination of 2-chlorobutane over Syntex alumina. Reaction conditions: 135°C, 100mg of catalyst and 110mlmin⁻¹ (145μmol·min⁻¹) total flow rate, GHSV= 55000h⁻¹.

	Try 1	Try 2*	Try 3
40 ml of NaOH scrubber in different concentration (x), mmoles	17.72	160	104
After reaction (duration in minute)	1250	1310	1212
Final concentration. No. of moles of HCl required to reach end point, mmoles	-31.58	106.2	37.2
Total HCl made from reaction, mmoles	49.3	53.6	66.78
Conv, %HCl per feed	26	28	38
Conv, %Hydrocarbon product per feed	40	36	33
Chlorine balance (%)	68	78	115
Carbon balance (%)	100	99	99

* Refer to Appendix D for a sample calculation of chloride analysis by neutralisation titration.

Consequently, a *Kitagawa* Drager hydrochloride detector tube²⁶ was used to analyse the amount of exit HCl from the reaction. However, the detector tube has a detection limit of up to 1200ppm, and the yield of HCl was always greater than 1200ppm. We conclude that only qualitative analysis of HCl was performed for the future studies.

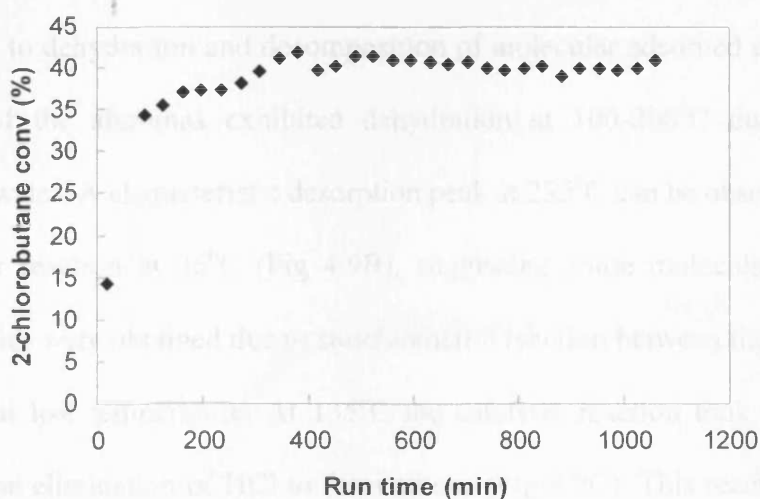
4.2.2.2 Catalyst deactivation

In order to investigate the catalyst life, extended reaction times up to 18h were studied. Fig 4.8 illustrates the reaction profile for dehydrochlorination of 2-chlorobutane over Syntex alumina, as a representative result. Prior to the reaction, a space velocity of 55000h⁻¹ and 100mg of catalyst were employed. A similar reaction profile to that of the activated alumina after reaction at 135°C with 33000h⁻¹ of space velocity (Fig 4.6) can be observed. The conversion of 2-chlorobutane was initially low, but increased to reach a maximum conversion of about 40% and close to 100% of butene selectivity. The absence of a catalyst deactivation can be observed. In

addition, by using only 0.1g of γ -Al₂O₃ catalyst (0.98mmol·g⁻¹) was able to convert 473mmol·g⁻¹ in 18h, indicating a catalytic reaction.

This effect may be ascribed to weak adsorption of chlorinated compound on the catalyst surface that increases the surface acidity, followed by desorption of alkene after losing an electron and elimination of HCl. This postulation is supported by the FTIR spectroscopic studies of the dehydrochlorination process over alumina that was performed by Ballinger and Yates²⁷, and Busca and coworkers²⁸. They agreed that the reaction begins with a rapid and reversible adsorption of a chlorinated compound on the catalyst surface, while a nucleophilic substitution occurs to give strongly adsorbed alkoxide species. Elimination of HCl occurs forming the alkene, restoring the surface oxide atom. It is worth noting that the catalyst deactivation has been reported on the catalytic dehydrochlorination of heavily chlorinated compounds^{8,29} (i.e. trichloroethane and 1,1,2,2-tetrachloroethane) over alumina, where the activity decreased with time due to surface coverage of organic compounds.

Fig 4.8: Catalytic activity for Syntex alumina. Reaction conditions: 135°C for 18h, 100mg of catalyst and 100ml/min total flow rate (GHSV= 55000h⁻¹).



4.2.3 Post-reaction analysis

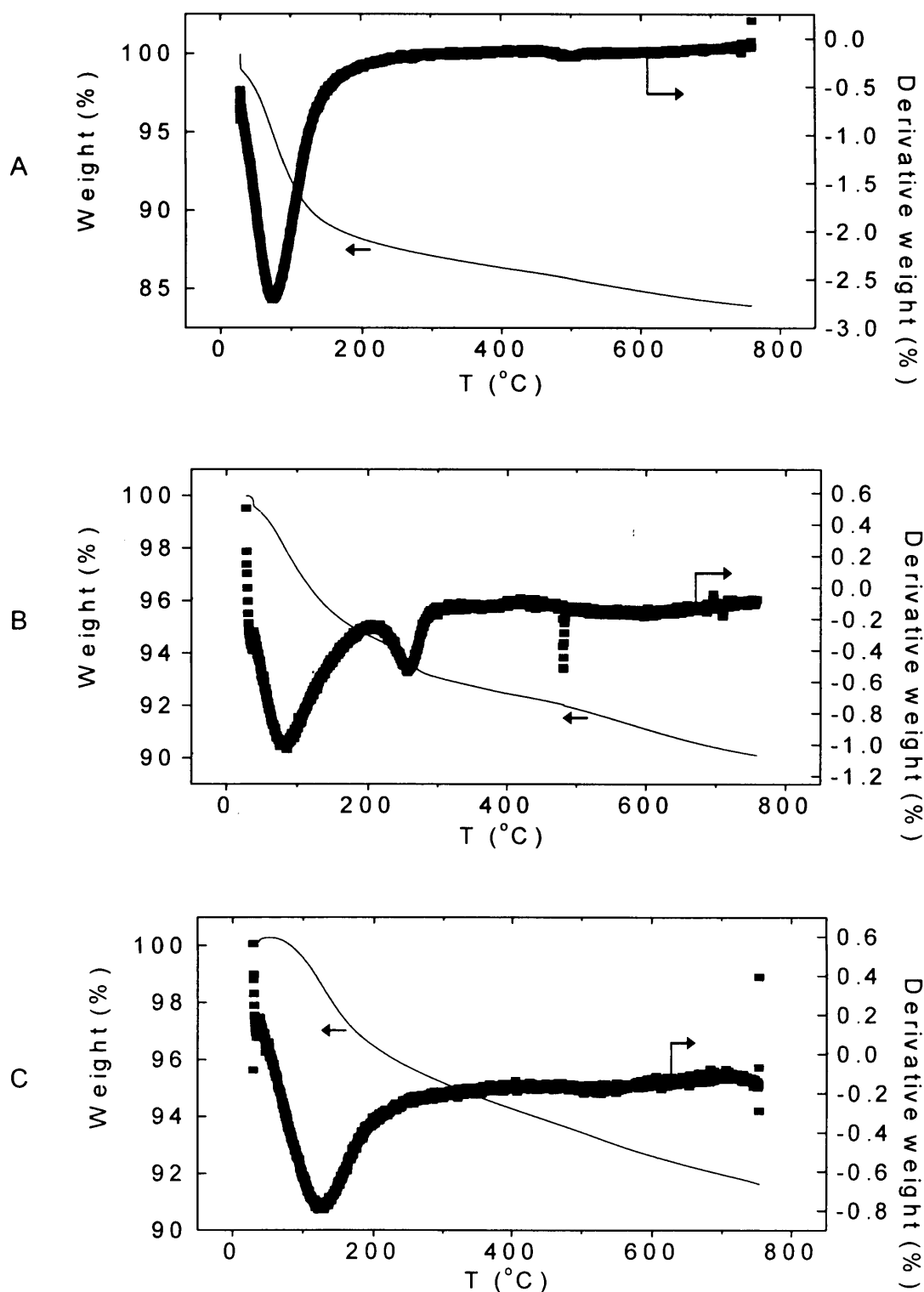
After 2-chlorobutane (2-CB) conversion at 135°C, visual examination of the used alumina catalysts revealed a pale yellow colour instead of the original white powder. The sample lost the pale yellow colour after it was heat-treated at 120°C, implying some molecular adsorption of organochlorides was obtained on the catalyst surface. The post-reaction analysis of the used catalyst was performed by XRD, TGA, XPS and TPD of ammonia.

Powder x-ray diffraction (XRD) was employed to investigate changes in the crystalline structure for the activated alumina after the dehydrochlorination reaction. The XRD patterns of the used aluminas revealed only the broad peaks due to γ -alumina phase, same as the fresh alumina catalysts (Fig 4.2). The absence of a sharp peak implies that the adsorption of a chlorinated compound (or chlorination) over the activated alumina may be occurred at the catalyst surface but definitely not in the bulk.

Thermogravimetric analysis (TGA) was performed over fresh and used alumina catalysts at reaction temperature of 35°C (close to room temperature) and at 135°C to compare the thermal stabilities. The TGA curves revealed typical plots for aluminas due to dehydration and decomposition of molecular adsorbed chlorides (Fig 4.9). Each of the aluminas exhibited dehydration at 100-200°C due to loss of physisorbed water. A characteristic desorption peak at 255°C can be observed for used alumina after reaction at 35°C (Fig 4.9B), suggesting some molecularly adsorbed chloride species were obtained due to stoichiometric reaction between the reactant and the catalyst at low temperature. At 135°C the catalytic reaction took place, which encourages the elimination of HCl to form alkene (Fig 4.9C). This reaction proceeds *via* a surface adsorption-desorption that explain the absence of a desorption peak at

255°C for this catalyst. The results fit the idea that the reaction begins with a weakly adsorbed and reversible adsorption of a chlorinated compound on the catalyst surface.

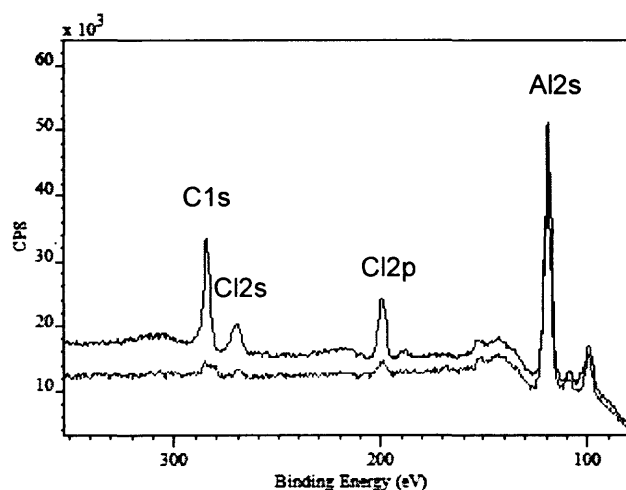
Fig 4.9: TGA curves for activated aluminas (Synetix) with temperature ramp rate of $20^{\circ}\text{C}\cdot\text{min}^{-1}$. A is the fresh alumina, B is the used alumina after reaction at 35°C (close to room temperature) and C is the used alumina after reaction at 135°C .



On the other hand, XPS spectra of activated aluminas (Synetix) before and after the reaction were recorded, as shown in Fig 4.10. The result indicates that the fresh sample contains residual carbon and chlorine species, which are attributed to some contamination during sample handling. Post reaction analysis of activated alumina shows significant increase in the intensity of the carbon and chlorine peaks. The observation of the chlorine peak agreed with the hypothesis that a surface interaction between the chlorinated compound and the alumina surface occurs. In addition, the increase in the concentration of carbon species on alumina surface after reaction suggested that some carbonaceous product or intermediate may be formed during the dehydrochlorination reaction.

Finally, the quantitative chloride analysis by columetric titration over the used alumina shows about 5% w/w of chloride was adsorbed on the alumina.

Fig 4.10: XPS spectra of alumina (Synetix). Top: Sample after reaction for 24h; Bottom: Fresh sample.



4.2.3.1 Increases in surface acidity

Selective chemisorption of ammonia was performed over the used alumina to determine the acidity after the dehydrochlorination reaction. It was assumed that one molecular of ammonia could react with one corresponding acid site. Table 4.4 shows

the acid properties for activated aluminas (Synetix), before and after the reaction. The TPD-NH₃ desorption peak of the used alumina at 204°C was close to that of the fresh alumina. This implied that acid sites of similar strength were present. In addition, the result revealed a significant increase in the amount of acid sites, from 96 μmol·g⁻¹ of adsorbed ammonia for the fresh alumina to 219 μmol·g⁻¹ for the used alumina. The chemisorption of ammonia confirmed the increase of surface Lewis acid sites on activated alumina that may be the active site for the dehydrochlorination reaction.

Table 4.4: NH₃ chemisorption of activated alumina (Synetix), before and after dehydrochlorination reaction.

samples	Acidity (NH ₃) of Al ₂ O ₃	
	Fresh	Used
BET (m ² ·g ⁻¹)	290	265
TPD, T _{max} (°C)	200	204
Active sites (μmol·g ⁻¹)	96	219
Active sites (molecule·m ⁻² × 10 ¹⁶)	20	51

4.3 Effects of acid treatment

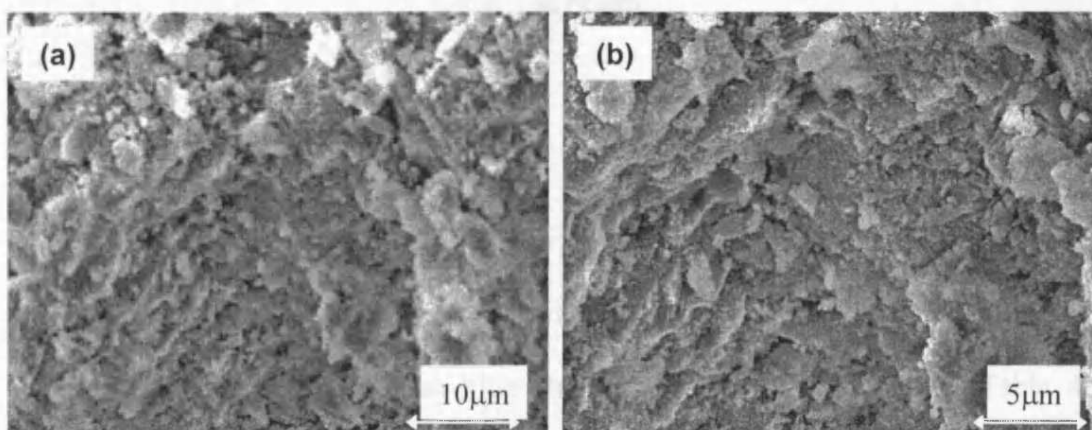
γ-alumina (Synetix) has been chlorinated with hydrogen chloride to observe the effect of this treatment on modifying the morphology and surface chemistry of alumina, as well as its catalytic performance for the dehydrochlorination of 2-chlorobutane. From the previous section, activated alumina was active for the dehydrochlorination of 2-chlorobutane, which is attributed to the large amount of surface Lewis sites of alumina. The conversion was improved upon chlorination of the alumina. Therefore, the alumina treated with hydrogen chloride (Al₂O₃-HCl) was prepared; the aim was to develop a better catalyst for the dehydrochlorination reaction.

4.3.1 Catalyst characterisation

N_2 -adsorption (BET) was performed to determine the surface area and porosity of the HCl-treated alumina. The BET plot revealed a typical type II isotherm (see Appendix C) for Al_2O_3 -HCl. The Al_2O_3 -HCl has a BET surface area of $270m^2g^{-1}$, a total pore volume of $0.36cm^3g^{-1}$ with average pore size diameter of 3.5nm, close to that of pure $\gamma-Al_2O_3$. The slight decrease in surface area indicates only moderate modification of the $\gamma-Al_2O_3$ support structure. The pore distribution of Al_2O_3 -HCl shows the accessible pore structure of the $\gamma-Al_2O_3$ support is still intact. The sample does not exhibit vast changes, which can normally be observed with blockage of the surface active sites and acid attack. X-ray diffraction analysis (XRD) of the Al_2O_3 -HCl displayed similar pattern to the amorphous $\gamma-Al_2O_3$ support (Fig 4.2).

Additionally, the scanning electron micrographs (SEM) of Al_2O_3 -HCl shows the sample was in an amorphous form, as illustrated in Fig 4.11. The pictures show aggregates of activated alumina in sphere and other shapes of varying size. Small particles less than $1\mu m$ in diameter can be observed on the surface of the sample. The result indicates that some smaller particles of pure alumina have been dissolved during the acid-treatment⁴.

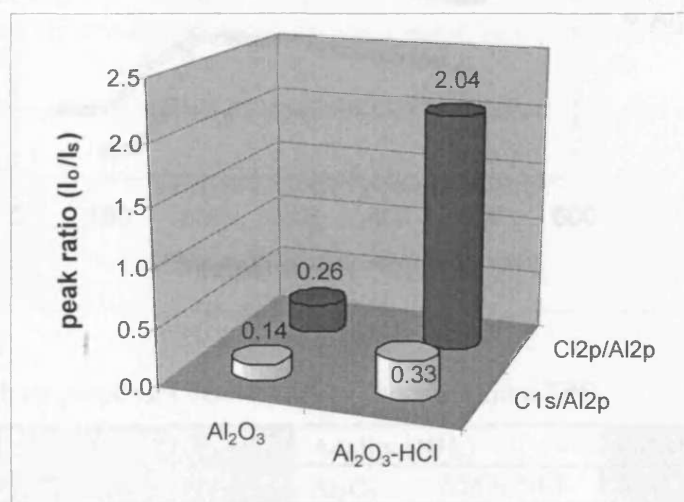
Fig 4.11: SEM of HCl-treated alumina. (a) $\times 5000$ and (b) $\times 8400$ of magnification.



4.3.1.1 Surface compositions by x-ray photoelectron spectroscopy (XPS)

XPS was used to observe the surface composition of HCl-treated alumina. The histogram in Fig 4.12 compares the peak intensity ratio of $\text{Al}_2\text{O}_3\text{-HCl}$ and pure $\gamma\text{-Al}_2\text{O}_3$ obtained from XPS. The I_0/I_s intensity ratio was calculated by dividing the XPS intensity of the overlayer to the support. The result revealed a significant increase in the intensity ratio for carbon and chloride species. The increase in the chloride peak ratio indicates that the higher concentration of surface chloride was obtained after the HCl-treatment. The slight decrement of the BET surface area for $\text{Al}_2\text{O}_3\text{-HCl}$ may be attributed to monolayer coverage of surface chloride that blocked the surface active sites of $\gamma\text{-Al}_2\text{O}_3$ support. On the other hand, the increase in the intensity ratio for the carbon peaks shows the carbon contamination occurred in the preparation procedure.

Fig 4.12: C1s/Al2p and Cl2p/Al2p peak area ratio calculated from XPS for pure alumina and acid-treated alumina.



4.3.1.2 Acid-base properties by chemisorption of NH_3 and CO_2

Selective chemisorptions of NH_3 and CO_2 were used to examine the change in acid-base properties for alumina after the acid-treatment ($\text{Al}_2\text{O}_3\text{-HCl}$). Table 4.5 shows the amount of acid-base sites and the acid-base strength with the assumption of

one molecule of the adsorbed probe reacts with one corresponding site. One desorption peak was observed for the NH_3 -TPD of Al_2O_3 -HCl at 260°C (Fig 4.13). The higher desorption peak temperature for Al_2O_3 -HCl than $\gamma\text{-Al}_2\text{O}_3$, indicating that acid sites with stronger acidity (Bronsted sites) was obtained³⁰. The measurement of the amount of acid sites for Al_2O_3 -HCl also rises from 96 to $457\mu\text{mol}\cdot\text{g}^{-1}$. The result indicates that significant increase in both the amount of acid sites and acidity for alumina after the HCl-treatment (Al_2O_3 -HCl).

Fig 4.13: TPD of ammonia adsorbed at 100°C over HCl-treated alumina, followed by a temperature programmed from 100 to 500°C with $20^\circ\text{C}\cdot\text{min}^{-1}$ ramp rate.

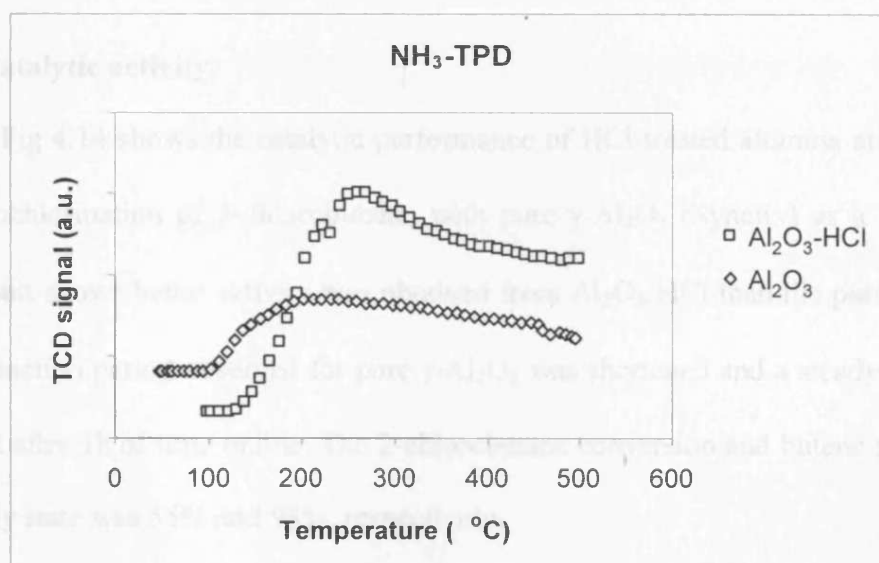


Table 4.5: Acid-base properties determined by chemisorption/ TPD

samples	Acidity (NH_3)		Basicity (CO_2)	
	Al_2O_3	Al_2O_3 -HCl	Al_2O_3	Al_2O_3 -HCl
TPD, T_{max} ($^\circ\text{C}$)	200	260	115	120
Active sites ($\mu\text{mol}\cdot\text{g}^{-1}$)	96	457	95	24
Active sites ($\text{molecule}\cdot\text{m}^{-2}\times 10^{16}$)	20	102	20	5

On treating the alumina with HCl, a labile surface chlorine species was formed as a result of the weak interaction between the very weak Lewis base hydrogen chloride and alumina^{31,32}. The presence of this chlorine species modified the defect spinel structure of γ -alumina (tetrahedral Al^{3+}), resulted in the presence of sites with

different strength of acidity. The enhancement of acidity may be due to the replacement of OH groups by Cl, resulting in surface Al^{3+} atoms in a disordered O/Cl environment.

The TPD- CO_2 of $\text{Al}_2\text{O}_3\text{-HCl}$ reveals only one broad peak at 120°C , similar as the pure $\gamma\text{-Al}_2\text{O}_3$ (Fig 4.5). Quantitative analysis of the amount of surface basic sites shows significant reduction of the active sites after the HCl-treatment. The result indicates that the surface chlorine species formed has blocked the basic sites of alumina, which are believed to be the surface O atom (O^{2-})^{24,33}.

4.3.2 Catalytic activity

Fig 4.14 shows the catalytic performance of HCl-treated alumina at 135°C on dehydrochlorination of 2-chlorobutane, with pure $\gamma\text{-Al}_2\text{O}_3$ (Synetix) as a reference. The result shows better activity was obtained from $\text{Al}_2\text{O}_3\text{-HCl}$ than the pure $\gamma\text{-Al}_2\text{O}_3$. The induction period observed for pure $\gamma\text{-Al}_2\text{O}_3$ was shortened and a steady state was reached after 1h of time online. The 2-chlorobutane conversion and butene selectivity at steady state was 55% and 98%, respectively.

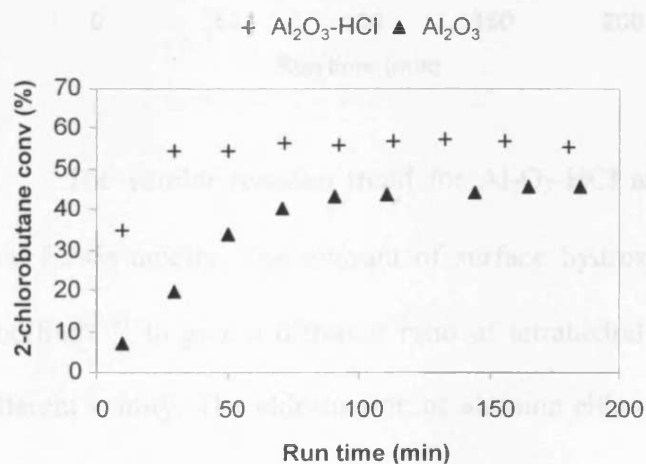


Fig 4.14: Catalytic activity for $\text{Al}_2\text{O}_3\text{-HCl}$ (+), where Synetix $\gamma\text{-Al}_2\text{O}_3$ (▲) used as a reference.

Reaction conditions: 135°C for 3h, 100mg of catalyst and $60\text{ml}\cdot\text{min}^{-1}$ total flow rate ($\text{GHSV} = 33000\text{h}^{-1}$).

The product distributions were dominated by the isomers of butene and hydrochloric acid, with isomers of octene as major by-product, as shown in Fig 4.15. The selectivity for different isomers of butene was 7% for 1-butene, 46% for trans-2-butene and 45% for cis-2-butene, with less than 2% of octene was detected. The cis-2-butene was found to be the preferential product and the cis/trans ratio was close to unity. These observations implied that the dehydrochlorination of 2-chlorobutane over $\text{Al}_2\text{O}_3\text{-HCl}$ was acid catalysed^{9,24}. As the reaction was acid-catalysed, the higher activity of $\text{Al}_2\text{O}_3\text{-HCl}$ was consistent with the stronger acidity that was obtained, compared to pure $\gamma\text{-Al}_2\text{O}_3$. However, the strong interaction between the $\text{Al}_2\text{O}_3\text{-HCl}$ and the reactant was also accompanied by increase amount of by-products, which may be due to the ability of strong acid sites to promote further side reaction.

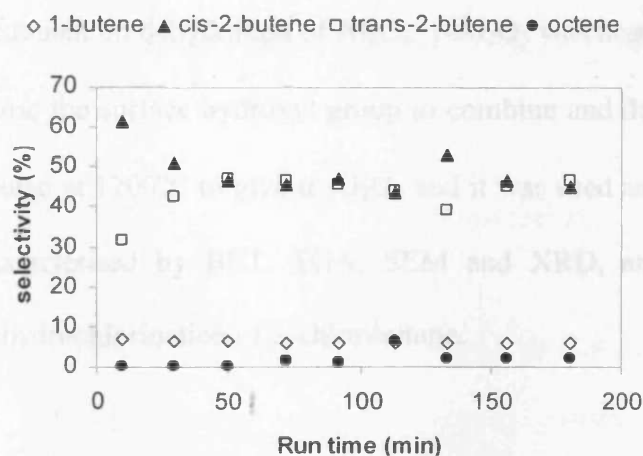


Fig 4.15: Different product distributions for $\text{Al}_2\text{O}_3\text{-HCl}$ at 135°C .

The similar reaction trend for $\text{Al}_2\text{O}_3\text{-HCl}$ and pure $\gamma\text{-Al}_2\text{O}_3$ was a result of their Lewis acidity. The amount of surface hydroxyl group on the $\gamma\text{-Al}_2\text{O}_3$ can be modified^{27,31} to give a different ratio of tetrahedral and octahedral structure, hence, different acidity. The chlorination of alumina either by acid-treatment or a period of 2-chlorobutane dehydrochlorination, results in a more active species formed. These active species are believe to be the weakly adsorbed surface chloride that increases the coverage of Lewis acid sites by replacing the surface OH group with Cl, and thus an

increase in activity. Furthermore, it is interesting to note that the dehydrochlorination of 1,1,1-trichloroethane is catalysed by γ - Al_2O_3 which has been chlorinated with CCl_4 or COCl_2 ³⁴. The chlorination of γ - Al_2O_3 promotes Lewis acidity; however, chlorination with HCl does not result in a catalyst for this reaction.

4.4 Effects of thermal treatment

In general, alumina shows strong surface acidity when heated to temperatures above 500°C ¹⁶. The structure morphology, surface chemistry and the acid-base properties of alumina changes subjected to different degree of dehydration^{1,4,27}. As mentioned before, γ - Al_2O_3 was prepared by heat-treating at 500°C , while α - Al_2O_3 was obtained with dehydration at above 1000°C . In order to examine the effects of thermal treatment on dehydration of Al_2O_3 , γ - Al_2O_3 was heat-treating at 800°C (Al_2O_3 -800) to cause the surface hydroxyl group to combine and desorbs as water. γ - Al_2O_3 was also heated at 1200°C to give α - Al_2O_3 and it was used as a reference. These samples were characterised by BET, TGA, SEM and XRD, and were tested for the catalytic dehydrochlorination of 2-chlorobutane.

4.4.1 The thermal stability of Al_2O_3

N_2 -adsorption (BET) and thermogravimetric analysis (TGA) was used to examine the thermal stability of Al_2O_3 with increasing temperature, as illustrated in Fig 4.16. The dashed line represents the surface area data obtained from literature¹. N_2 -adsorption for alumina calcined at 500 (γ - Al_2O_3), 800 (Al_2O_3 -800) and 1200°C (α - Al_2O_3) gives a BET area of 290, 180 and $5\text{m}^2\text{g}^{-1}$, respectively. The result shows that the specific surface area decreased significantly with increasing temperature. The TGA curve of Al_2O_3 shows an inflexion point at 100 - 200°C , which was attributed to

the loss of physisorbed water. Continuous weight losses were observed from 200°C and reached a plateau at 900°C. The result indicates the transformation of γ - Al_2O_3 into different transition states¹⁻⁴ with increasing temperature eventually becoming the most stable α - Al_2O_3 .

Fig 4.16: Combined data from N_2 -adsorption and TGA over heat-treated alumina with increasing temperature. *Reference data obtained from Kirk-Othmer Encyclopedia of Chemical Technology¹

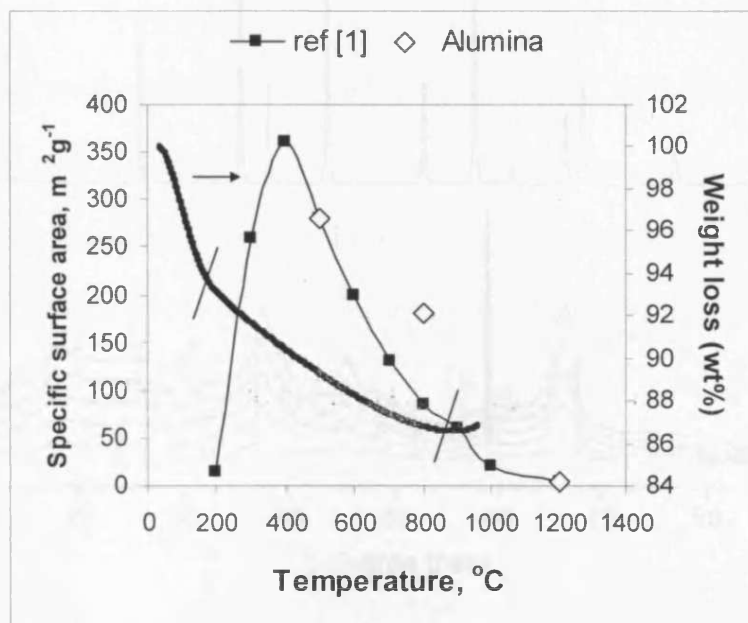
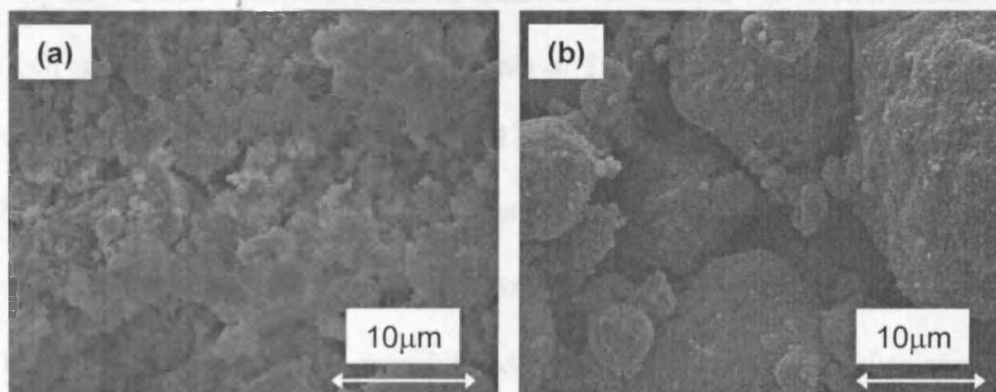


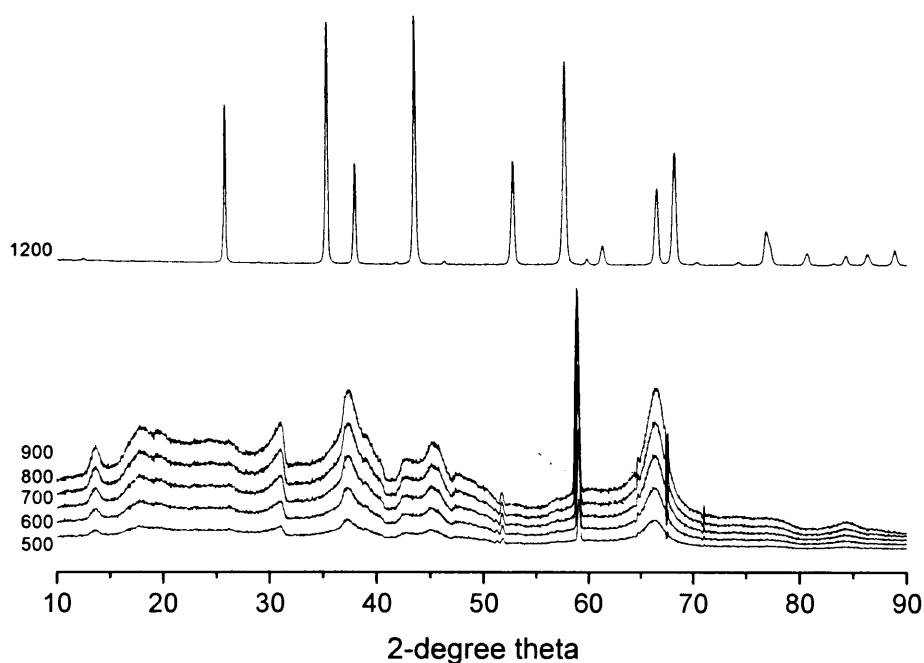
Fig 4.17: SEM micrograph of alumina calcined at a. 800°C (Al_2O_3 -800, c.a. $\times 6070$) and b. 1200°C (α - Al_2O_3 , c.a. $\times 5000$)



Scanning electron microscopy (SEM) was employed to determine the shape and size of the particles. The result showed that Al_2O_3 -800 appeared in an amorphous

form and the aggregates of alumina in flake clusters shape that can be observed whose diameter is approximately $5\mu\text{m}$, as shown in Fig 4.17. In addition, the SEM micrograph of $\alpha\text{-Al}_2\text{O}_3$ (Al_2O_3 heated at 1200°C) shows a different morphology obtained that large crystalline cluster was formed with diameter greater than $10\mu\text{m}$.

Fig 4.18: XRD patterns of alumina with increasing temperature



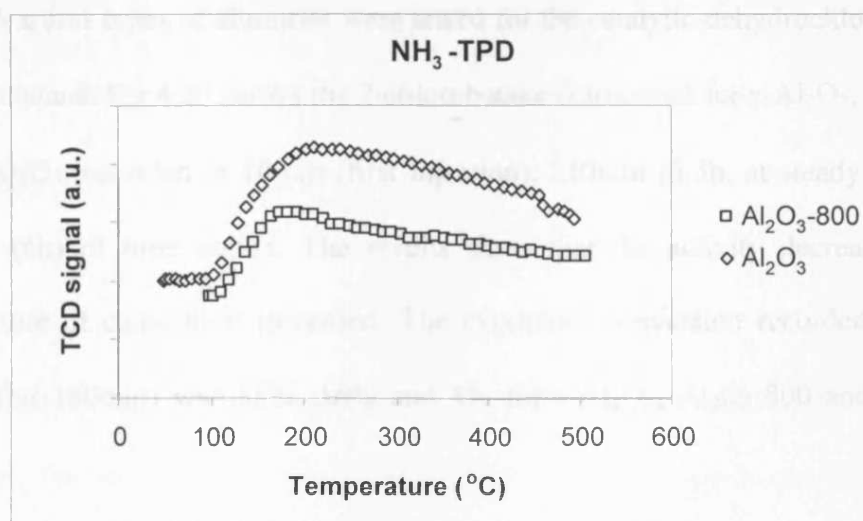
Nonetheless, *in-situ* x-ray diffraction analysis (XRD) was performed to identify the various crystalline phase of alumina. The sample was heated inside the *in-situ* cell under flow of air with a ramp rate of $20^\circ\text{C}\cdot\text{min}^{-1}$. The XRD patterns were collected at 500, 600, 700, 800, 900 and 1200°C with a scanning time of 30min. Fig 4.18 shows the XRD patterns of alumina with increasing temperature. The result clearly shows that the $\gamma\text{-Al}_2\text{O}_3$ phase was stable up to 900°C . After further dehydration at 1200°C , the γ -phase was transformed to the α -phase, which displayed high crystallinity with sharp peaks at 2θ of 25.5° , 35.1° , 37.8° , 43.4° , 52.5° , 57.5° , 66.5° and 68.2° observed. The results show that the crystalline structure of aluminas was dependent on the pre-treatment conditions. Transition aluminas including γ , η , χ , ρ or

α -phase have been reported^{1,3}, however, other phases of alumina have not been observed in our study apart from γ - and α -alumina phases.

4.4.1.1 Changes in acid-base properties

To determine the acid-base properties of various types of alumina, selective chemisorption using NH_3 or CO_2 as a probe was performed. As shown in Table 4.6, the amount of adsorbed ammonia for Al_2O_3 -800 was greater than the pure $\gamma\text{-Al}_2\text{O}_3$. Fig 4.19 shows the NH_3 -TPD peak temperatures at 200°C , suggests the presence of acid sites with medium strength that was similar to $\gamma\text{-Al}_2\text{O}_3$. $\alpha\text{-Al}_2\text{O}_3$ does not exhibit any adsorption-desorption with the probes due to its general chemically inert properties and low surface area¹. The result shows that the dehydration of alumina at 800°C favours the formation of acidic sites with intermediate strength. Peri *et al*³⁵ proposed a detailed scheme for the surface of γ -alumina heat-treated at 800°C , five different kinds of isolated hydroxyl groups were identified by IR spectroscopy. Heating Al_2O_3 causes Al-OH groups to combine and desorb as water, exposing Al^{3+} , Lewis acid sites, and O^{2-} basic sites^{22,27,33}.

Fig 4.19: TPD of NH_3 adsorbed at 100°C , followed by desorption with temperature programmed from 100 to 500°C at $20^\circ\text{C}\cdot\text{min}^{-1}$.



Echigoya and Cornelius *et al*^{16,36} put forward the suggestion that the acidic sites of alumina after high temperature dehydration were formed by lattice distortion. As the temperature of heat-treatment is raised, a water molecule is removed from two hydroxyl groups attached to Al atoms to form an Al-O-Al link. The lattice distortion between the Al-O-Al links become greater with increasing distance due to further dehydration, which is responsible for the acid strength. In the case of basicity, the amount of basic sites has significant reduced compared to the γ -alumina. The TPD- CO_2 peak temperature at 120°C indicated weak basic sites were obtained that was due to the O^{2-} sites of alumina surface.

In conclusion, the thermal treatment of alumina has modified the structures of alumina (tetrahedric or octaheric) and has altered the acid-base properties.

Table 4.6: Acid-base properties determined by chemisorption/ TPD

samples	Acidity (NH_3)		Basicity (CO_2)	
	Al_2O_3	Al_2O_3 -800	Al_2O_3	Al_2O_3 -800
TPD, T_{max} (°C)	200	200	115	120
Active sites ($\mu\text{mol.g}^{-1}$)	96	134	95	36
Active sites ($\text{molecule.m}^{-2} \times 10^{16}$)	20	45	20	12

4.4.2 Catalytic activity

Various types of aluminas were tested for the catalytic dehydrochlorination of 2-chlorobutane. Fig 4.20 shows the 2-chlorobutane conversion for γ - Al_2O_3 , Al_2O_3 -800 and α - Al_2O_3 , recorded at 10min (first injection), 210min (3.5h, at steady state) and 360min (6h) of time online. The results show that the activity decreases as the temperature of calcination increased. The maximum conversion recorded at steady state (after 180min) was 38%, 16% and 4% for γ - Al_2O_3 , Al_2O_3 -800 and α - Al_2O_3 ,

respectively. The selectivity to isomers of butene was similar for all aluminas and was always above 99%.

The decrease in activity for Al_2O_3 -800 was not expected, as we have mentioned that the high activity of Al_2O_3 was attributed to the large amount of acidic sites, the stronger acidity of Al_2O_3 -800 is preferential for the reaction. We suggest that the surface hydroxyl group are important for the catalyst dehydrochlorination of 2-chlorobutane. The dehydration of Al_2O_3 at 800°C induces lattice distortion of Al-OH structure and show increases in acidity; however, it also results in the removal of surface hydroxyl groups as water decrease the activity.

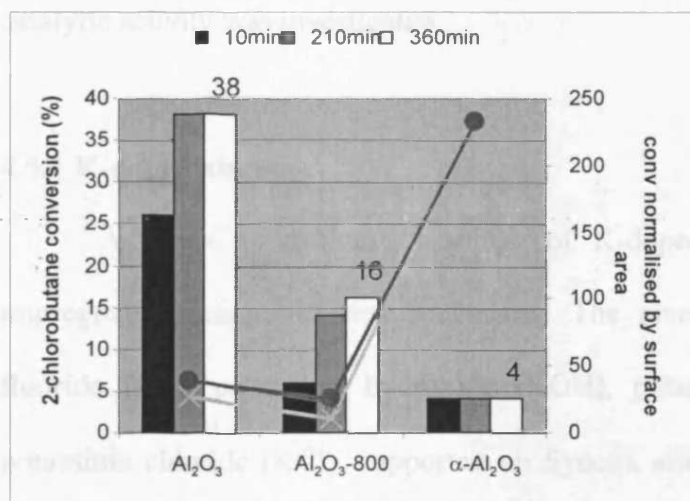


Fig 4.20: Catalytic activity for various types of alumina, include pure γ - Al_2O_3 (500°C), Al_2O_3 -800 and α - Al_2O_3 (1200°C). Secondary Y-axis shows the conversion after normalised by the surface area.

Reaction conditions: 135°C for 6h, 100mg of catalyst and $60\text{ml}\cdot\text{min}^{-1}$ total flow rate

On the other hand, α - Al_2O_3 is a crystallite compound with low surface area. It has been well-known for its inert properties¹ and its low surface area has discouraged interaction between the reactant and catalyst surface. Thus, low activity for α - Al_2O_3 was obtained.

4.5 Alkaline-doped alumina

Most of the alkaline-doped oxides show surface basicity. So far, the surface acidic site has been proven to be important for the catalytic dehydrochlorination of 2-

chlorobutane, but the Al_2O_3 -800 whose has lower activity. However, we cannot rule out the presence of the basic sites in alumina that might contribute to the catalytic activity due to an acid-base cooperative effect^{24,33}. Basic sites are indispensable for stabilizing carbonium ions³⁷. The acidic site is important for the abstraction of the Cl^- , whereas the intermediate carbonium ion is bound to the basic site over a hydrogen bridge bond. Therefore, we studied the use of a series of alkaline-doped alumina catalysts as base catalysts for the catalytic dehydrochlorination of 2-chlorobutane. Two types of alkaline-doped alumina catalysts were prepared, the K-doped and Na-doped alumina catalysts. The correlation between the acid-base properties and the catalytic activity was investigated.

4.5.1 K-doped aluminas

A series of different loadings of K-doped aluminas were prepared by impregnation using different precursors. The precursors used include potassium fluoride (KF), potassium hydroxide (KOH), potassium carbonate (K_2CO_3), and potassium chloride (KCl), supported on Syntex alumina ($\gamma\text{-Al}_2\text{O}_3$). These catalysts were characterised by employing N_2 -adsorption, AAS, XRD, SEM, TPR and selective chemisorption of CO_2 techniques. Finally, a selection of K-doped aluminas were tested for the catalytic dehydrochlorination of 2-chlorobutane.

4.5.1.1 The characteristic of K-doped aluminas

4.5.1.1.1 BET surface area

Table 4.7 shows the surface area data for different types of K-doped aluminas obtained from N_2 adsorption with the K metal loadings determined by atomic absorption spectroscopy (AAS). The results show that the BET surface area is not

significantly altered by addition of small amount of potassium salt (<5wt%). However, a decrease in BET surface area can be observed for the 10wt% and 20wt% K-doped aluminas. The result indicates that good dispersions can be achieved by impregnating small loadings of potassium compounds on the alumina support. Higher potassium loadings resulted in a decrease in BET surface area, which may be due to the limitation of impregnation method that caused multi-layer coverage of compounds and blocked the surface active sites of alumina²³. Note that the estimated experimental error for BET area is approximately 5%.

Table 4.7: The BET area and actual K loadings for K-doped alumina catalysts.

Samples	$\mu\text{mol K}$ per gram of $\gamma\text{-Al}_2\text{O}_3$	BET (m^2g^{-1})
$\gamma\text{-Al}_2\text{O}_3$	0	290
1wt%KF- Al_2O_3	172	300
5wt%KF- Al_2O_3	860	270
10wt%KF- Al_2O_3	1720	231
20wt%KF- Al_2O_3	3440	159
0.2wt%KOH- Al_2O_3	35	313
0.5wt%KOH- Al_2O_3	89	313
1wt%KOH- Al_2O_3	178	280
5wt%KOH- Al_2O_3	890	280
10wt%KOH- Al_2O_3	1780	239
20wt%KOH- Al_2O_3	3560	161
1wt% K_2CO_3 - Al_2O_3	72	310
1wt%KCl- Al_2O_3	134	300

4.5.1.1.2 X-ray diffraction (XRD)

X-ray diffraction analysis was performed to investigate the crystalline phase of K-doped alumina catalysts. Various loadings of KOH, KF, K_2CO_3 and KCl were supported on $\gamma\text{-Al}_2\text{O}_3$. All of the K-doped aluminas exhibited the XRD pattern of the initial $\gamma\text{-Al}_2\text{O}_3$ support, except for KCl- Al_2O_3 and KF- Al_2O_3 .

The XRD pattern of KCl- Al_2O_3 shows the crystalline KCl was formed readily even at low potassium loading. 2θ of 28.5° , 40.5° and 50.2° were assigned to the

presence of crystalline KCl phase as indicated later in Fig 4.29. On the other hand, Fig 4.21 illustrates the XRD patterns of KF-Al₂O₃ with 1, 5, 10 and 20wt% of loadings. The patterns showed that absence of sharp peaks for 1 and 5wt% of KF-Al₂O₃, indicating good dispersion of potassium species on the γ -Al₂O₃ support. The sample became more crystalline when the KF content was increased. For 10wt% KF-Al₂O₃, sharp peaks at 2 θ of 31.1°, 38.8° and 44.8° are attributed to the existence of KOH and/or K₂CO₃. Both KOH and K₂CO₃ have the most intense peak at 2 θ of 30.9° and 31.0°, respectively, which is hard to distinguish. The XRD pattern for 20wt% of KF-Al₂O₃ shows distinctive peaks at 2 θ of 29.8°, 36.6°, 42.8° and 53.2°, suggesting the formation of K₃AlF₆ crystalline phase. It is known that a K₃AlF₆ is formed by the reaction of aqueous KF and alumina^{38,39}.

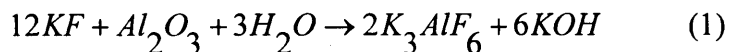
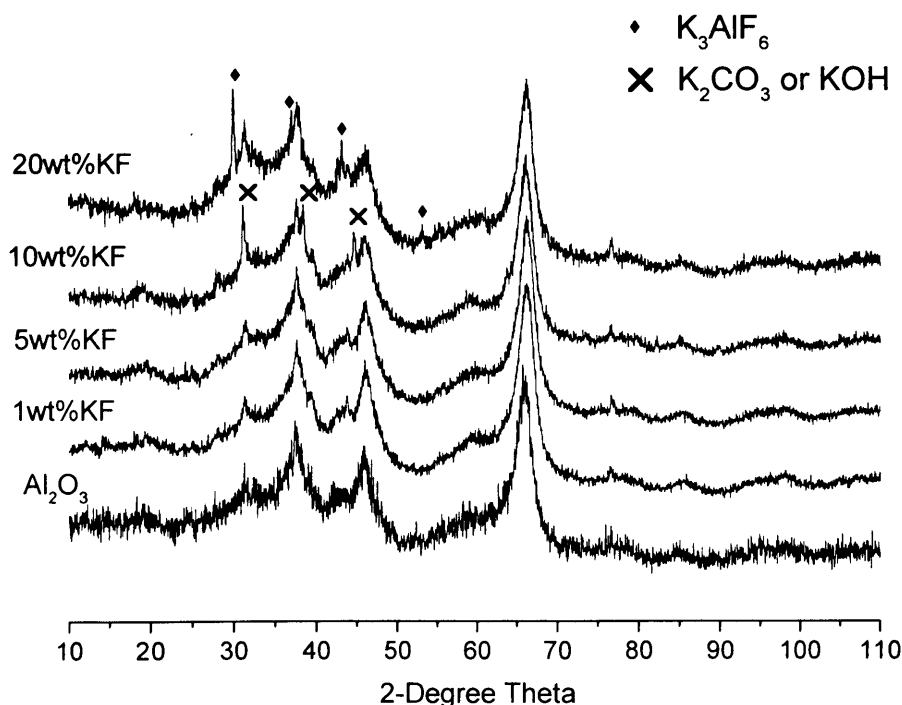


Fig 4.21: XRD patterns of KF-Al₂O₃ catalysts.



Weistock *et al* found the presence of potassium carbonate by IR spectroscopy³⁹. Based on these results, they concluded that the formation of potassium hydroxide and/or carbonate was a consequence of the reaction of potassium fluoride with alumina. The carbonate was formed by the reaction of atmosphere CO₂, and KOH formed by reaction (1) during the drying procedure

4.5.1.1.3 Scanning electron microscopy (SEM)

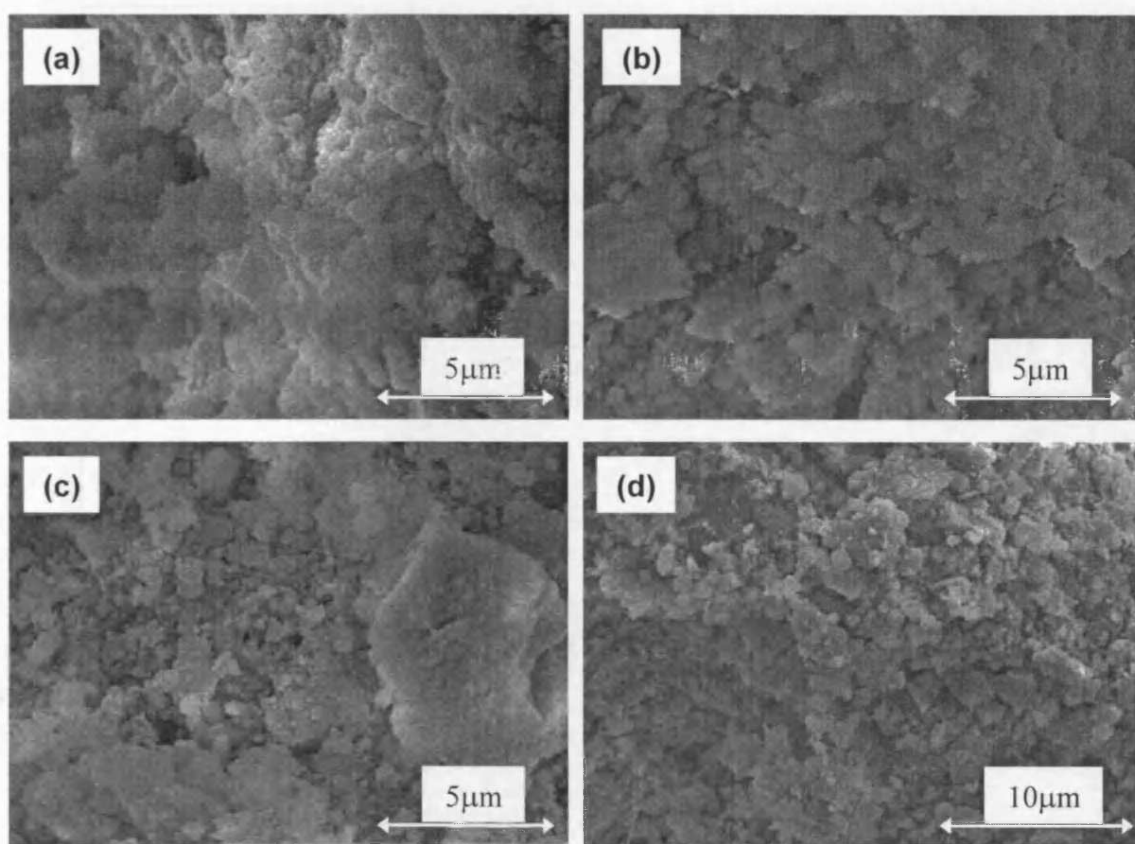
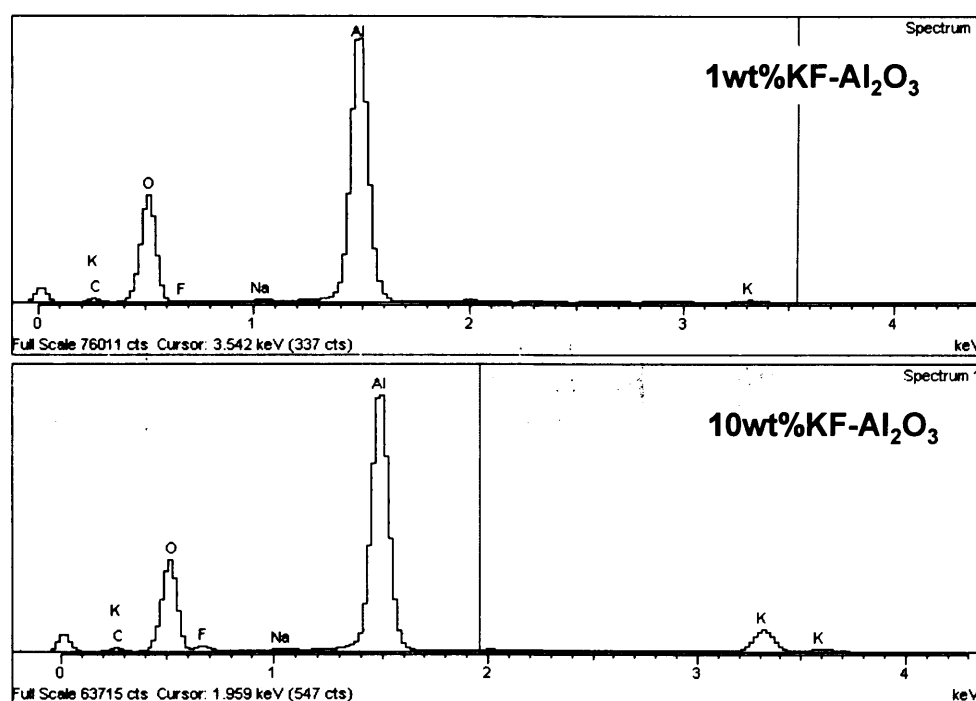


Fig 4.22: SEM of KF-Al₂O₃ and KOH-Al₂O₃ catalysts. (a) 1wt% KF, magnification ×12000, (b) 10wt% KF, ×12000, (c) 1wt% KOH, ×12000, and (d) 10wt% KOH, ×6500 of magnification.

Scanning electron microscopy was used to identify the shape and size for K-doped alumina catalysts. Fig 4.22 shows the SEM micrograph for KOH-Al₂O₃ and KF-Al₂O₃ with 1wt% and 10wt% of loadings. All samples revealed an amorphous form, similar as the γ -Al₂O₃ support. The pictures show aggregates of particles in sphere and other shapes, with about 1 μ m size in diameter.

While performing the SEM analysis, EDX x-ray analysis of $\text{KF-Al}_2\text{O}_3$ catalysts was also taken to confirm the composition of the samples. As shown in Fig 4.23, the presence of the fluorine peak for 10wt% $\text{KF-Al}_2\text{O}_3$ confirmed the presence of fluoride. The absence of a fluorine peak for 1wt% $\text{KF-Al}_2\text{O}_3$ was due to the low KF loading and the result was consistent with the decrease in the intensity for the potassium peak.

Fig 4.23: EDX spectrum of $\text{KF-Al}_2\text{O}_3$ catalysts.



4.5.1.1.4 Basic sites on K-doped alumina

Selective chemisorption of carbon dioxide was performed to determine the amount and the strength of basicity for various types of K-doped alumina catalysts. It was assumed that one molecule of carbon dioxide reacts with one basic site. Table 4.8 shows the basic properties for different loadings of KOH, KF, K_2CO_3 and KCl supported on alumina catalysts. The chemisorption of carbon dioxide over different loadings of $\text{KOH-Al}_2\text{O}_3$ ranges from 0.2wt% to 5wt% of KOH, revealed an increase of the amount of basic site as the KOH loading increased. The result indicates that the

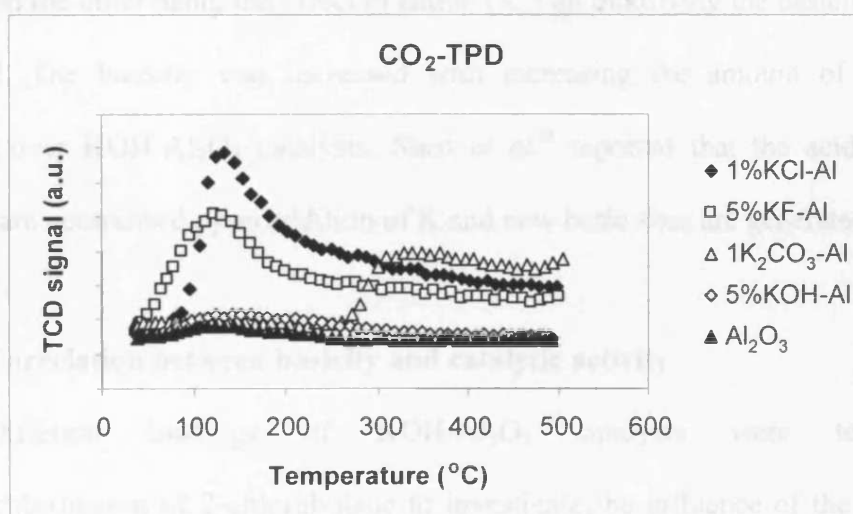


addition of 1wt% of KOH has doubled the number of basic site of γ -Al₂O₃. The TPD desorption peak temperature at 120°C suggests that the KOH-Al₂O₃ catalysts consist of basic sites with intermediate strength, similar to γ -Al₂O₃ (Fig 4.24).

Table 4.8: Basic properties of K-doped alumina catalysts.

Catalysts	TPD		Adsorbed CO ₂ (Basic site)	
	T _{max} (°C)	(molec·m ⁻²)×10 ¹⁶	μmol·g ⁻¹	
γ -Al ₂ O ₃ (Synetix)	120	20	95	
0.2%KOH-Al ₂ O ₃	120	16	84	
0.5%KOH-Al ₂ O ₃	120	31	163	
1% KOH-Al ₂ O ₃	120	40	186	
5% KOH-Al ₂ O ₃	120	69	334	
1%KF-Al ₂ O ₃	100	32	157	
5%KF-Al ₂ O ₃	120	37	166	
1%K ₂ CO ₃ -Al ₂ O ₃	310	60	309	
1%KCl-Al ₂ O ₃	120	38	188	

Fig 4.24: TPD of CO₂ adsorbed over K-doped aluminas at 40°C, followed by desorption with temperature programmed from 40 to 500°C at 20°C·min⁻¹.



The addition of various potassium precursors with the same loading (1wt %) shows the number of basic sites per m² for the K-doped alumina decrease followed the order: K₂CO₃ > KOH ≈ KCl > KF. The TPD results revealed that except for K₂CO₃-Al₂O₃, other potassium precursors show the presence of weak basic sites that

was close to γ - Al_2O_3 . K_2CO_3 - Al_2O_3 revealed stronger basicity with desorption peak observed at 310°C . The result indicates that the basicity of K-doped aluminas was influenced by the precursor used.

Handa *et al*⁴⁰ studied the characterisation of strong bases by performing the isomerisation of 2,3-dimethylbut-1-ene and the decomposition of 2-methyl-3-butyn-2-ol as test reactions. The isomerisation of 2,3-dimethylbut-1-ene is a base-catalysed reaction, and is useful for determining the relative activities of strong bases. The decomposition of 2-methyl-3-butyn-2-ol is a suitable reaction to discriminate acidic and basic catalysts^{41,42}. They conclude that the basicity of various potassium compounds followed the order: $\text{K}_2\text{CO}_3 > \text{KOH} > \text{KF}$. Our results are consistent with the basicity order that reported by Handa *et al*, supporting the effects of the anion on the catalyst basicity.

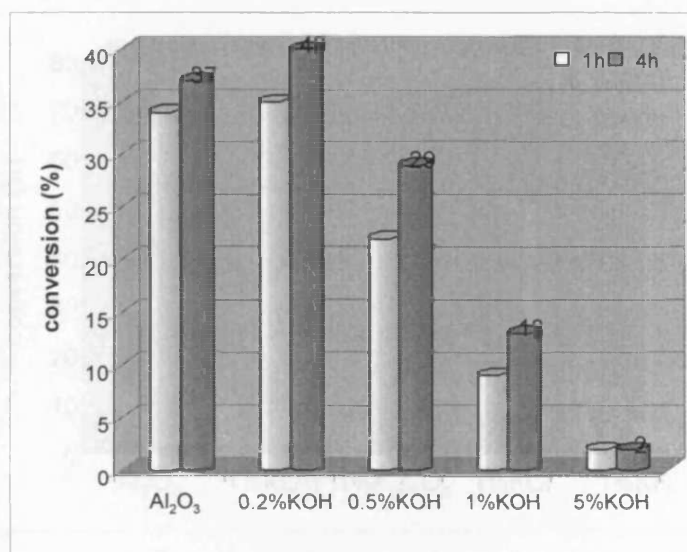
On the other hand, the effect of cation (K^+) on modifying the basicity was also observed. The basicity was increased with increasing the amount of potassium loadings over $\text{KOH-Al}_2\text{O}_3$ catalysts. Shen *et al*⁴³ reported that the acidic sites of alumina are neutralised upon addition of K and new basic sites are generated.

4.5.1.2 Correlation between basicity and catalytic activity

Different loadings of $\text{KOH-Al}_2\text{O}_3$ catalysts were tested for dehydrochlorination of 2-chlorobutane to investigate the influence of the potassium loadings (K^+) on the activity. Fig 4.25 shows the conversion of 2-chlorobutane at 135°C recorded at 1h and 4h (under steady state reaction) over various loadings of $\text{KOH-Al}_2\text{O}_3$ ranging from 0.2wt% to 5wt% loadings. The conversion shows slight increase with the addition of small KOH loading (0.2wt %). However, the conversion decreases as the KOH loading is increased. The addition of 1wt% of KOH decreased

the conversion to less than half. The catalyst becomes relatively inactive with higher loadings (>1wt%) of KOH on alumina. The result indicates that the addition KOH on alumina blocked the active sites of alumina and resulted in a decrease on activity. Further additions of KOH causes further deactivation.

Fig 4.25: 2-chlorobutane conversion recorded at 1h and 4h time online over different loadings of KOH- Al_2O_3 catalysts ranges from 0.2 to 5wt%. Reaction conditions: 135°C, 100mg of samples weight and 100ml·min⁻¹ of total flow rate (GSHV=55000h⁻¹).

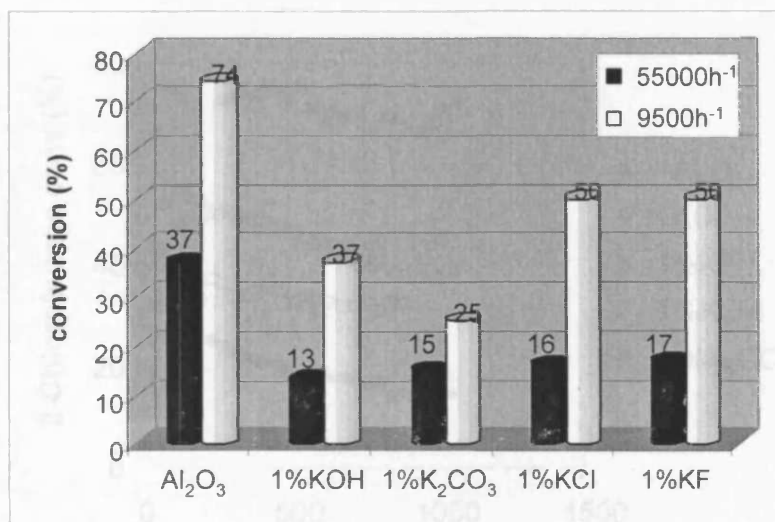


These data proposed that the exposed $\gamma\text{-Al}_2\text{O}_3$ surface catalysed the dehydrochlorination of 2-chlorobutane. As we mentioned before, the addition of K^+ increased the basicity and neutralised the acidic sites of $\gamma\text{-Al}_2\text{O}_3$ support⁴³. Thus, the deactivation of catalysts upon increasing K^+ loadings (and basicity), strongly support the proposal that the dehydrochlorination of 2-chlorobutane is acid-catalysed, exceptional case to $\text{Al}_2\text{O}_3\text{-800}$. The Lewis acid site of alumina is the active site for this reaction.

On the other hand, a series of K-doped alumina catalysts prepared by using different precursors with the same loading were compared. 1wt% of KF, KOH, K_2CO_3 and KCl were supported on $\gamma\text{-Al}_2\text{O}_3$. Fig 4.26 illustrates the conversion for various types of K- Al_2O_3 catalysts with the same loading. Under normal reaction

conditions (with GHSV=55000h⁻¹), all K-doped alumina catalysts exhibited similar 2-chlorobutane conversion which ranges from 13 to 17% with approximately 5% of experimental error. Therefore, the reactions over K-doped aluminas were repeated with a slight change of reaction condition from GHSV of 55000h⁻¹ to 9500h⁻¹.

Fig 4.26: 2-chlorobutane conversion recorded at 4h (under steady state reaction) over various K-doped alumina catalysts with same loading. The reaction was performed 135°C with GHSV of 55000 or 9500h⁻¹.



The reactivity over different types of K-doped alumina at 135°C with GHSV of 9500h⁻¹, followed the order of KCl ≈ KF > KOH > K₂CO₃. This is exactly the opposite to the order of the catalyst basicity. Presumably the abstraction of the chloride ion is the rate determining step; when the chloride interacts with the Lewis acid sites, some of the electronic charge was transferred to the cation. When a more basic carbonate was present, the carbonate competes with the chloride to interact with the cation³⁷ and results in a decrease in activity. Thus, the influence of the anion is evidenced.

Based-on the results, a relationship has been found between the total amount of base and the catalytic activities of K-doped aluminas that is the activity decrease with increasing amount of basic sites. The effect of anions was less profound than

cations, may be due to the greater difficulty of varying anions (and different basicity)³⁷. However, the fact that the dehydrochlorination activity increases in the opposite order as the base amounts, indicates that the presence of basic sites inhibited the catalyst activity.

4.5.1.2.1 Catalytic performance

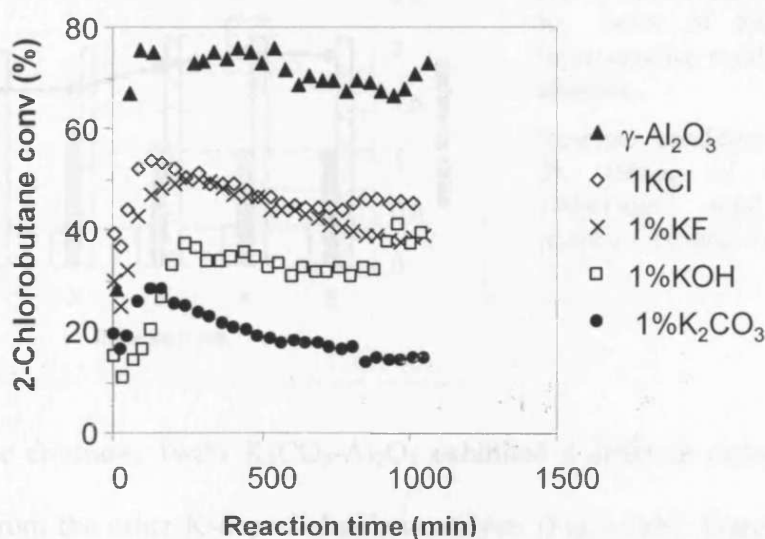


Fig 4.27: Reaction profiles for dehydrochlorination of 2-chlorobutane over various K-doped alumina catalysts at 135°C. Reaction conditions: 300mg of sample weight and 60mlmin⁻¹ total flow rate (GHSV= 9500h⁻¹).

Fig 4.27 illustrates the reaction profile for catalytic dehydrochlorination of 2-chlorobutane over a series of 1wt% of K-doped aluminas, with $\gamma\text{-Al}_2\text{O}_3$ as a reference. The results show similarity to that of the pure $\gamma\text{-Al}_2\text{O}_3$, in which the conversion was initially low and increased slowly until a steady state was reached. These agree with the proposal that the exposed alumina surface is the active site for the reaction. There is no significant deactivation can be observed for K-doped alumina catalysts.

Despite the addition of K^+ on alumina resulting in a decrease in conversion, all the K-doped alumina catalysts were found highly selective to the isomers of butene with 100% selectivity and no by-product was detected. All K-doped alumina catalysts except for $\text{K}_2\text{CO}_3\text{-Al}_2\text{O}_3$, exhibited a similar product distribution. The 1wt% KOH-

Al_2O_3 for the dehydrochlorination of 2-chlorobutane is used as a representative result. As shown in Fig 4.28a, the results illustrate that cis-2-butene is the dominant product, followed by trans-2-butene and 1-butene, the ratio being about 60%, 30% and 10%, respectively. The preferential formation of cis-2-butene indicates that the reaction was acid-catalysed⁹⁻¹¹.

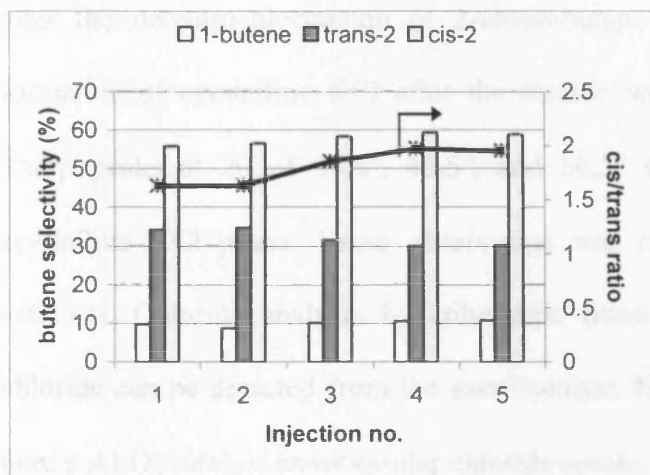


Fig 4.28a: Product distribution for 1wt% of $\text{KOH-Al}_2\text{O}_3$ as representative result for K-doped alumina.

Reaction conditions: 135°C for 5h, 100mg of catalyst and $100\text{ml}\cdot\text{min}^{-1}$ total flow rate ($\text{GHSV}=55000\text{h}^{-1}$).

On the contrary, 1wt% $\text{K}_2\text{CO}_3\text{-Al}_2\text{O}_3$ exhibited a different order of product distribution from the other K-doped alumina catalysts (Fig 4.28b). Trans-2-butene is the main product, followed by the cis-2-butene and 1-butene. This catalytic behaviour indicates a different mechanism might take place for $\text{K}_2\text{CO}_3\text{-Al}_2\text{O}_3$ catalyst. The preferential formation of trans-2-butene indicates strong basicity for $\text{K}_2\text{CO}_3\text{-Al}_2\text{O}_3$ catalyst.

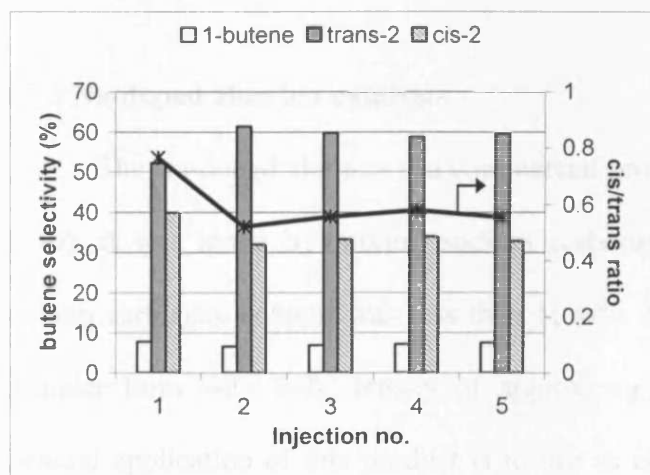


Fig 4.28b: Product distribution for 1wt% of $\text{K}_2\text{CO}_3\text{-Al}_2\text{O}_3$.

4.5.1.3 Post-reaction analysis

X-ray diffraction was performed to observe the changes on the crystalline phase for the used catalysts. 5wt% KF-Al₂O₃ was used as a representative result for all K-doped alumina, except for KCl- Al₂O₃ whose contains chloride in the fresh catalyst. Fig 4.29 depicts the XRD patterns of 5wt%KF-Al₂O₃ catalysts, before and after the dehydrochlorination of 2-chlorobutane. The results clearly showed the formation of crystalline KCl after the sample was exposed to the 2-chlorobutane. Sharp peaks at 2θ of 28.5°, 40.5°, and 50.2° were assigned to the presence of crystalline KCl phase. Same observation was obtained for all K-doped alumina catalysts. Chloride analysis by columetric titration indicated that about 5wt% of chloride can be detected from the used catalyst. Note that all K-doped aluminas and pure γ-Al₂O₃ catalyst show similar chloride uptake of 5.5wt% ± 1.5.

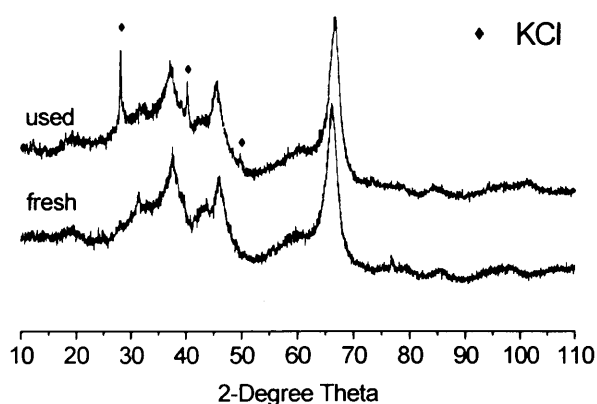


Fig 4.29: 5wt%KF-Al₂O₃ before and after reaction. Sharp peaks at 28.5°, 40.5° and 50.2° of 2θ revealed the existence of KCl for the used catalyst.

4.5.2 Na-doped alumina catalysts

The Na-doped alumina is a commercial product supplied by Syntex (Puraspec 2240). It was made by mixing sodium carbonate and alumina trihydroxide. The sodium carbonate content was less than 10wt%. Na-doped alumina is supplied in a granular form with bulk density of approx. 1g·ml⁻¹, pH 9.5 and is hygroscopic. General application of this product is to use as chloride removal in the purification

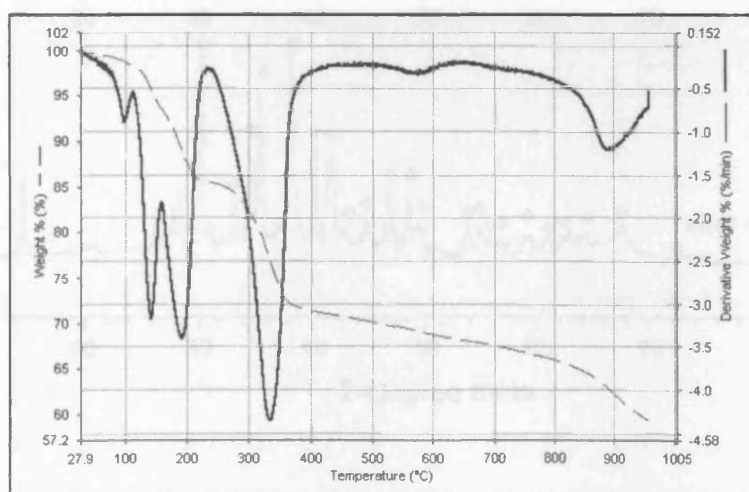
system The BET area was $100\text{m}^2\text{g}^{-1}$. The Na-doped alumina was characterised by thermogravimetric analysis (TGA), nitrogen adsorption (BET) and x-ray diffraction (XRD) techniques. Finally, Na-doped alumina was also tested for the catalytic dehydrochlorination of 2-chlorobutane.

4.5.2.1 Catalyst characterisations

4.5.2.1.1 Thermogravimetric analysis (TGA)

Fig 4.30 illustrates the TGA pattern for the sodium alumina sample. The result showed that the sample exhibited numerous weight losses at $100\text{-}250^\circ\text{C}$, 350°C , 550°C and 900°C . Weight losses occurring below 400°C are ascribed to the dehydration of Na-doped alumina and the decomposition of aluminium trihydroxide. Heating alumina at above 500°C causes the loss of surface hydroxyl group⁴⁴. The weight loss at 850°C could be attributed to the decomposition of sodium carbonate, as the carbonates generally decomposed at high temperature ($>500^\circ\text{C}$). The result indicates that several transition states can be obtained for Na-doped alumina dependent on the pre-treatment temperature used. Thus, Na-doped alumina was pre-treated by heating at 400°C for 3h before use.

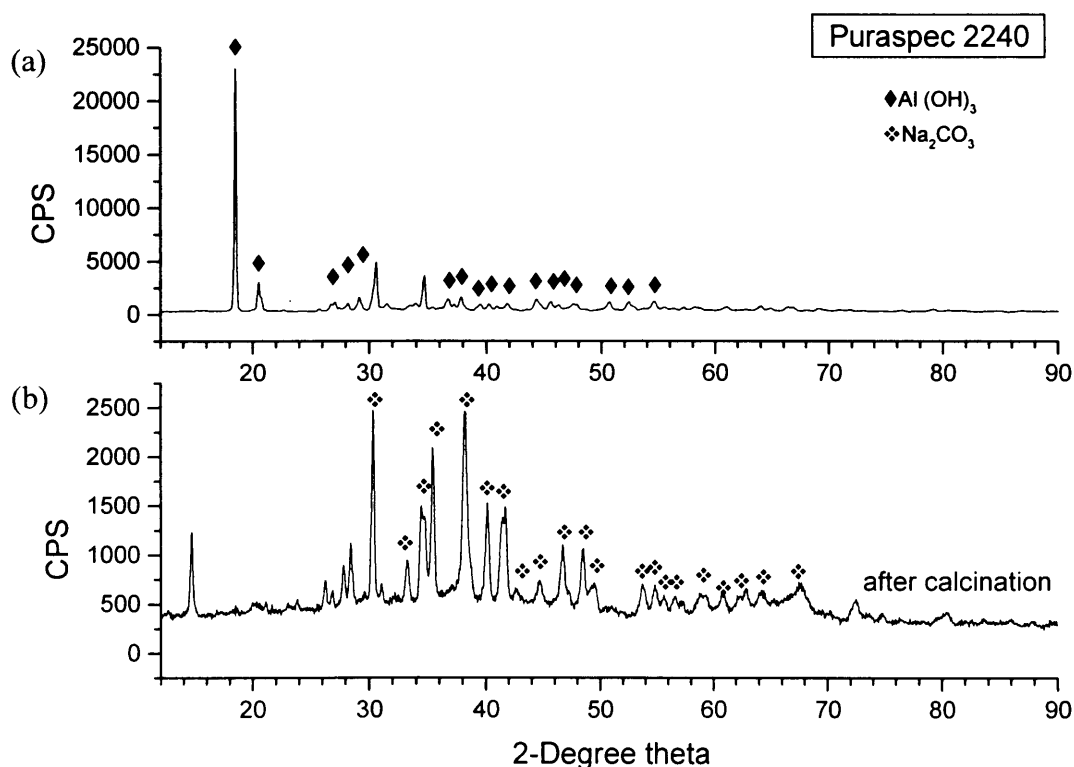
Fig 4.30: TGA analysis of the Na-doped alumina catalyst



4.5.2.1.2 X-ray diffraction (XRD)

Fig 4.31 shows the XRD patterns of the Na-doped aluminas: the fresh sample and the sample after the thermal treatment at 400°C. The result clearly shows the high crystallinity of the fresh Na-doped alumina, mostly dominated by aluminium trihydroxide. Sharp peaks due to the presence of aluminium trihydroxide and sodium carbonate can be observed. The XRD patterns of the sample after pre-treatment by heating at 400°C, revealed only the crystalline sodium carbonate phase. These results suggest that the fresh sample was comprised of aluminium trihydroxide and sodium carbonate. Decomposition of aluminium trihydroxide to form amorphous alumina occurred during the calcination step with crystalline sodium carbonate being predominant.

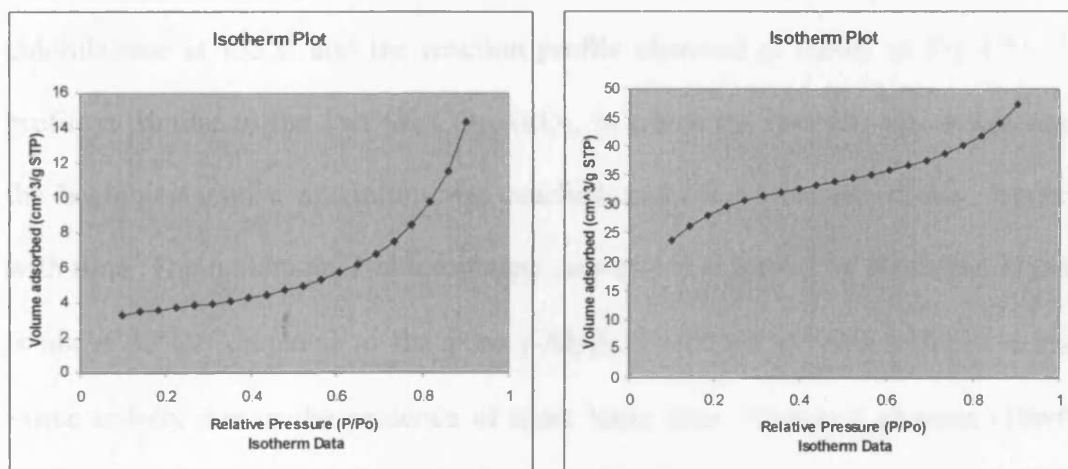
Fig 4.31: XRD patterns of Na-doped alumina catalysts. (a) Fresh sample and (b) sample after calcination at 400°C.



4.5.2.1.3 N₂-adsorption (BET)

N₂-adsorption was performed to observe the BET isotherms of Na-doped aluminas before and after the calcination. Fig 4.32 shows a type III¹⁵ isotherm was observed for the fresh Na-doped alumina, indicating weak interaction between the adsorbate-adsorbent as a consequence of large amount of water retention on the sample. After the sample was heated at 400°C, a typical type II BET plot was obtained (also see Appendix C). The BET isotherm shows the Na-doped alumina after calcination has a surface area of approx. 100m²g⁻¹. These results are consistent with the TGA curves and the XRD spectra, that the initial Na-doped alumina is rich in water content and with high crystallinity. A more stable amorphous compound was formed after the calcination at 400°C and has BET area of 100m²g⁻¹.

Fig 4.32: BET isotherm of 10wt% Na₂CO₃-Al₂O₃ catalyst: (a) fresh sample, and (b) after calcination.



4.5.2.1.4 Basic sites of Na-doped alumina

The amount of basic sites and the strength of basicity for Na-doped alumina were measured by the adsorption and desorption of carbon dioxide (TPD-CO₂). Table 4.9 shows the basic properties for Na-doped alumina with K₂CO₃-Al₂O₃ and pure γ -Al₂O₃ as references. The amount of adsorbed carbon dioxide per site is the greatest for

Na-doped alumina, and the TPD peak temperatures revealed the presence of weak basic sites, which is different from that of the $\text{K}_2\text{CO}_3\text{-Al}_2\text{O}_3$ but same as the pure $\gamma\text{-Al}_2\text{O}_3$ (see Fig 4.24). The strong basicity of Na-doped alumina may be attributed to the high Na_2CO_3 loadings on Al_2O_3 .

Table 4.9: Basic properties of Na-doped alumina

samples	Basicity (CO_2)		
	Na-doped Al_2O_3 (10wt% $\text{Na}_2\text{CO}_3\text{-Al}_2\text{O}_3$)	1wt% $\text{K}_2\text{CO}_3\text{-Al}_2\text{O}_3$	$\gamma\text{-Al}_2\text{O}_3$
BET (m^2g^{-1})	100	310	290
TPD, T_{max} ($^\circ\text{C}$)	100	310	120
Active sites ($\mu\text{mol.g}^{-1}$)	201	309	95
Active sites ($\text{molecule.m}^{-2} \times 10^{16}$)	121	60	20

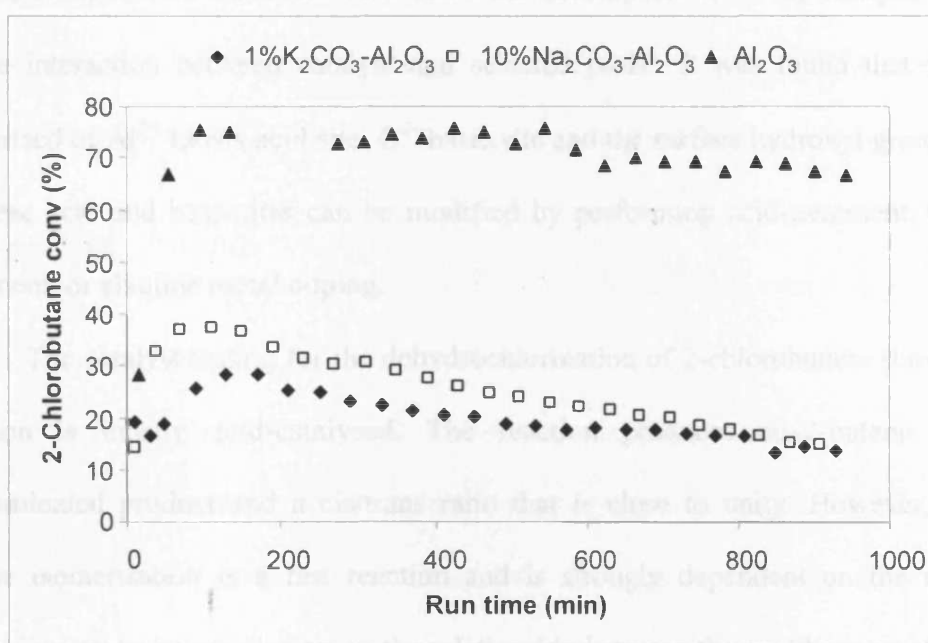
4.5.2.2 Catalytic activity

Na-doped alumina was tested for the catalytic dehydrochlorination of 2-chlorobutane at 135°C and the reaction profile observed is shown in Fig 4.33. The profile is similar to the $1\text{wt}\%\text{K}_2\text{CO}_3\text{-Al}_2\text{O}_3$, in which the reaction was increasing at the beginning until a maximum was reached, and the conversion slowly decreases with time. The maximum 2-chlorobutane conversion achieved by Na-doped alumina is about 40%. Compared to the pure $\gamma\text{-Al}_2\text{O}_3$, Na-doped alumina exhibits a much lower activity due to the presence of more basic sites. Na-doped alumina (10wt%) whose has larger amount of basic sites than $1\text{wt}\%\text{K}_2\text{CO}_3\text{-Al}_2\text{O}_3$ shows better activity.

The result suggests that the high reactivity of the Na-doped alumina (10wt%) may be due to the contribution of the bifunctional effect of the carbonates that can also serve as a Lewis acid site, apart from neutralising the acidic site of alumina. However, the carbonate Lewis acid site reacted strongly with the 2-chlorobutane reactant to form NaCl crystallites that cause catalyst deactivation. The product distribution for Na-doped alumina is exactly the same as for $1\text{wt}\%\text{K}_2\text{CO}_3\text{-Al}_2\text{O}_3$. The catalyst was

100% selective to the isomers of butene and HCl. The preferential formation of trans-2-butene indicates the basic properties of Na-doped alumina, followed by cis-2-butene and 1-butene. The reaction possibly proceeds *via* an E1cB mechanism on a base catalyst⁹⁻¹¹, the reaction begins with the rupture of the C-H bond. After the strong interaction between the reactant and catalyst, irreversible chlorination of catalyst resulted in poisoning of the catalyst.

Fig 4.33: Reaction profile for Na-doped alumina ($\text{Na}_2\text{CO}_3\text{-Al}_2\text{O}_3$), $\text{K}_2\text{CO}_3\text{-Al}_2\text{O}_3$ with pure $\gamma\text{-Al}_2\text{O}_3$ as references. Reaction conditions: 135°C, 300mg of sample and $60\text{ml}\cdot\text{min}^{-1}$ of total flow (GHSV=9500 h^{-1}).



A post reaction analysis by x-ray diffraction (XRD) was performed over Na-doped alumina to observe the changes on the crystalline phase. As with all alkaline doped catalysts, the NaCl crystallites are readily formed. Nonetheless, quantitative chloride analysis by coulometric titration shows that the chloride uptake for $\text{Na}_2\text{CO}_3\text{-Al}_2\text{O}_3$ was as much as 10wt%.

4.6 Conclusions

Several alumina-based catalysts obtained from acid-treatment, thermal treatment and alkali-doping were characterised using BET, XRD, SEM, XPS, TGA and TPD techniques. XRD patterns showed the initial crystalline phase of each catalyst that the amorphous material was obtained in most cases, except for the α -alumina and sodium-alumina. The result was always in agreement with the BET surface area obtained ranging between $190\sim 290\text{m}^2\text{g}^{-1}$. The SEM micrograph also revealed the amorphous surface of the catalyst. XPS was employed to monitor the surface composition. TGA and TPD show the decomposition of the catalyst, as well as the interaction between catalyst and selected probe. It was found that $\gamma\text{-Al}_2\text{O}_3$ comprised of Al^{3+} Lewis acid site, O^{2-} basic site and the surface hydroxyl group. Each of these acid and base sites can be modified by performing acid-treatment, thermal treatment, or alkaline metal doping.

The catalyst testing for the dehydrochlorination of 2-chlorobutane showed the reaction is mostly acid-catalysed. The reaction produces cis-2-butene as the predominated product and a cis/trans ratio that is close to unity. However, as the butene isomerisation is a fast reaction and is strongly dependent on the reaction kinetic, we make no conclusion on the relationship between the acid-base reaction and the cis/trans ratio. On the other hand, it was found that the dehydrochlorination reaction took place at the Lewis acid site of $\gamma\text{-Al}_2\text{O}_3$, and the acidity can be improved *via* chlorination or thermal treatment. However, the increase in acidity by thermal treatment at above 800°C over $\gamma\text{-Al}_2\text{O}_3$ resulted in the loss of surface hydroxyl groups, and hence, a decrease on activity. This suggests that the importance of the surface hydroxyl groups on alumina in the dehydrochlorination of 2-chlorobutane. The butene selectivity for alumina was always above 99.9%, with trace amount of octene detected

as secondary hydrocarbon product. HCl was the only chlorinated product obtained from the reaction and was collected in a sodium hydroxide solution for further analysis. Unfortunately, quantitative analysis was not possible by neutralisation titration due to rapid pH change at the end point. The HCl detector tube was used to perform qualitative analysis and to confirm the production of HCl.

Doping alkaline on γ -Al₂O₃ were also prepared to study the catalytic dehydrochlorination of 2-chlorobutane over base catalysts. All the base catalysts tested were shown lower conversions than pure alumina. The addition of alkaline metal inhibited the performance of the γ -alumina, causes loss of the Lewis acid sites as a consequence of neutralisation. Nevertheless, decreasing the metal loading (< 0.5wt%) regenerated the Lewis sites of alumina. The result indicates that the exposed alumina surface was the active site for the reaction. Note that all base catalysts gave 100% selectivity to butene with no by-products detected. Special attention was paid to the K₂CO₃-Al₂O₃ and Na₂CO₃-Al₂O₃ catalysts that form trans-2-butene as the most selective product. This indicates a base-catalysed dehydrochlorination reaction may occur over these catalysts. It is important to mention that although the catalytic dehydrochlorination occurs mostly *via* the acid sites, we cannot deny the ability of basic sites to stabilise the carbocation might be beneficial to the catalytic activity.

Post reaction analysis by XRD, XPS and coulometric titration methods clearly show that chlorination of all catalysts occurred in bulk (alkaline-metal) and on the surface (alumina-based) of the catalyst. The chloride formation gives rise to a change of the surface properties. Quantitative chloride analysis of used catalysts show the chloride uptake was between 5~10 % by weight.

References

1. M. Howe-Grant, Kirk-Othmer Encyclopedia of Chemical Technology (1985). John Wiley & Sons. Vol 2, Aluminium and Alloys, p140; Aluminates, p197; Aluminum oxides, p218.
2. Butler and Harrod, "Inorganic Chemistry, Principle and Applications". (1989), The Benjamin/ Cummings Publishing Company, Inc.
3. Well, "Structural Inorganic Chemistry", Clarendon Press Oxford.
4. F. A. Cotton and G. Wilkinson, "Advanced Inorganic Chemistry". 5th edition, John Wiley & Sons. 211
5. S. Yamaguchi, *Nippon Kagaku Kaishi (1921-47)*, **55** (1934) 1227-31 & 1232-5
6. E.W. Gardiner, J. W. Greene, A.L. Lyman (1937), US 2082203 19370601
7. H. Tominaga, T. Nakamura, H. Arai, T. Kunugi, *Kogyo Kagaku Zasshi*, **74:2** (1971) 199-203
8. A. Suzuki, K. Sakuma, T. Onda, *Kogyo Kagaku Zasshi*, **74:7** (1971) 1375-7
9. I. Mochida, A. Uchino, H. Fujitsu, K. Takeshita, *Journal of Catalysis*, **43:1-3** (1976) 264-72
10. I. Mochida, J. I. Take, Y. Saito, Y. Yoneda, *Journal of Organic Chemistry*, **32** (1967) 3894
11. I. Mochida, Y. Akio, A. Kato, T. Seiyama, *Journal of Organic Chemistry*, **39:25** (1974) 3785-7
12. I. Mochida, A. Uchino, H. Fujitsu, K. Takeshita, *Journal of Catalysis*, **51:1** (1978) 72-9
13. H. Vinek, H. Noller, *Zeitschrift fuer Physikalische Chemie (Muenchen, Germany)*, **102:5-6** (1976) 255-65
14. H. Vinek, H. Noller, *Zeitschrift fuer Physikalische Chemie (Muenchen, Germany)*, **102:5-6** (1976) 247-54
15. Attard and Barnes, "Surfaces". (1998), Oxford University Press.
16. K. Tanabe, "Solid Acids and Bases: their catalytic properties". (1970), Academic Press
17. M.C. Abello, A. P. Velasco, .O.F. Gorritz, J.B. Rivarola, *Applied Catalysis A-General*, **129** (1995) 93-100
18. H. Pines and W. O. Haag, *Journal of American Chemical Society*, **82** (1960) 2471
19. E. P. Parry, *Journal of Catalysis*, **2** (1963) 371
20. H. Pines and J. Manassen, "Advances in Catalysis". (1966), Academic Press. 16: p. 49
21. S.G. Hindin, S. W. Weller, *Journal of Physical Chemistry*, **60** (1956) 1501
22. H. Knozinger, G. Buhl, K. Kochloeff, *Journal of Catalysis*, **24** (1972) 57
23. M.V. Twigg, "Catalyst Handbook". 2nd edn. (1989) London, England, Wolfe Publishing Ltd.
24. H. Hattori, *Chemical Review*, **95** (1995) 537-558
25. J. Mendham, R.C. Denney, J.D. Barnes, M. Thomas, "Vogel's Quantitative Chemical Analysis". 6th edition (2000), Prentice Hall. p. 341
26. Kitagawa HCl detector tube no. 173SA,
http://www.komyokk.co.jp/pdata/tpdf/173SA_1.pdf
27. T.H. Ballinger, Jr. J. T. Yates, *Journal of Physical Chemistry*, **96:3** (1992) 1417-23
28. C. Pistarino, E. Finocchio, G. Romezzano, F. Bricchese, R. Di Felice, and G. Busca; M. Baldi, *Industrial & Engineering Chemistry Research*, **39** (2000) 2752-2760

-
29. Z. Czarny, B. Malinowska, E. Stec, A. Malik, *Przemysl Chemiczny (in polish)*, **53**:1 (1974) 23-6
 30. I. Kiricsi, J. B. Nagy, *Applied Catalysis A-General*, **271** (2004) 27-38
 31. C.H. Barclay, H. Bozorgzadeh, E. Kemnitz, M. Nickkho-Amiry, D.E.M. Ross, T. Skapin, J. Thomson, G. Webb, J.M. Winfield, *Journal of the Chemical Society, Dalton Transactions*, **1** (2002) 40-47
 32. J. Thomson, G. Webb, J.M. Winfield, *Journal of Molecular Catalysis*, **67** (1991) 117
 33. E. Iglesia, D. G. Barton, J.A. Biscardi, M.J.L. Gines, S.L. Soled, *Catalysis Today*, **38** (1997) 339-360E.
 34. J. Thomson, G. Webb, J.M. Winfield, *Journal of Molecular Catalysis*, **68**:3 (1991) 347-54
 35. J. B. Peri, *Journal of Physical Chemistry*, **69** (1965) 211
 36. E. Echigoya, a dissertation presented to Tokyo Inst. Of Technology in partial fulfilment of the requirements for the PhD degree (1957); E. B. Corneliuss, T.H. Milliken, A.G. Oblad, *Journal of Physical Chemistry*, **59** (1955) 809.
 37. H. Noller, W. Kladnig, *Catalyst Review- Science and Engineering*, **13** (1976) 149-207
 38. H. Handa, T. Baba, H. Sugusawa, Y. Ono, *Journal of Molecular Catalysis A: Chemical*, **134** (1998) 171-177
 39. L.M. Weistock, J. M. Stevenson, *Tetrahedron Letters*, **27** (1986) 3845
 40. H. Handa, Y. Fu, T. Baba, Y. Ono, *Catalysis Letters*, **59** (1999) 195-200
 41. H. Lauron-Pernot, F. Luck, J.M. Popa, *Applied Catalysis*, **78** (1991) 213
 42. M. Huang, S. Kaliaguine, *Catalysis Letters*, **18** (1993) 373
 43. J. Shen, R. D. Cortright, Y. Chen, J. A. Dumesic, *Journal of Physical Chemistry*, **98** (1994) 8067-8073
 44. J.M. Wang, M. Yamaguchi, I. Goto and M. Kumagai, *Physical Chemistry Chemical Physics (PCCP)*, **2** (2000) 3007-3015

5 ZIRCONIA PROMOTED CATALYSTS

Pure Zirconia (ZrO_2)
Zirconia-alumina ($ZrO_2-Al_2O_3$)
Alkaline-doped zirconia-alumina

5.1 Introduction

In this chapter, we applied the use of zirconia promoted catalysts to dehydrochlorinate the 2-chlorobutane for the first time. Pure zirconia, zirconia-alumina and alkaline doped zirconia-alumina were prepared, and the distinctive characteristics as well as the catalytic activity were examined. The characterisation techniques employed include nitrogen-adsorption (BET), x-ray diffraction (XRD), thermogravimetric analysis (TGA), chemisorption/ temperature programmed desorption (TPD) of carbon dioxide and ammonia, x-ray photoelectron spectroscopy (XPS) and x-ray fluorescence (XRF).

5.2 Pure zirconia

Zirconia consists of both acidic and basic properties¹⁻³, has an extremely high melting point (2700°C) and exceptional resistance to attack by both acids and alkalis, and good mechanical properties. It is a promising catalytic material that commonly applied as a catalyst in reactions such as esterification, alkene hydrogenation², and dehydration-dehydrogenation of 2-propanol³. Although zirconia shows interesting catalytic properties, its behaviour is still unclear. Extensive studies have been made on the effect of the synthetic procedure⁴ and calcination temperature^{3,5}, the effects of the zirconium precursor used^{6,7}, ageing time and pH⁸, could vastly change the textural properties and acid-base properties of zirconia obtained.

Zirconia is known to exist in monoclinic, tetragonal and cubic phases, and as an amorphous solid. The monoclinic form is thermodynamically stable under ambient conditions, while the tetragonal and cubic phases are metastable. Below 420-450°C the solid obtained is amorphous. The various crystal forms of zirconia were strongly dependent on the preparation method^{3,9}. The normal procedure used to prepare zirconia consists of calcinations of its hydroxide (hydroxylated gel) which is by hydrolysis of zirconium salt^{3,10}. This gel presents two different kind of hydroxyl groups, associated (hydrogen-bonded) and isolated (non-hydrogen-bonded), the ratio of these hydroxyl groups decide the active phase formed (tetragonal or monoclinic). The tetragonal form presents better textural and acid-base properties than the monoclinic and therefore, is the one most used in catalysis¹¹.

Few studies have been reported relate to the use of zirconia as a catalyst for catalytic dehydrochlorination. Recently, Moon *et al*¹² reported the deactivation behaviour of Pd catalysts on different supports (i.e. Al₂O₃, ZrO₂, TiO₂, etc.) in the hydrodechlorination of chloropentafluoroethane (CF₃CF₂Cl). The result shows that the deactivation of the Pd catalyst was mainly caused by sintering of Pd particles. The sintering of Pd particles on the catalyst surface was promoted by the reaction of hydrogen fluoride with the support of the catalysts. Later, Rama Rao *et al*^{13,14} suggest some modifications to Pd/Al₂O₃ and Pd/C by incorporation of ZrO₂ in order to enhance their CFC hydrodehalogenation abilities. The advantage of Pd-ZrO₂/C is that the catalyst is susceptible to HF released during the hydrogenolysis forming ZrF⁴⁺, which is responsible for creating electron-deficient environment at the vicinity of Pd site, thus, enhancing the selectivity to HFC-32. Furthermore, Zacheis *et al*¹⁵ performed the radiolytic degradation of hexachlorobenzene on ZrO₂. However, zirconia was found to be inefficient in promoting radiation induced catalysis.

In this work, we studied the thermal stability, textural properties and acid-base properties of two zirconia catalysts, a precipitation prepared zirconia ($\text{ZrO}_2\text{-P}$) by hydrolysis of zirconyl oxynitrate ($\text{ZrO}(\text{NO}_3)_2$) solution with ammonia solution at constant pH of 7-8. After the gel was formed, the sample was filtered and dried in oven without delay. A commercial zirconia from Aldrich ($\text{ZrO}_2\text{-ADH}$) was used as a comparative material. Finally, the zirconia catalysts are tested for the catalytic dehydrochlorination of 2-chlorobutane at 135°C . All samples were calcined in air at 600°C for 24h before use.

5.2.1 The characteristics of pure zirconia

5.2.1.1 Thermal analysis of the ZrO_2

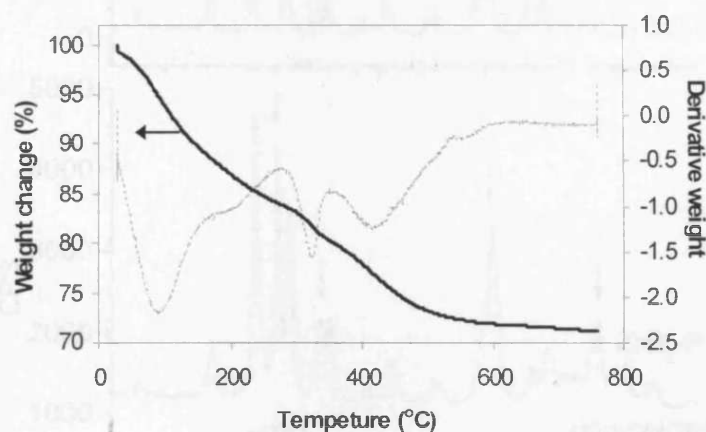


Fig 5.1: TGA of hydrous ZrO_2

The thermogravimetric analysis (TGA) was performed to observe the thermal stability of the uncalcined ZrO_2 catalysts with respect to the changes in weight as a function of temperature. Fig 5.1 illustrates the typical TGA pattern of dried zirconia gel⁵, where continuous weight losses occurred over the whole range of temperature studied from ambient to 800°C . Two desorption peaks were observed at 100°C and 200°C , corresponding to the loss of physisorbed water and crystalline water,

respectively. At 320°C and 420°C, two significant weight losses are ascribed to the incomplete decomposition of the hydroxylate gel, consequently the transformation of an amorphous material to crystalline phase³ The final sample weight loss is about 30% of the initial sample weight.

5.2.1.2 Textural properties

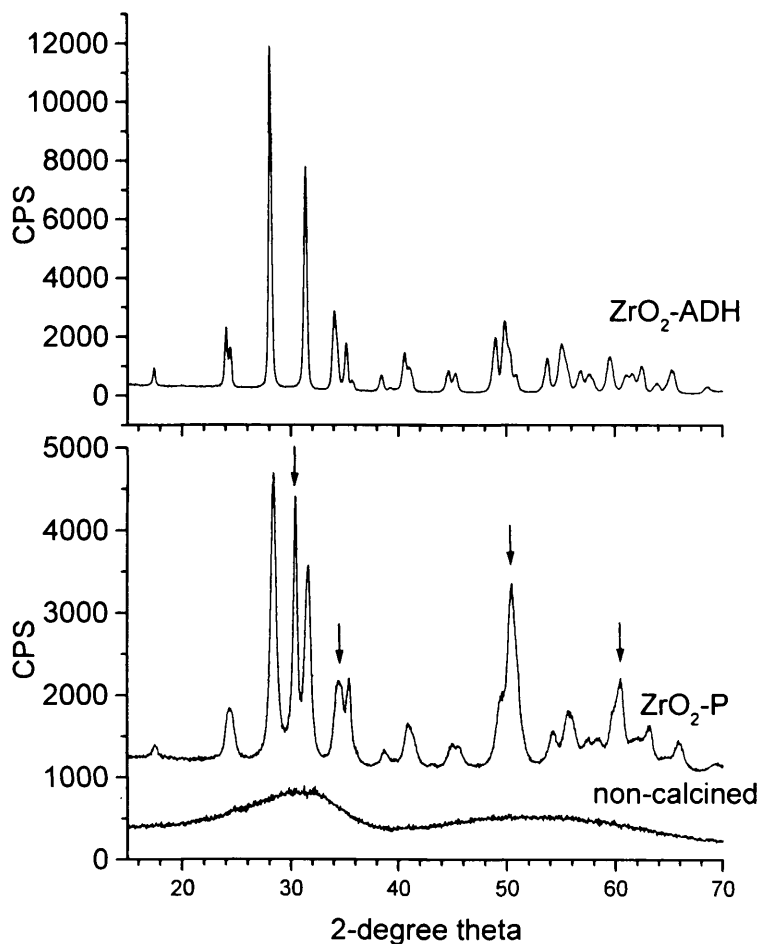
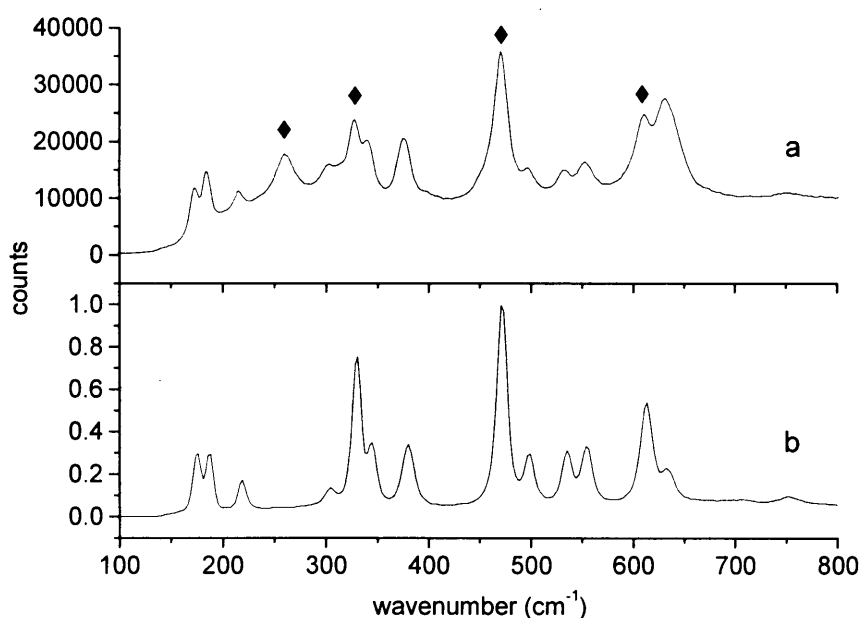


Fig 5.2: XRD patterns of uncalcined ZrO₂ gel, calcined ZrO₂-P and ZrO₂-ADH at 600°C. Arrow- tetragonal or cubic phase ZrO₂

Fig 5.2 shows the XRD patterns for the uncalcined ZrO₂, calcined ZrO₂-P and ZrO₂-ADH commercial zirconia at 600°C. The two broad peaks for zirconia gel in the range of 2θ from 18° to 40° and from 40° to 70° are typical^{3,4}, indicating an amorphous compound was obtained. After the calcination at 600°C, XRD patterns of

zirconia samples show numerous sharp peaks, indicating a crystalline compound was obtained. The XRD pattern of ZrO_2 prepared by precipitation method (ZrO_2 -P) displayed a combine mixture of stable monoclinic phase (baddeleyite) and a metastable phase which could be tetragonal or cubic phase. On the other hand, the XRD pattern of commercial zirconia from Aldrich (ZrO_2 -ADH) shows a completely crystalline material was obtained with the monoclinic phase was dominant. The result indicates that the commercial zirconia has undergone a different treatment in catalyst preparation to form the more thermodynamically stable and preferential monoclinic phase. Unfortunately, the XRD patterns of cubic and tetragonal zirconia modifications are nearly identical and are difficult to differentiate between each other.

Fig 5.3: Raman spectra of ZrO_2 samples: (a) a predominantly monoclinic sample with 'metastable' tetragonal species obtained by calcining ZrO_2 -P at $600^\circ C$ (diamonds indicate strongest peaks resulting from tetragonal phase); (b) a monoclinic Baddeleyite sample.



The tetragonal and cubic phases may however be identified and distinguished by Raman spectroscopy⁵. Tetragonal zirconia is expected to yield a spectrum consisting of six Raman bands (with frequency at about 148, 263, 325, 472, 608 and 640cm^{-1}), while cubic zirconia is expected to yield a single Raman band centred at 490cm^{-1} . Fig 5.3 shows the Raman spectra of ZrO_2 -P calcined at $600^\circ C$ and a

monoclinic zirconia (Baddeleyite) as reference. The absence of a band at 490cm^{-1} and the presence of the four strongest bands for tetragonal zirconia indicate that the tetragonal phase rather than cubic phase was obtained.

Nitrogen adsorption isotherms obtained for both zirconia ($\text{ZrO}_2\text{-P}$ and $\text{ZrO}_2\text{-ADH}$) revealed a “Type II” behaviour (see Appendix C), which indicate a non-porous ($>50\text{nm}$) material was obtained. The BET surface areas for $\text{ZrO}_2\text{-P}$ and $\text{ZrO}_2\text{-ADH}$ were $27\text{m}^2\text{g}^{-1}$ and below $10\text{m}^2\text{g}^{-1}$, respectively. The total pore volume is about $0.0368\text{cm}^3\text{g}^{-1}$. The relatively low BET surface area of pure zirconia was ascribed to the degree of surface diffusion against temperature^{3,5}. Two processes were identified for this matter: (i) crystallite growth of ZrO_2 and an accompanying phase transformation; and (ii) inter-crystallite sintering that becomes more pronounced with increasing temperature. The BET surface data are consistent with the XRD patterns of ZrO_2 that the commercial zirconia ($\text{ZrO}_2\text{-ADH}$) appeared to be more crystalline than the precipitation prepared zirconia ($\text{ZrO}_2\text{-P}$).

5.2.1.3 Acid-base properties of ZrO_2

Acid-base properties were studied by employing selective chemisorption and temperature programmed desorption (TPD) of reactive probe molecule include ammonia (total acidity) and carbon dioxide (basicity). It was assumed that one molecule of the reactive probe could react with one corresponding site. Table 5.1 presents the acid-base data obtained for pure zirconia samples from chemisorption-TPD. It is clear that the commercial zirconia ($\text{ZrO}_2\text{-ADH}$) has larger number of acid and base sites than the precipitation prepared zirconia ($\text{ZrO}_2\text{-P}$). The broad peak at temperature ranges from 100 to 300°C for TPD- NH_3 and about 140°C for TPD- CO_2 , indicating that the pure zirconia was comprised of weak acidic sites and weak basic

sites^{1-3,16}. However, due to the fact that pure ZrO₂ catalysts exhibited generally low surface area (<27m²g⁻¹), the TPD desorption peak obtained was unclear, as shown in Fig 5.4. Therefore, the strength of acidity and basicity of pure ZrO₂ catalysts was not compared.

Fig 5.4: TPD of ammonia adsorbed at 100°C over precipitation prepared ZrO₂, followed by desorption from ambient to 500°C at ramp rate of 20°C·min⁻¹

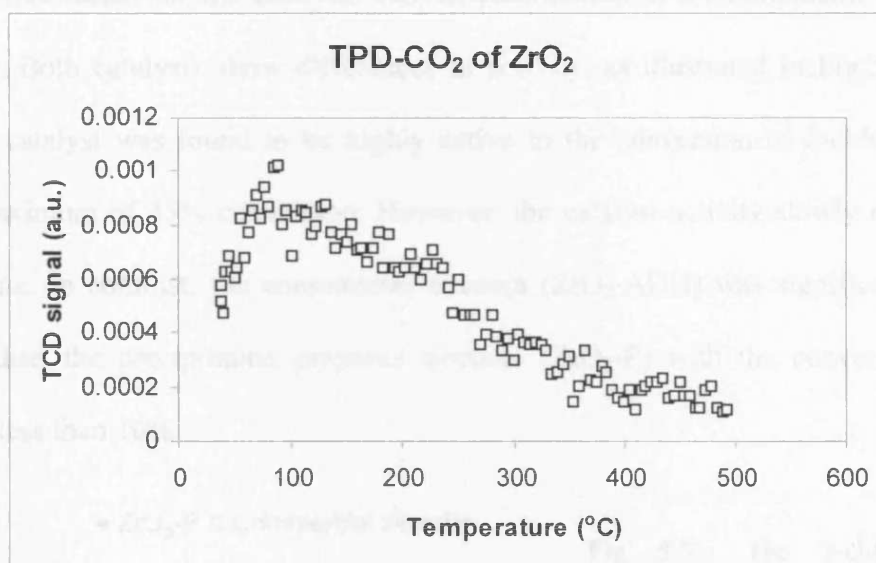


Table 5.1: Acid-base properties for pure zirconia from chemisorption and desorption of ammonia and carbon dioxide.

samples	Acidity (NH ₃)		Basicity (CO ₂)	
	ZrO ₂ -P	ZrO ₂ -ADH	ZrO ₂ -P	ZrO ₂ -ADH
TPD, T _{max} (°C)	100-300		140	
Active sites (μmol.g ⁻¹)	16	186	41	192
Active sites (molecule.m ⁻² × 10 ¹⁶)	36	1100	92	1200

It was believed that the weak acidic site is due to the presence of Zr⁴⁺ Lewis acid site, while the O²⁻ is responsible for the basic site on the surface of zirconia. Considering the difference in the specific surface area of the samples, the number of acid and base sites was normalised by the specific surface area for each sample. The result shows that the ZrO₂-P catalyst contains higher proportion of basic site than ZrO₂-ADH, where the base to acid site ratio for ZrO₂-P and ZrO₂-ADH were 2.5 and

1.0, respectively. It is clear that the preparation method is a crucial factor for obtaining ZrO_2 catalyst with suitable surface properties.

5.2.2 ZrO_2 as dehydrochlorination catalyst

Precipitation prepared zirconia (ZrO_2 -P) and commercial zirconia (ZrO_2 -ADH) were tested for the catalytic dehydrochlorination of 2-chlorobutane at $135^\circ C$ for 20h. Both catalysts show differences in activity, as illustrated in Fig 5.5a. The ZrO_2 -P catalyst was found to be highly active to the conversion of 2-chlorobutane with maximum of 45% conversion. However, the catalyst activity slowly decreased with time. In contrast, the commercial zirconia (ZrO_2 -ADH) was significantly less active than the precipitation prepared zirconia (ZrO_2 -P) with the conversion was always less than 10%.

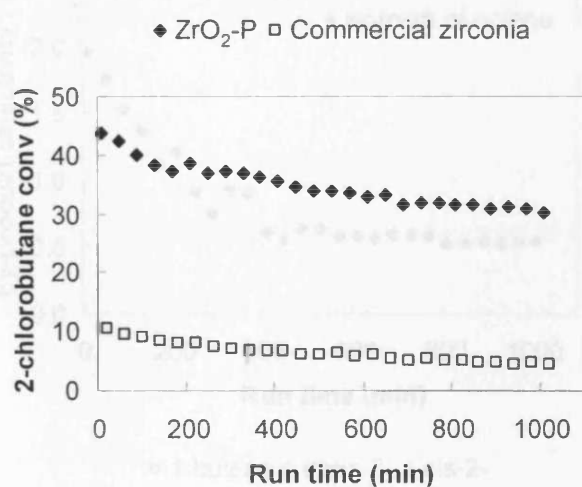


Fig 5.5a: The 2-chlorobutane conversion for ZrO_2 -P and commercial zirconia (ZrO_2 -ADH).

Reaction conditions: $135^\circ C$ for 20h, 100mg of catalyst and $100\text{ml}\cdot\text{min}^{-1}$ of feed flowrate ($GHSV=55000\text{h}^{-1}$). 30000ppm of gas concentration.

In addition to the high activity, ZrO_2 catalysts also revealed high selectivity to the formation of butene isomers and hydrogen chloride. The butene selectivity obtained for ZrO_2 -P and ZrO_2 -ADH were 98% and 100%, respectively. The 100% selectivity obtained for commercial ZrO_2 may be due to the low activity. The precipitation prepared ZrO_2 showed a lower selectivity, compared to $\gamma\text{-Al}_2\text{O}_3$ catalyst

(>99%). The decrease in butene selectivity was due to the formation of octenes as the secondary hydrocarbon product. Fig 5.5b shows the selectivity of isomers of octene over ZrO_2 -P catalyst changes with time. The result clearly shows that more octene isomers were formed at the initial reaction when the activity was high. The catalyst became more selective to butene isomers as the reaction proceeds and reached a steady state with 99.5% selectivity obtained after approximately 8h. The result indicates that the formation of the isomers of octene was possibly due to a further reaction caused by dimerisation of butenes over ZrO_2 -P catalyst. Note that quantitative result for the different isomers of octene was not obtained due to its low concentration (<2% of total product) and the hydrogen chloride was the only chlorinated product obtained from the reaction.

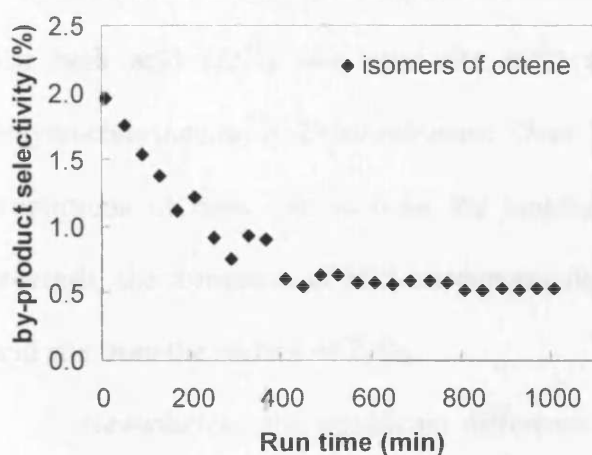


Fig 5.5b: Isomers of octene, by-product selectivity for ZrO_2 -P catalyst.

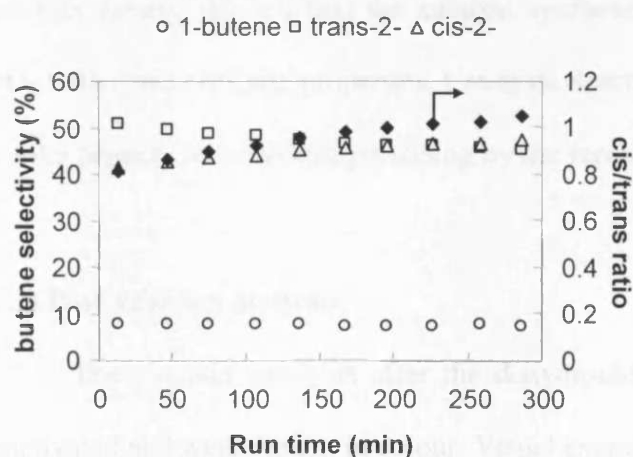


Fig 5.5c: Product distribution for ZrO_2 -P catalyst.

The products distribution changed continuously according to the reaction time. Fig 5.5c shows the products distribution of the butene isomers over ZrO_2 -P catalyst at 135°C. The result shows that the formation of the trans-isomer was slightly preferred than the cis-isomer at the initial reaction when the activity was high, while the formation of cis-isomer was predominant when the reaction reached a steady state. The butene selectivities at steady state were 7% (1-butene), 47% (cis-2-butene) and 45% (trans-2-butene). The ratio of cis to trans isomer was compared and the value was always close to unity.

As we have mentioned before, the formation of the preferential cis or trans isomers revealed the acid-base properties of the catalyst. Mochida *et al*^{17,18} has reported the formation of preferential cis isomers on acid catalyst and the trans isomers on base catalyst for dehydrochlorination reaction.. Thus, the results indicate that both acid (Zr^{4+}) and base site (O^{2-}) act as active sites on the catalytic dehydrochlorination of 2-chlorobutane. Over the fresh ZrO_2 catalyst surface, high proportions of basic site activate the lengthening of C-H bond. As the reaction proceeds, the formation of HCl encourages the abstraction of Cl^- ion by the Lewis acid site from the surface of ZrO_2 .

Nevertheless, the significant difference in activity between the two zirconia catalysts clearly showed that the catalyst synthesis is a crucial factor for obtaining ZrO_2 with good catalytic properties. Catalysts deactivation was observed possibly due to coke deposition or surface poisoning by the formation of organic chlorides.

5.2.3 Post-reaction analysis

The zirconia catalysts after the dehydrochlorination of 2-chlorobutane were deactivated and were darkened in colour. Visual examination of the used ZrO_2 -P catalyst

revealed a dark-brown in colour. This indicates a possibility of coke deposition occurred during the reaction. Alternatively, changes in the metal transition state could also affect the appearance of the catalyst.

X-ray photoelectron spectroscopy (XPS) analysis was performed to observe the surface composition of the used $\text{ZrO}_2\text{-P}$ catalyst, as shown in Fig 5.6. The result shows that the used catalyst gives a slight increase on the C1s peak intensity by 25%, by comparing the peak intensity ratio ($I_{\text{C}}/I_{\text{Al}}$) of the used sample to the fresh sample. It is important to note that the chlorine species were not detected on these catalysts, neither before nor after reaction, as judged from the absence of a Cl 2s peak at *ca* 275 eV binding energy (the Cl 2p peak overlaps with the Zr 3d features). The result suggests that the catalyst deactivation occurred as a consequent of coke depositions. The absence of a chloride peak expelled the possibly formation of surface chloride. The elemental chloride analysis by columetric titration shows negligible amount of chloride was detected from the used $\text{ZrO}_2\text{-P}$ catalyst.

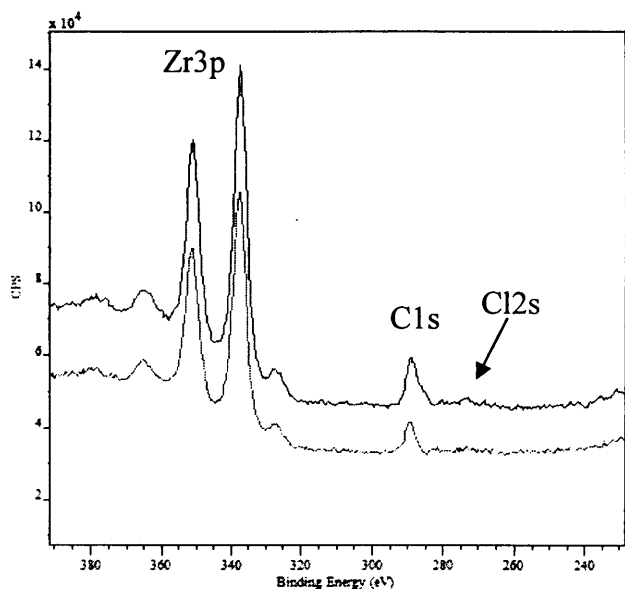


Fig 5.6: XPS spectra of $\text{ZrO}_2\text{-P}$ catalysts, before (bottom) & after (top) reaction.

5.3 Supported zirconia on alumina

Zirconia was found to be highly active for the dehydrochlorination of 2-chlorobutane in spite of its generally low surface area and poor pore structure. This material is often combined with cationic dopant (Y_2O_3 , Cr_2O_3 , MgO , CaO or La_2O_3), which contributed to stabilization of zirconia in which the sintering and phase transition is suppressed^{6,19}. Anionic dopant (SO_4^{2-} , CO_3^{2-} or Cl^-) is used to modify the surface properties of zirconia²⁰. Indeed, it is known that introducing alumina into zirconia delays the crystallization, increases the specific surface area and pore volume, and enhances the surface acidity of zirconia^{19,21}. Moreover, the $ZrO_2-Al_2O_3$ mixed oxide shows high strength, toughness, and seems to present interesting catalytic properties for the reduction of NO ^{22,23} and ethanol oxidation²⁴ reactions.

Only few studies were found from the literatures related to the use of zirconia-alumina as a catalyst for catalytic dehydrochlorination. A ternary oxides of Ti-Zr-Al has been prepared by coating alumina with a THF solution of $Ti(OCHMe_2)_4$ and $Zr(OCHMe_2)_4$, to use as a support for Pd catalyst²⁵. The catalytic performance of Pd/Ti-Zr-Al in the hydrodechlorination of 1,2-dichlorobenzene exceeded that of the corresponding single oxide catalysts. The enhanced activity may be attributed to the interaction between the support and the metal or the ability of the support to adsorb the reactant. Similar conclusion was drawn by Srinivas *et al*²⁶, in investigating the effect of support modification on the chlorobenzene hydrodechlorination on Pt/ Al_2O_3 catalysts. Al_2O_3 was modified with ZrO_2 using an organometallic precursor.

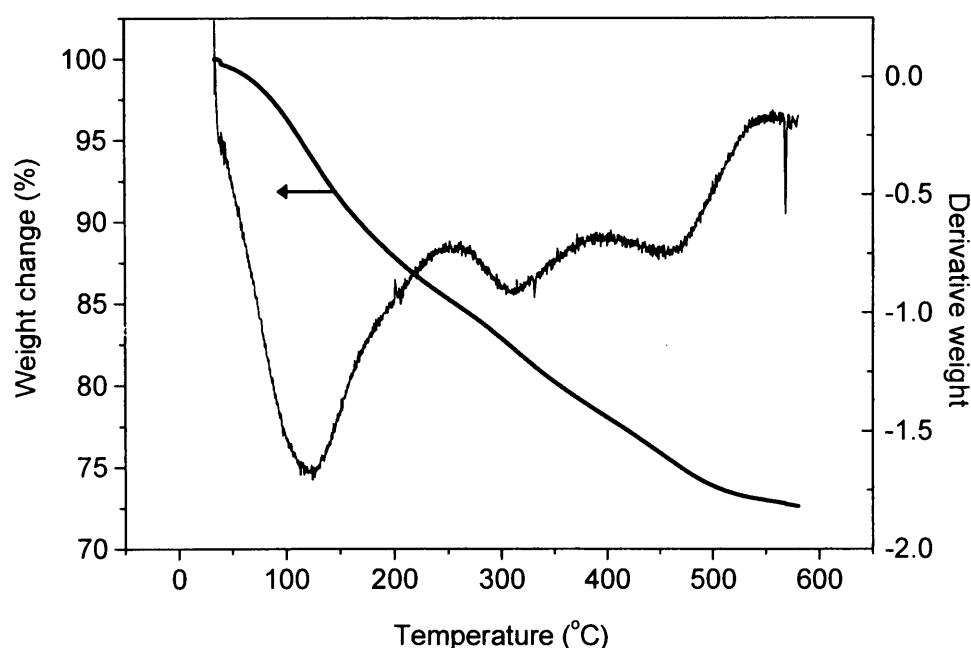
Therefore, our goal is to combine the advantages of zirconia and alumina, thereby to develop a new catalyst with better stability and activity for the catalytic dehydrochlorination of 2-chlorobutane. Three $ZrO_2-Al_2O_3$ mixed oxides were prepared, by *wet impregnation of $ZrO(NO_3)_2$ in dilute HNO_3 on alumina, dry*

impregnating (incipient wetness) the $ZrO(NO_3)_2$ on alumina, and by co-precipitation of $Al(NO_3)_3$ and $ZrO(NO_3)_2$ in dilute HNO_3 , namely ZA-I, ZA-H and ZA-C. The synthesis and characterisation of $ZrO_2-Al_2O_3$ was studied by employing techniques include TGA, XRF, N_2 -adsorption (BET), XRD, XPS and TPD.

5.3.1 Characteristic of zirconia-alumina catalysts

5.3.1.1 Thermal analysis of zirconia-alumina

Fig 5.7: TGA curve of fresh $ZrO_2-Al_2O_3$ gel



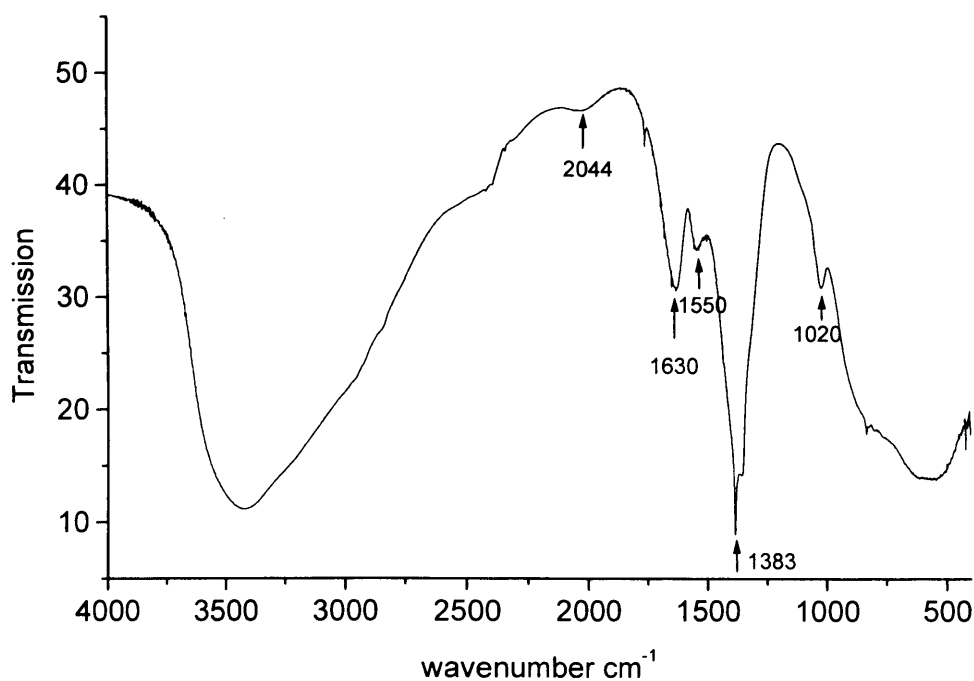
Thermogravimetric analysis (TGA) of $ZrO_2-Al_2O_3$ was performed to observe the weight changes as a function of temperature. Fresh ZrO_2 gel prepared by wet impregnation (ZA-I) with 50wt% contents of zirconyl oxynitrate ($ZrO(NO_3)_2$ in HNO_3) was used as a representative result for all $ZrO_2-Al_2O_3$ catalysts. Fig 5.7 illustrates the TGA curve of this sample, where the sample exhibited three significant weight losses due to desorption at 120°C, 300°C and 460°C. The result is similar to that of the pure zirconia, suggests that the weight losses were mostly attributed to the presence of zirconia. The first weight loss at 120°C was due to the removal of

physisorbed water. Two weight losses at 300°C and 460°C observed are due to the decomposition and desorption of the residual zirconium nitrate or zirconium hydroxylate gel. Note that the γ -alumina support does not exhibit any significant weight loss in the range of temperature used. Thus, $\text{ZrO}_2\text{-Al}_2\text{O}_3$ catalysts were calcined at 500°C for 3h under static air, to form stabilised $\text{ZrO}_2\text{-Al}_2\text{O}_3$ mixed-oxides.

5.3.1.2 Infrared spectroscopy (IR)

In order to obtain more insight into the transformation of the precursor to the stabilised $\text{ZrO}_2\text{-Al}_2\text{O}_3$ mixed oxide, the samples were studied with IR. Fig 5.8a & b show the IR spectra for pure ZrO_2 , $\gamma\text{-Al}_2\text{O}_3$ support and $\text{ZrO}_2\text{-Al}_2\text{O}_3$ mixed oxides (ZAI & ZAC with 50wt% contents of Zr salt) after the calcination, where the uncalcined $\text{ZrO}_2\text{-Al}_2\text{O}_3$ gel (ZAI with 50wt% contents of Zr salt) was used as a reference.

Fig 5.8a: IR spectrum of fresh $\text{ZrO}_2\text{-Al}_2\text{O}_3$ gel (ZA-I) with 50wt% contents of Zr salt.



Broad band in the $4000\text{-}2500\text{cm}^{-1}$ region was assigned to the OH stretching vibration modes. It diminishes after calcination, but it does not disappear (Fig 5.8a & b). The result indicates that large amount of water retention observed for the alumina-based catalyst was due to the hygroscopic nature of γ -alumina support. At 2044cm^{-1} , a band is observed in the spectrum of fresh $\text{ZrO}_2\text{-Al}_2\text{O}_3$ gel (Fig 5.8a) and supposing at 2104cm^{-1} for the calcined samples (Fig 5.8b) are assigned to the stretching vibrations of Zr-O-Al bond^{23,27}. The band diminution in the calcined samples is due to lattice structural rearrangement. The vibration band at 1630cm^{-1} and at 1640cm^{-1} after the thermal treatment was attributed to the physisorbed water²⁸. The band peaking at 1550 and 1383cm^{-1} in the spectrum of the fresh sample are shifted to 1520 and 1388cm^{-1} for the calcined ones. These two bands are attributed to the carboxylic or carbonate species²⁹. The wet impregnation prepare $\text{ZrO}_2\text{-Al}_2\text{O}_3$ (ZA-I) revealed more intense peaks than co-precipitation prepared $\text{ZrO}_2\text{-Al}_2\text{O}_3$ (ZA-C), suggesting a structural change in the γ -alumina support as a result of different preparation method.

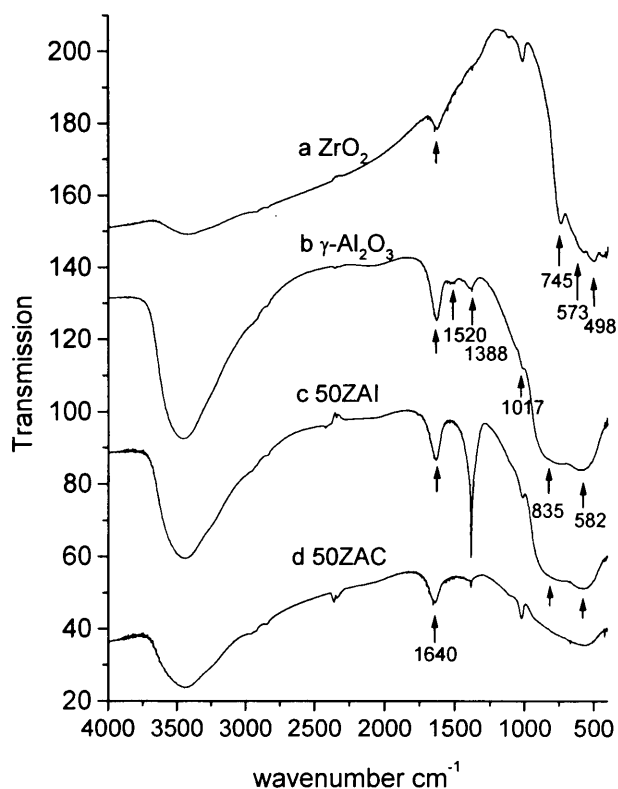


Fig 5.8b: Infra-red spectra in the range from 400 to 4000cm^{-1} .

a. Pure zirconia, **b.** γ -alumina support, **c.** 50wt% $\text{ZrO}_2\text{-Al}_2\text{O}_3$ by wet impregnation (50ZA-I) and **d.** 50wt% $\text{ZrO}_2\text{-Al}_2\text{O}_3$ by co-precipitation (50ZA-C).

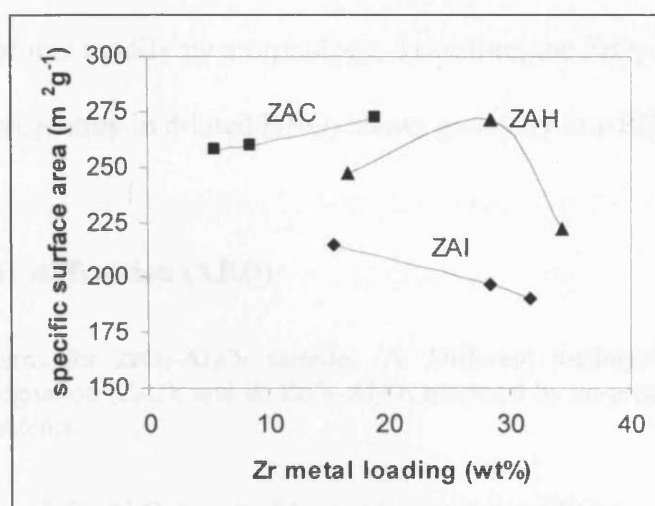
The low energy region of the spectra corresponds to the deformation vibration of the link Zr-O-Al²⁷. In this region, the vibration stretches at 745, 573, 498cm⁻¹ are assigned to pure zirconia and 835, 582cm⁻¹ assigned to γ -alumina support. The IR spectrum of the wet impregnation prepared ZrO₂-Al₂O₃ (ZAI) resembled the vibration band of the γ -alumina support. However, the diminution of these bands for co-precipitation prepared ZrO₂-Al₂O₃ (ZAC) indicates a different structure rearrangement of Zr-O-Al may be obtained.

5.3.1.3 Physical properties of zirconia-alumina

Nitrogen-adsorption was performed to determine the BET surface areas for different preparations of ZrO₂-Al₂O₃ mixed-oxides of 25, 50 and 75wt% Zr salt contents. The elemental composition of total Zr metal loading for each sample was obtained from the x-ray fluorescence analysis (XRF). Table 5.2 shows a summary of the BET data and the actual metal loading for different ZrO₂-Al₂O₃ samples. The original γ -alumina support has a BET area about 300m²g⁻¹. Addition of zirconia to alumina decreased the BET area of alumina and the value ranges between 190 and 271m²g⁻¹. Then again, the mixing of Al₂O₃ and ZrO₂ clearly shows improvement on the overall textural properties of ZrO₂, considering the stable monoclinic form of ZrO₂ are generally exhibited low surface area and poor pore structure¹⁹.

Table 5.2: BET surface areas and actual metal loadings for different types of ZrO₂-Al₂O₃ catalysts

	BET (m ² /g)			Actual ZrO ₂ loading (wt%)		
	ZA-I	ZA-C	ZA-H	ZA-I	ZA-C	ZA-H
25wt% ZrO ₂ -Al ₂ O ₃	215	258	247	15.4	5.6	16.6
50wt% ZrO ₂ -Al ₂ O ₃	190	260	271	31.7	8.5	28.3
75wt% ZrO ₂ -Al ₂ O ₃	197	272	222	28.4	18.8	34.2

Fig 5.9: The BET surface area Vs the actual zirconium metal loading

The BET area changes according to the metal contents of $\text{ZrO}_2\text{-Al}_2\text{O}_3$, and a non-linear correlation was obtained dependent on the preparation method used. As shown in Fig 5.9, the co-precipitation prepared $\text{ZrO}_2\text{-Al}_2\text{O}_3$ (ZAC) samples whose contain less than 20wt% metal contents, show high surface area ranges from 258 to $272\text{m}^2\text{g}^{-1}$. The BET areas increase with increasing metal loadings. The result indicates a well-dispersed and homogeneous mixing of ZrO_2 and Al_2O_3 obtained. On the other hand, $\text{ZrO}_2\text{-Al}_2\text{O}_3$ samples prepared from impregnation method (dry or wet) resulted in samples with high ($222\text{-}271\text{m}^2\text{g}^{-1}$) and low surface area ($190\text{-}215\text{m}^2\text{g}^{-1}$), and with high Zr metal contents (Table 5.2).

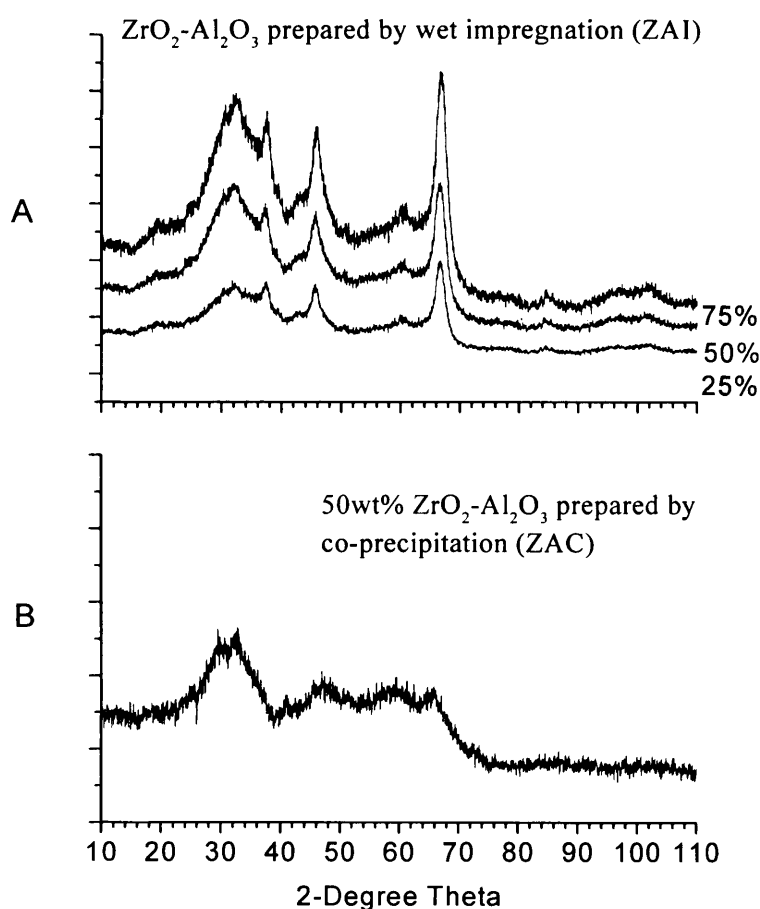
The elemental zirconium determined from XRF analysis shows metal contents between 15 to 35wt%. The higher metal loadings for impregnation prepared samples (ZAH & ZAI) than co-precipitation (ZAC), may be due to the washing step in the preparation of ZAC has removed the incompletely decomposed zirconium residual. Between the impregnation prepared $\text{ZrO}_2\text{-Al}_2\text{O}_3$ samples (ZAI & ZAH), ZAH shows higher BET area than ZAI.

Two possible explanations for this latter were proposed: (i) the solubility of zirconyl nitrate with or without presence of an acid, resulting in different degree of

crystallite growth^{3,5} that blocked the surface area of alumina; and (ii) acid attack on the γ -alumina support that modify its morphology. Therefore, the $\text{ZrO}_2\text{-Al}_2\text{O}_3$ samples prepared by wet impregnation in diluted HNO_3 shows generally low BET area.

5.3.1.4 Powder x-ray diffraction (XRD)

Fig 5.10: XRD patterns for $\text{ZrO}_2\text{-Al}_2\text{O}_3$ samples. A. Different loadings of $\text{ZrO}_2\text{-Al}_2\text{O}_3$ prepared by wet impregnation (ZAI); and B. $\text{ZrO}_2\text{-Al}_2\text{O}_3$ prepared by co-precipitation (ZAC) with 50wt% Zr salt contents.



X-ray diffraction was employed to observe the crystallinity of $\text{ZrO}_2\text{-Al}_2\text{O}_3$ samples. Fig 5.10 illustrates the XRD spectra of various loading of $\text{ZrO}_2\text{-Al}_2\text{O}_3$ samples prepared by wet impregnation (ZAI) as a representative result for impregnation prepared samples (ZAI & ZAH) and the co-precipitation prepared $\text{ZrO}_2\text{-}$

Al_2O_3 (ZAC) with 50wt% metal contents. Broad peaks at 2θ of 32.8° , 37.4° , 46.0° and 66.8° were due to the γ -alumina phase. The absence of a sharp peak for solid ZrO_2 suggests that the particles are well dispersed on the alumina support. As shown in Fig 5.10B, the co-precipitation prepared ZrO_2 - Al_2O_3 sample (ZAC) shows lower crystallinity than the impregnation prepared one (ZAI & ZAH). The absence of the XRD pattern for γ -alumina phase indicates a structure rearrangement of Zr-O-Al occurred.

These results are consistent with the observations from IR and BET. By introducing Al_2O_3 to ZrO_2 leads to samples with a specific area and morphology close to that of the alumina. The IR band at 1388 , 835 , 582cm^{-1} assigned to the γ -alumina support were observed in the impregnation prepared ZrO_2 - Al_2O_3 (ZAI) but disappears in the co-precipitation one (ZAC). This is in agreement with the XRD patterns of ZAC that show differences in morphology.

It is proposed that the differences between two samples (impregnation and co-precipitation) can be due to the fraction by which means the metal was incorporated^{21,22}. During the synthesis step, co-precipitation between two nitrates affects the final structure of the mixed-oxide to form sample with large surface area if compared with the sample in which the metal was incorporated on the calcined γ -alumina. The amount of ZrO_2 incorporated in to the alumina would be different. Therefore, the density of Zr-O-Al bonds form on the catalyst surface is different for each other.

5.3.1.5 X-ray photoelectron spectroscopy (XPS)

XPS analysis was performed to estimate the elemental composition and dispersion at the surface level of ZrO_2 - Al_2O_3 catalysts. XPS spectra were measured

for the 25, 50 and 75wt% ZrO₂-Al₂O₃ catalysts prepared by co-precipitation (ZAC) and wet impregnation (ZAI). All spectra yield a Zr 3d_{5/2} peak at binding energy in the range of 182 ± 0.5eV, which indicates the presence of zirconium (IV) dioxide at the catalyst surface³⁰. Since the intensity of the zirconium signal relative to that of the support is decided by the ZrO₂ contents of the catalyst and by the dispersion over the support, the intensity ratio I_{Zr}/I_{Al} was used as an estimation of the surface dispersion for ZrO₂-Al₂O₃ samples (Table 5.3). The results show that the zirconium intensity increase as the ZrO₂ loading increases. The intensity ratio value of the sample prepared by the co-precipitation method (ZAC) is significantly larger than the impregnation prepared one (ZAI) with the same ZrO₂ loading. This indicates that the dispersion of ZrO₂-Al₂O₃ sample prepared by co-precipitation is higher than that of the wet impregnation sample. Low dispersion of the ZrO₂-Al₂O₃ samples prepared by wet impregnation may be due to the formation of large clusters. The results are consistent with the proposal that the co-precipitation method yields catalysts with homogeneous dispersed of small particles on the support, while the crystallite growth^{3,5} occurred on the impregnated catalyst that results in low dispersion obtained.

Table 5.3: Intensity ratio of the Zr3d and Al2p peaks in the XPS spectra of ZrO₂-Al₂O₃ catalysts prepared by co-precipitation (ZAC) and wet impregnation method (ZAI)

Sample	Actual ZrO ₂ loadings (wt%)	I_{Zr}/I_{Al} , Intensity ratio
<i>prepared by wet impregnation (ZAI)</i>		
25 ZAI	15.4	1.43
75 ZAI	28.4	1.83
50 ZAI	31.7	2.06
<i>prepared by co-precipitation (ZAC)</i>		
25 ZAC	5.6	2.45
50 ZAC	8.5	2.81
75 ZAC	18.8	4.91

5.3.2 Catalytic activity

5.3.2.1 Optimisation of ZrO₂ loadings

Table 5.4: The 2-chlorobutane conversion activities for ZrO₂-Al₂O₃ samples at steady state after 4h time online. *Reaction conditions: 135°C for 5h, 100mg of catalyst and total gas flow of 100ml·min⁻¹ (GHSV = 55000h⁻¹). Feed concentration was 30000ppm*

Actual metal loadings, wt% (sample)	Conversion after 4h (%)	Normalised by surface area
<i>prepared by wet impregnation (ZAI)</i>		
15.4 (25 ZAI)	12	15.2
31.7 (50 ZAI)	46	65.8
28.4 (75 ZAI)	16	22.1
<i>prepared by dry impregnation (ZAH)</i>		
16.6 (25 ZAH)	46	50.6
28.3 (50 ZAH)	57	57.2
34.2 (75 ZAH)	49	60
<i>prepared by co-precipitation (ZAC)</i>		
5.6 (25 ZAC)	34	35.8
8.5 (50 ZAC)	51	53.3
18.8 (75 ZAC)	47	47

25, 50 and 75wt% of ZrO₂-Al₂O₃ catalysts prepared by co-precipitation (ZAC) and impregnation (ZAI & ZAH) were tested for the catalytic dehydrochlorination of 2-chlorobutane. Table 5.4 shows the conversion at 4h time online and the conversion after normalised by the surface area over various types of ZrO₂-Al₂O₃ catalysts. The result shows that the 50wt% ZrO₂ loading catalysts exhibited the highest conversion. The general reactivity trend for different loading of ZrO₂-Al₂O₃ catalysts is: 50wt% > 75wt% > 25wt% and ZAH > ZAC > ZAI. The result indicates that the lower activity was obtained with high ZrO₂ loading attributed to the poor structure properties due to formations of multilayer adsorption. The theoretical monolayer coverage was estimated to be approximate 8wt% of ZrO₂ supported on alumina. It is important to mention that both ZrO₂ and Al₂O₃ are active to the decomposition of 2-chlorobutane.

5.3.2.2 Catalytic activity over $ZrO_2-Al_2O_3$ catalysts

Fig 5.11: Conversions and selectivity for various $ZrO_2-Al_2O_3$ catalysts, pure $\gamma-Al_2O_3$ and ZrO_2 were used as references. Reaction conditions: $135^\circ C$, 100mg of catalyst and total gas flow of $100ml \cdot min^{-1}$ ($GHSV = 55000h^{-1}$). Feed concentration is 30000ppm.

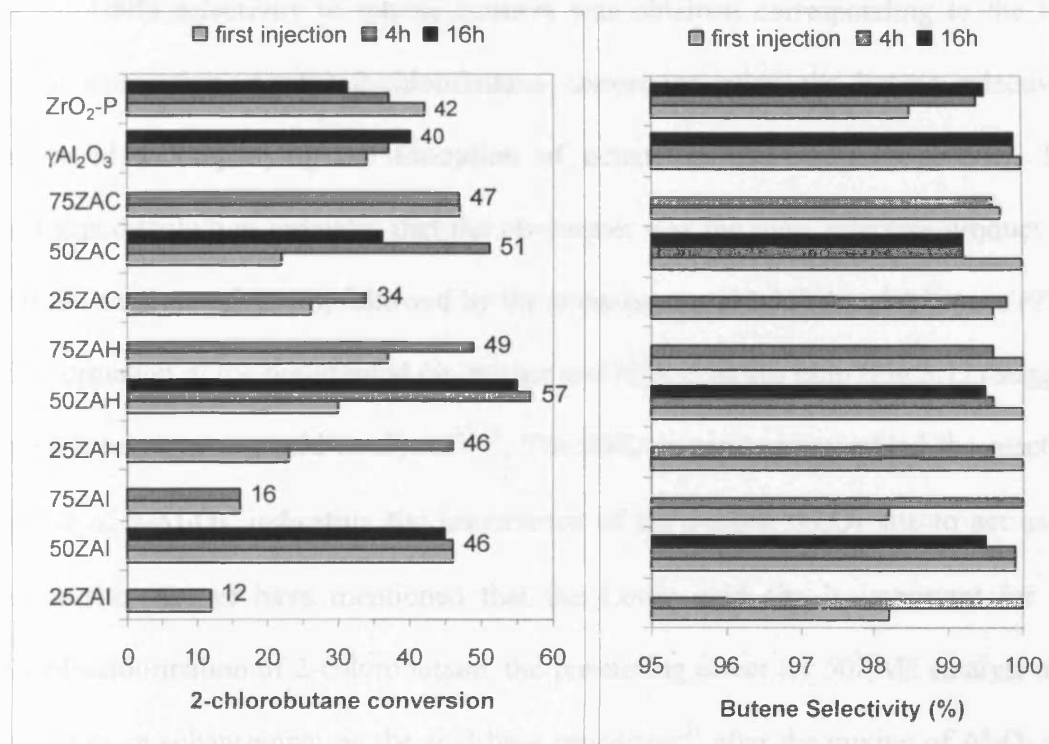


Fig 5.11 demonstrates the 2-chlorobutane conversion and the butene selectivity at $135^\circ C$ over various $ZrO_2-Al_2O_3$ catalysts recorded at the first injection, after 4h and after 16h time on stream to observe the reaction trend. Pure $\gamma-Al_2O_3$ and ZrO_2 prepared by precipitation (ZrO_2-P) were used as references. The result shows that addition of ZrO_2 to Al_2O_3 yield catalysts with good and bad catalytic properties, dependent on the preparation method used and the ZrO_2 loadings. Among all the catalysts tested, the $ZrO_2-Al_2O_3$ prepared by dry impregnation (ZAH) with 50wt% zirconium salt contents exhibited the best activity, 57% of 2-chlorobutane conversion and above 99.5% of butene selectivity can be obtained (Fig 5.11). The catalyst showed low initial conversion (first injection, 10-15min after reaction began), and the

reaction conversion was increased before it reached a steady state with 57% conversion (4h). The deactivation of catalyst was not observed in the range of experiment duration (16h).

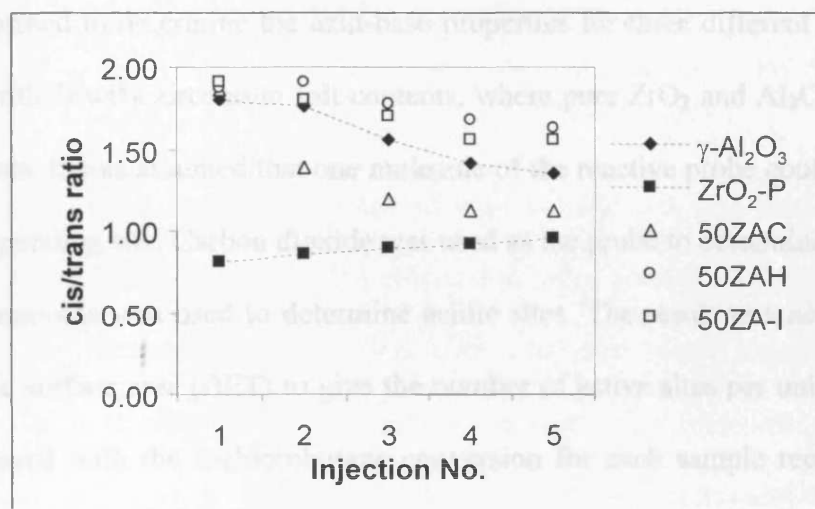
100% selectivity to butene isomers was obtained corresponding to the low initial conversion. As the 2-chlorobutane conversion raise, the butene selectivity decreased accompanying the formation of octene as the major by-product. The products distribution indicates that the cis-isomer was the most selective product for 50ZAH catalyst (55-59%), followed by the trans-isomer (32-35%) and 1-butene (9%). The formation of the preferential cis-isomer and high cis/trans ratio (Fig 5.12) suggest that the reaction was acid-catalysed^{17,18}. The 50ZAH catalyst resembled the reaction profile of γ -Al₂O₃, indicating the importance of the expose Al₂O₃ site to act as an active site. As we have mentioned that the Lewis acid site is important for the dehydrochlorination of 2-chlorobutane, the promoting effect for 50ZAH catalyst may be due to an enhancement on the acid-base properties²¹ after the mixing of Al₂O₃ and ZrO₂. Lahousse *et al*²¹ concluded from his studies of acid-base properties of ZrO₂-Al₂O₃ mixed-oxide, that the Lewis acidity of ZrO₂-Al₂O₃ samples increased with the alumina contents, whereas the Bronsted basicity of ZrO₂ decreased sharply after introducing alumina.

Nonetheless, the ZAH catalysts with 25wt% and 75wt% of zirconium contents showed lower conversions than the 50wt% one (Fig 5.11), implying that the ratio of ZrO₂ to Al₂O₃ or acid to base sites are possibly be important for ZrO₂-Al₂O₃ in the catalytic dehydrochlorination reaction.

Followed by the 50ZAH catalysts, was the ZrO₂-Al₂O₃ prepared by co-precipitation method with 50wt% zirconium salt contents (50ZAC). The catalyst showed maximum 2-chlorobutane conversion at 51% and butene selectivity at about

99.1% (Fig 5.11). The reaction trend was: low conversion at the beginning (first injection), after a reaction maximum was reached to give 51% conversion (at 4h) the catalyst deactivated with time and stabilised at 38% of 2-chlorobutane conversion. The butene selectivity was 100% at the first injection when the conversion was low. When the conversion reached the maximum (4h), the butene selectivity was at the lowest with a value of 99.1%. There was not further decrease of butene selectivity can be observed. The result indicates that mixing ZrO_2 and Al_2O_3 with co-precipitation method generates sites, which is more selective to the octene formation than the dry impregnation one, as the gas-chromatography analysis clearly shows increasing amount of butene isomers formation. The deactivation of catalyst may be due to the production of these non-volatile hydrocarbons and consequently coke deposition.

Fig 5.12: Cis to trans-2-butene ratio calculated from the butene selectivity



It is likely that the surface structural defects²² (Al-O-Zr) has been created, which justifies the different values of acidity and hence the occurrence of side reactions. In fact, the product distribution and the cis/trans ratio (Fig 5.12) indicated that the reaction is acid-catalysed, in which the formation of cis-2-butene is preferred and the cis/trans ratio is close to unity. The difference in activity for 25wt% and

75wt% ZrO₂-Al₂O₃ catalysts prepared by co-precipitation (ZAC) was again agreed with the proposal that the ratio of the ZrO₂ and Al₂O₃ or acid and base may be important for the reaction.

Finally, the wet impregnated ZrO₂-Al₂O₃ catalysts (ZAI) show generally low conversion compare to other ZrO₂-Al₂O₃ catalysts with same ZrO₂ contents. This is because of the crystallite growth³ or sintering of crystallite⁵ on wet impregnated catalysts (ZAI), resulting in low dispersion of ZrO₂ and less active site for the reaction to occur. Note that the reaction trend of ZAI catalysts is very similar to that of the ZAH catalysts.

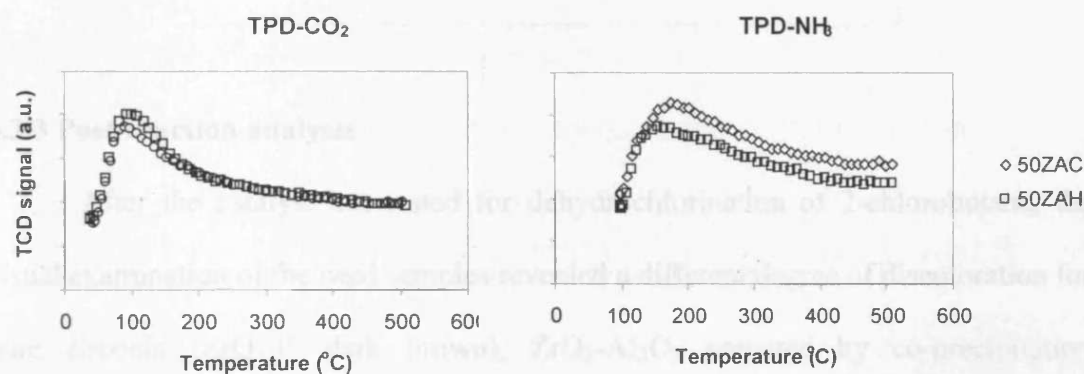
5.3.2.3 Correlation between acid-base properties and catalytic activity

Selective chemisorption and desorption (TPD) of ammonia and carbon dioxide were performed to determine the acid-base properties for three different ZrO₂-Al₂O₃ catalysts with 50wt% zirconium salt contents, where pure ZrO₂ and Al₂O₃ were used as references. It was assumed that one molecule of the reactive probe could react with one corresponding site. Carbon dioxide was used as the probe to determine basic sites, whereas ammonia was used to determine acidic sites. The result was normalised by the specific surface area (BET) to give the number of active sites per unit area and it was compared with the 2-chlorobutane conversion for each sample recorded at 1h time online (Table 5.5).

The TPD of CO₂ for Al₂O₃-based catalysts show desorption peak at about 120°C, indicates the presence of weak basic site with similar strength. Meanwhile, the TPD of NH₃ of ZrO₂-Al₂O₃, ZrO₂ and γ -Al₂O₃ catalysts revealed desorption peak in between 100-300°C centred at 200°C, implying that the presence of weak acid site (Lewis site) with similar strength was obtained for all samples. Lahousse *et al*²¹

reported the presence of Bronsted basicity for zirconia, and the addition of alumina to zirconia does not modify the acidity of alumina but markedly decreases the Bronsted basicity of zirconia. On the other hand, the selective chemisorption of NH_3 and CO_2 shows that by mixing ZrO_2 and Al_2O_3 increases the numbers of both acid and base sites compare to the original $\gamma\text{-Al}_2\text{O}_3$. These evidenced that the promotional effect for $\text{ZrO}_2\text{-Al}_2\text{O}_3$ catalyst was attributed to the increase number of acid and base sites, hence enhancement on activity.

Fig 5.13: TPD of CO_2 at 40°C and NH_3 at 100°C , followed by desorption up to 500°C with $20^\circ\text{C}\cdot\text{min}^{-1}$ of ramp rate

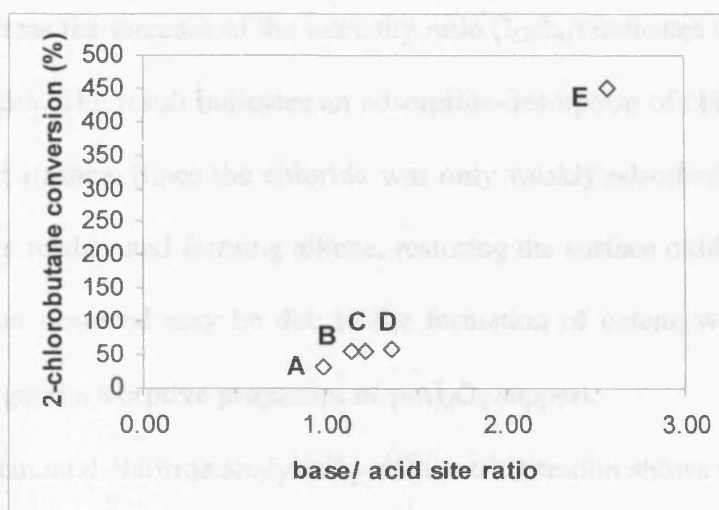


A correlation between the ratio of base to acid site and the activity was proposed. As showed in Fig 5.14, the conversion (after normalised by surface area) increases with increasing ratio of base/acid site. The result suggests that the importance of orientation of the acid-base pair site for acid-base bifunctional catalysis. The basic sites are vital for stabilising the carbonium ion and the acid sites are important for abstraction of Cl^- ions^{2,31}.

Table 5.5: The acid-base properties for $\text{ZrO}_2\text{-Al}_2\text{O}_3$ catalysts with 50wt% ZrO_2 loading.

Catalysts	TPD ($^\circ\text{C}$)		No. of molecules/sites/ $\text{m}^2 \times 10^{16}$		Ratio of base/ acid	Conversion at 1h (%)
	CO_2	NH_3	CO_2 (base)	NH_3 (acid)		
$\gamma\text{-Al}_2\text{O}_3$	115	200	20	20	0.99	34
$\text{ZrO}_2\text{-P}$	140	100-300	92	36	2.57	42
50ZAC	100	200	43	35	1.22	47
50ZAI	115	200	42	37	1.14	36
50ZAH	120	200	38	28	1.36	55

Fig 5.14: A correlation between ratio of base to acid site and the activity for various catalysts. **A.** γ - Al_2O_3 , **B.** ZrO_2 - Al_2O_3 by wet impregnation (50ZAI), **C.** by co-precipitation (50ZAC), **D.** by dry impregnation (50ZAH), and **E.** Pure zirconia (ZrO_2 -P).



5.3.3 Post-reaction analysis

After the catalyst has tested for dehydrochlorination of 2-chlorobutane, the visual examination of the used samples revealed a different degree of discoloration for pure zirconia (ZrO_2 -P, dark brown), ZrO_2 - Al_2O_3 prepared by co-precipitation (50ZAC, brown), by wet impregnation (50ZAI, yellow) and by dry impregnation (50ZAH, light yellow) with 50wt% zirconium salt contents. In order to obtain better understanding of the catalyst performances, the used catalysts were analysed by x-ray photoelectron spectroscopy (XPS) and chloride elemental analysis.

XPS analysis was employed to examine the surface compositions for the fresh and used ZrO_2 - Al_2O_3 catalysts by different preparation methods. All spectra were corrected from shift, based on the Al 2p binding energy of 74.2eV. Table 5.6 shows the intensity ratio of C 1s to Al 2p ($I_{\text{C}}/I_{\text{Al}}$) and Cl 2s to Al 2p ($I_{\text{Cl}}/I_{\text{Al}}$) from XPS analysis over wet impregnated (ZAI) and co-precipitated ZrO_2 - Al_2O_3 catalysts (ZAC) with 50wt% zirconium salt contents. The result showed that after 20h of exposure in dehydrochlorination of 2-chlorobutane for the samples, both ZrO_2 - Al_2O_3 catalysts

(ZAI & ZAC) revealed increase in carbon and chloride peaks intensity. The increased of intensity ratio (I_C/I_{Al}) for C 1s peak suggests the possibly that coke deposition had occurred, whereas the increase of the intensity ratio (I_{Cl}/I_{Al}) indicates the formation of surface chlorides. The result indicates an adsorption-desorption of chlorides occurred on the catalyst surface. Since the chloride was only weakly adsorbed, elimination of HCl took place readily and forming alkene, restoring the surface oxide atom^{32,33}. The coke deposition occurred may be due to the formation of octene with high boiling point, and the good adsorptive properties of γ -Al₂O₃ support.

The elemental chloride analysis by columetric titration shows that the chloride uptake for ZrO₂-Al₂O₃ catalysts was about 6wt%. Note that the chloride uptake γ -alumina was about 5wt% and the pure zirconia does not absorb any chloride.

Table 5.6: Determination of change of intensity ratio for C1s to Al2p (I_C/I_{Al}) and Cl2s to Al2p (I_{Cl}/I_{Al}) from XPS over fresh and used ZrO₂-Al₂O₃ catalysts prepared by wet impregnation (ZAI) and co-precipitation (ZAC) with 50wt% zirconium salt contents.

Reaction time (h)	I_C/I_{Al}		I_{Cl}/I_{Al}	
	50ZAC	50ZAI	50ZAC	50ZAI
0h	0.276	1.16	0.435	0.65
20h	0.929	1.36	0.933	1.34

5.4 Alkaline-doped zirconia-alumina catalysts

Zirconia-alumina mixed oxides were active catalysts for the dehydrochlorination of 2-chlorobutane. However, addition of zirconia to alumina decreases the butene selectivity of pure alumina due to increasing amount of octene formation. Since alkaline-doped alumina catalysts have shown good selectivity to the production of isomers of butene, KOH was added to the ZrO₂-Al₂O₃ mixed-oxide to investigate their catalytic activity in the dehydrochlorination of 2-chlorobutane.

5.4.1 KOH/ZrO₂-Al₂O₃ and ZrO₂/KOH-Al₂O₃

5.4.1.1 Catalysts characterisation

KOH/ZrO₂-Al₂O₃ and ZrO₂/KOH-Al₂O₃ catalysts were prepared by introducing the second and third metal salt followed the sequence as indicated. KOH/ZrO₂-Al₂O₃ termed KZA catalyst, was prepared by impregnating 1wt% of KOH solution on the ZrO₂-Al₂O₃ support prepared by co-precipitation (ZAC) with 50wt% of zirconium salt contents. ZrO₂/KOH-Al₂O₃ termed ZKA catalyst was prepared by impregnating 50wt% of ZrO(NO₃)₂ on 1wt% KOH-Al₂O₃ catalyst. These samples were characterised by BET, XRD, TPD before it was tested for the dehydrochlorination of 2-chlorobutane.

Nitrogen adsorption (BET) was performed to investigate the textural properties of KOH/ZrO₂-Al₂O₃ and ZrO₂/KOH-Al₂O₃ catalysts. As shown in Table 5.7, the ZrO₂-Al₂O₃ and KOH-Al₂O₃ supports showed 260m²g⁻¹ and 280m²g⁻¹ of specific surface area. As soon as the third metal was introduced to the support, the BET area reduced by approximately 15% to give 229m²g⁻¹ for KOH/ZrO₂-Al₂O₃ and 237m²g⁻¹ for ZrO₂/KOH-Al₂O₃. The reduction of specific surface area indicates that the introduction of the third metal by impregnation method resulting in crystallite growth⁵ that block the surface area of the support. The actual zirconium (or ZrO₂) and the potassium loadings were determined from XRF and AA (Table 5.7), were showed differences in the fraction by which means the zirconium metal was incorporated.

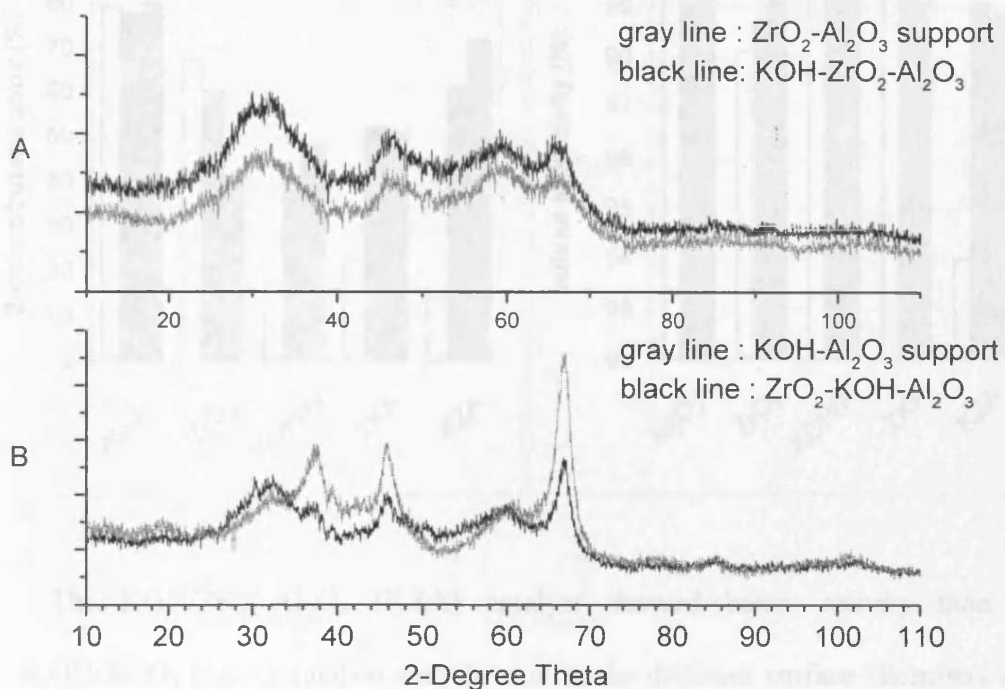
Table 5.7: BET area of various combinations of KOH/ZrO₂-Al₂O₃ catalysts. Results from XRF and AA were enclosed as references.

Catalysts	BET (m ² g ⁻¹)	XRF (wt% Zr)	AA (wt% K)
1wt%KOH/50wt% ZrO ₂ -Al ₂ O ₃ (KZA)	229	21.4	0.7
50wt%ZrO ₂ /1wt% KOH-Al ₂ O ₃ (ZKA)	237	8.8*	0.7
50wt% ZrO ₂ -Al ₂ O ₃ (ZAC)	260	28	-
1wt% KOH-Al ₂ O ₃	280	-	0.7

*XRF data were obtained from the industrial research laboratory. We do not fully agree with the result obtained.

XRD patterns of $\text{KOH/ZrO}_2\text{-Al}_2\text{O}_3$ and $\text{ZrO}_2/\text{KOH-Al}_2\text{O}_3$ catalysts show that amorphous materials were obtained, as shown in Fig 5.15A & B. The XRD pattern of $\text{KOH/ZrO}_2\text{-Al}_2\text{O}_3$ catalyst was the same as the $\text{ZrO}_2\text{-Al}_2\text{O}_3$ support, indicates a good dispersion of KOH was obtained. On the other hand, the XRD pattern of $\text{KOH-Al}_2\text{O}_3$ support revealed sharp peaks at 2θ of 32.8° , 37.4° , 46.0° and 66.8° evidenced the presence of γ -alumina phase. In contrast, addition of ZrO_2 to $\text{KOH-Al}_2\text{O}_3$ yielded sample with low crystallinity, suggesting the possibly formation of amorphous ZrO_2 structure.

Fig 5.15: XRD patterns of $\text{KOH/ZrO}_2\text{-Al}_2\text{O}_3$ (KZA) and $\text{ZrO}_2/\text{KOH-Al}_2\text{O}_3$ (ZKA), where the supports were used as references

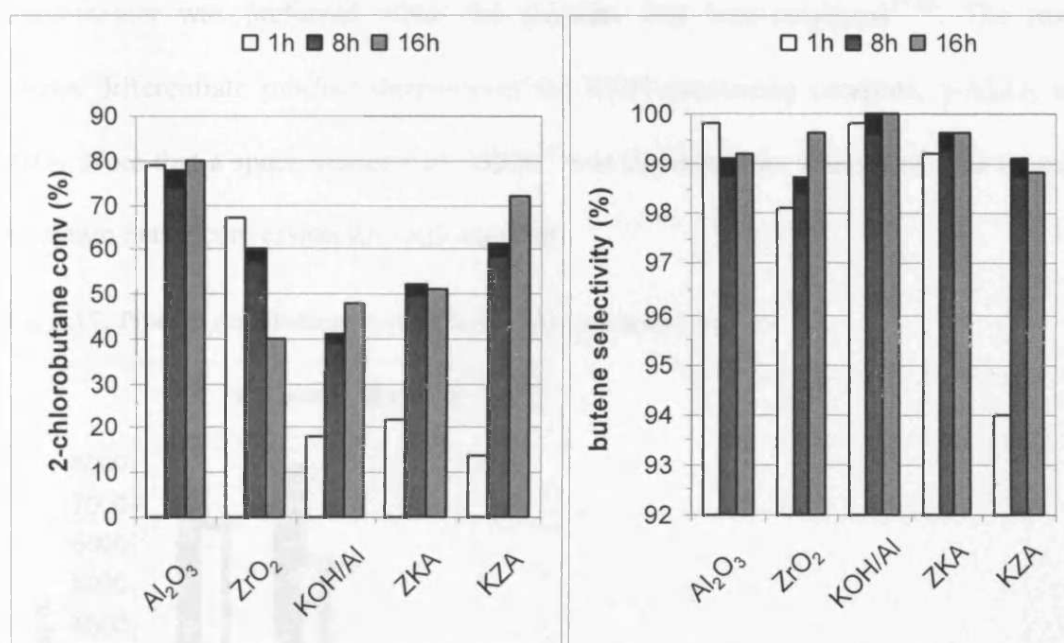


5.4.1.2 Catalytic activity

$\text{KOH/ZrO}_2\text{-Al}_2\text{O}_3$ (KZA) and $\text{ZrO}_2/\text{KOH-Al}_2\text{O}_3$ (ZKA) catalysts were tested on the catalytic dehydrochlorination of 2-chlorobutane. Fig 5.16 shows the catalytic performances for $\text{KOH/ZrO}_2\text{-Al}_2\text{O}_3$ and $\text{ZrO}_2/\text{KOH-Al}_2\text{O}_3$ catalysts at 135°C . Pure γ -

Al_2O_3 , zirconia ($\text{ZrO}_2\text{-P}$) and 1wt% of $\text{KOH}/\text{Al}_2\text{O}_3$ were used as references. The results show that the mixture of KOH , ZrO_2 and Al_2O_3 (KZA & ZKA) yielded catalyst with lower conversion compare to $\text{ZrO}_2\text{-Al}_2\text{O}_3$. This is consistent with the tendency of the addition of KOH neutralised the acidity of the support and showed increase in basicity.

Fig 5.16: 2-Chlorobutane conversion and butene selectivity for $\text{KOH}/\text{ZrO}_2\text{-Al}_2\text{O}_3$ (KZA) and $\text{ZrO}_2/\text{KOH-Al}_2\text{O}_3$ (ZKA) catalysts. Pure alumina, zirconia and 1wt% $\text{KOH}/\text{Al}_2\text{O}_3$ were used as references. Reaction conditions: 135°C , 300mg of catalyst and total gas flow of $60\text{ml}\cdot\text{min}^{-1}$ ($\text{GHSV} = 9509\text{h}^{-1}$). Feed concentration is 22000ppm.

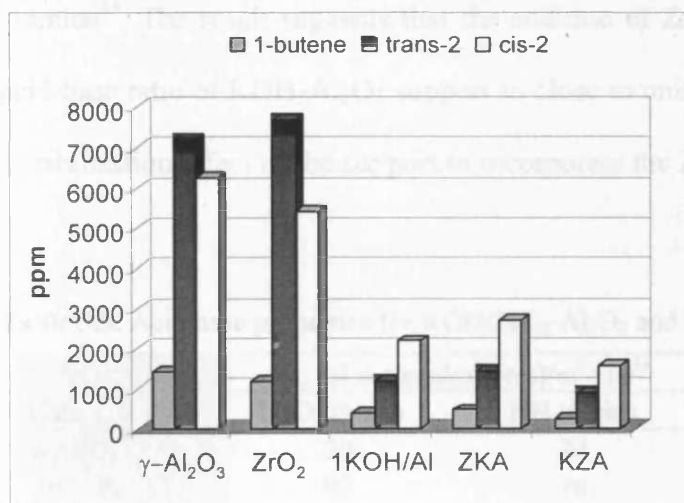


The $\text{KOH}/\text{ZrO}_2\text{-Al}_2\text{O}_3$ (KZA) catalyst showed better activity than the $\text{ZrO}_2/\text{KOH-Al}_2\text{O}_3$ (ZKA) catalyst may be due to the different surface chemistry as a result of different metal incorporation. The order of the 2-chlorobutane conversion at 16h for various catalysts decreases accordingly: $\gamma\text{-Al}_2\text{O}_3$ (80%) > $\text{KOH}/\text{ZrO}_2\text{-Al}_2\text{O}_3$ (72%) > $\text{ZrO}_2/\text{KOH-Al}_2\text{O}_3$ (52%) > 1% $\text{KOH}/\text{Al}_2\text{O}_3$ (48%) > ZrO_2 (40%). The products selectivities revealed that all catalysts tested were highly selective to isomers of butene with above 98.5% of selectivity at steady state. The order of butene

selectivities at 16h for various catalysts decreases according to: 1%KOH/Al₂O₃ > ZrO₂/KOH-Al₂O₃ > ZrO₂ > γ-Al₂O₃ > KOH/ZrO₂-Al₂O₃.

Fig 5.17 shows the product distribution of various catalysts for dehydrochlorination of 2-chlorobutane at 135°C. The results show that KOH/ZrO₂-Al₂O₃ (KZA) and ZrO₂/KOH-Al₂O₃ (ZKA) yield cis-2-butene as dominant product. On the contrary, trans-2-butene is preferred over pure γ-Al₂O₃ and pure ZrO₂ catalyst. The cis-isomer was predominant when the reaction was acid-catalysed, while the trans-isomer was preferred when the reaction was base-catalysed^{17,18}. The result shows differentiate product distribution for KOH-containing catalysts, γ-Al₂O₃ and ZrO₂. Note that a space velocity of 9509h⁻¹ was dedicated for this set of data in order to obtain better conversion for each catalyst.

Fig 5.17: Product distribution over various types of catalysts at 1h



5.4.1.2.1 Correlation between acid-base properties and catalytic activity

The acid-base pair concepts are often invoked to explain the catalytic properties. The KOH/ZrO₂-Al₂O₃ and ZrO₂/KOH-Al₂O₃ catalysts were characterised by the selective adsorption and temperature programmed desorption (TPD) analysis to

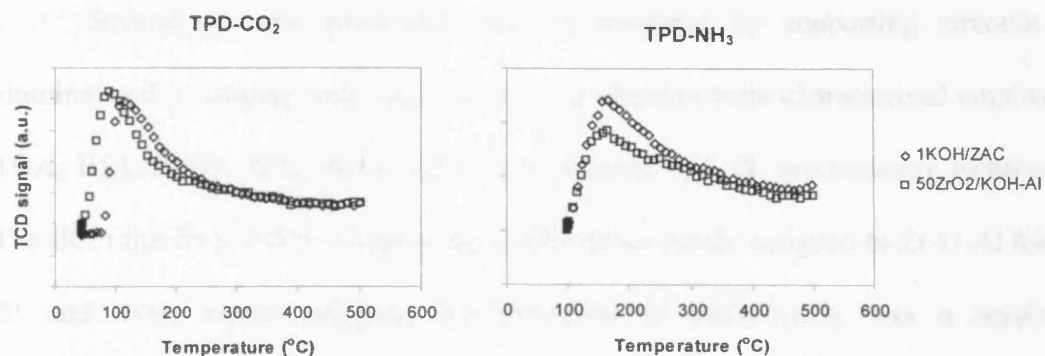
observe the change in acid-base properties after the additions of KOH. Table 5.8 shows the acid-base properties of various catalysts and its catalytic conversion at 1h time online. The amount of acid-base sites were quantified by adsorbing acidic (CO_2) and basic (NH_3) probes to the samples with the assumption of one molecule of reactive probe could react with one corresponding site.

TPD of CO_2 and NH_3 revealed desorption peaks temperature at 120 and 170°C (Fig 5.18), respectively, indicating the presence of weak base and weak acid sites. The result indicates that addition of 1wt%KOH to $\text{ZrO}_2\text{-Al}_2\text{O}_3$ increased the amount of basic sites significantly and decreased in acidity. On the other hand, the addition of ZrO_2 to $\text{KOH-Al}_2\text{O}_3$ decreases the basicity and increase the acidity slightly. We propose that $\text{KOH/ZrO}_2\text{-Al}_2\text{O}_3$ catalyst experienced the same effect as the addition of KOH to $\gamma\text{-Al}_2\text{O}_3$, that the addition of KOH neutralised the Lewis acid sites of alumina³⁴. The result suggests that the addition of ZrO_2 to $\text{KOH-Al}_2\text{O}_3$ modifies the acid-base ratio of $\text{KOH-Al}_2\text{O}_3$ support to close to unity (base/acid = 1.05), and shows a stabilisation effect of the support to incorporate the ZrO_2 active phase¹⁹⁻²¹.

Table 5.8: Acid-base properties for $\text{KOH/ZrO}_2\text{-Al}_2\text{O}_3$ and $\text{ZrO}_2/\text{KOH-Al}_2\text{O}_3$ catalysts

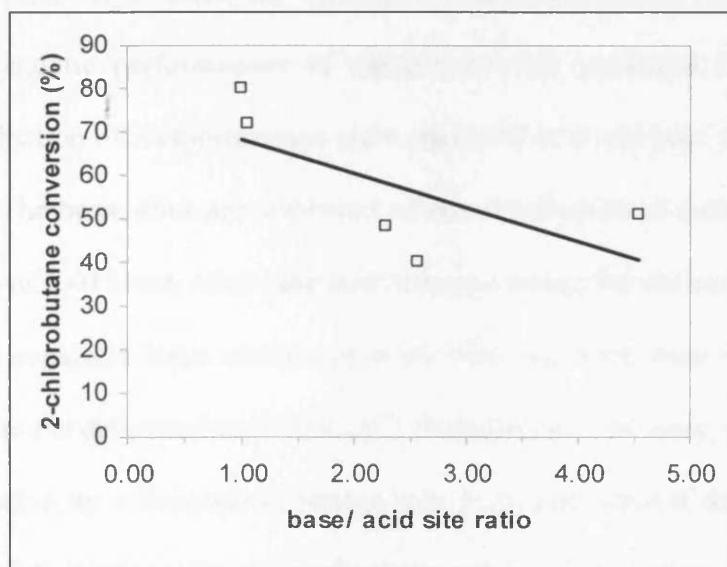
Catalysts	No. of molecules/sites/ $\text{m}^2 \times 10^{16}$		Ratio of base/ acid	Conversion at 1h (%)
	CO_2 (base)	NH_3 (acid)		
$\gamma\text{-Al}_2\text{O}_3$	20	20	0.99	80
$\text{ZrO}_2\text{-P}$	92	36	2.57	40
1% KOH/Al	41	18	2.28	48
50ZAC	43	35	1.22	-
KZA	100	22	4.55	51
ZKA	23	22	1.05	72

Fig 5.18: TPD of CO₂ at 40°C and NH₃ at 100°C, followed by desorption up to 500°C with 20°C·min⁻¹ ramp rate



A correlation between the acid-base properties and the catalytic activity was proposed. Referring to Fig 5.19, the results indicate that the 2-chlorobutane conversion increases with increasing amount of acidic sites. Despite the KOH/ZrO₂-Al₂O₃ (KZA) catalyst exhibited strong basicity, the catalyst was active to the 2-chlorobutane conversion to give 50% conversion, indicates that both acid and base sites are involved in catalytic dehydrochlorination of 2-chlorobutane. In this case, the acidic site is contributed to the abstraction of chloride, while the basic site serves hydrogen-activation and stabilisation of the carbonium ion^{2,31}.

Fig 5.19: Acid-base properties versus activity



5.5 Conclusions

Several zirconia promoted catalysts prepared by supporting zirconia on alumina, and by doping with base on zirconia-alumina were characterised employing TGA, BET, XRD, TPD, XPS, XRF, AA, Raman, and IR spectroscopy techniques. The IR of the $\text{ZrO}_2\text{-Al}_2\text{O}_3$ samples show adsorption bands assigned to Zr-O-Al bands. IR and TGA results support the formation of $\text{ZrO}_2\text{-Al}_2\text{O}_3$ was a result of decomposition of hydroxylate gel and desorption of residual nitrate. X-ray diffraction patterns do not identify crystalline structures corresponding to ZrO_2 , neither for $\text{ZrO}_2\text{-Al}_2\text{O}_3$ samples nor alkaline-doped samples. The samples after the calcination are appeared in amorphous forms. These results are always in agreement with the BET surface area determined, in which the mixing of ZrO_2 and Al_2O_3 yield catalyst with large surface area and good textural stabilities. XRF and AA confirmed the metal loadings, and XPS monitored the surface composition with prediction of surface chemistry. It was observed that $\text{ZrO}_2\text{-Al}_2\text{O}_3$ prepared by co-precipitation exhibited better dispersion of ZrO_2 . The acid-base properties study of $\text{ZrO}_2\text{-Al}_2\text{O}_3$ shows addition of ZrO_2 to Al_2O_3 increased both the acid and basic sites of Al_2O_3 .

The catalytic performances of various zirconia promoted catalysts for the dehydrochlorination of 2-chlorobutane show that both acid and base sites took part in the reaction. The basic sites are attributed to the stabilisation of carbonium ions and the activation of C-H bond, where the acid sites encourage the abstraction of Cl^- ions. Pure zirconia consisted large amount of weak acid and weak base sites, and it was highly active to the dehydrochlorination of 2-chlorobutane. However, the high activity was accompanied by a decrease in butene selectivity and catalyst deactivation. This was due to the formation of non-volatile hydrocarbons (octenes) as a consequent of side reaction causes surface poisoning by coke deposition. The absence of a chlorine

peak from XPS and the chloride analysis by coulometric titrations expelled the possibility of surface poisoning by organic chloride adsorptions. On the other hand, catalyst screenings of $ZrO_2-Al_2O_3$ showed an optimum loading of 50wt% of zirconium salt contents. The catalyst testing examined for $ZrO_2-Al_2O_3$ catalysts show enhancement on activity of the pure alumina and zirconia single oxide. It was due to the improvement in the textural properties and the surface acid-base properties by introducing zirconia to alumina. The order of the activity based on the TON is the catalyst prepared by co-precipitation (ZAC) > dry impregnation (ZAH) > wet impregnation (ZAI). The order of the 2-chlorobutane conversion for the top three active catalysts is ZAH > ZAC > ZAI of 50wt% zirconium salt contents. Note that the base to acid sites ratio seems to be important for the catalytic dehydrochlorination of 2-chlorobutane.

The 50wt% ZAH catalyst exhibited the best activity with high conversions and selectivity. The catalyst resembled the reaction trend of alumina and do not deactivate with time. Meanwhile, the 50wt% ZAC catalyst also showed high conversion of 2-chlorobutane. However, the butene selectivity was lower than the 50wt% ZAH catalyst due to increasing amount of octene with respond to the generation of more structural defect sites that justifies the values of acidity and hence the occurrence of side reactions. Finally, the ZAI catalyst showed general lower activity due to the sintering of crystallite on the surface during the catalyst preparation, resulting in low dispersion of ZrO_2 and less active to dehydrochlorination of 2-chlorobutane. The products distribution indicated that the cis-2-butene was the most selective product for $ZrO_2-Al_2O_3$ catalysts, and the surface acidity increased with the reaction time. A correlation between the acid-base properties and catalytic activity was evidenced. Post-reaction analysis showed proofs for the coke depositions and surface chlorination

of $\text{ZrO}_2\text{-Al}_2\text{O}_3$ catalysts due to the ability of the support to adsorb the reactants and the products.

Lastly, by introducing KOH to $\text{ZrO}_2\text{-Al}_2\text{O}_3$ (KOH/ $\text{ZrO}_2\text{-Al}_2\text{O}_3$ or $\text{ZrO}_2\text{/KOH-Al}_2\text{O}_3$) showed less active in the dehydrochlorination of 2-chlorobutane compare to the pure γ -alumina and zirconia single oxide. The addition of KOH increased the basicity of the catalysts and neutralised the Lewis acid sites that serve as the active sites.

References

1. H. Hattori, *Chemical Review*, **95** (1995) 537-558
2. K. Tanabe, T. Yamaguchi, *Catalysis Today*, **20** (1994) 185-198
3. M.A. Aramedia, V. Borau, C. Jimenez, J.M. Marinas, A. Porras, F.J. Urbano, *J. Chem. Soc, Faraday Transaction*, **93**: 7 (1997) 1431
4. P. Afanasiev, A. Thiollier, M. Breyse, J.L. Dubois, *Topics in Catalysis*, **8** (1999) 147-160
5. P.D.L. Mercera, J.G. Van Ommen, E.B.M. Doesburg, A.J. Burggraaf, and J.R.H. Ross, *Applied Catalysis*, **57** (1990) 127-148.
6. A. Kaddouri, C. Mazzocchia, E. Tempesti and R. Anouchinsky, *Journal of Thermal Analysis*, **53** (1998) 97-109.
7. R. Srinivasan, B. H. Davis, *Catalysis Letters*, **14** (1992) 165-170
8. G.K. Chuah, S. H. Liu, S. Jaenicke, J. Li, *Microporous and Mesoporous Materials*, **39** (2000) 381-392
9. M. Howe-Grant, Kirk-Othmer Encyclopedia of Chemical Technology (1985). John Wiley & Sons. **24**: p. 888
10. F. Albert Cotton, G. Wilkinson, "Advanced Inorganic Chemistry". 5th edition (1988), John Wiley and Son.
11. M. Shibagaki, *Fine Chemicals*, **21** (1992) 5
12. D.J. Moon, M. J. Chung, K.Y. Park, S. I. Hong, *Applied Catalysis A: General*, **168** (1998) 159-170
13. S.C. Shekhar, J. K. Murphy, P.K. Rao, K.S. Rama Rao., *Applied Catalysis A: General*, **271** (2004) 95-101
14. J.K. Murthy, S. C. Shekhar, V.S. Kumar, K.S. Rama Rao, *Catalysis Communications*, **3** (2002) 145
15. G.A. Zacheis, K. A. Gray, P.V. Kamat, *Journal of Physical Chemistry B*, **105** (2001) 4715-4720
16. C. Su, J. Li, D. He, Z. Cheng, Q. Zhu, *Applied Catalysis A: General*, **202** (2000) 81-89
17. I. Mochida, A. Uchino, H. Fujitsu, K. Takeshita, *Journal of Catalysis*, **43**: 1-3 (1976) 264-72

18. I. Mochida, Y. Anju, A. Kato, T. Seiyama, *Journal of Organic Chemistry*, **39**: 25 (1974) 3785-7
19. O.V. Metelkina, V.V. Lunin, V.A. Sadykov, G.M. Alikina, R.V. Bunina, E.A. Paukshtis, V.B. Fenelonov, A.Y. Derevyankin, V.I. Zaikovskii, U. Schubert, J.R.H. Ross, *Catalysis Letters*, **78**: 1-4 (2002) 111-114
20. C.R. Vera, J. M. Parera, *Journal of Catalysis*, **165/6** (1997) 254-262
21. C. Lahousse, A. Aboulayt, F. Mauge, J. Bachelier and J.C. Lavalley, *Journal of Molecular Catalysis* **84** (1993) 283-297.
22. S. Castillo, M. Moran-Pineda, R. Gomez, *Catalysis Communications* **2** (2001) 295-300.
23. M. Moran-Pineda, S. Castillo, T. Lopez, R. Gomez, Cordero-Borboa, O. Novaro, *Applied Catalysis B: Environmental*, **21** (1999) 79-88
24. J.L. Lakshmi, T.R.B. Jones, M. Gurgi, J.M. Miller, *Journal of Molecular Catalysis A: Chemical* **152** (2000) 99-110.
25. A. Gampine, D. P. Eyman, *Journal of Catalysis*, **179** (1998) 315-325
26. S.T. Srinivas, P. S. Sai Prasad, P. Kanta Rao, *Catalysis Letters*, **50**: 1/2 (1998) 77-82
27. M.L. Balmer, F. F. Lange, C.G. Levi,, *Journal of American Ceramic Society*, **77** (1994) 2069
28. T. Lopez, A. Romero, R. Gomez, *Journal of Non-Crystallite Solids*, **127** (1991) 105
29. A. Vazquez, T. Lopez, R. Gomez, A. Bokhimi, O. Morales, and Novaro, *Journal of Solid State Chemistry*, **123** (1997) 161
30. A.C.Q.M. Meijers, A. M. de Jong, L.M.P. van Gruijthuijsen, J.W. Niemantsverdriet, *Applied Catalysis*, **70** (1991) 53-71
31. H. Noller, W. Kladnig, *Catalyst Review- Science and Engineering*, **13** (1976) 149-207
32. T.H. Ballinger, J. J. T. Yates, *Journal of Physical Chemistry*, **96**: 3 (1992) 1417-23
33. C. Pistarino, E. Finocchio, G. Romezzano, F. Bricchese, R. Di Felice, and G. Busca; M. Baldi, *Industrial & Engineering Chemistry Research*, **39** (2000) 2752-2760
34. J. Shen, R. D. Cortright, Y. Chen, J. A. Dumesic, *Journal of Physical Chemistry*, **98**: (1994) 8067-8073

6 SILVER DOPED CATALYSTS

Silver-doped alumina

Al₂O₃-SS/ α -Al₂O₃/ SiO₂/ BN as alternative support

Silver-doped silica

Silver-doped zirconia-alumina

6.1 Introduction

Silver containing catalysts are particularly interesting in catalytic dehalogenation due to the existence of silver ions in more than one valence state which are able to donate and accept halogen ions freely¹. Since 1960s, the silver containing catalysts have been widely used for dechlorination include photocatalytic^{2,3}, radiolytic⁴, electrochemical⁵ and catalytic reductive reactions. Jusaburo *et al*⁶ investigated the catalytic activity of Raney nickel in reductive dehalogenation of chlorobenzene and was found that the addition of metals such as Pd, Mo, Cu and Ag served as promoters within certain ranges.

Later, Anju and Mochida⁷ performed the dehalogenation of haloethanes and halopropanes over metals (Cu, Ag, Au, Fe, Co, Ni, Pd, and Pt) supported by silica gel. The dechlorination reactivities of cis- and trans-1,2-dichloroethylene and the dechlorination products from dl- and meso-2,3-dichlorobutane were observed from the basis of stereoselectivity. The order of catalytic activities among the metals for the dehalogenation of haloethanes was: Pt > Cu \approx Ni > Ag \approx Co \approx Pd > F \approx Au. The author emphasized the differences in the reaction mechanism for the decomposition of haloethanes and halopropanes, and a conclusion was drawn from the results that the dehalogenation of haloalkanes on metal proceeds through a radical step-by-step mechanism.

Simkovich and Wagner⁸ were the first to report the roles of ionic point defects, which are the effects of electrons and electron holes (electronic effect) on the catalytic

dehydrochlorination of tertiary butyl chloride with pure and doped AgCl catalysts. Hauffe and Sitabkhan⁹, J. Maier^{10,11}, Ng and Leung^{12,13} subsequently prepared AgCl doped with Al₂O₃ or SiO₂, CuCl₂ and first-row transition metal chlorides to perform similar studies on the influence of ionic point defects in the same reaction.

Patent studies by Ito¹⁴ and Schoebrechts¹⁵ for reductive dechlorination and metal-catalysed reductive dechlorination of chlorinated hydrocarbons byproducts and waste products to less chlorinated hydrocarbons have been well established. For instance, hydrogenation of 1,2-dichloropropane with hydrogen in the presence of a supported catalyst such as Pt, Pd, Ru, Ir, Cu, Ag in elemental or compound form, gave a high degree of conversion and selectivity. In particular, the synthesis process, catalyst characterisations and the use of Pd-Ag/SiO₂ sol-gel catalysts^{16,17} for selective hydrodechlorination of 1,2-dichloroethane into ethylene has been studied extensively. Recently, Pd/SiO₂, Ag/SiO₂ and Cu/SiO₂ cogelled xerogel catalysts¹⁸ were synthesized for the same reaction.

In our studies, the catalytic dehydrochlorination of 2-chlorobutane using Ag/ γ -Al₂O₃, Ag/SiO₂ and Ag/ZrO₂-Al₂O₃ catalysts were compared, and the interactions between metal-support were investigated. These catalysts were prepared by impregnating the silver nitrate on the desired support and were characterised by BET, XRD, XPS, TPR and TGA for the physical and structural properties, and the thermal stability, before being tested for the catalytic properties.

6.2 Silver-doped alumina

Ag/ γ -Al₂O₃ catalysts have been studied extensively due to its application in catalytic combustion to control emission of NO, volatile organic compounds and automotive exhausts^{19,20}. However, few studies have been published for catalytic

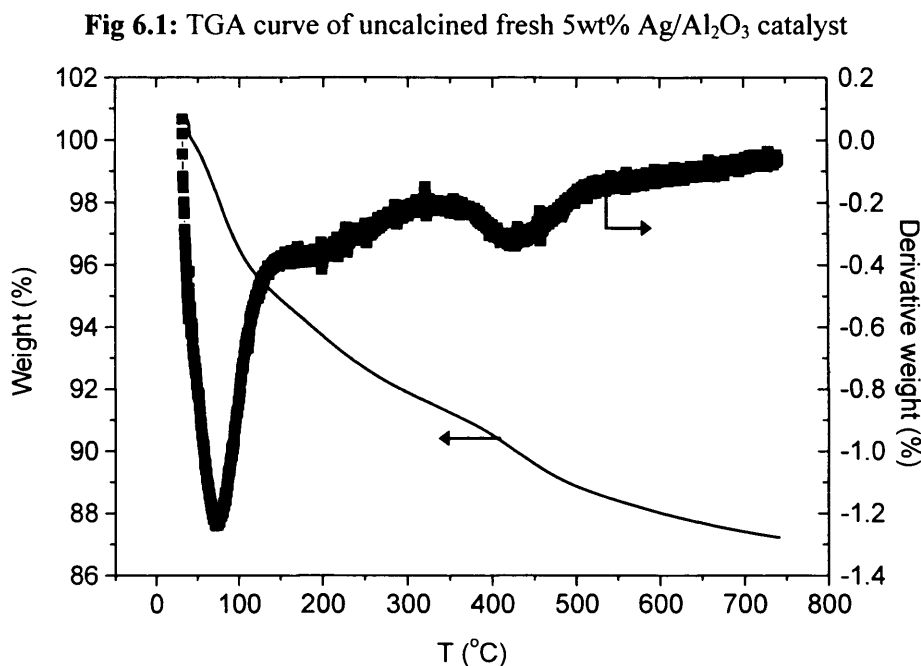
dehydrochlorination. Since γ - Al_2O_3 support was found active for the 2-chlorobutane conversion and the addition of silver to alumina can promote the interactions between the metal-support²¹, hence improvement on the surface properties. Our goal is to combine the advantageous of the highly reactive noble metal with highly absorptive γ - Al_2O_3 support and to develop a catalyst which exhibits high activity to the catalytic dehydrochlorination of 2-chlorobutane. A series of $\text{Ag}/\gamma\text{-Al}_2\text{O}_3$ catalysts with Ag loadings ranging from 1 to 20wt% was prepared using the incipient wetness impregnation method. The metal loading was confirmed by the atomic absorption spectroscopy.

6.2.1 Catalyst characterisation

Fig 6.1 shows the typical TGA curve for uncalcined $\text{Ag}/\gamma\text{-Al}_2\text{O}_3$ catalysts with 5wt% of AgNO_3 on alumina as a representative result. At temperature ramp of $20^\circ\text{C}\cdot\text{min}^{-1}$, two broad peaks at 100-300°C and 420°C were observed. The peak at 100-300°C was due to loss of physisorbed and crystalline water. At 420°C, the weight loss was assigned to the decomposition of silver nitrate. In addition, the detachment of surface hydroxyl group of alumina^{22,23} starts at temperature above 450°C. It is worth to note that the amount of total weight loss decreases according to the increasing silver loadings corresponding to the decrease of surface water with the additions of silver.

Wang *et al*²² suggested that the silver loading gradually reduces the degree of dehydration of γ -alumina over 500°C, indicating a correlation between the surface hydroxyl group and the silver loading. An interaction between the small amounts of Ag^+ with the basic $-\text{OH}$ species produces acidic proton, which becomes additional loading sites for Ag^+ . Various loadings of $\text{Ag}/\text{Al}_2\text{O}_3$ catalysts were calcined at 450°C

under static air for 3h before used. The final sample weight loss was between 5 and 15% of the initial sample weight.



6.2.1.1 Physical properties of Ag/Al₂O₃ catalysts

Nitrogen adsorption was performed to examine the textural properties of Ag/Al₂O₃ catalysts after the calcination. The BET plot revealed a type II isotherm (see Appendix C) suggesting a non-porous material was obtained. Fig 6.1 shows the BET surface area or various loadings of Ag/Al₂O₃ catalyst with the actual metal loadings determined by atomic absorption. The results show that the increasing silver loadings decrease the BET surface area. This phenomenon may be due to the occurrence of multilayer coverage as a result of large particles formed on alumina surface. The theoretical Ag loading estimated for the monolayer coverage is about 8wt%.

On the other hand, the x-ray diffraction (XRD) patterns for the calcined Ag/Al₂O₃ catalysts were collected. As shown in Fig 6.2a, the XRD pattern for pure AgNO₃ after the calcination shows the presence of metallic Ag, and possibly Ag₂O

crystalline phases. Sharp peaks at 2θ of 38.1° , 44.3° , 64.4° , 77.5° and 81.5° were assigned to the metallic silver phase. Unfortunately, we are not able to distinguish the crystalline Ag_2O from the metallic Ag phase, as the most intense diffraction peak was overlapping each other at 38.1° . No XRD peaks attributed to the crystalline silver metal can be observed for 1wt% Ag/ Al_2O_3 catalyst due to the low Ag loading (Fig 6.2c). In contrast, distinct XRD patterns of the metallic silver peaks and γ -alumina were observed for the 5wt% Ag/ Al_2O_3 catalyst (Fig 6.2d). The peaks intensity decrease as the Ag loading increased. The XRD peaks assigned to the crystalline silver metal diminished with 20wt% Ag/ Al_2O_3 catalyst (Fig 6.2f).

Table 6.1: BET areas and total metal loading for Ag/ Al_2O_3 catalysts.

	BET (m^2g^{-1})	Metal loading from AA (wt% Ag)
$\gamma\text{-Al}_2\text{O}_3$	290	-
1wt%Ag/ Al_2O_3	251	0.8
5wt%Ag/ Al_2O_3	250	4.6
10wt%Ag/ Al_2O_3	243	9.2
20wt%Ag/ Al_2O_3	223	18.9

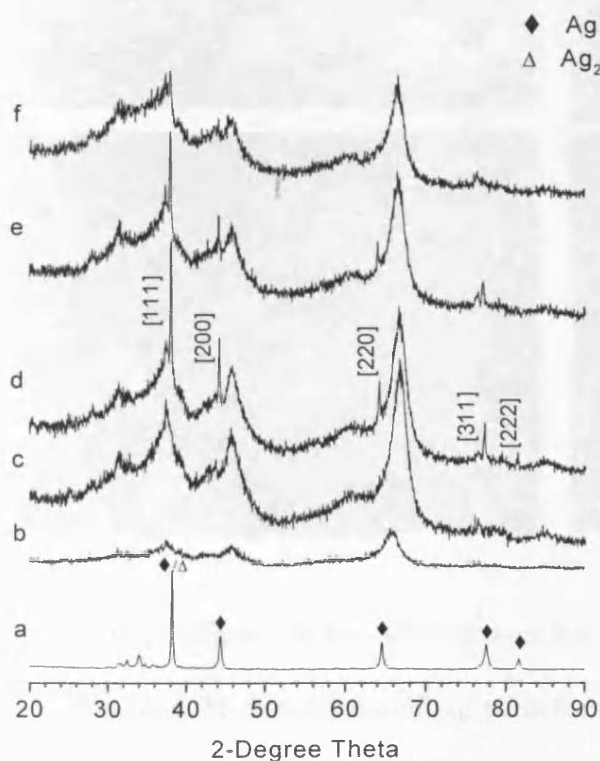


Fig 6.2: XRD patterns of Ag/ Al_2O_3 catalysts; calcined AgNO_3 and pure $\gamma\text{-Al}_2\text{O}_3$ were used as references.

a. Calcined AgNO_3 ,

b. $\gamma\text{-Al}_2\text{O}_3$,

c-f. 1, 5, 10 and 20wt% Ag/ Al_2O_3 catalysts.

The results indicate an unusual decrease in the degree of XRD line broadening peaks with increased metal loading above 1wt% Ag, corresponding to the presence of small particles at high loading samples. Hoost *et al*²¹ who studied the apparent metal dispersion of Ag/Al₂O₃ catalysts using the O₂ adsorption and H₂-O₂ titration methods, has observed this unusual trend for Ag/Al₂O₃ catalysts. The apparent dispersion increased with Ag loading and was attributed to a metal-support interaction^{21,22,24}. The observed trend of the XRD patterns suggesting a good dispersion of Ag particles and possibly formation of stable Ag aluminate²¹ structures may obtain.

Fig 6.3: SEM micrograph from Ag/Al₂O₃ catalysts. (a) 1wt% Ag/Al₂O₃, (b) 5wt% Ag/Al₂O₃, (c) 20wt% Ag/Al₂O₃ and (d) pure γ -Al₂O₃ support with magnification $\times 5000$.

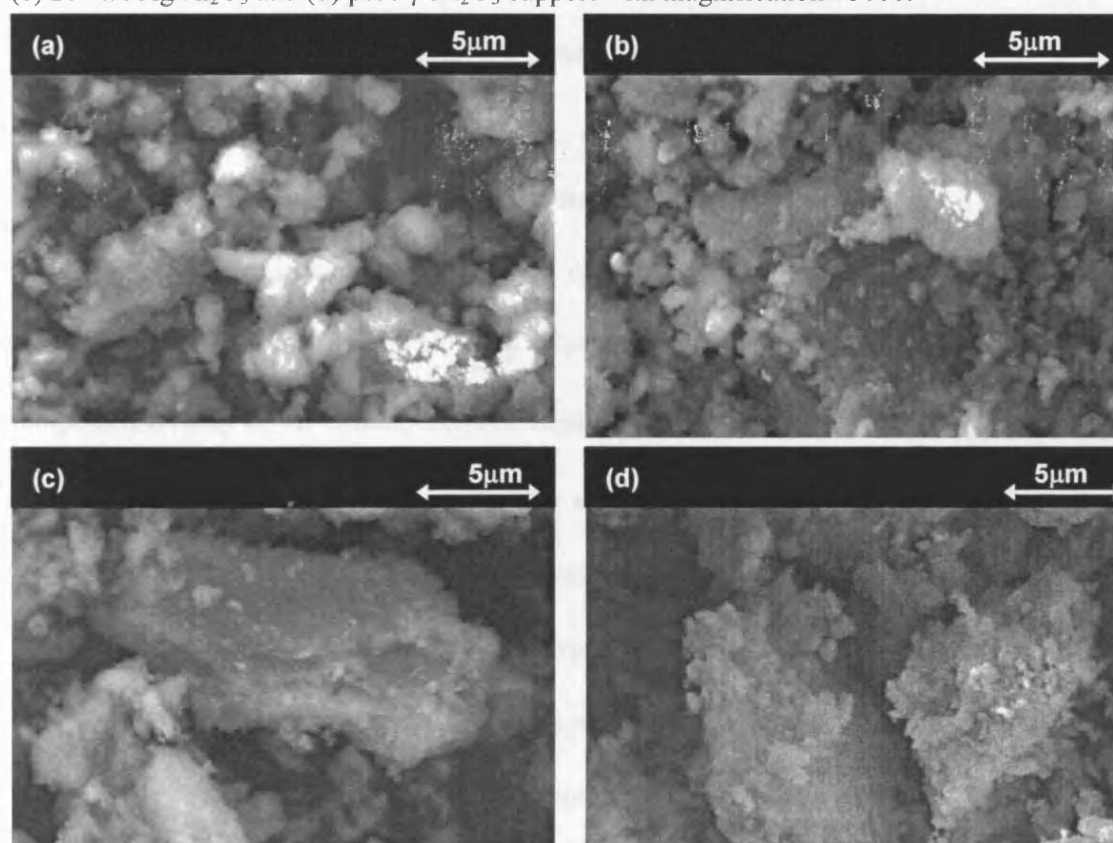


Fig 6.3 illustrates the SEM images for various loadings of Ag/Al₂O₃ catalysts to demonstrate the distribution of Ag particles and their morphology on the surface of Al₂O₃. As shown in Fig 6.3a, the surface of 1wt% Ag/Al₂O₃ was covered by particles

~2 μm in diameter with sphere shape. Fig 6.3b shows the image for 5wt% Ag/Al₂O₃ that revealed aggregates of varying shapes ranges from 1~5 μm in diameter. Fig 6.3c shows that the large particles of 20wt% Ag/Al₂O₃ in sizes of 7~15 μm in diameter, which is close to that of the pure γ -Al₂O₃ support (Fig 6.3d). The results indicate an amorphous surface was observed for Ag/Al₂O₃ catalysts attributed to the γ -Al₂O₃ support.

Indeed, the SEM was not suitable to identify either the silver oxide or the metallic silver particles due to the poor resolution with high magnification. XRD and SEM studies performed by Aoyama *et al*²⁴ showed particles growth in large size (~50nm, no XRD peaks) as a result of an interaction between Ag and the γ -Al₂O₃ support. The reduced Ag/Al₂O₃ showed generally small particles (~10nm).

6.2.1.2 Temperature programmed reduction (TPR)

TPR was performed over Ag/Al₂O₃ catalysts to examine the reduction process. A TPR was carried out by introducing 50ml·min⁻¹ of 10wt%H₂/Ar gas mixture at a temperature ramp of 10°C·min⁻¹. It was assumed that one Ag⁺ consumes ½ molecule of H₂. Fig 6.4 shows the TPR profiles for various loadings of γ -alumina support (a) and Ag/Al₂O₃ catalysts (b-e). Two reduction peaks were observed at temperature below 100°C. With 20wt% Ag/Al₂O₃ catalyst, two reduction peaks were observed at 50°C and 80°C, were attributed to the dispersed Ag₂O and the crystalline Ag₂O phase, respectively. The TPR-H₂ of pure Ag₂O was performed and was shown a reduction peak temperature at 90°C due to the crystalline Ag₂O phase. The reduction peaks were diminished and the peaks temperature was shifted to 50°C and 104°C with 10wt% Ag/Al₂O₃ catalyst. Only one reduction peak can be observed for 5wt% Ag/Al₂O₃, and the absence of a reduction peak for 1wt% Ag/Al₂O₃ due to the relatively low silver

contents. The results indicate that the H_2 consumption increases as the Ag loading increased. In addition, the 10wt% Ag/Al_2O_3 catalyst showed less dispersed than the 20wt% Ag/Al_2O_3 catalyst as the reduction peak was observed at higher temperature.

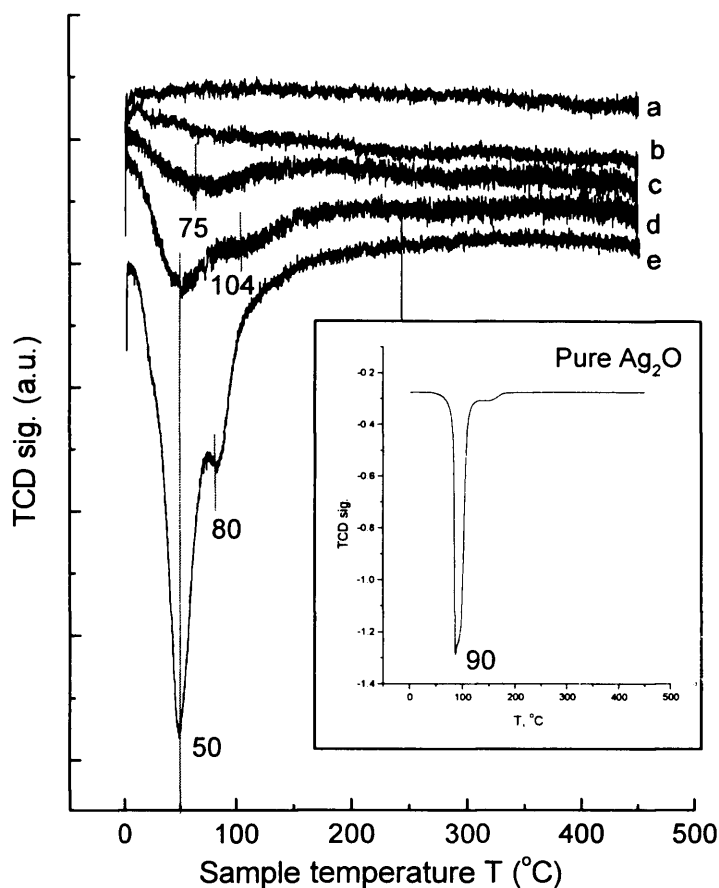


Fig 6.4: TPR of silver-doped catalysts. a. Pure γ -alumina, b. 1wt%, c. 5wt%, d. 10wt%, e. 20wt% Ag/Al_2O_3 . TPR of Pure Ag_2O as reference.

The results agreed with the profiles published by Luo *et al*¹⁹ that the reduction of dispersed Ag_2O phase occurring at a lower temperature compare to the crystalline Ag_2O phase. Yamashita *et al*²⁵ also reported that calcination of Ag/Al_2O_3 at high temperature induced an interaction between Ag and Al_2O_3 , resulting in the growth of the disordered silver oxide particles on Al_2O_3 .

The amount of hydrogen consumption was divided by the absolute metal loadings to give an estimation of the amount of reducible species, as shown in Table 6.2. The result shows the percentage of the reducible species increases with increasing Ag loading, which is consistent with the XRD results that the apparent dispersion

increases as the Ag loading was increased from 5wt% to 20wt%. The absence of a crystalline peak attributed to Ag_2O phase because of the dispersed Ag_2O phase was obtained. It is worth to mention that the percentage of total reducible species determined was relatively low ($\sim 1\%$), suggesting that metallic Ag^0 rather than oxidised Ag^+ particles were obtained. Note that the reduction of $\gamma\text{-Al}_2\text{O}_3$ was not observed under the condition used in this characterisation study.

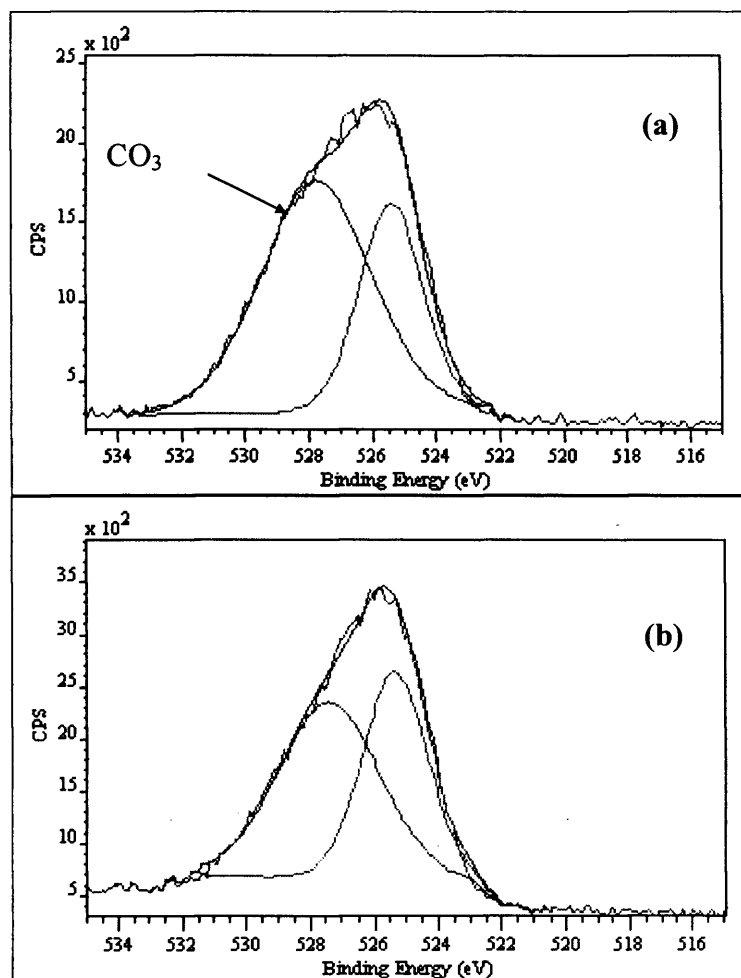
Table 6.2: An estimation of total reducible species for $\text{Ag}/\text{Al}_2\text{O}_3$ catalysts

	% reducible Ag compound/ total bulk Ag (%)
1wt% $\text{Ag}/\text{Al}_2\text{O}_3$	-
5wt% $\text{Ag}/\text{Al}_2\text{O}_3$	0.7
10wt% $\text{Ag}/\text{Al}_2\text{O}_3$	0.9
20wt% $\text{Ag}/\text{Al}_2\text{O}_3$	1.3

6.2.1.3 X-ray photoelectron spectroscopy (XPS)

X-ray photoelectron spectroscopy analysis (XPS) was performed to investigate the surface compositions and dispersion at the surface level of $\text{Ag}/\text{Al}_2\text{O}_3$ catalysts. XPS spectra for 5wt% and 20wt% $\text{Ag}/\text{Al}_2\text{O}_3$ catalysts were collected. All spectra yield a $\text{Ag } 3d_{5/2}$ peak at binding energy in the range of $367 \pm 0.5\text{eV}$ (taking $\text{Al } 2p$ at 72.9eV as reference), which indicates the presence of silver oxide. Analysing the electronic states of Ag was difficult through XPS spectra because the binding energy of various silver states were too close to analysed (368.3eV for metallic silver, 367.5eV for Ag_2O and 367.3 for AgO)²⁶. Note that a rapid discoloration of the catalyst was observed after the sample was exposed to the x-ray irradiation. Thus, a designed analysis procedure was performed to examine the effect of x-ray irradiation on the silver-doped alumina catalysts.

Fig 6.5: XPS spectra of O1s peak for 5% Ag/Al₂O₃, before (a) and after (b) the discoloration process.



XPS analysis was carried out using a monochromator and a flood gun to reduce the intensity of x-rays on the sample. After the XPS spectrum was collected, the monochromator was switched off and the sample was discoloured by treating with the standard x-ray source for 90min. Fig 6.5 illustrates the XPS spectra of 5wt% Ag/Al₂O₃ catalyst, before (a) and after (b) the discoloration process. O1s region showed a broad peak centred at 528eV. Assuming two overlapping peaks at 525eV and at 527.5eV were observed for the fresh sample before the discoloration (Fig 6.5a), the peak assigned to the silver carbonate at 527.5eV diminished after the x-ray irradiation (Fig 6.5b) but not disappear. The result indicates the presence of the surface carbonate on the fresh calcined Ag/Al₂O₃ catalyst. This species was partially

decomposed upon treatment due to generation of heat and electrons from the x-ray source. It was likely due to a surface contamination during the sample handling. However, this does not affect the final XPS results.

On the other hand, the peak intensity of the silver signal relative to that of the support is decided by the silver loadings of the catalyst and by the dispersion over the support. Therefore, the intensity ratio I_{Ag}/I_{Al} was used as an estimation of the surface dispersion for Ag/Al₂O₃ catalysts. The results show that the silver peak intensity increase as the silver loading increases. The intensity ratios for 5wt% and 20wt% Ag/Al₂O₃ catalysts were 0.48 and 2.04, respectively.

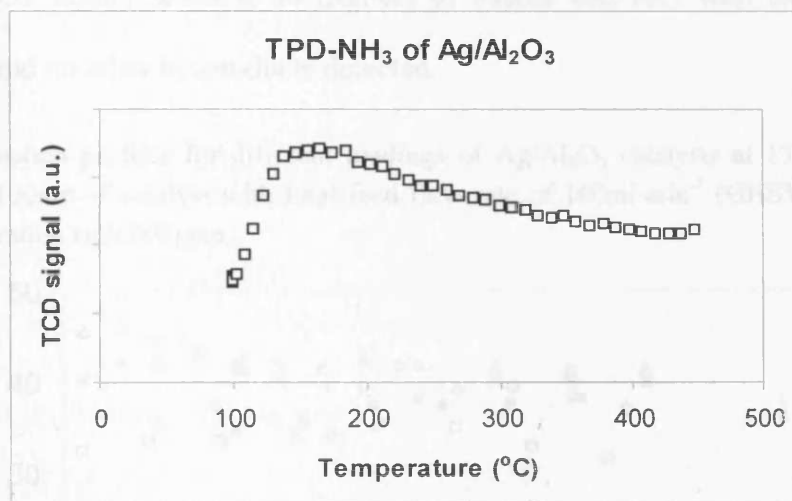
6.2.1.4 Selective chemisorption and desorption (TPD) of ammonia

Selective chemisorption and desorption of ammonia were employed to determine the amount of acid sites and the strength of acidity for Ag/Al₂O₃ catalyst, where 10wt% Ag/Al₂O₃ was used as a representative result. It was assumed that one molecule of ammonia could react with one acidic site. Table 6.3 shows the acid properties of a 10wt%Ag/Al₂O₃ catalyst.

Fig 6.6 shows the TPD curve for Ag/Al₂O₃ catalyst. Only one desorption peak can be observed at 160°C attributed to the weak interaction between the catalyst and the ammonia. The result indicates that the addition of 10wt% loading of Ag modified the acid properties of the support by produces fewer number of acid sites with weaker acidity. As mentioned before, the deposition of Ag on γ -Al₂O₃ by the impregnation induces metal-support interaction^{21,24} and modify the acid-base properties²² of the catalyst either through ion-exchange with the proton of an acidic OH or bonding with oxygen of basic -OH species with the Ag⁺ ions.

Table 6.3: Acid properties of 10wt%Ag/Al₂O₃ catalyst

samples	Acidity (NH ₃)	
	10wt%Ag/Al ₂ O ₃	Al ₂ O ₃
TPD, T _{max} (°C)	160	200
Active sites (μmol.g ⁻¹)	86	96
Active sites (molecule.m ⁻² × 10 ¹⁶)	21.4	20

Fig 6.6: TPD of ammonia adsorbed at 100°C, followed by desorption up to 450°C (the calcination temperature) at 20°C·min⁻¹

An Ag loading of >3wt% decreases the Lewis acid sites but increases the Bronsted acid-sites with medium NH₃ adsorption energy. A greater Ag loading induces interaction between NH₃ molecules and Ag oxides, leading to reduction of Ag oxides and dissociation of adsorbed NH₃. A large amount of Ag loading produces greatly enhanced basicity.

6.2.2 Catalytic activity

1, 5, 10 and 20 wt% Ag/Al₂O₃ catalysts were prepared by incipient wetness techniques and were tested for the dehydrochlorination of 2-chlorobutane at 135°C for 5h. Fig 6.7 shows the reaction profiles for various loadings of Ag/Al₂O₃ catalysts, using γ-alumina as a reference. The results indicate that all Ag/Al₂O₃ catalysts are active for the dehydrochlorination of 2-chlorobutane with conversions close to that of

the γ -alumina support, ranges between 34 and 42% recorded at steady state. 1wt% Ag/ Al_2O_3 catalyst exhibited similar reaction profile as the support, where the reaction begins with low conversion and gradually increases to reach a steady state. An Ag loading of greater than 1wt% diminished the induction period. Further addition of Ag loading to greater than 5wt% increases the conversion slightly. The Ag/ Al_2O_3 catalysts were highly selective to isomers of butene and HCl with close to 100% selectivity and no other by-products detected.

Fig 6.7: Reaction profiles for different loadings of Ag/ Al_2O_3 catalysts at 135°C. Reaction conditions: 100mg of catalyst with total feed flow rate of 100ml·min⁻¹ (GHSV = 55000h⁻¹). Gas concentration is 30000ppm.

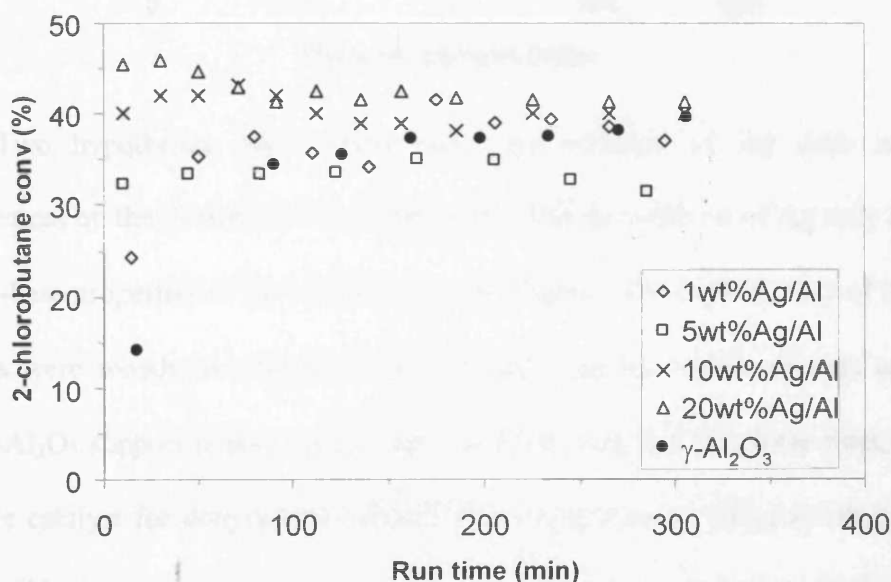
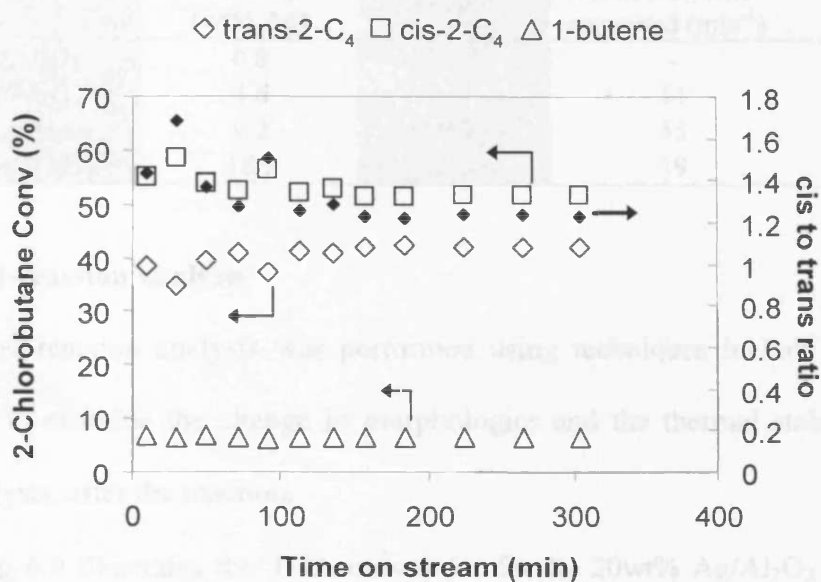


Fig 6.8 shows the products distribution of 20wt% Ag/ Al_2O_3 in dehydrochlorination of 2-chlorobutane at 135°C as a representative result. The results indicate that the formation of cis-2-butene was predominant, followed by trans-2-butene and 1-butene. The selectivity recorded at steady state was 52%, 42% and 6%, respectively. The formation of preferential cis-isomer implied that the reaction was acid-catalysed^{27,28}. Note that no deactivation of catalyst was observed throughout the experimental range.

Fig 6.8: Products distribution. The butene isomers selectivity and the cis/trans ratio for dehydrochlorination of 2-chlorobutane at 135°C were recorded over 20wt% Ag/Al₂O₃ catalyst.



Two hypotheses may explain why the addition of Ag does not show improvement on the overall activity. The first is that the addition of Ag only modified the acid-base properties of the γ -Al₂O₃ support slightly. The high activity of Ag/Al₂O₃ catalysts were mostly attributed to the exposed alumina surface (Lewis acid site). Since γ -Al₂O₃ support is amphoteric and consisted both acid and base sites, it makes an active catalyst for dehydrochlorination of 2-chlorobutane. The poor dispersion of the reducible Ag compound resulted on a poor Ag-support interaction obtained. Thus, no significant enhancement on activity can be observed.

Second, the oxidized Ag⁺ rather than the metallic Ag⁰ could be the active site for the reaction. The activity of Ag/Al₂O₃ catalysts was normalised by the total reducible Ag compound available. (from TPR). As shown in Table 6.4, per minute of the 2-CB molecule being converted for the 10wt% Ag/Al₂O₃ catalyst was the highest. Unfortunately, the poor dispersion of reducible Ag compound does not allow us to conclude at this point. Further investigation of this latter is required.

Table 6.4: Summary of the metal loadings, surface dispersion and catalytic activity recorded at steady state for Ag/Al₂O₃ catalysts

	Absolute loading (wt% Ag)	Ag _s /Ag _T (×100)	2-Chlorobutane	
			No. of molecule converted (min ⁻¹)	Conversion (%)
1wt% Ag/Al ₂ O ₃	0.8	-	-	39
5wt% Ag/Al ₂ O ₃	4.6	0.7	11	35
10wt% Ag/Al ₂ O ₃	9.2	0.9	53	40
20wt% Ag/Al ₂ O ₃	18.9	1.3	19	43

6.2.3 Post-reaction analysis

Post-reaction analysis was performed using techniques include TGA, XRD and XPS to examine the change in morphologies and the thermal stabilities of the used catalysts, after the reaction.

Fig 6.9 illustrates the TGA curves for 5wt%, 20wt% Ag/Al₂O₃ and γ -Al₂O₃ catalysts: fresh calcined samples (A), used samples after reaction at 35°C (B) and at 135°C (C). The TGA curves show similar trend to that of the pure γ -alumina (chapter 4). Each of the catalysts exhibited dehydration at 100-200°C due to loss of physisorbed water. The weight loss assigned to the physisorbed water on the fresh catalysts decreases as the Ag loadings increased (Fig 6.9A). For catalysts after reaction at 35°C, weight loss at 255°C can be observed indicating some molecularly adsorbed chloride species were obtained at low temperature (Fig 6.9B). It was believed that these stable chloride species were formed by stoichiometric reaction and the weight loss corresponding to the amount that was formed increases with increasing Ag loading. At 135°C the catalytic reaction occurred (Fig 6.9C), which encourages the elimination of HCl to form alkene. This reaction proceeding *via* a surface absorption-desorption that explain the absence of a desorption peak at 255°C for these catalysts.

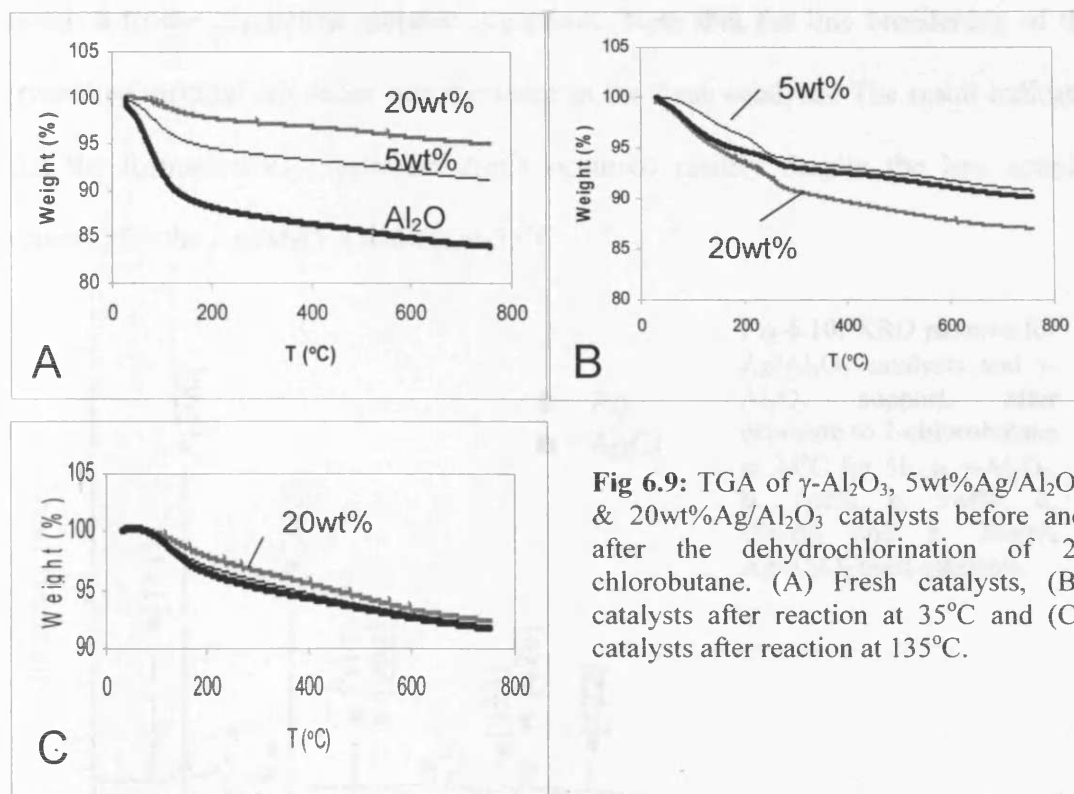


Fig 6.9: TGA of γ -Al₂O₃, 5wt%Ag/Al₂O₃ & 20wt%Ag/Al₂O₃ catalysts before and after the dehydrochlorination of 2-chlorobutane. (A) Fresh catalysts, (B) catalysts after reaction at 35°C and (C) catalysts after reaction at 135°C.

The results fit the idea that the catalytic reaction begins with a weakly absorbed and reversible adsorption of chlorinated compound on the catalyst surface. The addition of Ag on alumina enhanced the surface chloride formations and the catalytic activity.

Powder x-ray diffraction (XRD) and x-ray photoemission spectroscopy (XPS) techniques were employed to investigate changes in the crystalline structure and to monitor the surface composition for the Ag/Al₂O₃ catalysts after the dehydrochlorination reaction. Fig 6.10 shows the XRD patterns for various loadings of Ag/Al₂O₃ catalysts after reaction at 35°C, γ -Al₂O₃ after the same reaction was used as a reference. The results clearly show formation of crystalline AgCl phase for all Ag/Al₂O₃ catalysts after the reaction at 35°C, in which the diffraction peaks at 2θ of 27.8°, 32.2°, 46.2°, 54.8° and 57.5° were observed. The XRD line was broadened as the Ag loading increased. Sharp peaks at 2θ of 38.1°, 44.3°, 64.4°, and 77.5° were

assigned to the crystalline metallic Ag phase. Note that the line broadening of the crystalline metallic Ag phase was the same as the fresh catalysts. The result indicates that the formation of crystalline AgCl occurred readily despite the low activity obtained for the Ag/Al₂O₃ catalysts at 35°C.

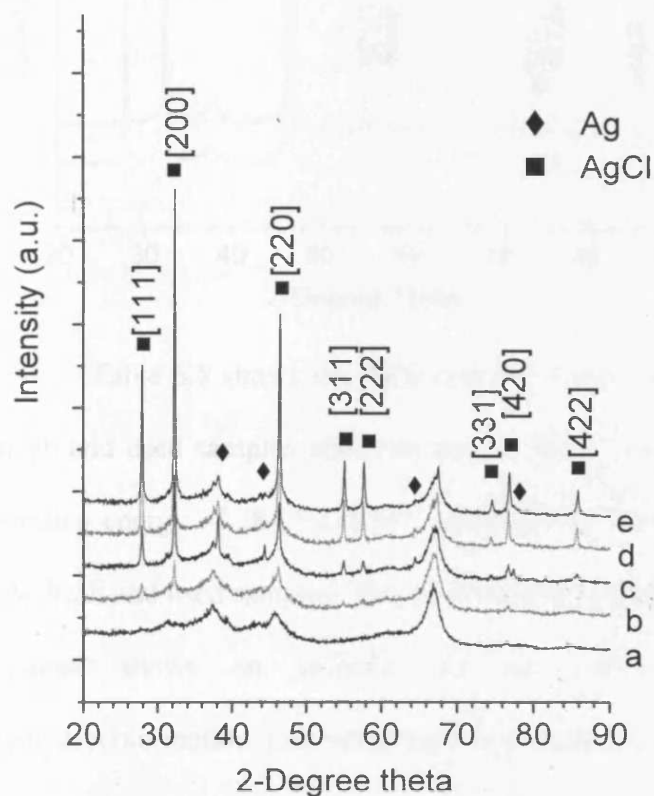


Fig 6.10: XRD patterns for Ag/Al₂O₃ catalysts and γ-Al₂O₃ support, after exposure to 2-chlorobutane at 35°C for 5h. **a.** γ-Al₂O₃, **b.** 1wt%, **c.** 5wt%, **d.** 10wt% and **e.** 20wt% Ag/Al₂O₃ used catalysts.

On the other hand, the XRD line broadening of crystalline AgCl phase also changes according to the increasing reaction temperature. Fig 6.11 shows the XRD patterns of 20wt% Ag/Al₂O₃ catalysts after reaction at 35°C and 135°C, used as a representative result. The result shows that the XRD patterns for crystalline AgCl obtained at 35°C exhibited higher crystallinity than the one obtained at 135°C. The result indicates that the catalyst is more prone to AgCl formation at 35°C when the activity was low. At 135°C the peak intensity was decreased accordingly, as the catalytic dehydrochlorination reaction took place. This is consistent with the TGA result that the diminution of the desorption peak at 255°C attributed to the molecularly adsorption of chloride for Ag/Al₂O₃ catalysts after reaction at 135°C.

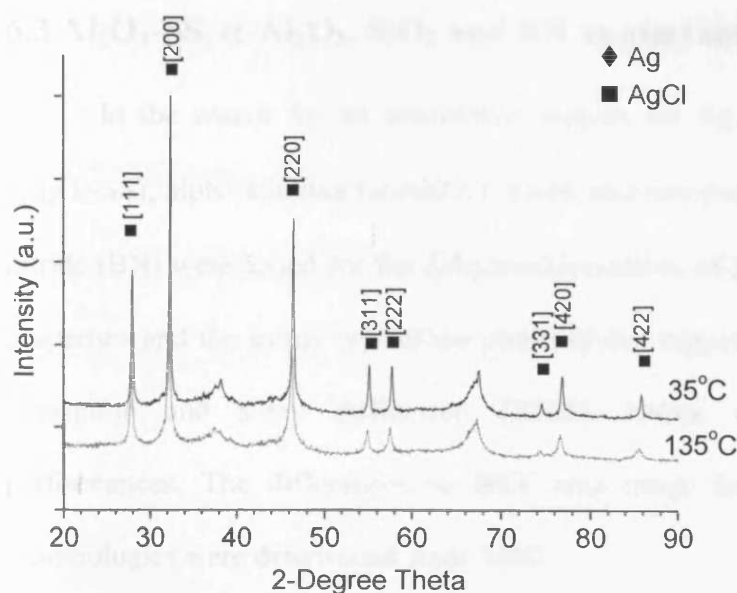


Fig 6.11: XRD patterns of 20wt% Ag/Al₂O₃ catalysts after reaction at 35°C and 135°C.

Table 6.5 shows the XPS data for 5wt% and 20wt% Ag/Al₂O₃ catalysts. The fresh and used samples after reaction at 135°C were compared. A C1s signal with a binding energy of $284.5 \pm 0.5\text{eV}$ attributed to the elemental carbon was observed in the fresh and used samples. The peak intensity ratio of C1s and Al2p peaks in the XPS spectra shows an increase of the surface carbon contents after the dehydrochlorination, indicating a possible coke formation on the catalyst surface.

Table 6.5: Intensity ratio of the C1s and Al2p peaks, and the cl2p and Al2p peaks in the XPS spectra of the Ag/Al₂O₃ catalysts before and after the reaction at 135°C

Sample	C1s/Al		cl2p/Al	
	fresh	used	fresh	used
5wt%Ag/Al ₂ O ₃	0.09	0.20	0.00	0.20
20wt%Ag/Al ₂ O ₃	0.09	0.45	0.00	0.27
Al ₂ O ₃	0.05	0.24	0.00	0.24

Then again, the spectra of the used samples after the reaction show Cl2p signal at a binding energy of 198.6eV. A significant increase of peak intensity ratio of Cl2p and Al2p, suggests a surface chlorination took place. The peak intensity ratio increased with increasing Ag loading shows that the addition of Ag resulting in more severe carbon deposition and surface chlorination.

6.3 Al₂O₃-SS, α -Al₂O₃, SiO₂ and BN as alternative supports

In the search for an alternative support for Ag catalyst, the Sasol alumina (Al₂O₃-SS), alpha-alumina (α -Al₂O₃), fused and non-porous silica (SiO₂) and Boron nitride (BN) were tested for the dehydrochlorination of 2-chlorobutane. The physical properties and the initial crystalline phase of the supports were characterised by N₂ adsorption and x-ray diffraction (XRD), before testing for their catalytic performances. The differences in BET area range from 2 to 477m²g⁻¹ and the morphologies were determined from XRD.

6.3.1 Catalytic performances

Al₂O₃-SS, α -Al₂O₃, SiO₂ and BN were tested for the dehydrochlorination of 2-chlorobutane at reaction temperatures between 35°C and 335°C with an interval of 100°C. Table 6.6 shows the 2-chlorobutane conversions for various supports recorded at different reaction temperatures at steady state. No “real” catalytic activity can be observed for all samples at 35°C except for the gas phase reaction²⁹ product was detected in trace amount. The result shows that the reaction was thermodynamically not favoured at 35°C with zero% conversion for all samples.

As mentioned previously in chapter 4, the catalytic activity for the γ -Al₂O₃ support starts at 135°C with a maximum conversion of 40% for Syntex alumina (Al₂O₃) and 48% for Sasol alumina (Al₂O₃-SS). In comparison, α -Al₂O₃, SiO₂ and BN were relatively inactive at this temperature. However, the catalyst performances changed over each catalysts with increasing temperature (>135°C). At 235°C, γ -Al₂O₃ catalysts show above 95% of 2-chlorobutane conversion, followed by electronic grade SiO₂ (94%), α -Al₂O₃ (88%), fused SiO₂ (11%) and BN (11%).

Table 6.6: 2-chlorobutane conversions for various supports recorded at different reaction temperatures. Reaction conditions: 0.1g of sample and 33000ppm of gas concentration.

Sample	BET (m^2g^{-1})	Reaction temperature			
		35°C	135°C	235°C	335°C
Al_2O_3	290	0	40	95	99
$\text{Al}_2\text{O}_3\text{-SS}$	195	0	48	96	99
$\alpha\text{-Al}_2\text{O}_3$	10	0	1	88	99
SiO_2 , fused	2	0	1	11	99
SiO_2 , high purity	477	0	4	94	99
BN	8	0	0	11	99

Attentions were drawn to the exceptional high catalytic performance of electronic grade SiO_2 and $\alpha\text{-Al}_2\text{O}_3$, despite the inherent “inert” properties³⁰. This suggests that the Al^{3+} ion, the surface hydroxyl group from Al_2O_3 and the silanol group from SiO_2 are possibly the active sites for the dehydrochlorination of 2-chlorobutane. The low activities for fused SiO_2 and BN may be due to their poor stabilities and unsuitable surface properties, which exhibited low specific surface area and poor pore structure. Note that a thermodynamically favoured gas phase decomposition of 2-chlorobutane starts above 285°C and is nearly total at 335°C.

6.3.2 Evaluation of different supported Ag catalysts

Supported Ag catalysts were prepared by impregnating silver nitrate on $\gamma\text{-Al}_2\text{O}_3$, $\alpha\text{-Al}_2\text{O}_3$ and SiO_2 to investigate their catalytic performances. Except for the $\alpha\text{-Al}_2\text{O}_3$, $\gamma\text{-Al}_2\text{O}_3$ and SiO_2 supports used are of high surface area, 290 and $477\text{m}^2\text{g}^{-1}$ respectively. 2-Chlorobutane conversion was measured over different supported Ag catalysts at 135°C and the results are shown in Table 6.7. The conversions were recorded at 3h time online. The results indicated that the 2-chlorobutane conversion for Ag/ Al_2O_3 and Ag/ $\text{Al}_2\text{O}_3\text{-SS}$ catalysts were about 40%. Ag/ $\alpha\text{-Al}_2\text{O}_3$ was relatively

inactive with only 1% conversion and Ag/SiO₂ exhibited high activity up to 59% conversions.

Table 6.7: 2-chlorobutane conversion of different supported Ag catalysts

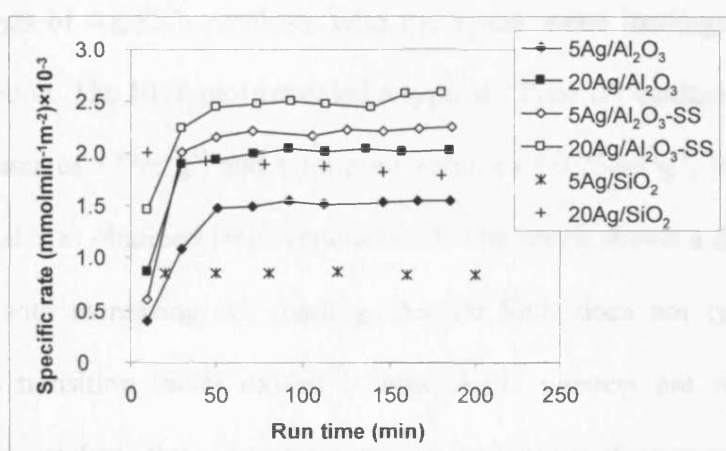
Samples	5wt% Ag		20wt% Ag	
	BET (m ² g ⁻¹)	conv (%)	BET (m ² g ⁻¹)	conv (%)
Ag/Al ₂ O ₃	250	35	223	41
Ag/Al ₂ O ₃ -SS	196	40	167	39
Ag/ α -Al ₂ O ₃	8	1	6	1
Ag/SiO ₂	455	34	365	59

This is not too surprising considering the various pre-treatment conditions, the effects of the promoter, and the influence of the support which is particularly important in heterogeneous catalysis. The low activity of Ag/ α -Al₂O₃ catalyst may be due to the low surface area and low acidity³¹ of the support, resulting in poor dispersion³² of large Ag particles that suppress the interaction between the reactant and the catalyst. Interesting result was observed for Ag/SiO₂ catalysts that the pure SiO₂ was inactive for dehydrochlorination of 2-chlorobutane at 135°C, but the addition of Ag yielded a catalyst which is highly active to the 2-chlorobutane conversion. Additionally, the conversion improved with increasing silver loading suggesting a correlation between the activity and the Ag loadings.

Fig 6.12 shows the reaction profiles for the different supported Ag catalysts, where the specific rates were obtained by normalising the reaction rate with the BET surface area. The results show similar reaction trend for Ag/Al₂O₃ (Synetix and Sasol) catalysts, where the reaction rate was low initially and increased gradually with time to reach a steady state. The Ag/SiO₂ catalysts exhibited a rather different reaction trend, in which the specific rate was at the maximum and was stabilised right from the beginning of the reaction. The different reaction trend obtained, suggesting a quite

different mechanism for both catalysts. The sequence of the specific rate decreases in the order of $20\text{wt}\%\text{Ag}/\text{Al}_2\text{O}_3\text{-SS} > 5\text{wt}\%\text{Ag}/\text{Al}_2\text{O}_3\text{-SS} > 20\text{wt}\%\text{Ag}/\text{Al}_2\text{O}_3 > 20\text{wt}\%\text{Ag}/\text{SiO}_2 > 5\text{wt}\%\text{Ag}/\text{Al}_2\text{O}_3 > 5\text{wt}\%\text{Ag}/\text{SiO}_2$. Further investigation is required in order to develop better understanding of the catalytic properties for Ag/SiO_2 catalysts,

Fig 6.12: Reaction profiles for various supported Ag catalysts at 135°C . Reaction conditions: 100mg of catalyst with total feed flow rate of 100mlmin^{-1} ($\text{GHSV} = 55000\text{h}^{-1}$). Gas concentration is 30000ppm .



6.4 Silver-doped silica catalysts

Although Ag/SiO_2 catalyst shows interesting catalytic properties, only few publications can be found on the used of this catalyst for dehydrochlorination reaction. Pd/SiO_2 , Ag/SiO_2 , Cu/SiO_2 , and $\text{Pd-Ag}/\text{SiO}_2$ sol-gel catalysts were synthesized and were studied extensively by Heinrichs and coworkers¹⁶⁻¹⁸ to prepare highly dispersed nano-metre size particles for selective hydrodechlorination of 1,2-dichloroethane. In our studies, a series of Ag/SiO_2 catalysts with different loadings ranging from 1 to $20\text{wt}\%$ of Ag were prepared by the incipient wetness technique to study the catalytic performance on dehydrochlorination of 2-chlorobutane. Ag/SiO_2

catalysts were characterised by BET, XRD and TPR, before were tested for the reaction.

6.4.1 Catalyst characterisation

6.4.1.1 Physical properties of Ag/SiO₂ catalysts

Nitrogen adsorption was performed to examine the textural properties of the Ag/SiO₂ catalysts after the calcination. Table 6.8 shows the BET surface areas for various loadings of Ag/SiO₂ catalysts with the actual metal loadings determined by atomic absorption. The BET plot revealed a typical “Type II” isotherm for SiO₂ with BET surface area of 477 m²g⁻¹ and total pore volume of 0.73 cm³g⁻¹, indicating a non-porous material was obtained (see Appendix C). The result shows a decrease of BET surface area with increasing Ag loading. As the SiO₂ does not typically interact strongly with transition metal oxides²⁰, large Ag₂O clusters are expected on the surface of this catalyst, thus, decreases on the specific surface area. Note that the theoretical monolayer coverage of Ag supported on SiO₂ is about 13wt%.

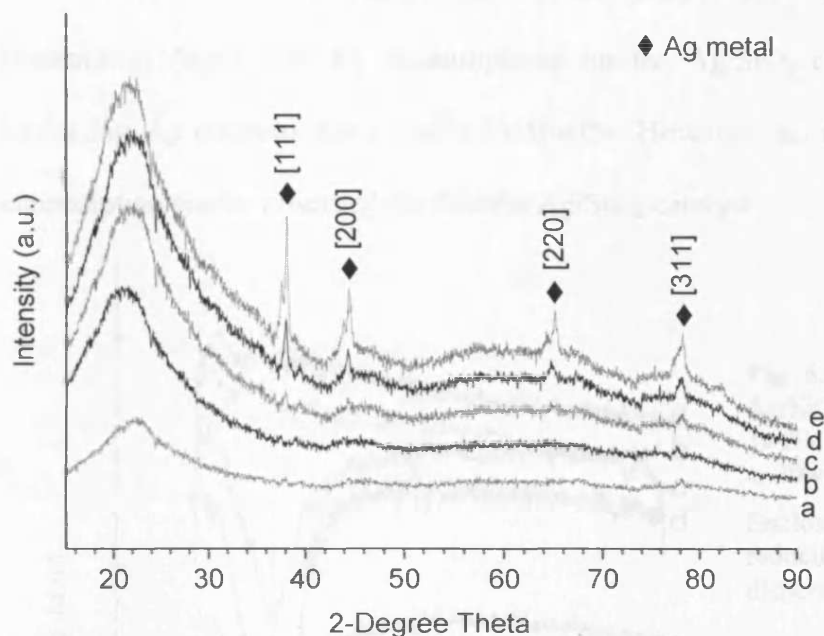
Table 6.8: BET surface areas determined from N₂-absorption and actual Ag loadings from AA for Ag/SiO₂ catalysts

	BET (m ² g ⁻¹)	metal loading from AA (wt% Ag)
SiO ₂	477	-
1wt%Ag/SiO ₂	470	1.2
5wt%Ag/SiO ₂	455	5.4
10wt%Ag/SiO ₂	420	9.2
20wt%Ag/SiO ₂	365	18.3

Fig 6.13 depicts the XRD patterns for the various loadings of Ag/SiO₂ catalysts. Broad peak at 2θ of 22° are due to the amorphous silica. XRD of the 1 and 5wt% Ag/SiO₂ catalysts revealed neither the presence of metallic silver nor silver oxide. The absence of a sharp peak in the XRD pattern, suggesting good dispersion of small silver particles was obtained. On the contrary, distinct XRD peaks at 2θ of

38.1°, 44.3°, 64.4°, and 77.5° were observed due to the presence of crystalline metallic Ag phase. The peak intensity increases as the Ag loading increased.

Fig 6.13: XRD patterns for fresh Ag/SiO₂ catalysts, where a. pure SiO₂, b. 1wt%, c. 5wt%, d. 10wt% and e. 20wt% Ag/SiO₂.



Since the XRD line broadening is a function of the crystallite size, the observation of broader XRD line indicates that large Ag clusters with poor dispersion were obtained for Ag/SiO₂ catalyst with high Ag loadings. The growth of silver particle is probably related to the ability of silver ions to rapidly diffuse in the oxide network. Besson *et al*³³ reported that random distribution of large Ag particles was due to the fast diffusion of Ag ions into the mesoporous film and was enhanced by the presence of silanol groups.

6.4.1.2 Temperature programmed reduction (TPR)

TPR was performed for the Ag/SiO₂ catalysts using 10%H₂/Ar to observe the reduction process. It should be note that one Ag⁺ could consume ½ molecule of H₂. Fig 6.14 illustrates the TPR profiles for 1, 5, 10 and 20wt% Ag/SiO₂ catalysts, pure

SiO₂ was used as a reference. Only one reduction peak can be observed at 53°C for the Ag/SiO₂ catalysts. No reduction process can be observed for 1wt% Ag/SiO₂ catalyst due to its relatively low Ag loading. The reduction peak at 53°C becomes more noticeable when the Ag loading was increased to above 5wt% attributed to the presence of Ag₂O. The H₂ consumptions for the Ag/SiO₂ catalysts increase with increasing Ag contents from 5wt% to 10wt%. However, no further increase of H₂ consumption can be observed for 20wt% Ag/SiO₂ catalyst.

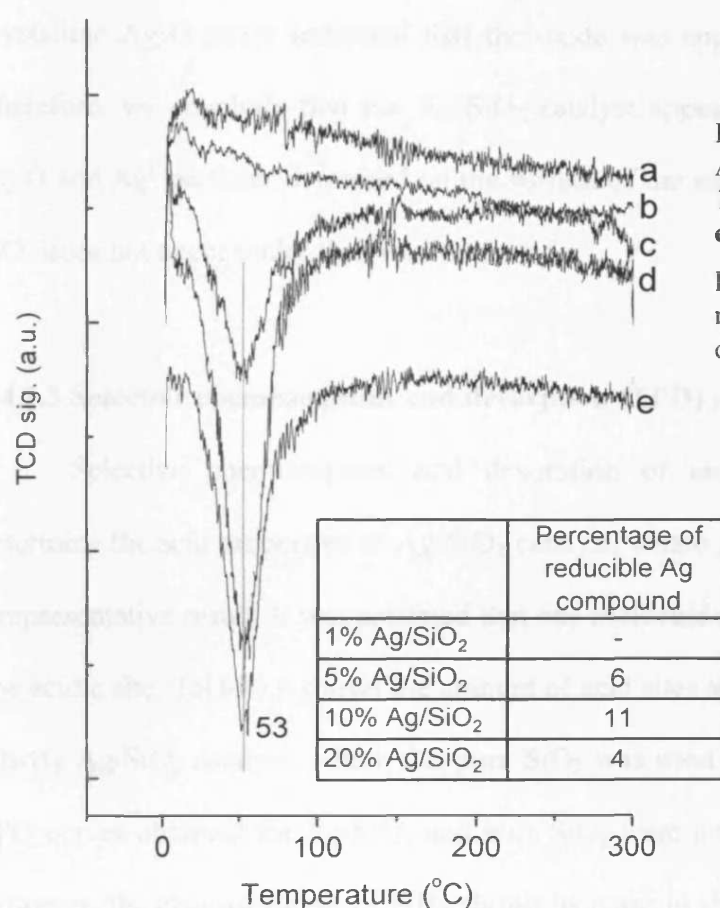


Fig 6.14: TPR profiles for Ag/SiO₂ catalysts. **a.** SiO₂, **b.** 1wt%, **c.** 5wt%, **d.** 10wt% & **e.** 20wt% of Ag/SiO₂.

Enclosed is a table of reducible Ag compound dispersion (%).

The results indicated that a saturation of hydrogen was achieved with 10wt% Ag/SiO₂ catalyst. The reduction process determined the amount of reducible species (Ag⁺ or Ag₂O) as well as the particle distribution of the catalyst. The addition of >10wt% of Ag showed no further H₂ consumptions, suggesting a decrease in amount

of reducible Ag compound due to the formation of large Ag_2O particles or Ag^0 metallic silver.

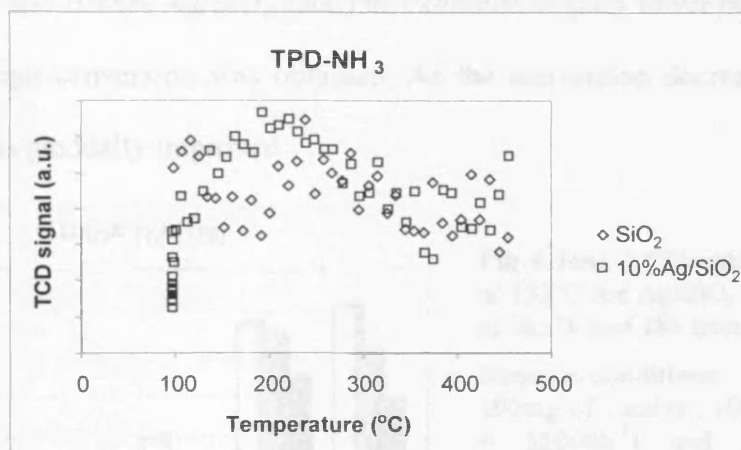
Based on the TPR results, the amount of reducible Ag compound was estimated by dividing the total H_2 consumptions to the total Ag loading. It is assumed that the Ag^+ or Ag_2O was the dominant phase of Ag reducible species. The percentage of reducible species for 5wt%, 10wt% & 20wt% Ag/SiO_2 , were 6%, 11% & 4%, respectively. Based on the XRD analysis, the absence of a XRD pattern attributed to crystalline Ag_2O phase indicated that the oxide was appeared in a dispersed phase. Therefore, we conclude that the Ag/SiO_2 catalyst appeared as a mixture of Ag^+ or Ag_2O and Ag^0 particles dispersed on the surface of the support. Note that reduction of SiO_2 does not occur under the condition used.

6.4.1.3 Selective chemisorption and desorption (TPD) of ammonia

Selective chemisorption and desorption of ammonia were employed to determine the acid properties of Ag/SiO_2 catalyst, where 10wt% Ag/SiO_2 was used as a representative result. It was assumed that one molecule of ammonia could react with one acidic site. Table 6.9 shows the amount of acid sites and the strength of acidity for 10wt% Ag/SiO_2 catalyst, where the pure SiO_2 was used as a comparison. The NH_3 -TPD curves obtained for Ag/SiO_2 and pure SiO_2 were unclear, as shown in Fig 6.15. However, the chemisorption of NH_3 shows increase in the number of acid sites. The addition of 10wt% loading of Ag on SiO_2 modified the acidity of the support to create more acidic sites with weaker strength. We propose that the addition of Ag on SiO_2 by the impregnation method generates the acidic site through ion-exchange of the surface silanol group by the Ag^+ ion. The mechanism was similar to that of the interaction between $\text{Ag}-\text{Al}_2\text{O}_3$ ²².

Table 6.9: Acid properties for 10wt%Ag/SiO₂ catalyst

samples	Acidity (NH ₃)	
	10wt%Ag/SiO ₂	SiO ₂
TPD, T _{max} (°C)	-	-
Active sites (μmol.g ⁻¹)	67	48
Active sites (molecule.m ⁻² × 10 ¹⁶)	10	6

Fig 6.15: NH₃ was adsorbed at 100°C, followed by desorption up to 450°C at 20°C·min⁻¹

6.4.2 Catalytic activity

1, 5, 10 and 20wt% Ag/SiO₂ catalysts were tested for the dehydrochlorination of 2-chlorobutane at 135°C and the activities are shown in Fig 6.16. The results clearly show that the addition of Ag on SiO₂ increase the 2-chlorobutane conversion significantly. The pure SiO₂ was not active for the dehydrochlorination of 2-chlorobutane, however, addition of small loading (1wt%) of Ag generates active sites for the reaction to give 10% of conversion. The 2-chlorobutane conversion increases with increasing Ag loadings. The maximum 2-chlorobutane obtained for each different loading Ag/SiO₂ catalysts was 32% for 5wt% Ag/SiO₂, 59% for 10wt% Ag/SiO₂ and 63% for 20wt% Ag/SiO₂ catalysts.

The reaction trend observed for Ag/SiO₂ catalysts was that the catalyst exhibited high initial conversion, but decreased with time. The catalyst deactivation

was more severe with high silver loadings. After 18h of operation, the 2-chlorobutane conversion was 9% (1wt%Ag), 26% (5wt%Ag), 46% (10wt%Ag) and 40% (20wt%Ag). The butene selectivity shows that the Ag/SiO₂ catalysts are highly selective to the desirable butene isomers. 1wt% and 5wt% Ag/SiO₂ catalyst show 100% selective to isomers of butene with no by-product can be detected. On the one hand, 10wt% and 20wt% Ag/SiO₂ catalysts exhibited slightly lower butene selectivity despite the high conversion was obtained. As the conversion decreases, the butene selectivity was gradually improved.

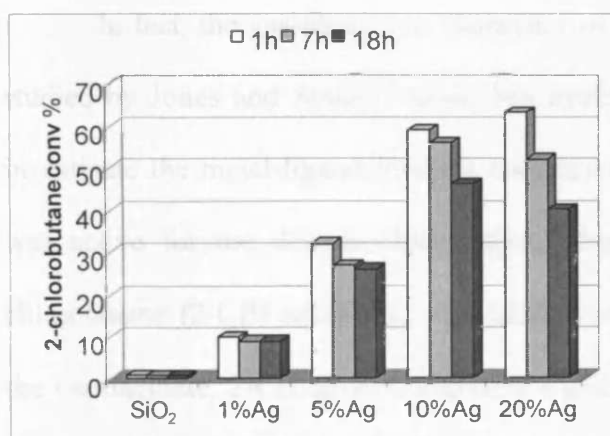


Fig 6.16a: 2-Chlorobutane conversion at 135°C for Ag/SiO₂ catalyst recorded at 1h, 7h and 18h time online.

Reaction conditions:
100mg of catalyst, 100mlmin⁻¹ (GHSV = 55000h⁻¹) and 30000ppm feed concentration.

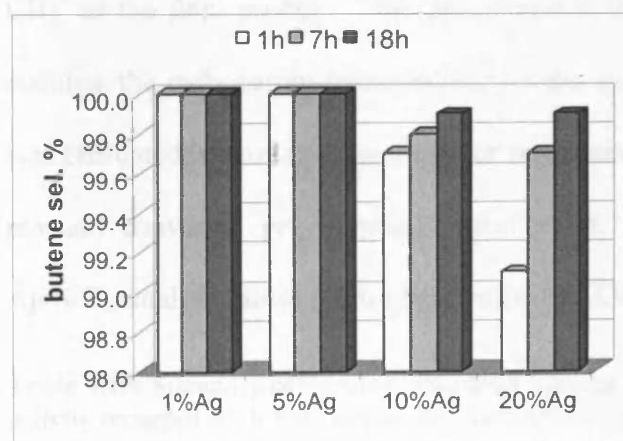


Fig 6.16b: Butene selectivity at 135°C for Ag/SiO₂ catalyst recorded at 1h, 7h and 18h time online.

Nevertheless, the product distribution indicates that the formation of cis-2-butene was predominant, followed by trans-2-butene and 1-butene. The butene selectivity is 51%, 43% and 5% for 10wt% Ag/SiO₂ catalyst, respectively. The formation of preferential cis-isomers indicated that the reaction was acid-catalysis^{27,28}.

Based on the results obtained, two suggestions were proposed. First, the catalyst activity is probably related to the Ag loadings and the dispersion of Ag particles. Compared to Ag/Al₂O₃ catalysts, Ag/SiO₂ catalysts clearly show improvement on the dispersion of Ag reducible species from the TPR result. Assuming that the Ag⁺ rather than the Ag⁰ was the active site for the reaction, the increase amount of these surface Ag⁺ species encourages a better interaction between the reactant and the catalyst. Thus, enhancement on activity can be observed with the increasing Ag loadings.

In fact, the gas-phase ion chemistry of Ag⁺ with the 2-chlorobutane has been studied by Jones and Staley³⁴ using ion cyclotron resonance (ICR) spectroscopy to investigate the metal-ligand binding energies studies. The result shows that the Ag⁺ was active for the dehydrochlorination, displacement, and/or condensation of 2-chlorobutane (2-CB) reactions. Ag(C₄H₈)₂⁺ and Ag(C₄H₈)(2-CB)⁺ were found to be the intermediate. 2-CB slowly displaces C₄H₈ from Ag(C₄H₈)₂⁺ to give Ag(C₄H₈)(2-CB)⁺ as the final product. This phenomenon indicates that the ability of Ag⁺ ion to stabilise the carbocation intermediate on the surface of catalyst. The catalyst activity was presented in terms of the turnover frequencies (TOF), the number of molecules of reactant converted per exposed metal atom, as shown in Table 6.10. The 5wt% Ag/SiO₂ catalyst shows the highest value of TOF.

Table 6.10: Summary of the absolute metal loading, the surface Ag atom and the catalytic activity recorded at 1h time online for Ag/SiO₂ catalysts

	Absolute loading (wt% Ag)	Ag _S /Ag _T (×100)	2-Chlorobutane	
			Per min of molecule (min ⁻¹)	Conversion (%)
1wt% Ag/SiO ₂	1.2	-	-	10
5wt% Ag/SiO ₂	5.4	6	11	32
10wt% Ag/SiO ₂	9.2	11	6	59
20wt% Ag/SiO ₂	18.3	4	9	63

Second is that the deposition of Ag on SiO₂ induces the interaction between metal-support¹⁹ generates the silanol group (acidic sites) with moderate acidity that served as the active site. The increase Ag loadings with good dispersion creates more defects, which enhanced the activity of the catalyst. However, the presence of these defect sites could also activated the formation of undesirable byproducts and resulting in a decrease in butene selectivity. The catalysts deactivation was possibly due to surface poisoning by the formation of stable AgCl, coking and metal sintering³⁵.

6.4.3 Post reaction analysis

After the dehydrochlorination reaction, discoloration of Ag/SiO₂ catalyst was observed. A comparison between the physico-chemical properties of the fresh catalyst and of the deactivated one was performed, employing the XRD, XPS and XRF techniques.

Fig 6.17: XRD patterns of Ag/SiO₂ catalysts after reaction at 135°C for 20h. a. 1wt%, b. 5wt%, c. 10wt% and d. 20wt% Ag/SiO₂.

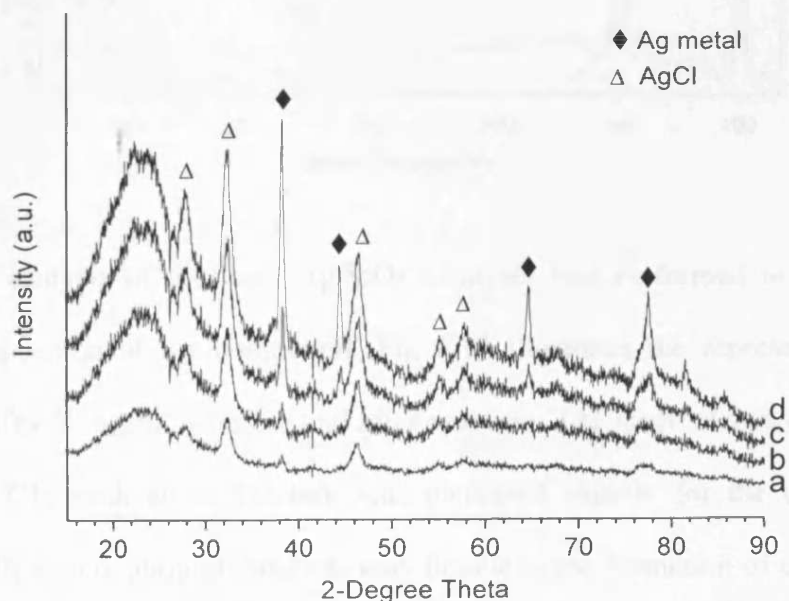
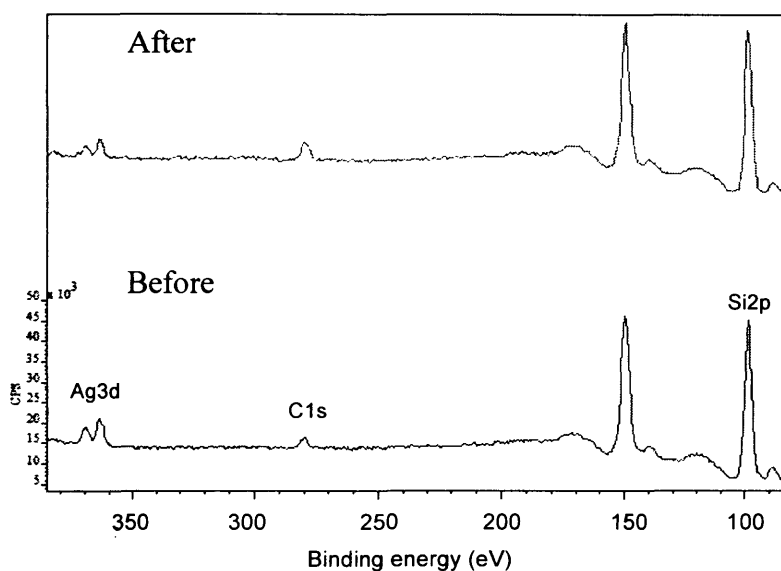


Fig 6.17 shows the XRD patterns of Ag/SiO₂ catalysts after the reaction at 135°C. The XRD pattern clearly shows the presence of crystalline AgCl phase for

Ag/SiO₂ catalysts after the reaction, as diffraction peaks at 2θ of 27.8°, 32.2°, 46.2°, 54.8° and 57.5° were observed. The peak line broadening increased with the increase of silver content indicates the transformation of dispersed Ag compound to crystallite AgCl. The sharp peaks at 2θ of 38.1°, 44.3°, 64.4°, and 77.5° attributed to the metallic Ag phase were observed and the peak intensity was the same as that of the fresh catalyst, implied that the Ag was remained as disperse phase. The result suggests that the formation of stable crystallite AgCl resulting in the disappearance of the free Ag⁺ species, hence, deactivation of catalyst.

Fig 6.18: XPS patterns of 10wt% Ag/SiO₂ after reaction.



XPS analysis of the used Ag/SiO₂ catalysts was performed to monitor the surface composition of the compound. Fig 6.18 illustrates the representative XPS spectra for 10wt% Ag/SiO₂ before and after reaction. The result shows that the peak intensity of C1s peak at *ca* 284.6eV was increased slightly for the used sample, suggesting the deactivation of catalysts may be due to the formation of carbonaceous species. Note that chlorine species were not detected on these catalysts, neither before nor after reaction, as judged from the absence of Cl2s (275eV) and Cl2p (199eV)

peaks, suggesting that surface chlorination had not occurred over the Ag/SiO₂ catalysts. Elemental analysis of used 5wt% and 10wt% Ag/SiO₂ catalysts by XRF shows that the chloride contents were 1.85 and 2.45wt% respectively. It is important to point out that the absence of a chloride peak in XPS is unusual, as the XRD and elemental analysis clearly showed the presence of crystalline silver chloride.

6.5 Silver-doped zirconia-alumina catalysts

From chapter 5, ZrO₂-Al₂O₃ catalysts were found active for the dehydrochlorination of 2-chlorobutane. Two types of ZrO₂-Al₂O₃ catalysts, prepared by incipient wetness (dry impregnation, ZAH) and by co-precipitation (ZAC), were used as the support for the supported Ag catalysts. 10wt% of Ag was impregnated on the ZrO₂-Al₂O₃ support by incipient wetness technique and the catalytic performances were determined. The BET surface areas and the morphologies of 10wt%Ag/ZrO₂-Al₂O₃ catalysts were characterised by N₂ adsorption, XRD and TPR.

6.5.1 Catalyst characterisations

6.5.1.1 Textural properties and crystalline phases

N₂ adsorption was performed over the 10wt%Ag/ZrO₂-Al₂O₃ catalysts to determine the BET surface areas. Table 6.11 shows the BET surface areas obtained for 10wt%Ag/ZrO₂-Al₂O₃ catalysts and the supports. The actual Ag loadings determined by atomic absorption were also included. The result shows that the BET surface area for 10wt%Ag/ZrO₂-Al₂O₃ was close to that of the support, which suggests that good dispersion of Ag particles was obtained to maintain the large surface area. This is in agreement with the XRD patterns of 10wt%Ag/ZrO₂-Al₂O₃

catalysts that revealed only the amorphous form of the supports and no sharp peak was detected.

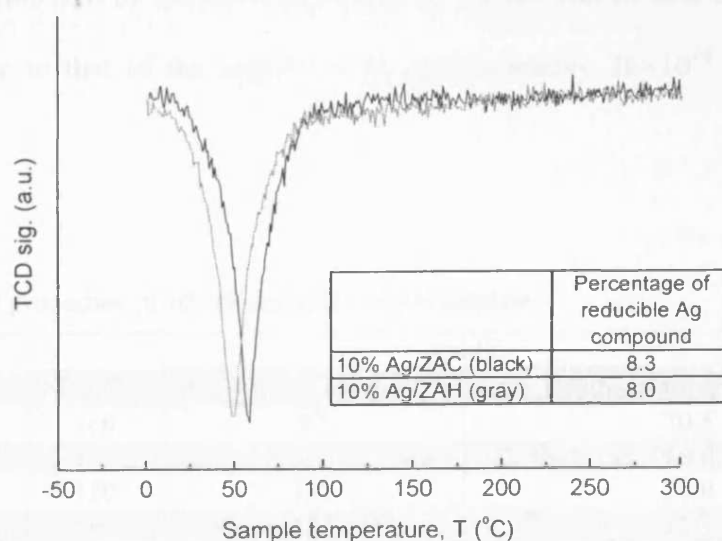
Table 6.11: BET areas and actual Ag loadings for Ag/ZrO₂-Al₂O₃ catalysts.

	BET (m ² g ⁻¹)	metal loading from AA (wt% Ag)
ZrO ₂ -Al ₂ O ₃ (ZAH)	271	-
ZrO ₂ -Al ₂ O ₃ (ZAC)	260	-
10wt%Ag/ZAH	276	9.4
10wt%Ag/ZAC	293	9.2

6.5.1.2 Temperature programmed reduction (TPR)

A TPR of Ag/ZrO₂-Al₂O₃ catalyst was performed to investigate the reduction process. 50ml·min⁻¹ of 10%H₂ in Ar gas mixture was passed through the sample at a temperature ramp of 20°C·min⁻¹. The TPR profiles for the two types of Ag/ZrO₂-Al₂O₃ catalysts were collected and are shown in Fig 6.19. Only one reduction peak was observed for Ag/ZrO₂-Al₂O₃ catalysts, with the reduction peak temperature at 49°C for 10wt%Ag/ZAC and 59°C for 10wt%Ag/ZAH. The low reduction peak temperature observed suggests that the dispersed Ag₂O phase¹⁹.

Fig 6.19: TPR profiles



The Ag reducible species contents was calculated by measuring the amount of H₂ consumption, assuming one atom of Ag consumes ½ a molecule of H₂. The reducible Ag dispersion is the ratio of the amount of reducible Ag compound to the total Ag of the catalyst. The result shows that both Ag/ZAH and Ag/ZAC catalysts of 10wt% Ag loading revealed similar dispersions at 8% and 8.3% respectively.

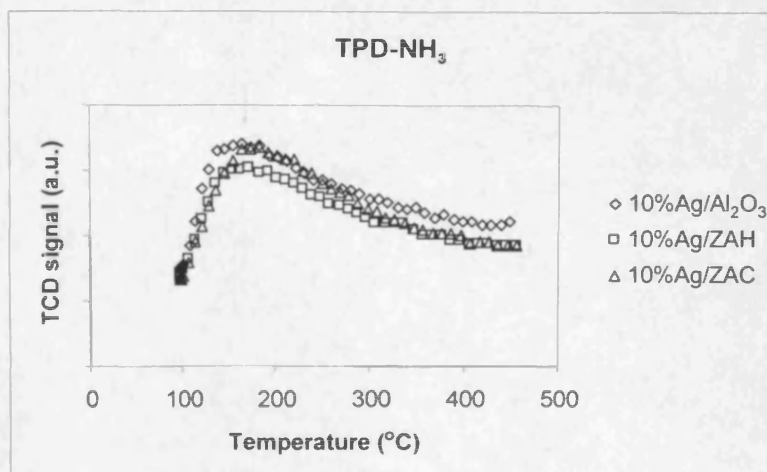
6.5.1.3 Selective chemisorption and desorption (TPD) of Ammonia

Selective chemisorption and TPD of ammonia were performed to examine the acid strength and to determine the number of acid sites of 10wt%Ag/ZrO₂-Al₂O₃ catalysts. It was assumed that one molecule of ammonia could react with one acidic site. Table 6.12 shows the acid properties of 10wt%Ag/ZrO₂-Al₂O₃ catalysts. In the case of Ag/ZAH catalyst, addition of Ag increased the number of acid sites of the catalyst. The TPD peak temperature indicates that weak acid sites of similar strength to that of the support were obtained (Fig 6.20). Meanwhile, the addition of Ag on ZAC support does not show any significant changes to the acidity of the support. Ag/ZAC catalyst might have consumed more ammonia molecules; however, after the number was normalised by the BET surface area, the number of acid sites per square metre was close to that of the support with approximately 26×10^{16} of active sites available.

Table 6.12: Acid properties of 10wt%Ag/ZrO₂-Al₂O₃ catalyst

Catalysts	Acidity		
	TPD (°C)	Active sites ($\mu\text{mol}\cdot\text{g}^{-1}$)	Active sites ($\text{molecule}\cdot\text{m}^2 \times 10^{16}$)
ZAH	160	92	20.5
10%Ag/ZAH	160	119	26.0
ZAC	180	112	26.0
10%Ag/ZAC	180	123	25.3

Fig 6.20: TPD of ammonia adsorbed at 100°C, followed by desorption up to 450°C at 20°Cmin⁻¹ ramp rate



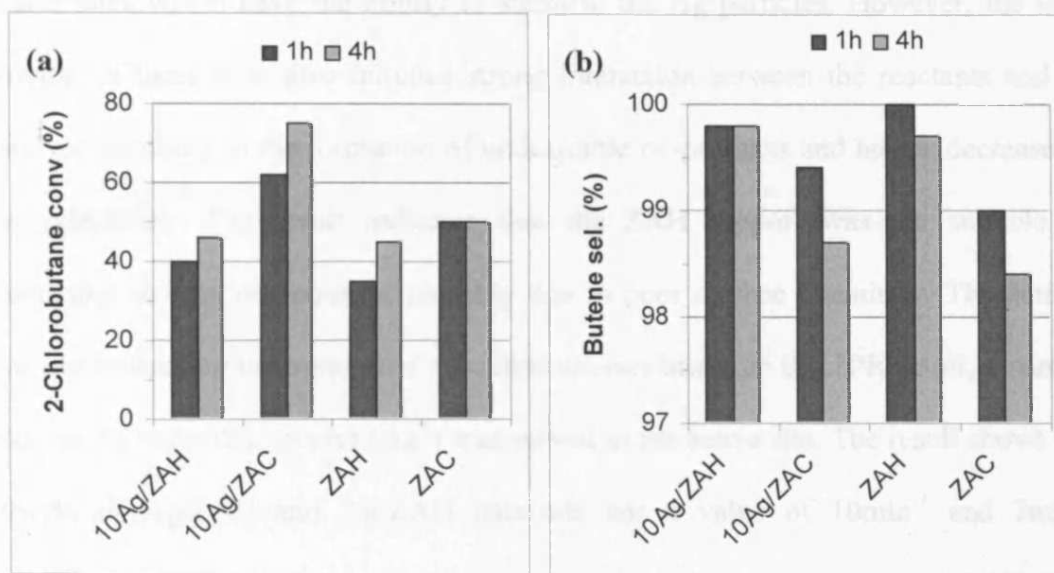
6.5.2 Catalytic activity

10wt% of Ag/ZAH and Ag/ZAC catalysts were tested for the dehydrochlorination of 2-chlorobutane at 135°C to investigate their catalytic performances. Fig 6.21 shows the conversion and selectivity recorded at 1h and 4h of time on stream for the Ag/ZrO₂-Al₂O₃ catalysts as well as the supports to use as comparison. The result shows that all Ag/ZrO₂-Al₂O₃ catalysts were active to the dehydrochlorination of 2-chlorobutane.

Outstanding activity was observed for the 10wt%Ag/ZAC catalyst with up to 74% of conversion achieved; compared to the 50% of conversion for the ZAC support. The addition of 10wt% of Ag on ZAC shows significant promotion effect and is the best conversion so far that has been achieved in this studies under this reaction condition. The reaction trend was started with low conversion initially and was increased gradually to reach a steady state at the maximum conversion. Conversely, the butene selectivity was started high (99.3%) when the conversion was low and was decreased slowly with time. The isomers of octene were found to be the only by-products from the reaction. This phenomenon was likely due to repeated

dehydrochlorination and displacement of 2-chlorobutane, resulting in formation of undesirable by-product and decreasing the butene selectivity.

Fig 6.21: 2-Chlorobutane conversion (a) and selectivity (b) for Ag/ZrO₂-Al₂O₃ catalysts and the supports recorded at 1h and 4h time on stream. Reaction conditions: 135°C of reaction temperature, 100mg of sample, 100mlmin⁻¹ of total flow rate (GHSV = 48000h⁻¹) and 27000ppm of feed concentration.



Meanwhile, the addition of Ag on ZAH does not show improvement on activity compare to that of the support. Both the 2-chlorobutane conversion and butene selectivity were the same to give 46% and nearly 100%, respectively. This observation has been noticed previously with the Ag/Al₂O₃ catalyst due to the poor dispersion of Ag particles on the support. The products distribution of Ag/ZrO₂-Al₂O₃ catalysts indicate that the formation of cis-2-butene was predominant, followed by the trans-2-butene and 1-butene. This implied that the reaction was acid-catalysed^{27,28}. Note that no deactivation of catalyst can be observed within the experimental range.

The results strongly support the postulates that both the Ag particles and the support are important for catalytic dehydrochlorination of 2-chlorobutane. The higher activity of 10wt% Ag/ZAC catalyst than the ZAC support in spite of the similar acidity, evidence the role of Ag particles to stabilise the carbocation intermediate³⁴

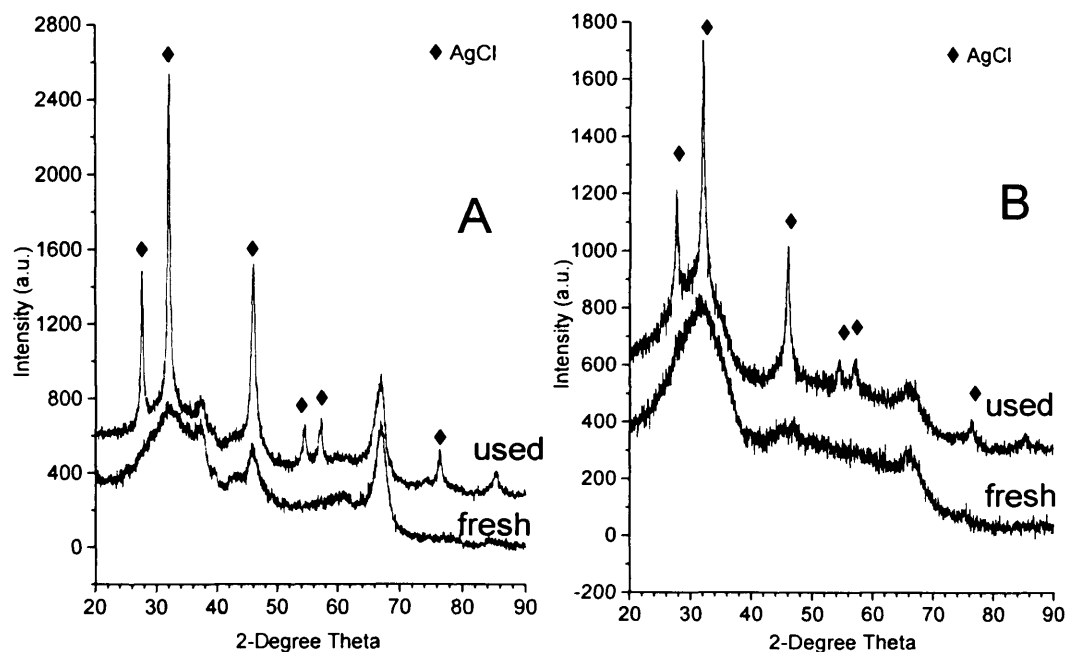
and to involve in the dehydrochlorination of 2-chlorobutane. As mentioned previously in chapter 5, the preparation of $\text{ZrO}_2\text{-Al}_2\text{O}_3$ by co-precipitation (ZAC) creates more acid and base sites than that of the impregnation one (ZAH). We suggest that the homogeneous mixing of ZrO_2 and Al_2O_3 by co-precipitation method (ZAC) create defect sites which have the ability to stabilise the Ag particles. However, the large amount of these sites also initiates strong interaction between the reactants and the catalyst, resulting in the formation of undesirable by-products and hence, decreases in the selectivity. The result indicates that the ZAH support was not suitable for stabilising the Ag compounds, possibly due to poor surface chemistry. The activity was normalised by the number of reducible species based on the TPR result, assuming that the Ag reducible species (Ag^+) was served as the active site. The result shows that 10wt% of Ag/ZAC and Ag/ZAH catalysts has a value of 10min^{-1} and 7min^{-1} , respectively.

6.5.3 Post-reaction analysis

XRD patterns of the used Ag/ $\text{ZrO}_2\text{-Al}_2\text{O}_3$ catalysts were collected to observe changes in the crystalline phase before and after the reaction.

Fig 6.22 depicts the XRD patterns of the fresh and used 10wt%Ag/ $\text{ZrO}_2\text{-Al}_2\text{O}_3$ catalysts. The results show that formation of crystallite AgCl observed for Ag/ $\text{ZrO}_2\text{-Al}_2\text{O}_3$ catalysts after the reaction. The diffraction peaks at 2θ of 27.8° , 32.2° , 46.2° , 54.8° , 57.5° and 76.7° were attributed to the presence of crystalline AgCl phase. The line broadening suggests that 10wt%Ag/ZAH obtained larger AgCl particles than 10wt%Ag/ZAC. Note that the metallic Ag phase was not observed at all in the XRD patterns neither before nor after the dehydrochlorination reaction.

Fig 6.22: XRD patterns of 10wt%Ag/ZrO₂-Al₂O₃ before and after reaction. A. Ag/ZAH and B. Ag/ZAC.



6.6 Conclusions

Silver-doped catalysts were prepared by impregnating 1, 5, 10 and 20wt% of Ag on γ -Al₂O₃, SiO₂ and ZrO₂-Al₂O₃ support *via* incipient wetness technique. The catalysts were characterised by TGA, BET, XRD, TPR, TPD, AA and XPS techniques before being tested for the dehydrochlorination of 2-chlorobutane. TGA and XRD results indicated an interaction between metal-support to produce catalyst with various dispersion of Ag particles. This apparent dispersion was found to be Ag loading dependent. XRD patterns showed the presence of crystalline metallic Ag for Ag/Al₂O₃ and Ag/SiO₂ catalysts, but not for Ag/ZrO₂-Al₂O₃ catalysts. AA was employed to determine the actual metal loadings and TPR was used to investigate the existences of reducible species and the temperature that a reduction took place. The TPR profile indicates that dispersed Ag₂O was obtained and the amount of reducible species was estimated by dividing the amount of H₂ consumption to the actual metal loading. The result showed largely difference in the reducible species contents

dependent on the support used, ranges from 0.7% to 11%. XPS monitor the surface composition of these catalysts. The selective chemisorption and TPD method determines the strength of acidity and the amount of acid sites, and this was used to differentiate between chemical properties for silver-doped catalysts and the support. A general loss of BET surface area for all the supported Ag catalysts was observed as the Ag loading was increased.

Two hypotheses were proposed to explain the catalyst performances of various supported Ag catalysts. The first is the acid-base properties of supported Ag catalysts. γ - Al_2O_3 support was active to the catalytic dehydrochlorination of 2-chlorobutane due to the presence of Lewis acid site. The addition of Ag on γ - Al_2O_3 only modified the acid-base properties slightly, and does not show any significant changes on the activity. In the case of Ag/ SiO_2 catalysts, the SiO_2 support is chemically inert and the addition of Ag generated the acidic sites through ion-exchange of the surface silanol group by the Ag^+ ion. Hence, the catalytic conversion increased with the increasing Ag loadings. The differences in catalyst performances for supported Ag on ZrO_2 - Al_2O_3 catalysts by co-precipitation (ZAC) and impregnation (ZAH), strongly agreed that the importance of the acid-base properties and surface chemistry of the support. The preparation of ZrO_2 - Al_2O_3 by co-precipitation method created more acid and base sites than impregnation, and exhibited better surface chemistry to stabilise Ag compound on the surface of the catalyst. Thus, highly active Ag/ZAC catalyst for dehydrochlorination of 2-chlorobutane was obtained. Secondly, the oxidation state and the dispersion of Ag particles are important for the catalyst performance. The oxidised Ag^+ rather than the metallic Ag^0 could be the active site for the reaction. The oxidised Ag^+ has the ability to stabilise the carbocation intermediate on the catalyst surface³⁴. The poor dispersion of Ag particles on Al_2O_3 support determined by TPR

(0.7-1.3% of surface Ag atom) explained the poor interaction between metal-support, resulting in no changes on activity for Ag/Al₂O₃ catalysts. The addition of Ag on SiO₂, ZAC and ZAH clearly showed better dispersion of Ag particles. The order of the 2-chlorobutane conversion over different supported Ag catalysts with same loading (10wt%) was Ag/ZAC > Ag/SiO₂ > Ag/ZAH > Ag/Al₂O₃. The order of the butene selectivity was Ag/Al₂O₃ ≈ Ag/ZAH > Ag/SiO₂ > Ag/ZAC. Note that only Ag/SiO₂ catalyst was exhibited catalyst deactivation.

Post-reaction analysis showed that the formation of stable AgCl crystallite occur readily. The catalyst deactivation observed for Ag/SiO₂ catalysts is due to the formation of stable AgCl resulting in the disappearance of Ag⁺ species. The XPS spectra show that surface chlorination of catalysts was only observed for catalysts that contains alumina (Ag/Al₂O₃ and Ag/ZrO₂-Al₂O₃). In addition, the XPS spectra also indicated a slight increase of the peak intensity ratio of C1s peak suggesting possible carbon deposition on the catalyst surface.

References

1. Robert H. Perry and Don W. Green, "Perry's Chemical Engineering Handbook" 7th edition, published by McGraw-Hill, 23-28
2. S. Kim, H. Park, W. Choi, *Journal of Physical Chemistry B*, **108**: 20 (2004) 6402-6411
3. E. Bae, W. Choi, *Environmental Science and Technology* **37** (2003) 147-152
4. I. Koichi, A. Koji, O. Hitoshi (2004), JP 2004201702 A2 20040722 20021118
5. H. Nagahiro, S. Keisuke, H. Seiji, H. Yoshio, *Journal of Electroanalytical Chemistry*, **568**: 1-2 (2004) 267-271
6. I. Jusaburo, *Nippon Kagaku Zasshi*, **81** (1960) 1354-61
7. Y. Anju, I. Mochida, H. Yamamoto, A. Kato, T. Seiyama, *Bulletin of the Chemical Society of Japan*, **45**: 8 (1972) 2319-23
8. G. Simkovich, C. Wagner, *Journal of Catalysis* **1** (1962) 521-525.
9. K. Hauffe, F. Sitabkhan, *Journal of Catalysis* **8** (1967) 340-347.
10. J. Maier, *Journal of Physical Chemical Solids*, **46**: 3 (1985) 309-320
11. J. Maier, P. Murugaraj, *Solid State Ionics* **40/41** (1990) 1017-1020.
12. C.F. Ng, K.S. Leung, *Journal of Catalysis* **89** (1984) 553-559.

13. C.F. Ng, K.S. Leung, *Journal of Catalysis* **67** (1981) 410-423.
14. L.N. Ito, A. D. Harley, M.T. Holbrook, D.D. Smith, C.B. Murchison, M.D. Cisneros (1994), WO 9407828 A1 19940414 19930813
15. J.-P. Schoebrechts, F. Janssens. (1996), WO 9616003 A1 19960530
16. B. Heinrichs, P. Delhez, J.-P. Schoebrechts, J.-P. Pirard, *Journal of Catalysis*, **172**: 2 (1997) 322-335
17. B. Heinrichs, F. Noville, J.-P. Schoebrechts, J.-P. Pirard, *Journal of Catalysis*, **192**: 1 (2000) 108-118
18. S. Lambert, C.Ceilier, P. Grange, J.-P. Pirard, B. Heinrichs, *Journal of Catalysis* **221** (2004) 335-346
19. M.-f. Luo, X. Yuan, X. Zheng, *Applied Catalysis A: General* **175** (1998) 121-129
20. K.A. Bethke, H.H.Kung, *Journal of Catalysis* **172** (1997) 93
21. T.E. Hoost, R.J.K., K.M. Collins, M.S. Chattha, *Applied Catalysis B: Environmental* **13** (1997) 59-67
22. Z.M. Wang, M. Yamaguchi, I. Goto, M. Kumagai, *Physical Chemistry Chemical Physics (PCCP)* **2** (2000) 3007-3015
23. H. Knozinger, P. Ratnasamy, *Catalysis Review-Science and Engineering* **17** (1978)
24. N. Aoyama, K. Yoshida, A. Abe, T. Miyadera, *Catalysis Letters* **43** (1997) 249-253
25. Y. Yamashita, N. Aoyama., N. Takezawa, K. Yoshida, *Journal of Molecular Catalysis A: Chemical* **150** (1999) 233-239
26. E. Seker, J.C., E. Gulari, P. Lorpongpaiboon, S. Osuwan, *Applied Catalysis A: General*, **183** (1999) 121
27. I. Mochida, A. Uchino., H. Fujitsu, K. Takeshita, *Journal of Catalysis* **43**:1-3 (1976) 264-72
28. I. Mochida, Y. Anju, A. Kato, T. Seiyama, *Journal of Organic Chemistry* **39**:25 (1974) 3785-7
29. D.H.R. Barton, P.F. Onyon, *Transaction Faraday Society* **45** (1949) 725-735.
30. F. Albert Cotton, G. Wilkinson, *Advanced Inorganic Chemistry*. 5th edition 1988: John Wiley and Son.
31. D.M. Minahan, G.B. Hoflund, W.S. Epling, D.W. Schoenfeld, *Journal of Catalysis* **168** (1997) 393-399.
32. S.R. Seyedmonir, J.K. Plischke, M.A. Vannice, H.W. Young, *Journal of Catalysis* **123** (1990) 534-549.
33. S. Besson, T. Gacoin, C. Ricolleau. J.-P. Boilot, *Chemical Communication* (2003) 360-361
34. R.W. Jones, R.H.S., *Journal of Physical Chemistry* **86** (1982) 1669-1674
35. B. Heinrichs, F.N., J.-P. Schoebrechts, J.-P. Pirard, *Journal of Catalysis* **220**:1 (2003) 215-225

7 CONCLUSIONS

& FUTURE WORK

7.1 Conclusions

The catalytic dehydrochlorination of 2-chlorobutane has been studied using alumina and zirconia catalysts, where silver used as promoters. The modified alumina (i.e. $\text{Al}_2\text{O}_3\text{-HCl}$, $\text{K-Al}_2\text{O}_3$), zirconia-alumina and silver-alumina catalysts were synthesized and characterised before being tested for catalytic activity.

During the blank reaction studies, one major problem experienced was the reproducibility of results. It was observed that the chlorobutane decomposed over the empty glass reactor tube due to an interaction between the reactant and the reactor wall. Reproducible results can only obtain after the reactor wall was coated with a carbonaceous film. This effect was more severe with the tertiary-butyl chloride, and the reactivity order followed 2-chloro-2-methylpropane (tertiary chloride) > 2-chlorobutane (secondary) > 1-chlorobutane (primary), the well-known order of the ease of chloride removal. Efforts have been made to overcome this problem. The reactor conditions were finally optimised to operate at temperature ranges between 35-235°C with a gas space velocity of 9500-55000h⁻¹ to give conversions between 0-80% depending on the catalyst used. 2-chlorobutane was used as the model compound of a weakly chlorinated volatile organic to study the catalytic dehydrochlorination.

γ -alumina was active for the catalytic dehydrochlorination of 2-chlorobutane due to the presence of Lewis acid sites. The different activities between two γ -aluminas from different suppliers (Synetix and Sasol), and the higher conversion

obtained for the acid-treated alumina ($\text{Al}_2\text{O}_3\text{-HCl}$), support the idea that the reaction was acid-catalysed. The lower conversion obtained for alumina after thermal-treatment at 800°C ($\text{Al}_2\text{O}_3\text{-800}$) emphasised the importance of the surface hydroxyl group of γ -alumina. Doping K or Na on alumina was found to inhibit the performance of the γ -alumina support, causes loss of the acidic sites as a result of neutralisation. The result indicated that the exposed alumina surface was served as the active sites, and can be regenerated by lowering the potassium loading. Although all results obtained support the postulation that the reaction as an acid-catalysed dehydrochlorination, in our opinion, basic sites are indispensable for a stabilising effect that may be beneficial to the catalytic activity. In fact, an acid-base bifunctional zirconia-alumina catalyst was proposed.

Mixing zirconia and alumina produces a catalyst with a large surface area ($190\text{-}290\text{ m}^2\text{g}^{-1}$) and good stability. IR studies evidenced the presence of the surface structural defects (Al-O-Zr), relates to the acid-base properties of the zirconia-alumina catalysts hence to the catalytic activity. The zirconia-alumina catalysts exhibited high performance for the catalytic dehydrochlorination of 2-chlorobutane and show better activity than the single oxide components. Among all zirconia-alumina catalysts (25, 50 & 75wt% of $\text{ZrO}(\text{NO}_3)_2$ loading) tested, zirconia-alumina with 50wt% of zirconyl nitrate loading showed the best activity, independent of the preparation method used. A correlation between the ratio of base to acid sites and the catalytic conversion was put forward. With gas hourly space velocity of 55000h^{-1} , the conversion (after normalised by surface area) increases with increasing ratio of base/acid site (ascending order). Alternatively, a linear relationship between the base/acid sites ratio and the conversion was obtained for the reaction performed at GHSV of 9500h^{-1} , in which the best conversion was obtained when the base/acid ratio was close to unity

(descending order). These results strongly support the acid-base bifunctional properties of zirconia-alumina catalysts for the catalytic dehydrochlorination of 2-chlorobutane, where the basic sites provide the stabilisation of the carbonium ion and the activation of the C-H bond, while the acid sites encourage the abstraction of Cl⁻ ions.

The catalytic studies of Ag-doped (Ag-promoted) catalysts for the dehydrochlorination of 2-chlorobutane, emphasised the importance of the Ag-support interaction. Various silver loading ranging from 1 to 20wt% were supported on γ -alumina, zirconia-alumina and silica prepared by the incipient wetness technique. TGA, XRD, and TPD analysis indicated the interaction between the silver species and the alumina support, resulting in differences with the Ag compound dispersion and acid-base properties for various supported silver catalysts. TPR confirmed the existence of reducible species was due to the dispersed silver oxide. Based-on the TPR result (H₂-consumption), we estimated the total available reducible species. Assuming that the Ag⁺ silver oxide rather than the Ag⁰ metallic silver was served as the active site, the very low contents of reducible species obtained (0.7-1.3%) for the Ag/Al₂O₃ catalysts may explain the rather insignificant effect on activity. Supporting Ag on zirconia-alumina and silica improved the Ag dispersion significantly (4-11%). It is important to note that the pure silica is not active for the dehydrochlorination of 2-chlorobutane. The addition of silver on silica induces interaction between metal and support, and generates active sites (acidic sites) for the reaction, and the conversion increases with increasing silver loading. An enhancement on activity was also observed for supported silver on co-precipitated zirconia-alumina (Ag/ZAC), but no significant changes for silver supported on impregnated zirconia-alumina (Ag/ZAH). The different catalytic performances for Ag/ZAC and Ag/ZAH, strongly suggest that

the silver dispersion as well as the acid-base properties were important for the dehydrochlorination of 2-chlorobutane.

Finally, we demonstrated the catalytic studies for the dehydrochlorination of 2-chlorobutane under inert condition is possible. γ -alumina, modified alumina, zirconia, zirconia-alumina and supported silver, all tested active for the dehydrochlorination of 2-chlorobutane as acid, base, acid-base bifunctional and noble metal catalysts.

7.2 Future work

The future challenge will be further investigating the influence of the structure properties on the catalytic performance of zirconia-alumina for the dehydrochlorination of 2-chlorobutane. The tetragonal form of zirconia is known to present better structure and acid-base properties¹.

The addition of noble metals to zirconia-alumina is an interesting research topic to investigate the metal-support interaction as a function of the preparation method, metal dispersion, particle size and structural and acid-base properties.

References

-
1. M. Shibagaki, *Fine Chemicals*, **21** (1992) 5

APPENDICES

- Appendix A: List of Priority Pollutants
- Appendix B: Physical Properties Data
- Appendix C: BET Isotherms
- Appendix D: Sample Calculations
- Appendix E: Case Studies
 - ❖ Chloride absorbent

Appendix A

Table A.1: Alphabetical Listing of Priority Pollutants^a

Acenaphthlene	Endosulfan and metabolites
Acrolein	Endrin and metabolites
Acrylonitrile	Ethylbenzene
Aldrin	Fluoranthene
Antimony and compounds	Haloethers
Arsenic and compounds	Halomethanes
Asbestos	Heptachlor and metabolites
Benzene	Hexachlorobutadiene
Benzidine	Hexachlorocyclohexane
Beryllium and compounds	Hexachlorocyclopentadiene
Cadmium and compounds	Isophorone
Carbon tetrachloride	Lead and compounds
Chlordane (technical mixture and metabolites)	Mercury and compounds
Chlorinated benzenes (other than dichlorobenzenes)	Napthalene
Chlorinated ethanes	Nickel and compounds
Chloroalkyl ethers	Nitrobenzene
Chlorinated naphthalene	Nitrophenols
Chlorinated phenols	Nitrosamined
Chloroform	Pentachlorophenol
2-chlorophenol	Phenol
chromium and compounds	Phthalate esters
copper and compounds	Polychlorinated biphenyls (PCBs)
cyanides	Polynuclear aromatic hydrocarbons
DDT and metabolites	Selenium and compounds
Dichlorobenzenes	Silver and compounds
Dichlorobenzidines	TCDD (2,2,7,8-tetrachlorodibenzo- <i>p</i> -dioxin)
Dichloroethylenes	Tetrachloroethylene
2,4-dichlorophenol	Thallium and compounds
dichloropropane and -propene	Toluene
dieldrin	Toxaphene
2,4-dimethylphenol	Vinyl chloride
dinitrotoluene	Zinc and compounds
diphenylhydrazine	

^a Clean Water Act (CWA) of 1977 copy from "Kirk-Othmer Encyclopedia of Chemical Technology" (1985) John Wiley & Sons. Vol.20, p 108.

Appendix B

Table B.1: Physical properties of reagents used*

	1-chlorobutane	2-chlorobutane	2-chloro-2-methylpropane
Boiling Point:	77 - 78 C	68 - 70 C	50 - 52 C
Melting Point:	-123 C	-140 C	-25 C
Flash Point:	20F	5 F	14 F
Explosion Limits in Air:			
Upper	10.1%	-	-
Lower	1.8%	-	-
Vapor Pressure:	80.1 mmHg @ 78.4 C	-	262.6 mmHg
Specific Gravity:	0.886	0.873	0.84
Vapor Density:			3.2 g/L

* Reference from Material Safety Data Sheet

Type II



- Multilayer adsorption (starting at B)
- Common for porous materials

Type IV



- Small ρ at low p
- Poor conductor at high p

Appendix C

C.1 BET isotherm¹

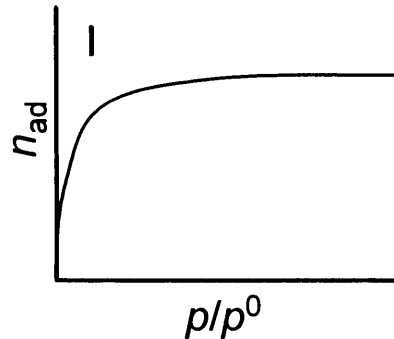
Type I Langmuir Adsorption Isotherm

Assumptions:

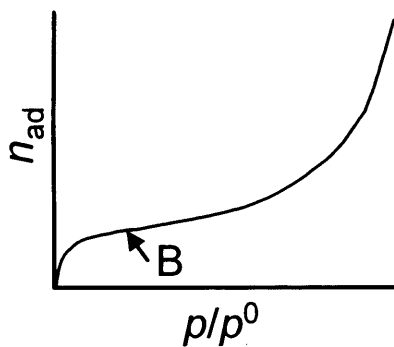
- homogeneous surface
(all adsorption sites energetically identical)
- monolayer adsorption (so no multilayer adsorption)
- no interaction between adsorbed molecules

$$\text{BET equation: } \frac{P}{N_s(P_0 - P)} = \frac{1}{NC} + \frac{(C-1)}{NC} \times \frac{P}{P_0}$$

where N_s can also be written in volume or mass.

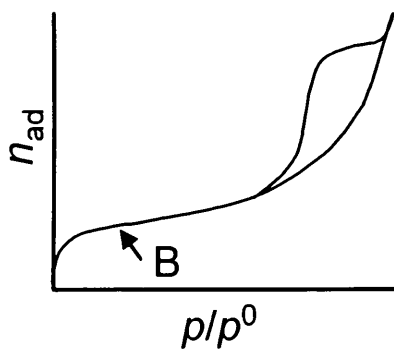


Type II



- Multilayer adsorption (starting at B)
- Common for pore-free materials

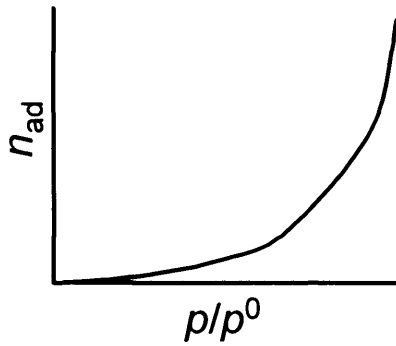
Type IV



- Similar to II at low p
- Pore condensation at high p

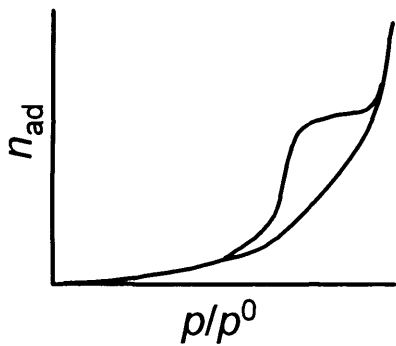
¹ Attard and Barnes, *Surface*, 1998, Oxford University Press.

Type III



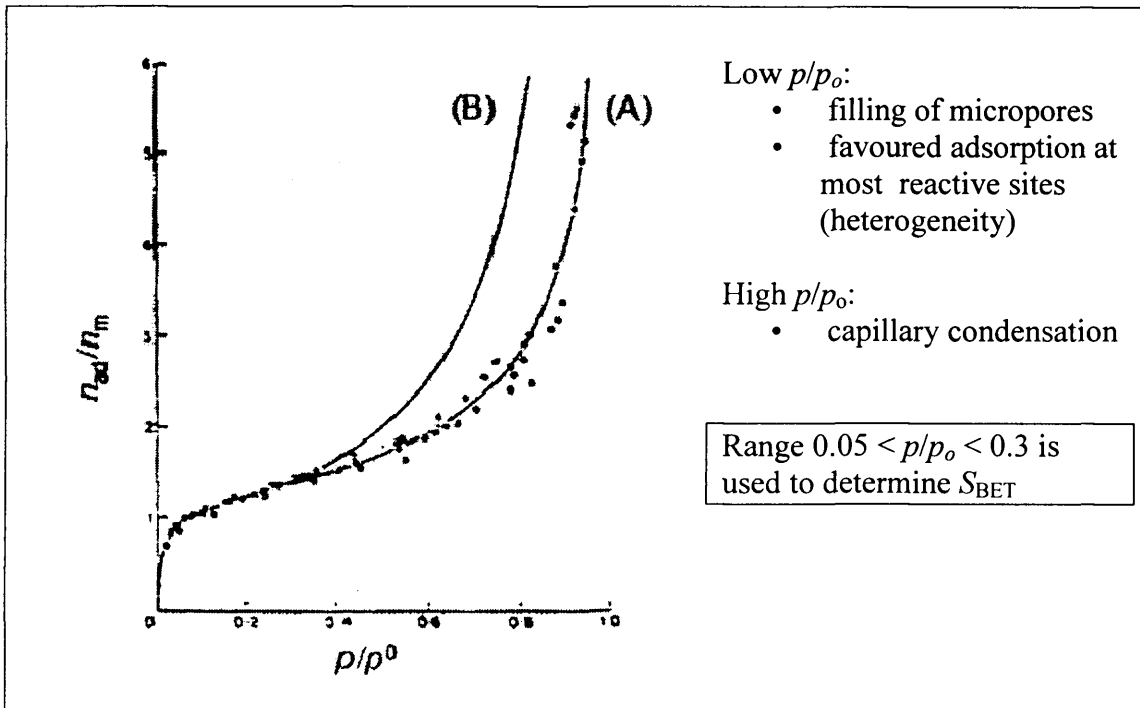
- Strong cohesion force between adsorbed molecules, e.g. when water adsorbs on hydrophobic activated carbon

Type V



- Similar to III at low p
- Pore condensation at high p

Figure C 1: Typical BET plot for non-porous silica (A) and alumina (B)²



² K.L. Yeung, Department of Chemical Engineering, Hong Kong University of Science and Technology, Lecture notes "Absorption and Catalysis"

Appendix D: Sample calculations

D1: A Typical Mass Balance sheet: Date 03/12/2003

Feed gas 3% of 2-CB in He Temperature 135 C

Catalyst g-Al₂O₃ Remark: sample w/o preactivation step

Sample weight 0.1003 g Bed size 0.11 ml

BET area 290 m²/g Total flow 110 ml/min (64ml 2-CB & 45ml make-up)

GHSV ~55000 h⁻¹ Response factor (RF) 2-CB y=3.7684x

isobutene y=3.7352x where x is the GC count*1000

octene y=2(3.7352x) y is the concentration in ppm

start time 12:10 discoloration end time 9:00 next day

total HCl to 36.2 mol in 24h

Exit gas	butene	2-CB	octene	butene	2-CB	octene	sum	butene	2-CB	octene	C bal	Reaction rate	mmolg	molecul/g	molecul/g min
Run time (min)	GC count*1000	B20*RF	B21*RF	B22*RF	selectivity*100	conv*100	F20/SUM	Exit/Feed	mmolg min	mmolg	molecul/g	molecul/g min			
18	1087	6597	4096	24860	0	28956	100.00	14	0.16	2.80	1.69E+21	9.37E+19			
90	2620	4955	9786	18672	0	28459	100.00	34	0.38	27.23	1.64E+22	2.28E+20			
126	2710	4863	10122	18326	0	28448	100.00	36	0.39	14.09	8.48E+21	2.36E+20			
162	2828	4730	10563	17825	0	28388	100.00	37	0.41	14.74	8.87E+21	2.46E+20			
198	2812	4679	10503	17632	0	28136	100.00	37	0.41	14.78	8.90E+21	2.47E+20			
234	2877	4784	10746	18028	0	28774	100.00	37	0.41	14.79	8.90E+21	2.47E+20			
270	2955	4777	11038	18002	7	29047	99.93	38	0.42	15.06	9.06E+21	2.52E+20			
306	3070	4658	11467	17553	7	29028	99.93	40	0.43	15.65	9.42E+21	2.62E+20			
342	3165	4481	11822	16886	7	28716	99.94	41	0.45	16.31	9.82E+21	2.73E+20			
378	3184	4375	11893	16487	7	28387	99.94	42	0.46	16.60	9.99E+21	2.78E+20			
414	3082	4639	11512	17482	7	29001	99.94	40	0.44	15.73	9.47E+21	2.63E+20			
450	3103	4575	11590	17240	7	28838	99.94	40	0.44	15.93	9.59E+21	2.66E+20			
486	3261	4563	12180	17195	15	29391	99.88	41	0.46	16.43	9.89E+21	2.75E+20			
522	3323	4648	12442	17516	15	29943	99.88	42	0.46	16.44	9.89E+21	2.75E+20			
558	3331	4743	12442	17874	15	30330	99.88	41	0.45	16.26	9.79E+21	2.72E+20			
594	3355	4814	12532	18141	15	30688	99.88	41	0.45	16.19	9.75E+21	2.71E+20			
630	3375	4853	12606	18288	15	30909	99.88	41	0.45	16.17	9.73E+21	2.70E+20			
666	3365	4896	12569	18450	15	31034	99.88	41	0.45	16.06	9.67E+21	2.69E+20			
702	3414	4917	12707	18529	15	31296	99.88	41	0.45	16.15	9.72E+21	2.70E+20			
738	3402	5061	12707	19072	15	31794	99.88	40	0.44	15.85	9.54E+21	2.65E+20			
774	3455	5041	12532	18997	15	31543	99.88	40	0.44	15.73	9.47E+21	2.63E+20			
810	3366	5010	12573	18880	15	31467	99.88	40	0.44	15.84	9.54E+21	2.65E+20			
846	3421	5061	12778	19072	15	31865	99.88	40	0.44	15.90	9.57E+21	2.66E+20			
882	3347	5162	12502	19452	15	31969	99.88	39	0.43	15.50	9.33E+21	2.59E+20			
918	3413	5055	12748	19049	15	31812	99.88	40	0.44	15.89	9.56E+21	2.66E+20			
954	3420	5078	12774	19136	15	31925	99.88	40	0.44	15.86	9.55E+21	2.65E+20			
990	3384	5095	12640	19200	15	31855	99.88	40	0.44	15.73	9.47E+21	2.63E+20			
1026	3437	5089	12838	19177	15	32030	99.88	40	0.44	15.89	9.57E+21	2.66E+20			
1062	3486	4978	13021	18759	15	31795	99.89	41	0.45	16.24	9.77E+21	2.72E+20			
1098	3480	4516	12998	17018	15	30032	99.89	39	0.48	17.16	1.03E+22	2.87E+20			
Standard deviat	49	180								473.03	2.85E+23				
average	3411	5009						100							
%error	1	4						6%							

D.2 Sample calculation for chloride analysis by acid-base neutralisation titration

A $145\mu\text{molmin}^{-1}$ of 2-chlorobutane (2-CB) fed into the reactor, which is equal to 38000ppm of gas concentration. The reaction has run for 1310min, and the Cl product was trapped in a 40ml of concentrated NaOH solution (4M). Find out: (1) how much of Cl product has been produced, if 59ml of 1.8M HCl is required to complete neutralise the scrubber. (2) What is the 2-chlorobutane conversion evaluated based on the Cl- product? (3) How much is the chloride balance? Assume an average of 36% of 2-chlorobutane conversion was achieved.

Answers

$$(1) \text{ Initial concentration of NaOH trap} = 40\text{ml} \times \frac{4\text{mmol}}{1\text{ml}} = 160\text{mmol}$$

After reaction for 1310min, 59ml of 1.8M HCl is required for complete neutralisation

$$59\text{ml} \times \frac{1.8\text{mmol}}{1\text{ml}} = 106.2\text{mmol} \text{ of NaOH was remained}$$

$\therefore 1\text{M NaOH} \rightarrow 1\text{M HCl}$

Therefore,

$$\begin{aligned} \text{Total consumption of NaOH} &= 160\text{ml} - 106.4\text{ml} \\ &= \boxed{53.6\text{ml}} \\ &= \text{Total HCl produced} \end{aligned}$$

(2) The reaction duration was 1310min with 2-CB feed flow rate of $145\mu\text{molmin}^{-1}$.

$$\begin{aligned} \text{Therefore, total feed of 2-CB to the reactor} &= \frac{145\mu\text{mol}}{\text{min}} \times 1310 \text{ min} \\ &= 190\text{mmol} \end{aligned}$$

Since the conversion can be evaluated by dividing the total production of chloride

$$\text{compound to the total feed (conv (\%))} = \frac{\text{total products}}{\text{total reactant in feed}} \times 100$$

$$\begin{aligned} \text{The 2-chlorobutane conversion} &= \frac{53.6\text{mmol}}{190\text{mmol}} \times 100\% \\ &= \boxed{28.2\%} \end{aligned}$$

(3) Because of the HCl is the only chlorinated product from the 2-CB conversion,

$$\begin{aligned} \text{Chlorine balance} &= \frac{\text{Total HCl produced}}{\text{Total 2-CB converted}} \times 100\% \\ &= \frac{53.6\text{mmol}}{190\text{mmol} \times 0.36} \times 100\% \\ &= \boxed{78.4\%} \end{aligned}$$

D.3 Monolayer coverage estimation

Ag-O	r_e		Ag ⁺	CN	r_i
Si-O	2.003			4	1.00
Zr-O	1.5097			6	1.15
Al-O	1.7116			8	1.28
	1.6176		Al ³⁺	4	0.39
				5	0.48
				6	0.54
O ²⁻	CN	r_i	Si ⁴⁺	4	0.26
	2	1.21		6	0.4
	6	1.4	Zr ⁴⁺	4	0.59
	8	1.42		6	0.72
Cl ⁻	6	1.81		8	0.84
OH ⁻	4	1.35		9	0.89
	6	1.37			

Taking the Ag/Al₂O₃ (~290m²g⁻¹) as an example, assume that the Ag⁺ was in a coordination of four. The maximum distance, Ag-O-Ag, was estimated as followed:

$$\begin{aligned}
 \text{The diameter of Ag}_2\text{O molecule} &= 4 \times (\text{Ag}^+)r_i + 2 \times (\text{Ag-O})r_e + 2 \times (\text{O}^{2-})r_i \\
 &= (4 \times 1.00) + (2 \times 2.003) + (2 \times 1.21) \\
 &= 10.426 \text{ \AA} \\
 &= 10.4 \times 10^{-10} \text{ m}
 \end{aligned}$$

$$\begin{aligned}
 \text{The surface area of single molecule} &= \frac{\pi d}{4} \\
 &= 8.54 \times 10^{-19} \text{ m}^2
 \end{aligned}$$

$$\begin{aligned}
 \text{The total number of molecules or sites} &= \frac{290 \text{ m}^2 \text{ g}^{-1}}{8.54 \times 10^{-19} \text{ m}^2} \\
 &= 3.4 \times 10^{20} \text{ per gram of sample}
 \end{aligned}$$

Since 1 mole consisted 6.023×10²³ atoms (Avogadro number), and the molecular mass of Ag₂O is 140.

$$\begin{aligned}
 \text{The monolayer coverage for Ag/Al}_2\text{O}_3 &= \left(\frac{3.4 \times 10^{20}}{6.023 \times 10^{23}} \right) \text{ mol} \times 140 \\
 &= 0.0784 \text{ g} \\
 &\approx \boxed{8 \text{ wt}\%}
 \end{aligned}$$

Appendix E: Case Studies – Chloride absorbent

A selection of catalysts include the precipitation prepared ZrO_2 , $\text{ZrO}_2\text{-Al}_2\text{O}_3$ by impregnation and co-precipitation (ZAH & ZAC), Ag/SiO_2 , and 1wt% $\text{KOH}/\gamma\text{Al}_2\text{O}_3$ were tested as an absorbent for the dehydrochlorination of t-butyl chloride. Prior to the reaction, 1% t-BuCl in N_2 gas mixture was fed into the reactor at ambient condition with gas hourly space velocity of 14000h^{-1} and gas concentration of 80ppm. 3ml of catalyst bed was used. The concentration of the exit gas was analysed by the gas-chromatography method.

Table E 1: The t-butyl chloride breakthrough results

Sample	Exit RCl	HCl	C=C
ZrO_2	√	√	√
50ZAC	×	√	√
50ZAH	√	×	√
10% Ag/SiO_2	×	×	√
1% KOH/Al	√	√	√

Table E 1 shows the results for each catalyst tested for the tertiary butyl chloride breakthrough experiment. Among all the catalysts, Ag/SiO_2 revealed to be the best absorbent for t-butyl chloride, the organochloride.

Fig E.1 shows the conversion of t-butyl chloride determined based-on the exit gas concentration. The result shows that 100% absorbance was obtained at the first hour of reaction. The t-butyl chloride conversion starts after 60min of operation with isobutene detected as the only product from the reaction. At 150min time online, the reaction reaches a steady state with maximum conversion of 46%. Note that neither t-butyl chloride nor HCl was detected throughout the 6h of experiment period.

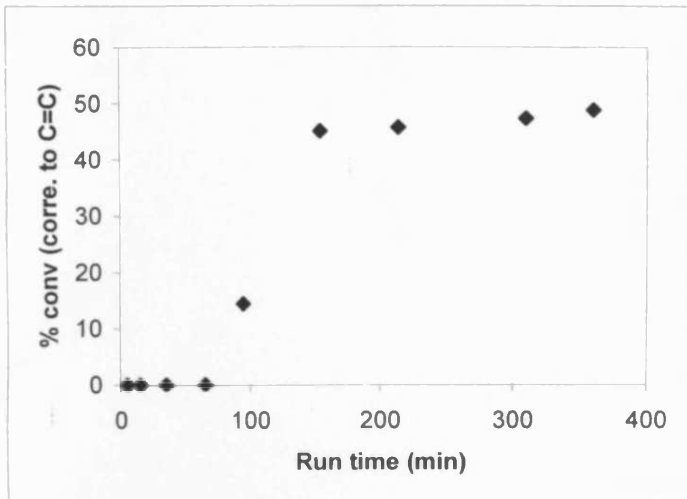


Fig E.1: The t-butyl chloride breakthrough examination over 10wt%Ag/SiO₂.

The result indicates that the 10wt%Ag/SiO₂ is active to the conversion of t-butyl chloride to isobutene despite the low reaction temperature at ambient condition. The absence of t-butyl chloride and HCl from the exit gas suggests the Ag/SiO₂ can be a promising chloride absorbent.

